

**Design and Applications
of
Luminescent Inorganic Complexes**

Thesis by

T. Mark McCleskey

In Partial Fulfillment of the Requirements
for the Degree of
Doctor of Philosophy

California Institute of Technology

Pasadena, California

1994

(Submitted September 1993)

Acknowledgments

I truly enjoyed my stay at Caltech thanks to the wonderful people I came to know over the years. When I first arrived, Bob Sweeney and Erica Harvey made sure that I had some kind of life outside of research by taking me hiking to places like Joshua Tree. John Brewer is a great friend, with whom I had many conversations concerning science, and sometimes just life in general. Horseback riding in Topanga Canyon with Liz Moress provided another nice way to get away from lab. Both John and Liz were fantastic traveling companions in Europe. Barry Ryan and Michael Lock (the Irish contingent) were kind enough to accompany me to just about every party within walking distance of Caltech one summer; I still recall my fingers on fire for a statue of liberty drink. In general, Barry, Michael, Sandi, Terry, Donny, Chrissie, Pat and Andy helped make Friday evenings at the Athenaeum more entertaining.

Jim Bailey and Maureen Hughes were two of the greatest postdocs. I learned how to golf and improved my pool game immensely with them; I now know that straddling the table is a key aspect for many pool shots. Jim and Soni were kind enough to feed me on several occasions, and Soni always had an entertaining story to tell. Although Jim and I were in Las Vegas during the Tailhook party, we were not involved in any way. Even through antagonistic times Julia Hodge has been a friend around lab. Wayne Larson has an amazingly creative sense of humor that has cheered many of my days here. Deborah Wuttke and I enjoyed some fine dining in the LA area (my advice is not to bet with her). Tim, Rhonda, Bob and Steve have all participated in some of the fun times I've had here.

I have to thank Tim, Tom, Gary, Andy, Brian, and everyone else on the chemistry soccer team that allowed me to learn the sport by playing with them. I will always appreciate those true blue Greyhounds such as Bill, Jim, and Toshi who showed up for the games while I was manager (even if most of them came 5 minutes late directly from the Ath). Don, Toshi and Jack have been great tennis partners. Jack also taught me to

play racquetball, but conveniently hurt his ankle when I finally won a match. Our French postdoc Eric taught me the fine game of squash. Eva kindly introduced me to the sport of ultimate last year, which usually involves throwing the disc around with a great group of people. The whole Grey group and assorted others have been instrumental in my skiing activities (especially since the only running car I have is a convertible VW bug). I'm not sure if I should thank Larry Henling for kicking my but up Chantry Flats more times than I care to remember, but the cycling was enjoyable.

In terms of science, the Gray group has been inspirational in many ways. Harry Gray is an amazing advisor who has allowed me to work on my own at times, and offered advice whenever asked. I hope I have learned a little of his ability to present the "Big Picture" to an audience of any level. Most importantly though, Harry cares about his students well being as well as their science. Jay Winkler has taught me many experimental and theoretical aspects of good science, including the fine art of artifact identification. He has also been willing to talk about science and answer curiosity questions at virtually any time. I'd like to thank the Gray group over the years and Vinny for insightful scientific discussions. Thanks to my amazing undergraduate advisor, Mitsuru Kubota, I spent last year teaching Freshman chemistry at Harvey Mudd College. Bob Cave, Bill Daub, Karry Karukstis, William Sly, and obviously Mits were all a part of making that a very pleasant experience. Thanks to Jack Mizoguchi (for instruction) and Jack Richards (for use of his lab space) I learned about molecular biology last year.

Finally, I need to thank a few special people: my Dad has always been very supportive and participated in more exciting aspects of my free time such as skiing and sky diving; I can't say enough about my Mom and stepdad (the convertible is the best hand-me-down ever received) who have encouraged me along the way; Eva has been a great supportive friend (she even proofread most of this thesis) and a wonderful traveling companion in Europe this summer. Dave and Carrie (from Mudd) and Dave, Trisha, and Alice (from Westport) have all been fantastic friends that I could always count on.

Abstract A series of Au(I) phosphine complexes were designed and synthesized to investigate the possibility of room temperature phosphorescence in solution from three different types of transitions: metal-to-ligand-charge-transfer in four coordinate monomers, $d\sigma^* \rightarrow p\sigma$ in Au(I) dimers, and $d \rightarrow p$ in two and three coordinate monomers. Solution emission was only observed from the three coordinate Au(I) complexes. The complex $\text{Au}_2(\text{dcpe})_3^{2+}$ (dcpe = 1,2-bis-dicyclohexylphosphinoethane) has two isolated AuP_3 units and emits at 508 nm in acetonitrile solution with a lifetime of 21 μs and a quantum yield of 0.8 (366 nm excitation). The emission has been assigned as a $^1A_1 \leftarrow E'(^3E'')$ transition with the corresponding absorption band at 370 nm. The excited state is a powerful reductant capable of reducing aryl halides.

Electron transfer (ET) rates were studied from the excited $\text{Au}_2(\text{dcpe})_3^{2+*}$ to a series of substituted pyridiniums (py^+). The low excited state reduction potential (Au(II)/Au(I)) of -2.3 V made it possible to study ET rates at driving forces as high as 2.1 eV. High driving force, bimolecular ET rates were also studied with $[\text{Ir}(\text{cod})(\text{pz})]_2$ (Ir_2 ; cod = cyclooctadiene, pz = pyrazole). The forward ET rates from Ir_2 to py^+ increase to the diffusion limit and remain diffusion limited at driving forces as high as 1.60 eV. The recombination ET rates from py^\cdot to Ir_2^+ show inverted behavior (rates decrease as the driving force increases) at driving forces > 0.85 eV, representing the first observation of inverted behavior for a bimolecular system. The discrepancy between the forward ET and recombination ET rates is explained by ET to low lying excited states.

On the basis of the emission observed from three coordinate Au(I) complexes, Au(I) was used as a probe for the coordination environment of the active site in *Pseudomonas auruginosa* azurin. The active site consists a copper center strongly bound to two histidines and a cysteine in a trigonal plane with a disputed axial interaction to Met121 3.1Å away. The Au(I)-WT-azurin is stable and emits at 580 nm, indicating that there is little or no interaction with the Met121.

Table of Contents

Acknowledgments	ii
Abstract	iv
List of Figures and Tables	vi
Chapter 1. Design and Applications of Luminescent Inorganic Complexes: An Introduction	1
Chapter 2. Characterization and Photophysics of Au(I) Phosphine Complexes	32
Chapter 3. Electron Transfer at High Driving Forces	119
Chapter 4. Luminescent Gold as a Probe for the Coordination Environment of the Active Site in Azurin.	193
Appendix 1 X-ray data for [Au ₂ (dcpe) ₂] (PF ₆) ₂ .	226
Appendix 2 X-ray data for [Au ₂ (dcpe) ₃][Au(CN) ₂] ₂ .	246
Appendix 3 Sample absorbance traces for recombination rates.	276
Appendix 4 Absorbance traces used to determine quantum yields.	284

Figure 1.1.	Jablonski diagram.	5
Figure 1.2.	Orbital energy diagrams of $\text{Ru}(\text{bpy})_3^{2+}$ and $\text{Re}(\text{O})_2(\text{py})_4^+$.	7
Figure 1.3.	Orbital energy diagram of PtPOP.	10
Figure 1.4.	Modified Latimer Diagram of $\text{Ru}(\text{bpy})_3^{2+}$.	13
Figure 1.5.	Scheme for the two electron transfer from Au(I).	16
Figure 1.6.	Reaction steps of photosynthesis.	19
Figure 1.7.	Marcus curve.	21
Figure 1.8.	Reorganization energy.	23
Figure 1.9.	Theoretical Marcus curve for the photosynthetic center.	26
Figure 1.10.	Ribbon diagram of <i>Pseudomonas aeruginosa</i> .	28
Table 2.1	Selected bond distances and bond angles for $[\text{Au}_2(\text{dcpe})_2] (\text{PF}_6)_2$.	37
Table 2.2	Selected bond distances and bond angles for $[\text{Au}_2(\text{dcpe})_3]$ $[\text{Au}(\text{CN})_2]_2$.	39
Figure 2.1.	Instrument configuration for emission spectra.	42
Figure 2.2	^{31}P NMR spectrum of $[\text{Au}_2(\text{dcpe})_3] (\text{PF}_6)_2$.	48
Figure 2.3.	Ortep drawing of $[\text{Au}_2(\text{dcpe})_2] (\text{PF}_6)_2$.	51
Figure 2.4.	Ortep drawing of $[\text{Au}_2(\text{dcpe})_3] [\text{Au}(\text{CN})_2]_2$.	53
Figure 2.5.	Absorption spectrum of $\text{Au}(\text{PPh}_3)_2 (\text{PF}_6)$, 21 μM .	56
Figure 2.6.	Absorption spectrum of $\text{Au}(\text{PCy}_3)_2 (\text{PF}_6)$, 100 μM .	58
Figure 2.7.	Absorption spectra of dppe(---), and $\text{Au}(\text{dppe})_2 (\text{PF}_6)$, 20 μM .	60
Figure 2.8.	Solid state emission spectrum of $\text{Au}(\text{dppe})_2 (\text{PF}_6)$.	62
Figure 2.9.	Absorption spectrum of $\text{Au}(\text{dcpe})_2 (\text{PF}_6)$, 43 μM .	65
Figure 2.10.	Absorption spectrum of $\text{Au}_2(\text{dcpe})_2 (\text{PF}_6)_2$, 73 and 730 μM .	67
Figure 2.11.	Absorption spectrum of $\text{Au}_2(\text{dcpe})_3 (\text{PF}_6)_2$, 5, 50, and 500 μM .	69
Figure 2.12.	Solid state emission spectrum of $\text{Au}_2(\text{dcpe})_2 (\text{PF}_6)_2$ at 77 K, 366 nm excitation.	71
Figure 2.13.	Solid state emission spectrum of $\text{Au}_2(\text{dcpe})_2 (\text{PF}_6)_2$ at room	

	temperature, 313 nm excitation.	73
Figure 2.14.	Emission spectrum of $\text{Au}_2(\text{dcpe})_2 (\text{PF}_6)_2$ at 77 K in a 4:1 ethanol:methanol glass, 313 nm excitation.	75
Figure 2.15.	Emission spectrum of $\text{Au}_2(\text{dcpe})_3 (\text{PF}_6)_2$ in acetonitrile solution at room temperature, 366 nm excitation, 10 μM .	77
Figure 2.16.	Excitation spectrum of $\text{Au}_2(\text{dcpe})_3 (\text{PF}_6)_2$ in acetonitrile solution at room temperature, 366 nm excitation, 10 μM .	79
Figure 2.17.	Absorption spectrum of $\text{Au}(\text{dipe})_2 (\text{PF}_6)$, 67 μM .	83
Figure 2.18.	Absorption spectrum of $\text{Au}_2(\text{dipe})_2 (\text{PF}_6)_2$, 85 μM .	85
Figure 2.19.	Absorption spectrum of $\text{Au}_2(\text{dipe})_3 (\text{PF}_6)_2$, 8 and 800 μM .	87
Figure 2.20.	Solid state emission spectrum of $\text{Au}_2(\text{dipe})_2 (\text{PF}_6)_2$ at room temperature, 313 nm excitation.	89
Figure 2.21.	Emission spectrum of $\text{Au}_2(\text{dipe})_3 (\text{PF}_6)_2$ in acetonitrile solution at room temperature, 366 nm excitation, 10 μM .	91
Figure 2.22.	Excitation spectrum of $\text{Au}_2(\text{dipe})_3 (\text{PF}_6)_2$ in acetonitrile solution at room temperature, 366 nm excitation, 10 μM .	93
Figure 2.23.	Absorption spectrum of $\text{Au}_2(\text{dppb})_3 (\text{PF}_6)_2$ in ethanol, 3 μM .	95
Figure 2.24.	Emission spectrum of $\text{Au}_2(\text{dppb})_3 (\text{PF}_6)_2$ in ethanol solution at room temperature, 366 nm excitation, 2 μM .	97
Figure 2.25.	Excitation spectrum of $\text{Au}_2(\text{dppb})_3 (\text{PF}_6)_2$ in ethanol solution at room temperature, 366 nm excitation, 2 μM .	99
Figure 2.26.	Energy surface diagram: a,b, and c represent the allowed vertical Frank-Condon transitions of $\nu_0-\nu_0$, $\nu_1-\nu_1$ and $\nu_1-\nu_2$.	102
Figure 2.27.	Absorption spectra of $[\text{Au}_2(\text{dcpe})_3] (\text{PF}_6)_2$ at 298 K (lower trace) and 77 K (upper trace).	104
Figure 2.28.	Emission spectra of $\text{ClAu}(\text{PPh}_3)$ with a, 0 (coincides with the baseline); b, 0.5; c, 1.0; d, 1.5; e, 2.0; f, 5.0; g, 9.0 equivalents	

	of PPh ₃ added.	106
Table 2.3	Excited state quenching rates of [Au ₂ (dcpe) ₃] (PF ₆) ₂ with aryl and alkyl halides.	110
Figure 2.29	Modified Latimer diagram for [Au ₂ (dcpe) ₃] (PF ₆) ₂ .	112
Figure 3.1.	Reactant and product energy surfaces for $\Delta G^{\circ} = 0$.	121
Figure 3.2.	Reactant and product energy surfaces for $\Delta G^{\circ} \approx \lambda$.	123
Figure 3.3.	Reactant and product energy surfaces for $\Delta G^{\circ} > \lambda$.	125
Figure 3.4	Theoretical Marcus plot of $\ln(k_{ET})$ vs $-\Delta G^{\circ}$.	127
Figure 3.5.	Coupling effects on the theoretical Marcus curve.	129
Figure 3.6.	Reorganization energy effects on the theoretical Marcus curve; $\lambda(a) = 0.5$ eV, $\lambda(b) = 1.0$ eV, $\lambda(c) = 1.5$ eV.	131
Figure 3.7.	Marcus plots for bimolecular ET; (a) shows the theoretical first order k_{ET} , and (b) shows the theoretical curve corrected for the diffusion limiting rate k_d .	135
Figure 3.8.	Laser arrangement for time resolved emission and absorption.	139
Figure 3.9.	Absorption spectrum of MeV ⁺ .	141
Figure 3.10.	Transient absorption spectrum of a solution containing MeV ²⁺ (380 μ M) and Ir ₂ (160 μ M) at 390 nm, excitation at 532 nm.	143
Figure 3.11.	Transient absorption spectrum of a solution containing MeV ²⁺ and Ir ₂ at 500 nm, excitation at 532 nm.	145
Figure 3.12.	Luminescence decay of Au ₂ (dcpe) ₃ ²⁺ , excitation 355 nm.	152
Figure 3.13.	Sample Stern Volmer plot with 3,4-dicyanopyridinium as the quencher.	154
Figure 3.14.	Marcus plot for the forward ET reactions between Au ₂ (dcpe) ₃ ²⁺ and a series of substituted pyridiniums.	156
Table 3.1.	Quenching rates and driving forces for the forward ET reactions between Au ₂ (dcpe) ₃ ²⁺ and a series of substituted pyridiniums.	158

Figure 3.15.	Kinetic scheme for bimolecular ET.	160
Figure 3.16.	Transient absorption spectrum of $\text{Au}_2(\text{dcpe})_3^{2+}$.	162
Figure 3.17.	Absorption spectrum of Ir_2 .	165
Figure 3.18.	Emission spectrum of Ir_2 .	167
Figure 3.19.	Transient absorbance trace used for the quantum yield determination with 3,4-dicyano-N-methylpyridinium.	169
Table 3.2.	Quenching rates and driving forces for the forward (k_q) ET reactions and the recombination (k_b) reactions between Ir_2 and a series of pyridiniums.	171
Figure 3.20.	Transient absorbance trace at 500 nm with Ir_2 and 3,4-dicyano-N-methylpyridinium, excitation at 532 nm; solid line is the best fit to bimolecular kinetics.	175
Figure 3.21.	Plot of $1/\Delta\text{absorbance}$ vs time for the recombination reaction with 4-cyano-N-methylpyridinium (squares), N-ethylisonicotinamide (triangles), N-ethylpyridinium (circles), and 2,6-dimethyl-N-methylpyridinium (asterisks).	177
Figure 3.22.	Marcus plot of forward (open circles) and recombination (filled circles) ET rates. The solid line is the best fit theoretical curve excluding the diffusion limited forward rates; $H_{ab} = 10 \text{ cm}^{-1}$, $\lambda = 0.85 \text{ eV}$.	179
Figure 3.23.	Tunneling effects; (a) in the normal region, (b) in the inverted region coupled to a low energy vibration, and (c) in the inverted region coupled to a high energy vibration.	183
Figure 3.24.	Distance effect on ET rates in the inverted region; (a) Marcus plot for the λ at the contact distance and (b) Marcus plot for the slightly larger λ at some distance d ($d >$ the contact distance).	185
Figure 3.25.	Enhancement of ET rates in the inverted region by low lying	

excited states; (a) ET to the LUMO on the acceptor, and (b) ET to a low lying excited state. Lower Marcus curves shows the rates for paths (a) and (b).

		187
Figure 4.1	Active site of <i>Pseudomonas aeruginosa</i> .	195
Figure 4.2.	FPLC trace for Au(I)-WT-azurin purification.	202
Figure 4.3.	Absorption spectrum of apo-WT-azurin.	204
Figure 4.4	Absorption spectrum of Au(I)-WT-azurin.	206
Figure 4.5.	Emission spectrum of apo-WT-azurin, 77 K glycerol:water glass.	208
Figure 4.6.	Emission spectrum of reduced-holo-WT-azurin, 77 K glycerol:water glass.	210
Figure 4.7.	Emission spectrum of holo-WT-azurin, 77 K glycerol:water glass.	212
Figure 4.8.	Emission spectrum of Au(I)-WT-azurin, 77 K glycerol:water glass.	214
Figure 4.9.	Luminescence decay of Au(I)-WT-azurin, 77 K glycerol:water glass.	216
Figure 4.10.	Excitation spectrum of Au(I)-WT-azurin.	218
Figure 4.11.	Theoretical active site for the Au(I)-Leu121 mutant.	222

Chapter 1.

Design and Applications of Luminescent Inorganic Complexes:

An Introduction

Introduction.

Luminescent complexes have provided a fascinating and diverse area of research. There are over 2000 papers on the classic inorganic complex $\text{Ru}(\text{bpy})_3^{2+}$ (bpy = 2,2'-bipyridine) alone. The great interest in this complex varies from use as a means for transferring light energy into useful chemical energy¹ to a photo-activated trigger for studying reactions on a fast time scale² to a luminescent probe of the environment.³ The extensive studies on $\text{Ru}(\text{bpy})_3^{2+}$ and other luminescent inorganic complexes has produced a wealth of information concerning the fundamental process of emission, making it feasible to design luminescent complexes. This thesis will focus on the design and characterization of a luminescent gold complex and examine the application of such a luminescent inorganic species to photo-reduce substrates, study the fundamental process of electron transfer, and probe the nature of the geometry in the active site of a protein.

The desire to harness the light energy by photo-reducing a substrate places a few requirements on the emission characteristics. In order for the excited state of the luminescent species to interact with other compounds it is necessary that the complex emit in solution with a lifetime which exceeds the time required for the two molecules to diffuse together. For most solutions the required lifetime is >1 ns. Emission at room temperature is also beneficial to facilitate both the study and possible applications of the luminophore. To purposely design a compound with such characteristics it is necessary to understand some of the basic aspects of luminescence.

Luminescence occurs when an electron decays from an excited state to the ground state by emitting a photon. The electron generally achieves this excited state through the absorption of a photon. The spin states involved in the transition have a large effect on the lifetime of the excited state. The complexes addressed in this thesis have diamagnetic ground states. The excited state will either be a singlet state if the excited electron remains paired with the electron remaining in the highest occupied molecular orbital (HOMO) of the ground state or a triplet if the electrons have the same spin. The spin

allowed singlet to singlet process (fluorescence) occurs on a shorter time scale (ps-ns) than the spin forbidden triplet to singlet process (phosphorescence; ns-s) in which spin angular momentum is not conserved. Therefore, phosphorescence is the desired decay path for long-lived emission in solution. Accessing the triplet excited state directly is a problem because the spin forbidden nature of the transition means there will be no absorption band. The excited triplet state may be accessed from the higher energy singlet excited state (there will be a strong absorption band for the allowed singlet to singlet transition; $\epsilon > 10,000$), but this spin crossover rate is usually much slower than the allowed fluorescence decay. For these reasons most organic compounds which luminesce fluoresce brightly but show very little phosphorescence. The bright fluorescence makes them useful as laser dyes, but they are not capable of bimolecular photochemistry.

Inorganic compounds with large metal centers provide a mechanism where spin angular momentum can couple with the orbital angular momentum. By changing orbital angular momentum concomitant with the spin angular momentum, the total angular momentum is conserved. As the spin change becomes more allowed, the spin crossover rate can become faster than fluorescence and the triplet excited state can be readily populated from the singlet excited state (Figure 1.1). Direct excitation to the triplet state becomes possible with measurable absorption bands ($\epsilon > 10$).⁴ The lifetime of the phosphorescence state decreases as the triplet to singlet transition becomes more allowed, offsetting the increased efficiency of populating the triplet excited state. The balance between the lifetime of the triplet state and the quantum yield for phosphorescence can be tuned by varying the metal center. Spin orbit coupling effects increase considerably with the size of the metal atom. Some inorganic species with third row metals display phosphorescence with quantum yields as high as 0.8 and lifetimes in solution as long as 25 μ s (substantially longer than the 1 ns required for bimolecular reactions).⁵ The compounds in this thesis utilize the third row metals Au and Ir for their spin orbit coupling ability.

Although the presence of the heavy metal atom helps to access the triplet excited state, it does not ensure emission. One must also consider the nature of the orbitals involved in the emission process. When the electron absorbs a photon it may go directly into the lowest unoccupied molecular orbital (LUMO) or into one of many higher lying orbitals. Inter-conversions between different excited states occurs in ≈ 10 fs.⁶ Emission on a picosecond or longer time scale will always come from the lowest energy excited state with singly occupied HOMO and LUMO orbitals (Figure 1.1). By engineering the appropriate HOMO and LUMO it is possible to design low-energy transitions which are more likely to lead to long lived excited states. One of the reasons for the vast interest in $\text{Ru}(\text{bpy})_3^{2+}$ is that it has a long-lived excited state (600 ns) at room temperature in acetonitrile. The emission of $\text{Ru}(\text{bpy})_3^{2+}$ transfers an electron from the ligand centered π^* (LUMO) to the metal centered d orbital (HOMO). The metal to ligand charge transfer (MLCT) transition is vital to the emission. It has been demonstrated that substituent changes on the bpy ligands which raise the ligand π^* orbital and bring the MLCT transition close in energy to the higher lying ligand field transition result in a shorter lifetime and an increase in photo-dissociation.⁷ These observations are even more pronounced for the isoelectronic $\text{W}(\text{CO})_5\text{X}$ (X is a substituted pyridinium) complexes,⁸ and are believed to be a result of a thermal equilibrium between the excited MLCT state and the excited ligand field state. As the two excited states become closer in energy, the excited ligand field state becomes occupied and provides the pathway for photo-dissociation.

The fact that d-d absorption transitions often lead to photo-dissociation instead of luminescence is expected from ligand field theory considerations. The energy of the d orbitals is determined by their interactions with the bonding electrons from the ligands. The lower energy orbitals are generally non-bonding and the higher energy d orbitals are M-L anti-bonding. In $\text{Ru}(\text{bpy})_3^{2+}$ the octahedral ligand environment splits the d orbitals into two degenerate sets. The low energy non bonding (or π back bonding) orbitals are

Figure 1.1. Jablonski diagram: S_0 is the ground state singlet; S_1 is the lowest energy excited state singlet; S_2 is a higher energy excited state singlet; T_1 is the lowest energy excited state triplet; k_F is the fluorescence decay rate; k_{NR} is the non-radiative decay rate; k_P is the phosphorescence decay rate; k_{SS} is the singlet to singlet interconversion rate; k_{ST} is the singlet to triplet crossover rate.

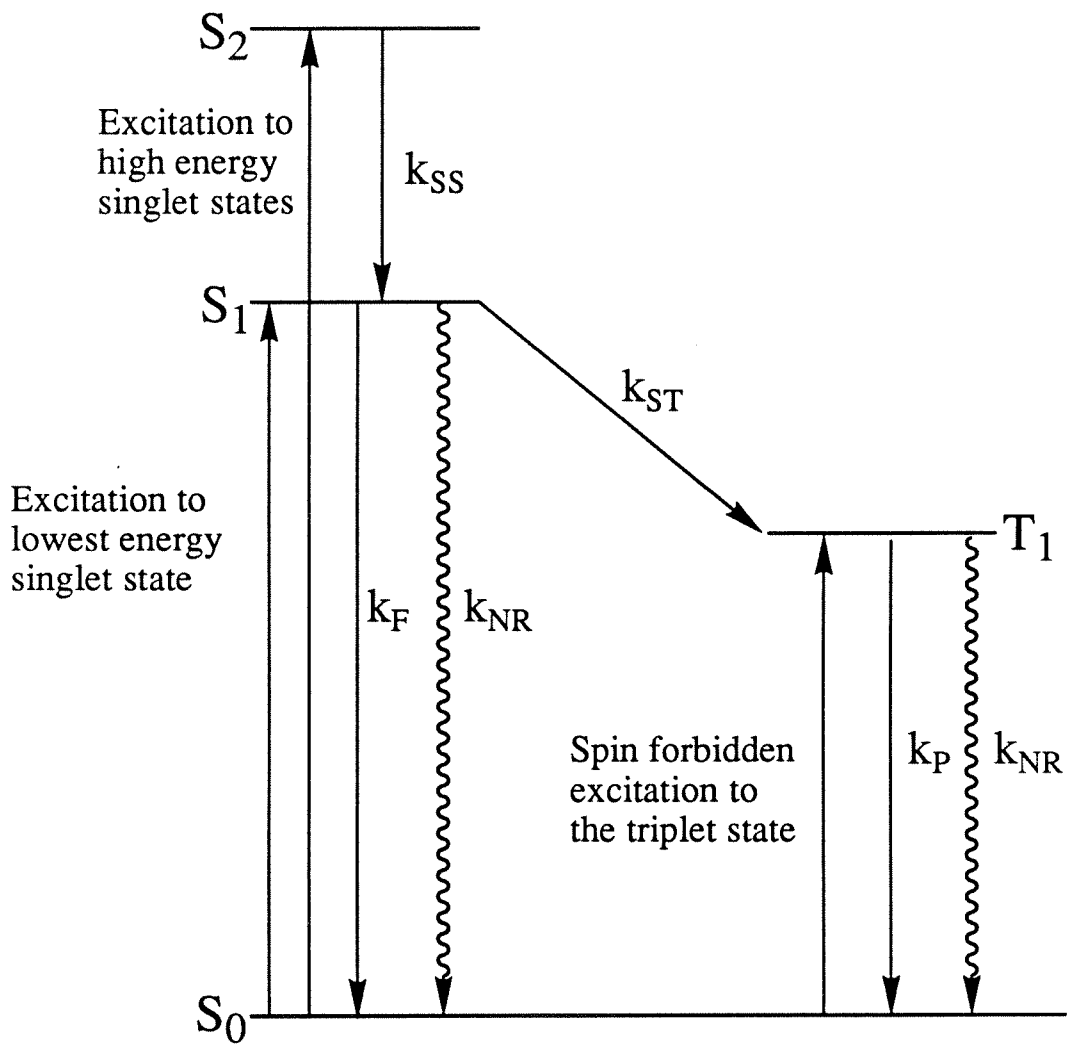


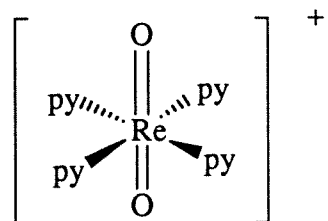
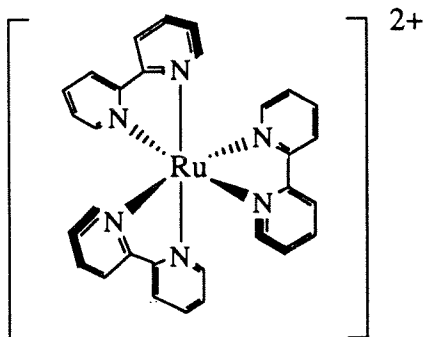
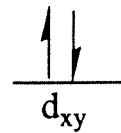
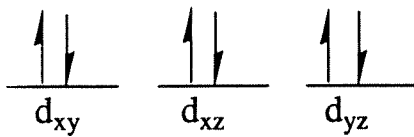
Figure 1.2. Orbital energy diagrams of $\text{Ru}(\text{bpy})_3^{2+}$ and $\text{Re}(\text{O})_2(\text{py})_4^+$.

$d_{z^2}, d_{x^2-y^2}$ ——— ———

 $\text{bpy } \pi^*$ ———

 d_{z^2} ———

 $d_{x^2-y^2}$ ———

 d_{xz}, d_{yz} ——— ———


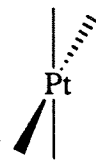
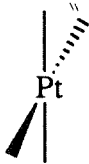
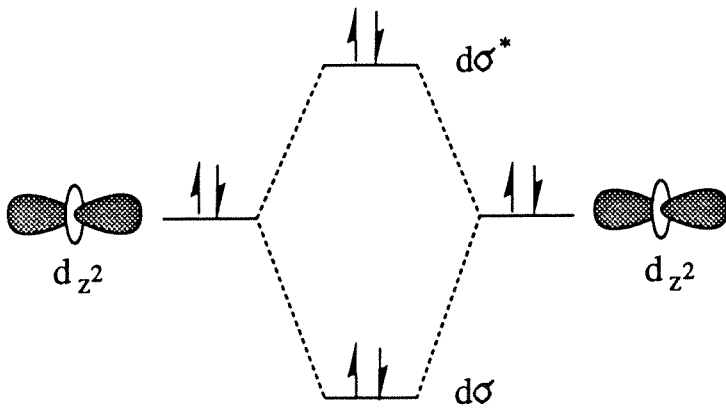
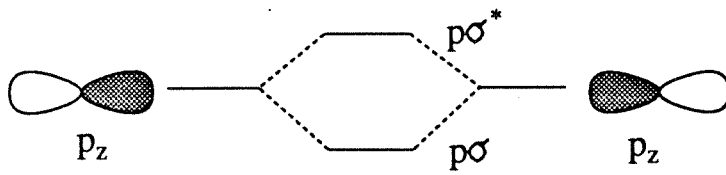
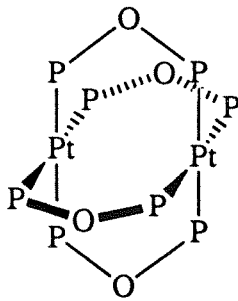
d_{xz} , d_{yz} , and d_{xy} . The high lying d_z^2 and $d_{x^2-y^2}$ orbitals are σ anti-bonding (Figure 1.2). The six d electrons of the Ru^{2+} center completely fill the non-bonding d orbitals. Ligand field excitation takes a d electron from a non-bonding orbital and places it into an anti-bonding orbital, causing the metal ligand bond to weaken enough to dissociate.

Emission in solution from a d-d transition is observed in multiply bonded species such as metal oxos ($M=O$) and metal nitridos ($M=N$). The compound $Re(py)_4O_2$ emits in acetonitrile solution with a lifetime of 10 μs .⁸ The emission transition of the d^2 species has been assigned as a $d_{xy} \leftarrow d_{xz} d_{yz}$ transition (Figure 1.2). The d_{xy} (HOMO) is a non-bonding orbital and the degenerate d_{xz} , d_{yz} (LUMOs) are π^* anti-bonding orbitals. When the electron is excited into the π^* orbital the π bond of the strong metal oxo double bond is weakened, but the σ bond remains intact preventing dissociation.

Room temperature luminescence in solution has been observed for a variety of d^8 - d^8 dimers. One such dimer is the completely inorganic complex PtPOP.⁵ The complex consists of two square planar Pt d^8 centers brought together in a face-to-face arrangement. The filled d_z^2 orbitals interact to form a bonding $d\sigma$ orbital and an anti-bonding $d\sigma^*$ orbital. The empty p_z orbitals interact in an analogous manner to form a bonding $p\sigma$ and an anti-bonding $p\sigma^*$ orbital (Figure 1.3). The lowest energy absorption transition is a $d\sigma^* \rightarrow p\sigma$ transition. This transition formally removes an electron from an anti-bonding orbital and places it into a bonding orbital, resulting in a stronger metal-metal bond. One can observe the increase in bond strength by excited state raman; the metal-metal bond stretch shifts from 118 cm^{-1} for the ground state to 156 cm^{-1} for the excited state.¹⁰ The Pt dimer emits in solution with a lifetime of 25 μs .

Two other types of transitions commonly observed are ligand to metal charge transfer (LMCT) transitions and intraligand transitions. The LMCT transition promotes an electron from a ligand based orbital to a metal centered orbital. The excited state orbital of an LMCT transition is usually a metal centered d orbital. As in the d-d transitions one must be careful to ensure that the metal orbital is non-bonding to observe

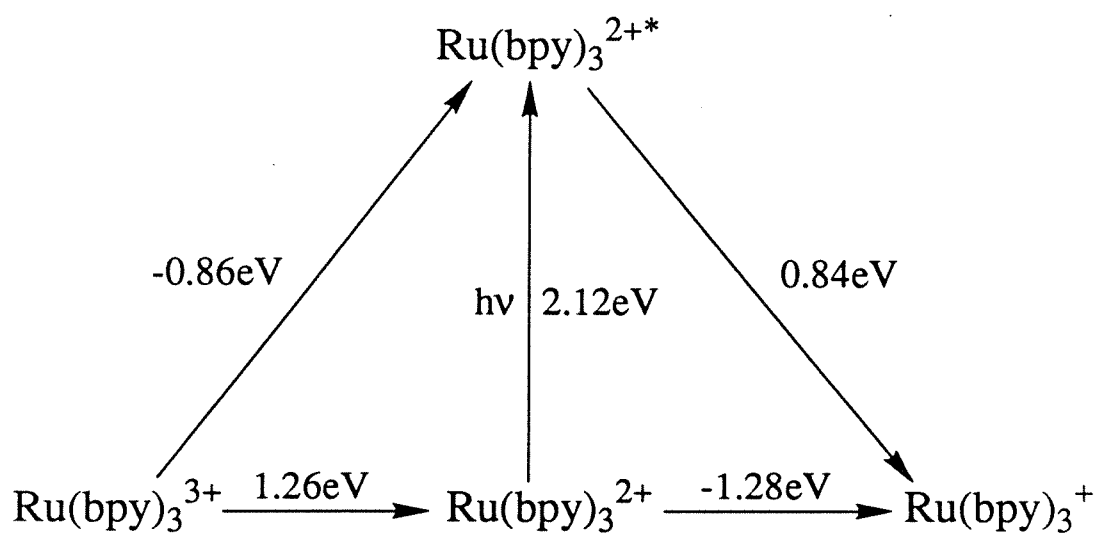
Figure 1.3. Orbital energy diagram of PtPOP.



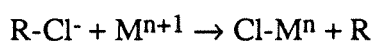
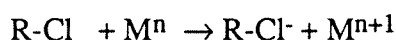
long-lived luminescence. Metals are also known to perturb intraligand transitions. In terms of luminescence, ligands that only fluoresce on their own have been observed to phosphoresce when ligated to a metal center. This heavy atom effect is a result of the spin orbit coupling mentioned earlier.

The research discussed in the second chapter started with the goal of designing a luminescent inorganic complex capable of using the absorbed light energy to reduce a substrate. Gold(I) was chosen as the metal center for a number of reasons: it is a third row metal with efficient spin orbit coupling for accessing the triplet excited state; gold(I) has a d^{10} configuration so none of the dissociative d-d transitions are possible; the oxidation of Au(I) produces Au(III) in a two electron process. Understanding the benefits of this last feature requires an examination of the process of photo-reduction. When a molecule absorbs a photon, the light energy stored in the excited state makes the complex both a better oxidant and a better reductant than the ground state. When the ground state acts as an oxidant the electron from the substrate must go into the LUMO, but in the excited state the substrate electron can fill the hole in the HOMO. In a similar manner the excited state acts as a better reductant because the electron transferred from the complex is the excited electron in the LUMO; the ground state must transfer an electron from the lower energy HOMO. Ruthenium trisbipyridine is an example of a complex which is stable in the ground state with respect to both oxidation to Ru^{3+} ($\Delta G (Ru^{2+}/Ru^{3+}) = 1.26$ eV) and reduction to Ru^{1+} ($\Delta G (Ru^{2+}/Ru^{1+}) = 1.28$ eV). In the excited state it can act as both an oxidant ($\Delta G (Ru^{2+*}/Ru^{1+}) = -0.84$ eV) and a reductant ($\Delta G (Ru^{2+*}/Ru^{3+}) = -0.86$ eV; Figure 1.4).³ The products of the photo-induced electron transfer can thermally react to regenerate the original ground state reactants, posing a major problem for converting sunlight energy into storable chemical energy. This unwanted back electron transfer will always be exoergonic for solar energy conversion processes, so the reaction must somehow be slowed kinetically. The two electron reduction capacity of Au(I) is one way to slow the back reaction. An excited Au(I) species can reduce a substrate by

Figure 1.4. Modified Latimer Diagram of $\text{Ru}(\text{bpy})_3^{2+}$.

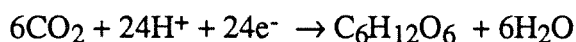
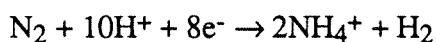
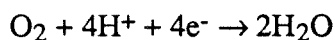


one electron and generate transient unstable Au(II) complex. The Au(II) complex rapidly disproportionates to Au(I) and Au(III) or donates a second electron to another molecule of substrate before back electron transfer to the Au(II) can occur (Figure 1.5). The two electron transfer to Au(III) is kinetically slow since it must proceed through the unstable Au(II) state. Alternatively, the two electron transfer from Au(I) can be carried out on a single substrate molecule in conjunction with transfer of an atom, such as Cl, from the substrate (R1). Such atom abstraction has a slow back rate because the atom must



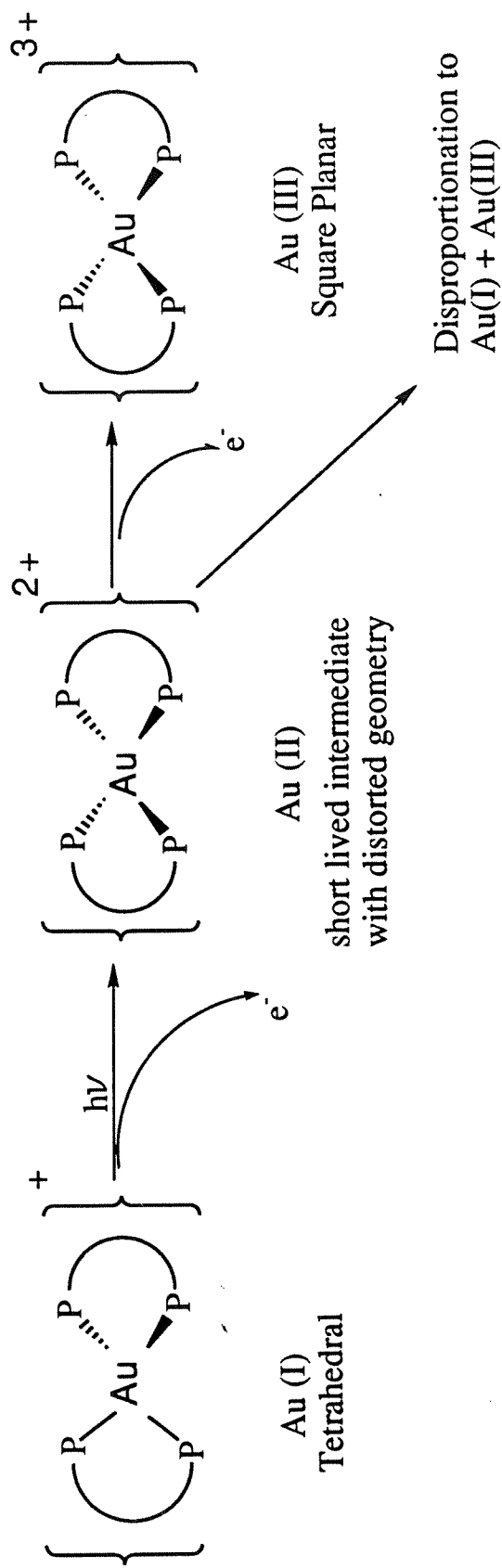
dissociate from the metal center.

Chapter three takes advantage of luminescence by using it as a trigger to initiate electron transfer. Electron transfer (ET) is the fundamental process by which all molecules are reduced or oxidized. Mammalian respiration, nitrogen fixation and photosynthesis are just three of the myriad of biological processes which require ET.



The ET rates can take place in less than a nanosecond, so conventional stop flow techniques that require mixing time for the reaction mixture to become homogeneous are too slow for studying ET. Long-lived excited states, however, provide a way to generate a homogeneous reaction mixture in the time required to absorb a photon \approx fs. As an example, one can study ET from Ru(bpy)₃^{2+*} to N-methyl pyridinium by first making a solution of Ru(bpy)₃²⁺ and N-methyl pyridinium; no reaction occurs initially because the ground state ruthenium complex is not a powerful enough reductant to reduce the pyridinium. Absorption of light from a laser pulse produces Ru(bpy)₃^{2+*} in \approx fs, allowing one to study the subsequent ET to the pyridinium. The limitation for observing

Figure 1.5. Scheme for the two electron transfer from Au(I).



Step 1) Absorption of light leads to an excited state complex that transfers one electron to produce an unstable gold (II) compound

Step 2) The unstable gold (II) compound thermally transfers a second electron

fast ET now becomes the duration of the laser pulse. This type of photo-triggering has enabled researchers to study ET in proteins¹¹ as well as many of the short-lived intermediates in photosynthesis.¹²

Photosynthesis begins with the absorption of light by a chlorophyll molecule. The excited electron then travels 17 Å to a bacteria pheophiton in 3 ps. The electron quickly moves on to quinone A in 200 ps (Figure 1.6).¹² This second step must compete with the highly exoergonic back reaction which produces the original ground states. The remarkable aspect of photosynthesis is that the reaction to the ground state is much slower (12 ns) than either of the first two forward ET steps despite the fact that there is a higher driving force, $-\Delta G$, for the back reaction. Understanding the long-lived charge transfer state which results from the slow back ET rate is crucial to the development of artificial photosynthesis. One hypothesis suggests poor coupling between the HOMO of the chlorophyll and the orbital of the bacteria pheophiton is responsible for the slow back rate. To account for the fast forward ET rate, the LUMO of the chlorophyll must be highly coupled to the bacteria pheophiton orbital. The difference in rates would require the coupling of the bacteria pheophiton orbital to the π^* orbital of the chlorophyll to be an order of magnitude greater than the coupling to the π orbital of the chlorophyll. The large coupling difference between two spatially similar orbitals is difficult to imagine.

A second explanation comes from the Marcus theory for ET,¹³ which predicts that the ET rates will increase exponentially as the driving force increase, reach a maximum, and then decrease exponentially as the driving force continues to increase (Figure 1.7). If the forward ET reaction is near the maximum of the Marcus curve then the higher driving force back reaction will be much slower. The maximum of the Marcus curve occurs when the driving force is equal to the reorganization energy. The reorganization energy is comprised of the energy required for the solvent dipoles to reorient as the charge transfers and the energy required for any bond length or bond angle changes (Figure 1.8). The photosynthetic center lies within the cell membrane so that the "solvent" is

Figure 1.6. Reaction steps of photosynthesis: P is the chlorophyll; Bph is the bacteria pheophiton; Q_a is quinone A; Q_b is quinone B.

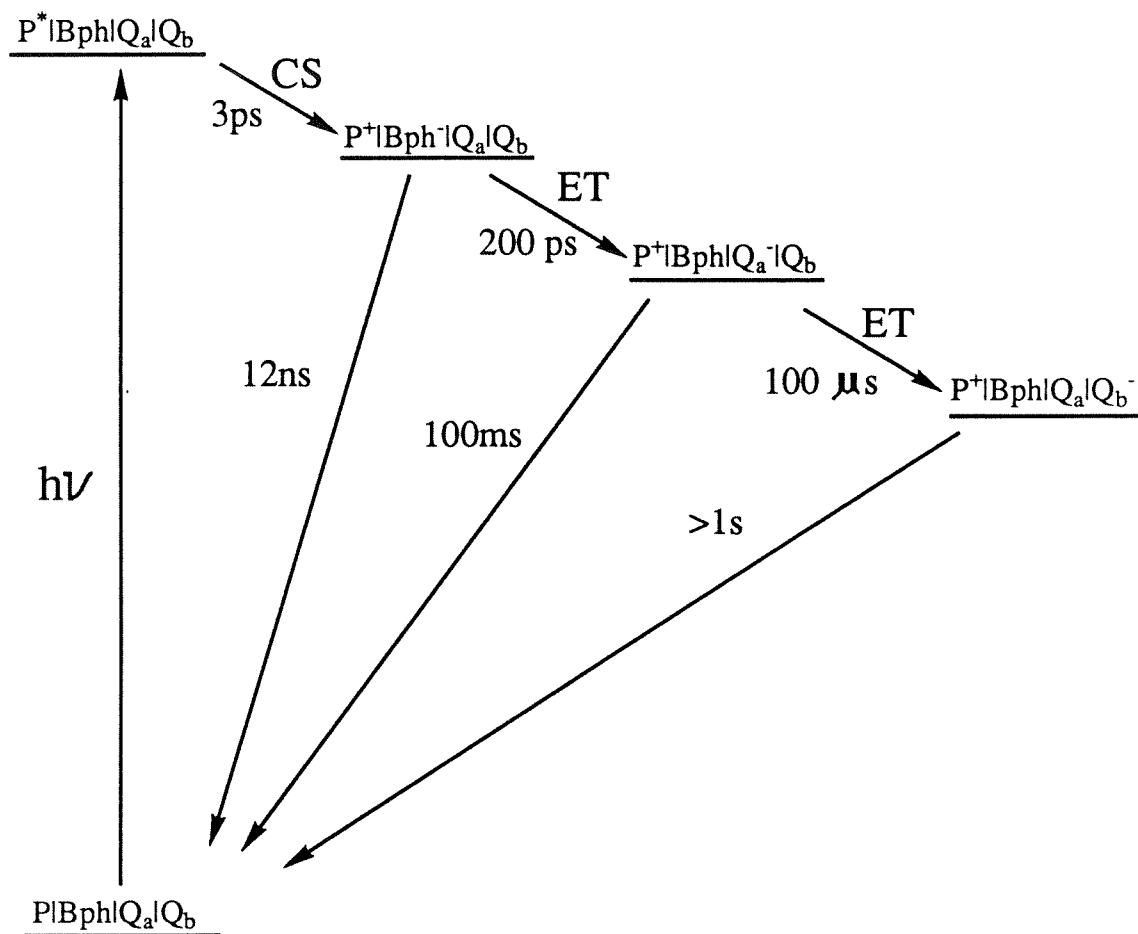


Figure 1.7. Marcus curve: k_{\max} is the maximum electron transfer rate.

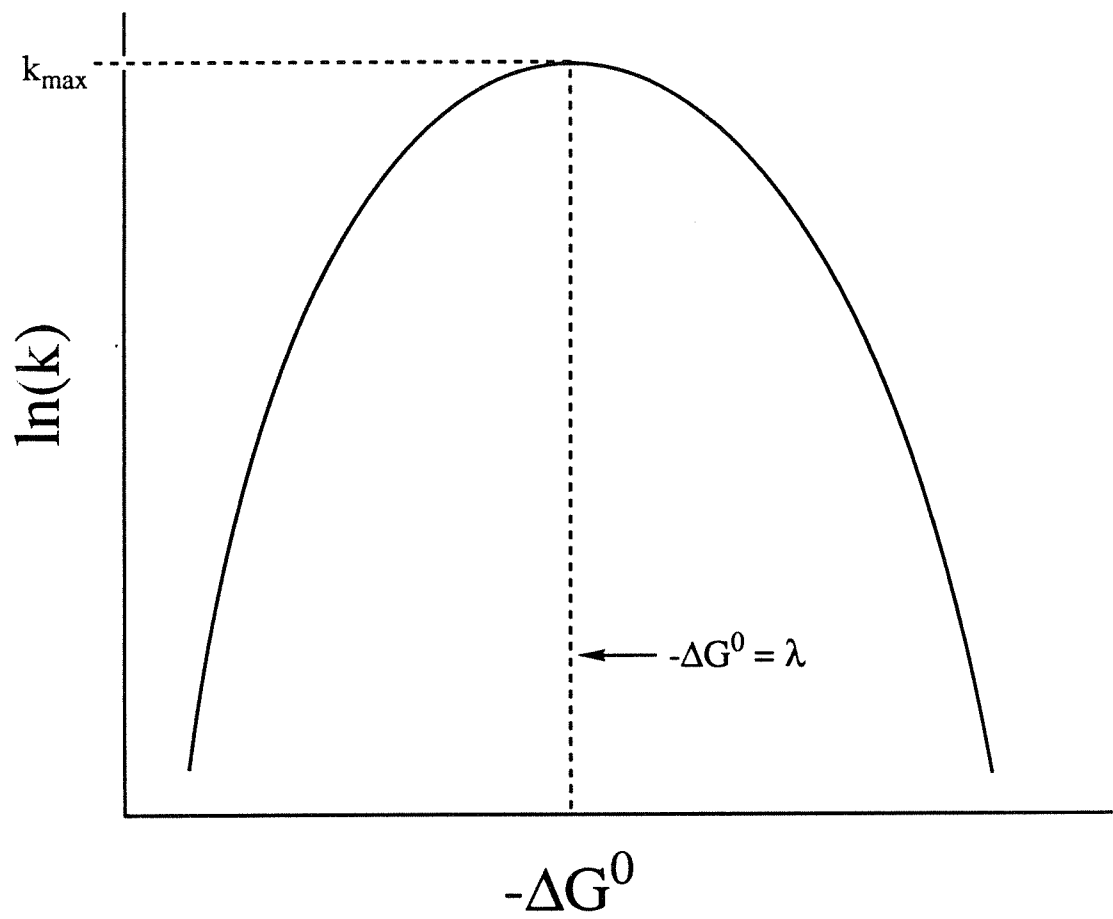
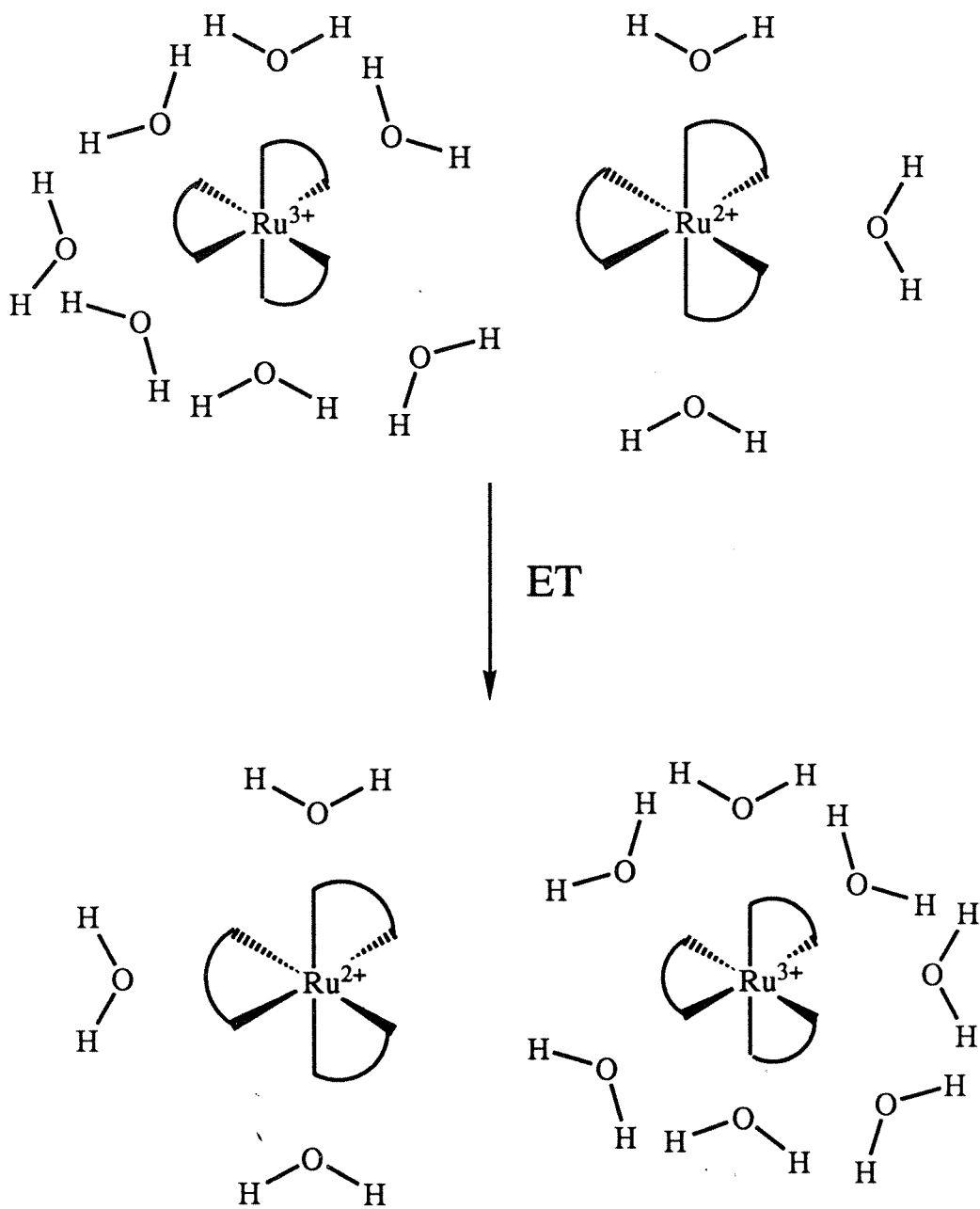


Figure 1.8. Reorganization energy.



essentially fixed in place. The lack of solvent reorganization leads to a low total reorganization energy (λ) and a very narrow Marcus curve (Figure 1.9). The fast initial ET step in photosynthesis can now be explained if the relatively low driving force is $\approx \lambda$ and lies at the top of the Marcus curve. The slow back rate is explained by the fact that it has a much higher driving force and will lie deep in the inverted part of the curve. Chapter three discusses the use of luminescent metal complexes to experimentally investigate ET rates at high driving force and verify the predicted inverted region.

For a luminescent complex, the lifetime, the emission maximum, and the intensity of the emission are all affected by the environment around the compound. The $\text{ReO}_2(\text{py})_4^+$ complex mentioned earlier emits strongly in an acetonitrile solution, but shows no evidence of emission in water; it is believed that the excited is deactivated through hydrogen bonding between a water proton and the oxo of the $\text{ReO}_2(\text{py})_4^+$. The phosphorescence lifetime of many inorganic complexes is drastically shortened in the presence of oxygen.¹⁴ The fact that luminescence can change drastically depending on the environment makes luminescent compounds useful as probes. Ethidium bromide is used as a marker for the presence of DNA in DNA gel separations because it fluoresces brightly when intercalated into DNA, but does not emit in water. Chapter four discusses the use of an emissive gold complex to probe the coordination site of azurin. Azurin is a small blue copper protein that functions as an ET protein (Figure 1.10). The active site is a type I copper site with a Cu^{2+} ion strongly bound to a cysteine and two histidines. The blue color arises from a cysteine to copper charge transfer band at 628 nm.⁹ When the protein accepts an electron the Cu^{2+} is reduced to Cu^+ , and the protein loses its blue color as the cysteine to copper charge transfer band moves to the UV. Despite crystal structures of both the reduced and oxidized forms of the protein,¹⁴ there is still some controversy in the literature as to how much the copper center interacts with the methionine at position 121. The crystal structure places the methionine 3.1 Å from the copper. Solomon and coworkers have used the crystal structure coordinates to perform

Figure 1.9. Theoretical Marcus curve for the photosynthetic center.

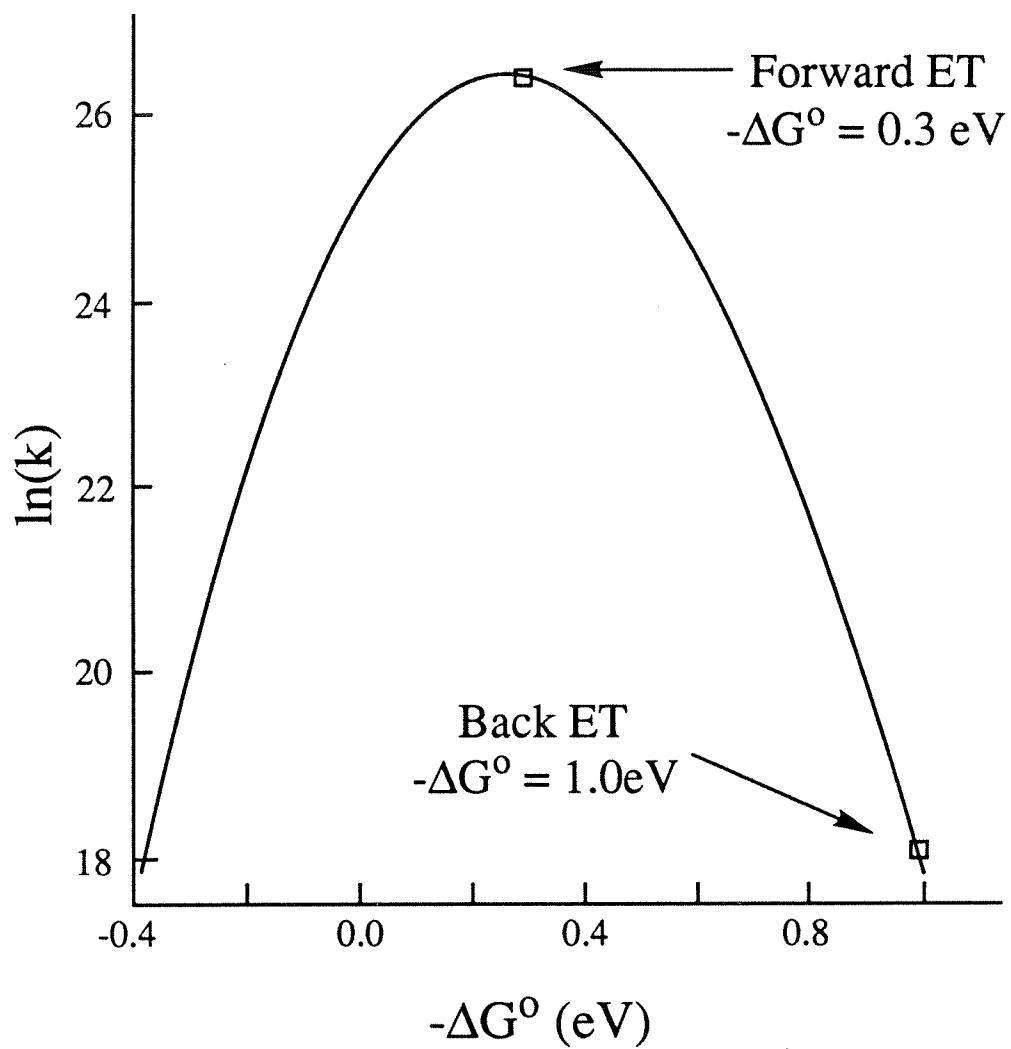


Figure 1.10. Ribbon diagram of *Pseudomonas aeruginosa*.



XCF-Xalpha calculations and report a 30% bond to the methionine.¹⁵ Chapter four reports a series of gold substituted azurins and their luminescence properties. Gold was placed in the active site because results on the emission from gold phosphines (see chapter two) show that three coordinate gold phosphoresces strongly, but four coordinate gold does not emit. Strong bonding with the methionine would lead to a non-emissive four coordinate gold(I) site. Little or no bonding interaction with the methionine would produce an emissive three coordinate gold(I) site.

References

- 1) Maestri, M.; Sandrini, D.; Balzani, V.; Mader, U.; Zelewski, A. *Inorg. Chem.* **1987**, *26*, 1323.
- 2) Balzani, V.; Bolletta, F.; Gandolfi, M.T.; Maestri, M. *Topics in Current Chemistry*, **1978**, *78*, 1-59.
- 3) Thorp, H.H.; Gray, H.B. *Photochemistry and Photobiology*. **1991**, *54*, 609-612.
- 4) Lever, A.B.P. *Inorganic Electronic Spectroscopy (second edition)*. **1984**, Elsevier, New York, New York.
- 5) Stiegman, A.E.; Rice, S.F.; Gray, H.B.; Miskowski, V.M. *Inorg. Chem.* **1987**, *26*, 1112-1116.
- 6) Turro, N.J. *Modern Molecular Photochemistry*. **1978**, Benjamin/Cummings Publishing Company, Menlo Park, California.
- 7) (a) Van Houten, J.V.; Watts, R.J. *Inorg. Chem.* **1978**, *12*, 3381-3385. (b) Durham, B.; Caspar, J.V.; Nagle, J.K.; Meyer, T.J. *J. Am. Chem. Soc.* **1982**, *104*, 4803.
- 8) Wrighton, M.S.; Abrahamson, H.B.; Morse, D.L. *J. Am. Chem. Soc.* **1976**, *98*, 4105-4109.
- 9) Winkler, J.R.; Gray, H.B. *Inorg. Chem.* **1985**, *24*, 346-355.
- 10) Che, C.M.; Butler, L.G.; Gray, H.B.; Crooks, R.M.; Woodruff, W.H. *J. Am. Chem. Soc.* **1983**, *105*, 5492-5494.
- 11) Winkler, J.R.; Gray, H.B. *Chem. Rev.* **1992**, *92*, 369-379.
- 12) Parson, W.W.; Ke, B. *Photosynthesis: Energy Conversion by plants and Bacteria, Vol. 1*. **1982**, Academic Press, New York, New York.
- 13) Marcus, R.A.; Sutin, N. *Biochim. Biophys. Acta* **1985**, *811*, 265-322.
- 14) Lowery, M.D.; Solomon, E.I. *Inorganica Chimica Acta*, **1992**, *198*, 233-243.
- 15) Shepard, W.E.B.; Anderson, B.F.; Lewandowski, D.A.; Norris, G.E.; Baker, E.N. *J. Am. Chem. Soc.* **1990**, *112*, 7817-7819.

Characterization and Photophysics
of
Gold(I) Phosphine Complexes

Background

Luminescence has been reported for a few dinuclear gold(I) complexes in solution.¹⁻⁴ Formulations of the electronic structures of the emissive states have emphasized the importance of Au-Au interactions by analogy to d^8-d^8 Pt₂⁵⁻⁶ and $d^{10}-d^{10}$ Pt₂⁷ species. A crystal structure of the luminescent [Au₂(dppm)₂] [BF₄]₂ (dppm = bis-(diphenylphosphino) methane) reports a Au-Au distance of 2.962 Å, significantly shorter than the sum of the van der Waals radii, 3.40 Å.¹ When the two d^{10} centers are brought together, the filled d_z^2 orbitals and the empty p_z orbitals interact in the same manner as discussed for PtPOP (Figure 1.3). The resulting $d\sigma^* \rightarrow p\sigma$ singlet transition is observed in the electronic absorption spectrum at 293 nm for [Au₂(dppm)₂] [BF₄]₂. The emission in solution ($\lambda_{\text{max}} = 593$ nm) has been assigned as the triplet $d\sigma^* \leftarrow p\sigma$ transition.³ The large Stokes shift of 17,300 cm^{-1} is similar to the shift (16,600 cm^{-1}) observed by Che et al. in the complex Au₂(dmb)(CN)₂ (dmb=1,8-di-isocyano-p-menthane).^{2a} The excitation spectrum reported by Che for the dmb compound is extremely intriguing because it differs markedly from the absorption spectrum. In general the excitation spectrum is expected to be nearly identical to the absorption spectrum. The excitation spectrum of Au₂(dmb)(CN)₂ shows only a single intense band at 350 nm which is lower in energy than any observable feature in the absorption spectrum, indicating that a small amount of a luminescent impurity may be responsible for the emission..

Introduction

Gold complexes have the potential to be strong photo-reductants. The Au(I) metal center has several advantageous features: it is a third row metal with efficient spin orbit coupling for accessing the triplet excited state, Au(I) has a d^{10} configuration so none of the dissociative $d \rightarrow d$ transitions are possible, and the oxidation of most Au(I) species produces a transient, unstable Au(II) moiety which will disproportionate or thermally transfer a second electron before back electron transfer can occur. Design of luminescent

complexes focused on three types of transitions: MLCT transitions, $d\sigma^* \rightarrow p\sigma$ transitions associated with the dimers, and $d \rightarrow p$ transitions in gold monomers.

The MLCT transition was chosen based on the long-lived luminescence of the MLCT state of $\text{Ru}(\text{bpy})_3^{2+}$. The complex $\text{Au}(\text{bis}(\text{-diphenylphosphino})\text{ethane})_2^+$ was synthesized to generate a low-lying MLCT state. The d $\text{Au-P } \sigma^*$ orbitals are pushed up in energy by the four highly-donating, bound phosphines and there exists a potentially accessible π^* orbital as the LUMO on the phosphine ligand. This type of MLCT transition should be more stabilizing than the MLCT of $\text{Ru}(\text{bpy})_3^{2+}$ since the electron is being removed from a metal centered $d \sigma^*$ orbital as opposed to a non-bonding metal centered d orbital.

The $d \text{ Au-Au } \sigma^* \rightarrow p \text{ Au-Au } \sigma$ transition was investigated, because previous literature reported the emission in solution from $\text{Au } d^{10}\text{-}d^{10}$ dimers as being analogous to the $d^8\text{-}d^8$ systems such as PtPOP. Dimers with ethyl butyl bridged chelating phosphines were synthesized for comparison to the literature methyl bridged chelating phosphines. Presumably the longer bridge would lead to a longer Au-Au distance, causing both the absorption and emission bands to move to higher energy.

Although there were no reports in literature of long-lived emission in solution from a $d \leftarrow p$ transition, the bonding character of the HOMO and LUMO justified investigation of the transition. The $d \rightarrow p$ transition involves removing an electron from the highest energy $d \text{ Au-L } \sigma^*$ orbital and placing it into a non-bonding p orbital; such transitions should lead to a contraction of the Au-L bonds as opposed to the dissociation associated with $d \rightarrow d$ transitions. The absence of a pathway for photo-dissociation enhances the possibility that the $d \rightarrow p$ excited state could be long-lived. Two and three coordinate gold phosphine complexes were prepared to generate low energy $d \text{ Au-P } \sigma^* \rightarrow p$ transitions. Four coordinate complexes were considered undesirable for $d \text{ Au-P } \sigma^* \rightarrow p$ transitions, because the p LUMO would be a $\text{M-L } \sigma^*$ type orbital as opposed to a non-bonding orbital.

Possible LMCT states were not investigated, because they would generate a Au(0) species which could plate out as metallic gold. Intraligand transitions were considered disadvantageous for photo reduction, because electron transfer produces a radical on the ligand which could lead to unwanted side reactions; the three transitions investigated all produce Au(II) centers upon oxidation and leave the ligands unperturbed.

Experimental Section

Materials Bis-(dicyclohexylphosphino)ethane, Bis-(dichlorophosphino)-ethane, Au shot, and hydrogen tetrachloroaurate (II) hydrate were purchased from Strem chemicals. All other solvents and materials were reagent grade and purchased from Aldrich Chemical Company unless otherwise noted. Distilled solvents were dried over CaH₂, except for tetrahydrofuran which was dried over sodium. Lifetime measurements, emission spectra and excitation spectra were all performed with degassed solutions. Solutions were degassed by cycling the solution through a freeze (10 minutes), pump (vacuum of 1×10^{-5} torr for 5 minutes), thaw (with a room temperature water bath) procedure at least four times.

X-ray Data Collection and Reduction for [Au₂(bis-(diphenylphosphino)ethane)₂] [(PF₆)₂] Crystals for X-ray diffraction were grown by recrystallization from CH₃CN/Et₂O. Crystal: square prism with cross-section 0.26 x 0.26 mm, 0.3 mm long with skewed ends; CAD-4 diffractometer; cell dimensions from 25 reflections with $39^\circ < 2\theta < 43^\circ$; no absorption correction ($I_{r_{max}}=1.2$, 2 data sets merged satisfactorily); $(\sin\theta/k)_{max}=0.66$; data collected to $2\theta = 56^\circ$, h from 0 to 21, k from 0 to 21, l from -16 to 6; three standard reflections, 230, 140, 22 $\bar{2}$, showed no variations greater than expected from counting statistics; 8221 reflections measured, 3805 independent; goodness of fit for merging 1.08; $(GOF) = [\sum_n w(F^2_{o(hkl)} - F^2_{avg(hkl)})^2 / (n-1)]^{1/2}$ for n observations of reflection hkl; $GOF_{merge} = [\sum_m w(GOF_{hkl})^2 / m]^{1/2}$, for m reflections with more than one contributor); $R_{merge}(\text{point group, } \bar{4}m2)$ for 3386 reflections with exactly 2 observations = 0.042; all

reflections used in solution and refinement of the structure; gold atom coordinates found from Patterson map, remainder of structure by successive structure factor-Fourier calculations; full matrix least squares refinement using F^2 values; hydrogen atoms placed by calculation 0.95 Å from their carbon atoms, with isotropic B's of 10.0 Å², hydrogen coordinates not refined but adjusted once near conclusion of refinement; 165 parameters refined, including scale factor, all refineable coordinates of non-hydrogen atoms and their anisotropic U_{ij} 's; final R 0.064 for 3525 reflections with $F_o^2 > 0$, 0.038 for 2440 reflections with $F_o^2 > 3\sigma(F_o^2)$, final goodness of fit 1.46. The absolute configuration for the structure was confirmed by refining both alternatives; the incorrect one gives R = 0.087 compared to R = 0.064 for the correct one. Variances ($\sigma^2(F_o^2)$), derived from counting statistics plus an additional term, $(0.014I)^2$, variances of the merged data by propagation of error plus another additional term, $(0.014I)^2$; ratio of maximum shift to error in final least squares cycle, 0.07 for cation, 0.36 for fluorine atoms of PF₆⁻ anion; one peak 2.7eÅ⁻³ between the two gold atoms, another 1.8 eÅ⁻³ 0.3Å from the gold atom, all other peaks less than 1.5 eÅ³, most negative peaks in the vicinity of PF₆⁻ ion; atomic scattering factors and dispersion corrections taken from Cromer and Waber; programs used were those of the CRYRM crystallographic computing system and ORTEP. Table 2.1 gives a list of selected bond distances and bond angles.

X-ray Data Collection and Reduction for [Au₂(bis-(dicyclohexylphosphino)ethane)₃] [(Au(CN)₂)₂] The crystal was prepared by the slow evaporation of methanol. Crystal: prism with cross section 0.08 x 0.16 x 0.22 mm, CAD-4 diffractometer; cell dimensions from 25 reflections with 30° < 2θ < 330; $(\sin\theta/\lambda)_{\max} = 0.59$; data collected to 2θ = 50°, h from -14 to 14, k from -15 to 15, l from -18 to 18; three standard reflections, 03 $\bar{3}$, 40 $\bar{1}$ and 013, showed no variations greater than expected from counting statistics; 15196 reflections measured, 7486 independent; goodness of fit for merging 1.02 ($GOF = [\sum_n w(F_o^2(hkl) - F_{avg}^2(hkl))^2 / (n-1)]^{1/2}$ for n

Table 2.1 Selected bond distances and bond angles for $[\text{Au}_2(\text{dcpe})_2] (\text{PF}_6)_2$.

Distance (Å)		Angle (°)	
Au - Au	2.935(1)	P1 - Au - P1	160.6(1)
Au - P1	2.314(2)	Au - P1 - C1	120.7(2)
P1 - C1	1.848(7)	Au - P1 - C10	109.1(3)
P1 - C10	1.819(10)	Au - P1 - C20	107.4(2)
P1 - C20	1.825(8)	C10 - P1 - C1	103.8(4)
C1 - C1	1.463(9)	C20 - P1 - C1	108.2(3)
		C20 - P1 - C10	107.0(4)
		C1 - C1 - P1	117.8(5)
		C11 - C10 - P1	109.4(6)
		C15 - C10 - P1	111.2(6)
		C21 - C20 - P1	112.8(6)
		C25 - C20 - P1	115.9(6)

Table 2.2 Selected bond distances and bond angles for $[\text{Au}_2(\text{dcpe})_3][\text{Au}(\text{CN})_2]_2$.

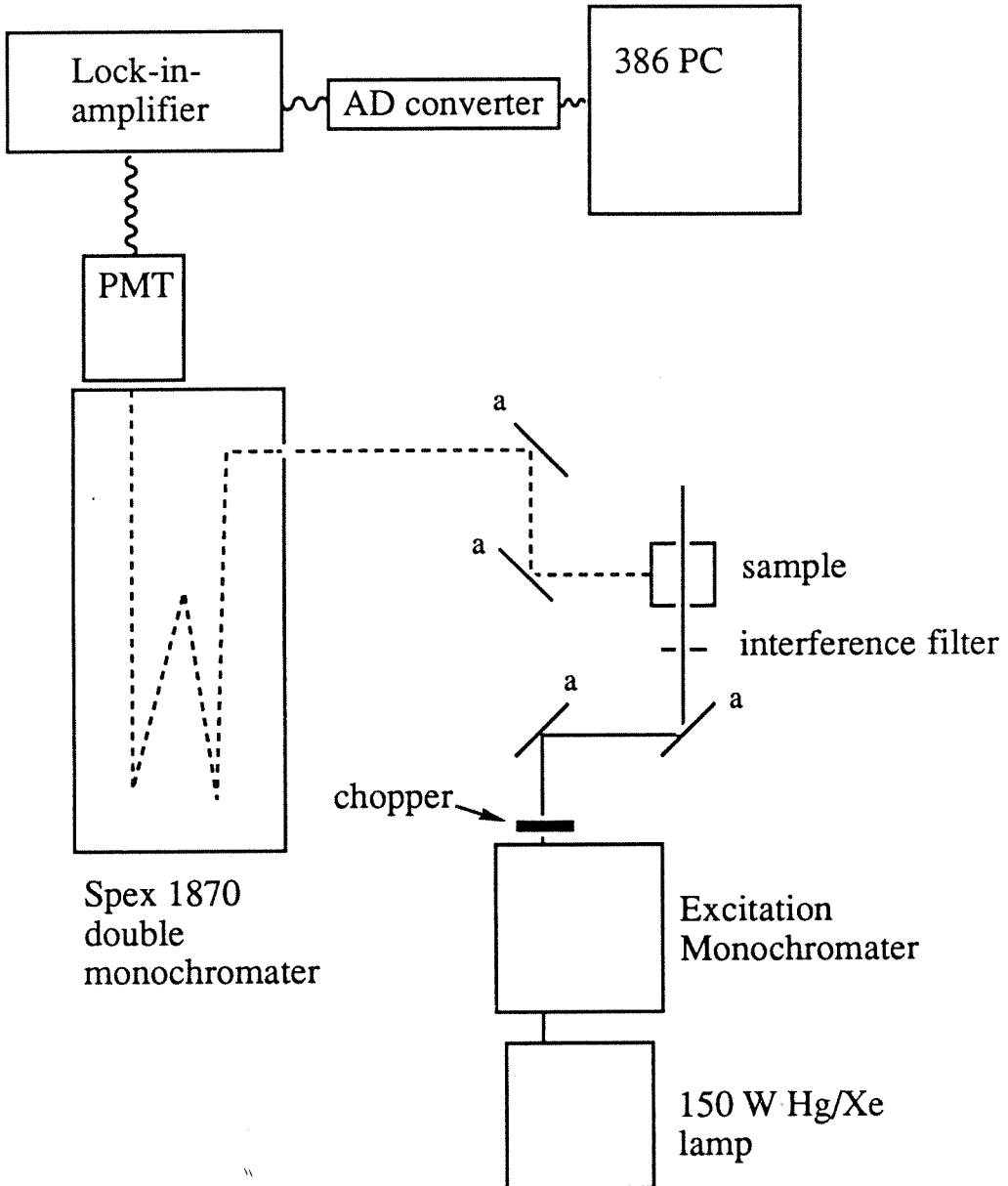
	Distance (Å)		Angle (°)
Au1 - P1	2.440(2)	P1 - Au1 - P2	87.4(1)
Au1 - P2	2.422(2)	P1 - Au1 - P3	136.9(1)
Au1 - P3	2.318(1)	P2 - Au1 - P3	135.3(1)
P1 - C1	1.849(6)	Au1 - P1 - C1	103.9(2)
P1 - C10	1.851(6)	Au1 - P1 - C16	118.0(2)
P1 - C16	1.846(6)	Au1 - P1 - C10	119.2(2)
P2 - C2	1.839(6)	C1 - P1 - C10	103.3(3)
P2 - C22	1.847(6)	C1 - P1 - C16	103.5(3)
P2 - C28	1.833(6)	C10 - P1 - C16	106.6(3)
P3 - C3	1.846(6)	Au1 - P2 - C2	103.9(2)
P3 - C34	1.846(6)	Au1 - P2 - C22	117.8(2)
P3 - C40	1.844(6)	Au1 - P2 - C28	119.4(2)
C1 - C2	1.531(8)	C2 - P2 - C22	103.6(3)
C3 - C3'	1.502(8)	C2 - P2 - C28	104.9(3)
		C22 - P2 - C28	105.4(3)
		Au1 - P3 - C3	116.4(2)
		Au1 - P3 - C34	113.6(2)
		Au1 - P3 - C40	112.3(2)
		C3 - P3 - C34	105.2(3)
		C3 - P3 - C40	103.5(3)
		C34 - P3 - C40	104.7(3)
		P1 - C1 - C2	114.8(4)
		P2 - C2 - C1	116.0(4)
		P3 - C3 - C3'	114.3(4)

observations of reflection hkl ; $GOF_{merge} = [\sum w(GOF_{hkl})^2/m]^{1/2}$, or m reflections with more than one contributor); $R_{merge}(\text{point group } \bar{1})$ for 6605 reflections with exactly 2 observations = 0.027; the final R for $F^2_o > 3\sigma$ was 0.0301; the final wR was 0.0030. Table 2.2 gives a list of selected bond angles and bond distances.

Spectroscopic Measurements All electronic absorption spectra were measured with a Cary-14 spectrophotometer. The ^{31}P NMR spectra were obtained with a JOEL 400 MHz NMR equipped with a broad band probe, except for the ^{31}P NMR spectrum of $\text{Au}_2(\text{dcp})_3^{2+}$ which was also measured on a Bruker AMX 500 MHz NMR and a JOEL 90 MHz NMR. All ^{31}P NMR shifts were measured in CD_3CN and are reported relative to phosphoric acid. A Beckman 4240 infrared spectrometer was used for IR measurements. Electrochemistry was performed with a model 173 potentiostat and a model 175 universal programmer from EG and G Princeton Applied Research. The experimental equipment for the emission spectra included: a 200W Xe/Hg lamp from Oriol as the source; a Spex 1681 monochromator for the excitation monochromator; an Oriol narrow bandpass interference filter; a Spex 1870 monochromator as the emission monochromator; a Hamamatsu R955 PMT as the detector; a model 186A lock in amplifier from EG and G Princeton Applied Research which was used to ratio the sample signal to a blank signal; an 386 PC to analyze the data (Figure 2.1).⁹ Excitation spectra were recorded with a SLM 8000 Fluorimeter.

Lifetime Measurements and Analyses Analyses for C, H and N were done at the Caltech Analysis Facility; analyses of all other elements were done at Galbraith Laboratories. The experimental apparatus for the lifetime measurements is described in chapter 3. The excitation source for the lifetime measurements was the third harmonic (355 nm) of a Quanta-Ray Nd-YAG laser with a 20 ns pulse width. The TBA salt of PtPOP was used as a standard for quantum yield measurements. Solutions of PtPOP and the gold complex to be measured were prepared with an absorbance of 0.1 at 366 nm to

Figure 2.1. Instrument configuration for emission spectra; "a" indicates an off axis parabolic broad band mirror with a focal length of 15 cm; the chopper enables the lock-in amplifier to reference the signal to a blank; the operating computer program was written Jim Bailey.



avoid self quenching of the emission. Emission spectra were taken using the equipment described above. The integrated areas under the emission bands were used to calculate the quantum yield, ϕ . The quantum yield of PtPOP in acetonitrile has been previously

$$\phi = \frac{\text{integrated area for sample}}{\text{integrated area for PtPOP}} * 0.8$$

reported as 0.8.¹⁰

Bis-(diisopropylphosphino)ethane (1)¹¹ A solution of 2 M isopropyl magnesium chloride (29 mL) was added dropwise under an argon atmosphere to a schlenk flask containing 55 mL of freshly distilled tetrahydrofuran (THF) and 2.0 g of 1,2-bis-(dichlorophosphino) ethane. The mixture was refluxed for ninety minutes and then allowed to cool to room temperature. Excess Grignard reagent was quenched by the slow, dropwise addition of saturated aqueous ammonium chloride. The resulting solution containing copious amounts of solid lithium chloride was extracted with 3 times with 60 mL portions of ether. The ether layers were combined and the ether was removed by rotary evaporation under reduced pressure. The product was then purified by vacuum distillation to yield a clear oil (2 mL) which was stored in an inert atmosphere. ³¹P NMR: 9.0 ppm (s).

1,3-Bis-(dicyclohexylphosphino)propane (2)¹² A solution of 2.5 M N-butyl lithium (20 mL) was added to a schlenk flask charged with 60 mL of Ar purged ether at -78°C. Following the slow addition (1 drop per second) of a solution of dicyclohexylphosphine (10 g) in 30 mL of ether, the mixture was allowed to stir for two hours. A solution of 1,3- dichloropropane (2.4 mL) in 30 mL of ether was added dropwise and the solution was warmed to room temperature. Removal of the solvent by rotary evaporation followed by vacuum distillation yielded a clear oil, which was stored in an inert atmosphere. ³¹P NMR: -5.3 ppm (s).

Au(SCH)(Cl) (3) Gold shot (1.48 g) was dissolved in 150 mL of aqua regia. Once dissolved (heating the mixture slightly sped up the dissolution process for large ingots of gold) the solution was concentrated to 5 mL by boiling. To remove any nitrates

the mixture was washed twice with 50 mL portions of concentrated HCl and reduced in volume to 5 mL by boiling after each addition of HCl. The resulting bright orange solution of auric acid (HAuCl_4) was then dissolved in 400 mL of ethanol and an excess (4 mL) of tetrahydrathiophene was added to solution. The solution turned bright orange for a few seconds and then clear as the white, product precipitated out of solution. The product was collected by vacuum filtration (2.18 g Yield: 91%). The isolated product can be stored for months in a freezer.

[Au(PPh₃)₂] [PF₆] (4) Compound **3** was suspended in 50 mL of freshly distilled dichloromethane. Two equivalents of triphenylphosphine were added and the mixture was stirred for 45 minutes. The solvent was removed by rotary evaporation under reduced pressure, yielding the solid Cl salt. The solid was then dissolved in 30 mL of water and a minimum of methanol. Addition of a solution of ammonium hexafluorophosphate in methanol lead to the precipitation of the product as a white solid. The solid was collected by vacuum filtration and dried overnight in a vacuum oven. Analysis Calculated for $\text{AuClP}_2\text{C}_3\text{H}_3\text{O}$: C, 57.12 ; H, 3.99. Found: C, 56.63; H, 4.09. ³¹P NMR: 42.64 ppm (s). Analysis calculated for $\text{AuP}_3\text{F}_6\text{C}_3\text{H}_3\text{O}$: C, 49.90; H, 3.49. Found: C, 50.13; H, 3.62.

[Au(P(C₆H₁₁)₃)₂] [PF₆] (5) This compound was made by a procedure analogous to that described for $[\text{Au}(\text{PPh}_3)_2] [\text{PF}_6]$. ³¹P NMR: 63.8 ppm (s).

[Au(1,2-bis-(diphenylphosphino)ethane)₂] [PF₆] A round-bottom flask was filled with 50 mL of freshly distilled dichloromethane, 200 mg (0.624 mmol) of **3** and 525 mg (1.320 mmol) of dppe. The solution was stirred for two hours. The solvent was then reduced in volume to 25 mL by rotary evaporation under reduced pressure. Addition of 50 mL of ether precipitated the product as a white powder which was collected by vacuum filtration (500 mg; Yield 71%). The powder was dissolved in 25 mL of methanol and water was added until the solution became slightly cloudy. Addition of a solution of ammonium hexafluorophosphate in methanol lead to the precipitation of the

PF₆ salt in product as a white solid. The solid was collected by vacuum filtration and dried overnight in a vacuum oven. ³¹P NMR: 44.76 ppm (s). Analysis calculated for AuP₅F₆C₅₂H₄₈: C, 54.85; H, 4.25. Found: C, 54.80; H, 4.33.

[Au(bis-(dicyclohexylphosphino)ethane)₂] [PF₆] A mixture of compound **3** (100 mg ; 0.31 mmol) and an excess of dcpe (920 mg; 2.1 mmol) in 50 mL of freshly distilled dichloromethane was stirred under argon at room temperature for one hour. The solvent was removed by rotary evaporation under reduced pressure to give a white powder. The powder was dissolved in a minimum of a 60:40 solution of methanol: water, and an excess of ammonium hexafluorophosphate in 1 mL of methanol was added to precipitate the PF₆ salt. The product was collected by vacuum filtration. ³¹P NMR: 30.01 ppm (s). Analysis calculated for AuP₅F₆C₅₂H₉₆: P, 13.05; F, 9.60; C, 52.61; H, 8.15. Found: P, 13.27; F, 9.33; C, 52.98; H, 8.20.

[Au₂(bis-(dicyclohexylphosphino)ethane)₂] [(PF₆)₂] A mixture of compound **3** (150 mg ; 0.47 mmol) and one equivalent of dcpe (210 mg; 0.50 mmol) in 50 mL of freshly distilled dichloromethane was stirred under argon at room temperature for one hour. The solvent was removed by rotary evaporation under reduced pressure to give a white powder. The powder was dissolved in a minimum of a 60:40 solution of methanol: water, and an excess of ammonium hexafluorophosphate in 1 mL of methanol was added to precipitate the PF₆ salt. The product was collected by vacuum filtration. ³¹P NMR: 51.39 ppm (s). Analysis calculated for Au₂P₆F₁₂C₅₂H₉₆: P, 12.15; F, 14.90; C, 40.85; H, 6.33. Found: P, 11.76; F, 14.61; C, 40.54; H, 6.27.

[Au₂(bis-(dicyclohexylphosphino)ethane)₃] [(PF₆)₂] A mixture of compound **3** (1.2 g; 3.75 mmol) and one and one half to two equivalents of dcpe (3.00 g; 7.1 mmol) in 50 mL of freshly distilled dichloromethane was stirred under argon at room temperature for one hour. The solvent was removed by rotary evaporation under reduced pressure to give a thick oil. Sonication in ether followed by rotary evaporation of the solvent yielded a white powder which may have a green tinge due to luminescence

(Yield: 95%). Metathesis to the PF_6 salt was accomplished quantitatively by dissolving the solid in a minimum amount of a 50:50 solution of methanol: water followed by addition of excess ammonium hexafluorophosphate in 1 mL of methanol. ^{31}P NMR: 64.4 ppm (d); 57.6 ppm (t) (Figure 2.2). Fine splitting in the doublet and triplet patterns due to the $\text{A}_2\text{BA}'_2\text{B}'$ is expected for the molecule. Spectra taken on a 400 MHz or 90 MHz NMR have increasingly complex patterns as the chemical shift difference between the two types of phosphines approaches the coupling value. Analysis calculated for $\text{Au}_2\text{P}_8\text{F}_{12}\text{C}_{78}\text{H}_{144}$: P, 12.70; F, 11.68; C, 48.00; H, 7.44. Found: P, 12.72; F, 11.42; C, 48.14; H, 7.13.

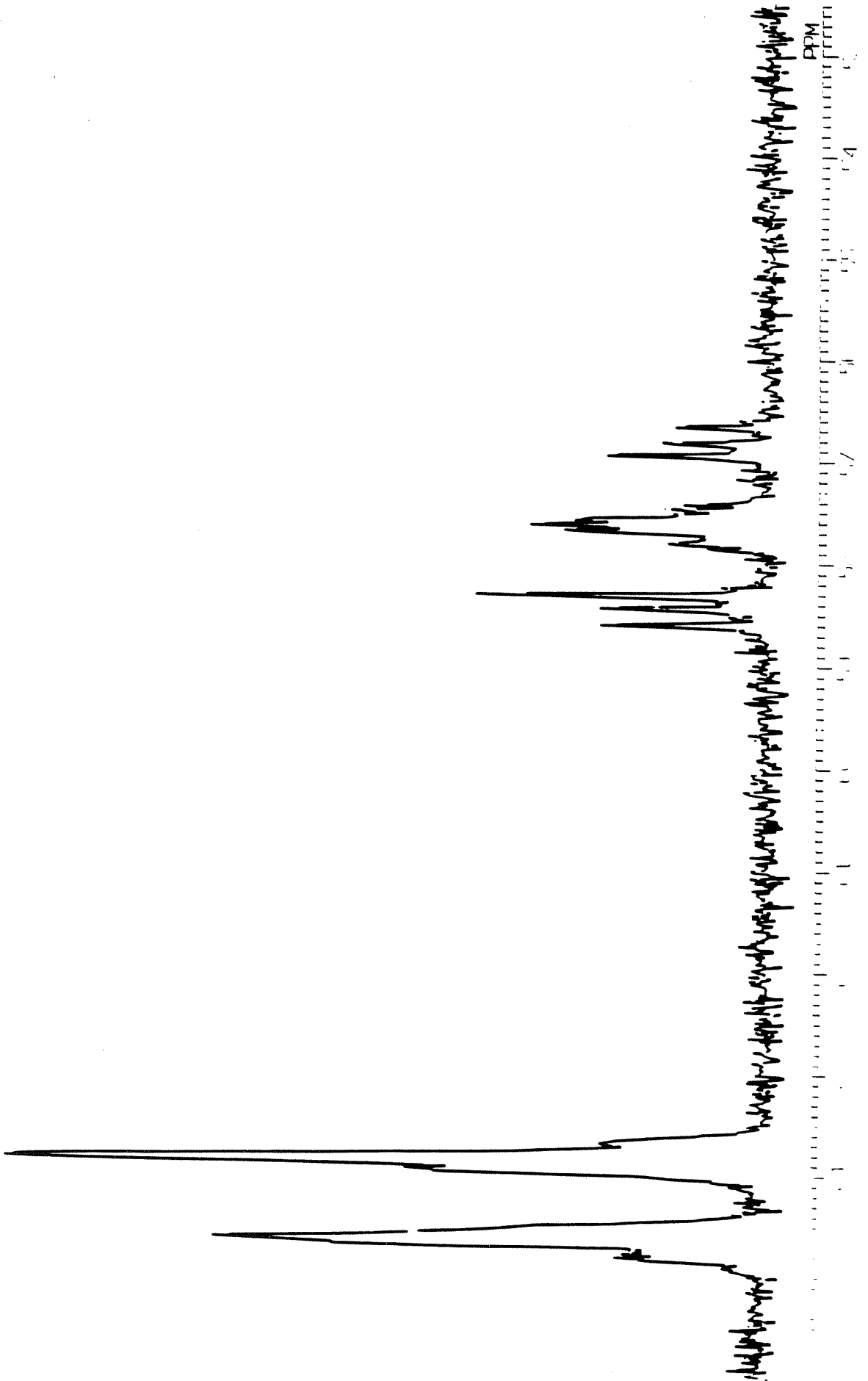
AuCN^{13} Gold powder (500 mg) was stirred in a solution of 400 mg KCN and 20 mL of distilled water overnight. The resulting clear solution was combined with 10 mL of concentrated HCl and brought to a boil. The product precipitated out as a yellow solid and was collected by vacuum filtration.

$[\text{Au}_2(\text{bis}(\text{dicyclohexylphosphino})\text{ethane})_3][(\text{Au}(\text{CN})_2)_2]$ A 100 mL round-bottom flask was filled with 50 mL of methanol, 223 mg AuCN and 423 mg of dcpe. The yellow solution was stirred until it turned clear, and the solvent was then removed by rotary evaporation under reduced pressure. The resulting white powder was dried overnight in a vacuum oven. IR: CN stretch 2125 cm^{-1} . ^{31}P NMR: 64.4 ppm (d); 57.6 ppm (t). Analysis calculated for $\text{Au}_4\text{P}_6\text{C}_{82}\text{H}_{144}\text{N}_4$: C, 45.60; H, 6.72; N, 2.60. Found: C, 45.20; H, 6.61; N, 2.58.

$[\text{Au}(\text{bis}(\text{diisopropylphosphino})\text{ethane})_2][\text{PF}_6]$ The 1,2-bis(diisopropylphosphino)ethane compounds were made according to procedures analogous to those previously described for the corresponding dcpe complexes. ^{31}P NMR: 41.63 ppm (s). Analysis calculated for $\text{AuP}_5\text{F}_6\text{C}_{28}\text{H}_{64}$: C, 38.81; H, 7.44. Found: C, 38.19; H, 7.37.

$[\text{Au}_2(\text{bis}(\text{diisopropylphosphino})\text{ethane})_2][(\text{PF}_6)_2]$ ^{31}P NMR: 60.94 ppm (s). Analysis calculated for $\text{Au}_2\text{P}_6\text{F}_{12}\text{C}_{28}\text{H}_{64}$: C, 27.83; H, 5.34. Found: C, 28.34; H, 5.37.

Figure 2.2 ^{31}P NMR spectrum of $[\text{Au}_2(\text{dcpe})_3](\text{PF}_6)_2$.



[Au₂(bis-(diisopropylphosphino)ethane)₃] [(PF₆)₂] ³¹P NMR: 74.05 ppm (d); 66.95 ppm (t). Analysis calculated for Au₂P₈F₁₂C₅₂H₉₆: C, 34.31; H, 6.58. Found: C, 34.51; H, 6.63.

[Au₂(bis-(diphenylphosphino)butane)₃] [(Cl)₂] A slight excess of 1,4-bis(diphenylphosphino)butane (300 mg) was added to a stirring solution of compound **3** (75 mg) in 50 mL of freshly distilled acetonitrile. The product precipitated out as a white powder and was collected by vacuum filtration. This compound has limited solubility in ethanol. ³¹P NMR: 30.47 ppm (s). The formulation of this compound as a triply bridged dimer is based on a combination of the analysis results and the singlet ³¹P NMR signal. The ³¹P NMR spectrum shows that all of the phosphines are equivalent, ruling out structures involving one chelating bidentate ligand and one bridging bidentate ligand.

Results and Discussion

Crystal Structures

The crystal structure for Au₂(dcpe)₂²⁺ features a binuclear complex bridged by two dcpe bidentate ligands (Figure 2.3). Each AuP₂ unit has a nearly linear geometry with a P-Au-P angle of 160.6°. The ethylene groups in the dcpe bridges are twisted to give a Au-Au separation of 2.936 Å. This distance is shorter than the van der Waals distance of 3.4 Å and is even shorter than that observed for the Au₂(dppm)₂²⁺, indicating a significant metal - metal interaction.

The structure for Au₂(dcpe)₃²⁺ shows each gold atom is bound to one chelating dcpe and one bridging dcpe (Figure 2.4). The slightly distorted trigonal planar geometry is quite unusual. Gold(I) complexes are almost exclusively linear or tetrahedral about the gold atom, with only a few examples of a trigonal planar environment.¹⁴⁻¹⁶ The distortion is due to the constrained, chelating dcpe unit, which binds with a P-Au-P angle of 87.4°. The other two P-Au-P angles which involve the bridging dcpe are 136.9°, and 135.3°. The bridging dcpe unit is extended to give a Au-Au distance of 7.050 Å; clearly no Au-Au interaction is present in this molecule.

Figure 2.3. Ortep drawing of $[\text{Au}_2(\text{dcpe})_2](\text{PF}_6)_2$; ellipses drawn at 50 % probability.

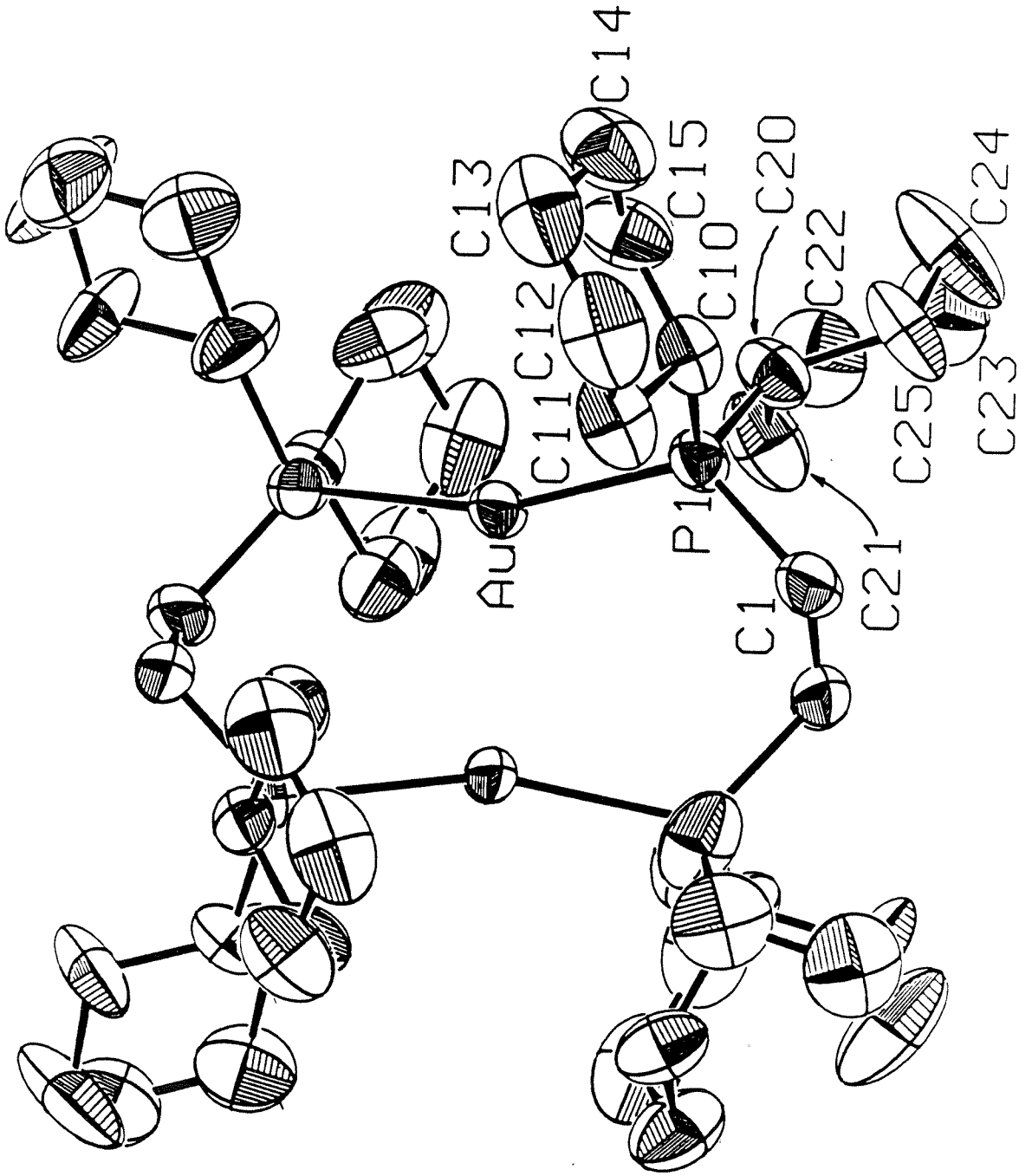
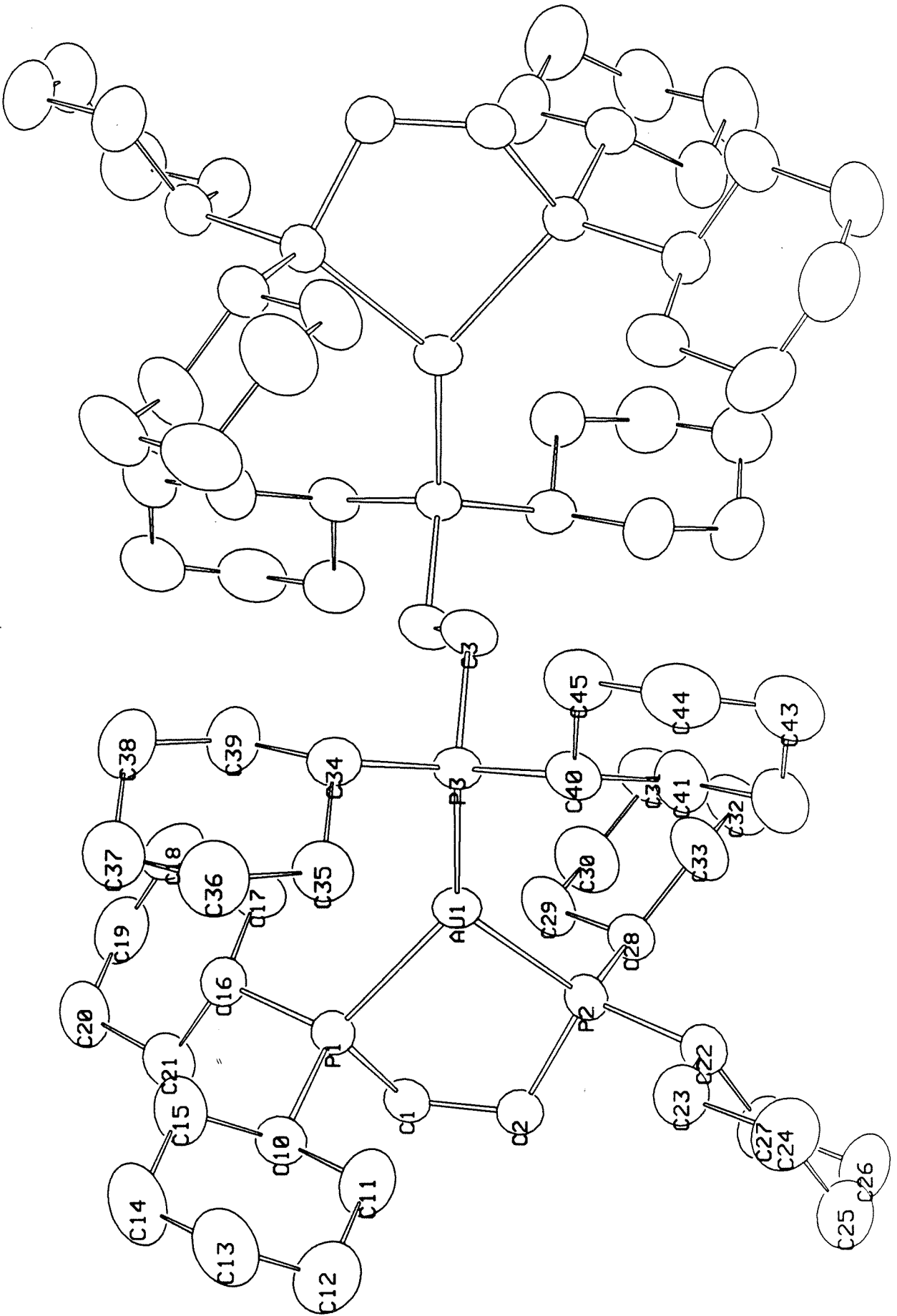


Figure 2.4. Ortep drawing of $[\text{Au}_2(\text{dcpe})_3][\text{Au}(\text{CN})_2]_2$; ellipses drawn at 50 % probability.



Electronic Absorption and Emission Spectra The complexes $\text{Au}(\text{PPh}_3)_2^+$, and $\text{Au}(\text{P}(\text{C}_6\text{H}_{11})_3)_2^+$ have similar electronic absorption spectra (Figures 2.5-2.6). The two lowest energy features appear at 275 nm ($\epsilon = 9,200 \text{ M}^{-1}\text{cm}^{-1}$) and 268 nm ($\epsilon = 11,800 \text{ M}^{-1}\text{cm}^{-1}$) for the triphenylphosphine complex and at 250 nm and 236 nm for the tricyclohexylphosphine complex. These two bands are attributed to $^1\Sigma_g \rightarrow ^1\Pi_u$ ($d_z^2 \rightarrow p_x, p_y$) and $^1\Sigma_g \rightarrow ^1\Pi_u$ ($d_{xz}, d_{yz} \rightarrow p_x, p_y$) transitions respectively. The d orbitals are pushed up in energy by the two phosphine ligands along the z axis, so the d_z^2 (σ^*) will be the HOMO and the d_{xz}, d_{yz} (π^*) will be slightly lower in energy. These assignments agree with analogous assignments made by Mason et al. for $\text{Au}(\text{PEt}_3)_2^+$ (PEt_3 is triethyl-phosphine).¹⁷

The electronic absorption spectra of the free ligand dppe and the four coordinate complex $\text{Au}(\text{dppe})_2^+$ are shown in Figure 2.7. The ligand spectrum has an absorption band at 252 nm ($\epsilon = 17,000 \text{ M}^{-1}\text{cm}^{-1}$) which can be assigned as a $\pi \rightarrow \pi^*$ transition. Upon coordination of two ligands to the Au center this transition moves to lower energy ($\lambda_{\text{max}} = 280 \text{ nm}$, $\epsilon = 34,700 \text{ M}^{-1}\text{cm}^{-1}$), and broadens substantially. At higher energy is the metal centered $d \rightarrow p$ transition, $^1A_1 \rightarrow ^1B_2$ ($d_{xz}, d_{yz} \rightarrow p_x, p_y$), which is both spin allowed and dipole allowed in the D_{2d} symmetry. The $d \rightarrow p$ transition is extremely high in energy since both p_x and p_y are σ anti-bonding for a four coordinate $\text{Au}(\text{I})$ complex. Mason and coworkers have observed a similar high energy metal centered transition with four monodentate phosphines bound to gold, and have assigned the transition as the analogous T_d transition $^1A_1 \rightarrow ^1T_2$ ($d_{xy}, d_{xz}, d_{yz} \rightarrow p_x, p_y, p_z$).¹⁸ In the D_{2d} symmetry the added electron density from the bridge between the chelating phosphines raises the energy of the p_z, d_{xz} , and d_{yz} orbitals. The solid emits at ($\lambda_{\text{max}} = 570 \text{ nm}$) room temperature (Figure 2.8); no emission is observed in solution at room temperature. Based on the assignment of the electronic absorption spectrum the emission has been ascribed to a ligand centered $\pi \leftarrow \pi^*$ emission. The large Stokes shift ($18,200 \text{ cm}^{-1}$) between the

Figure 2.5. Absorption spectrum of $\text{Au}(\text{PPh}_3)_2(\text{PF}_6)$, 21 μM .

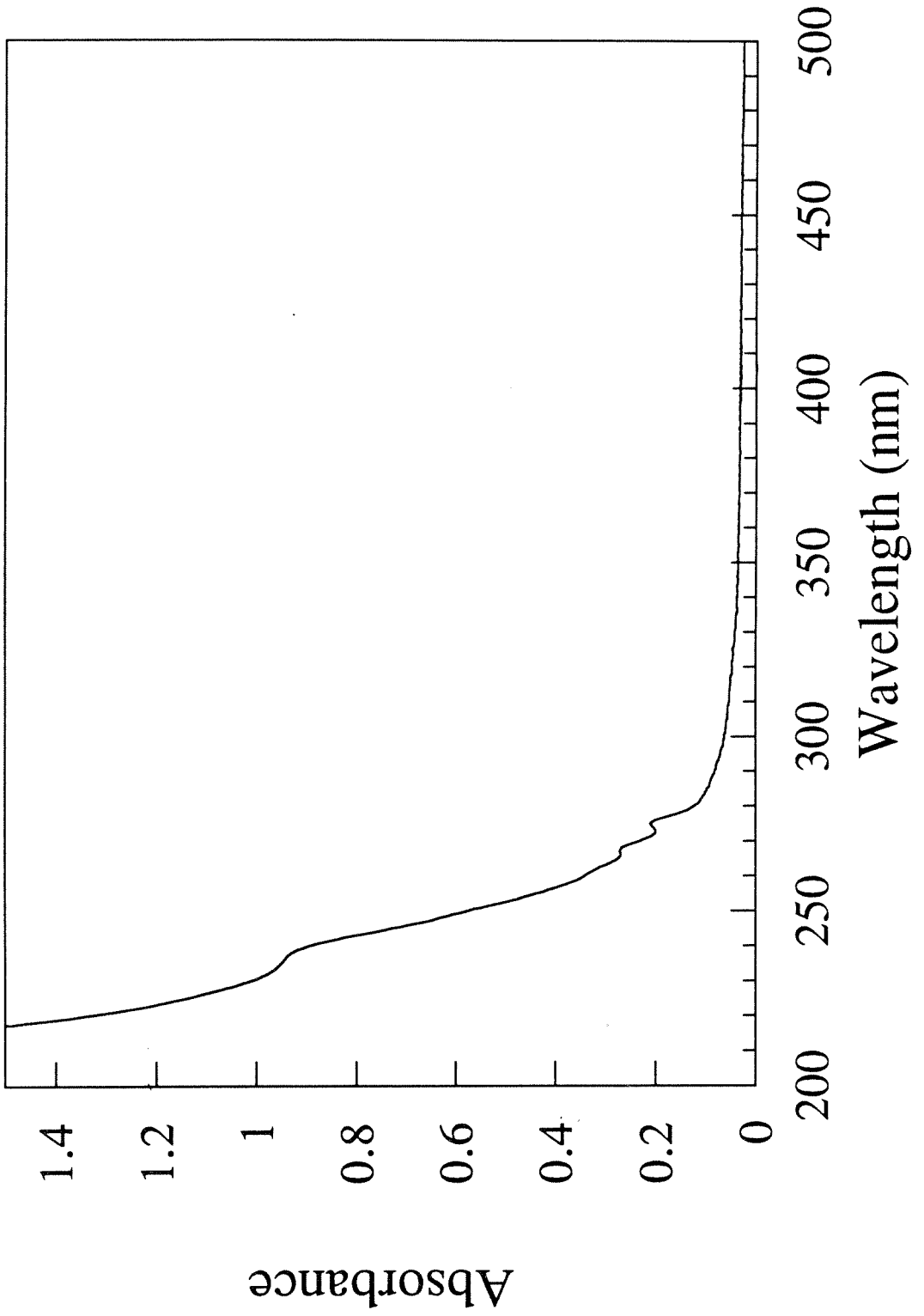


Figure 2.6. Absorption spectrum of $\text{Au}(\text{PCy}_3)_2(\text{PF}_6)$, 100 μM .

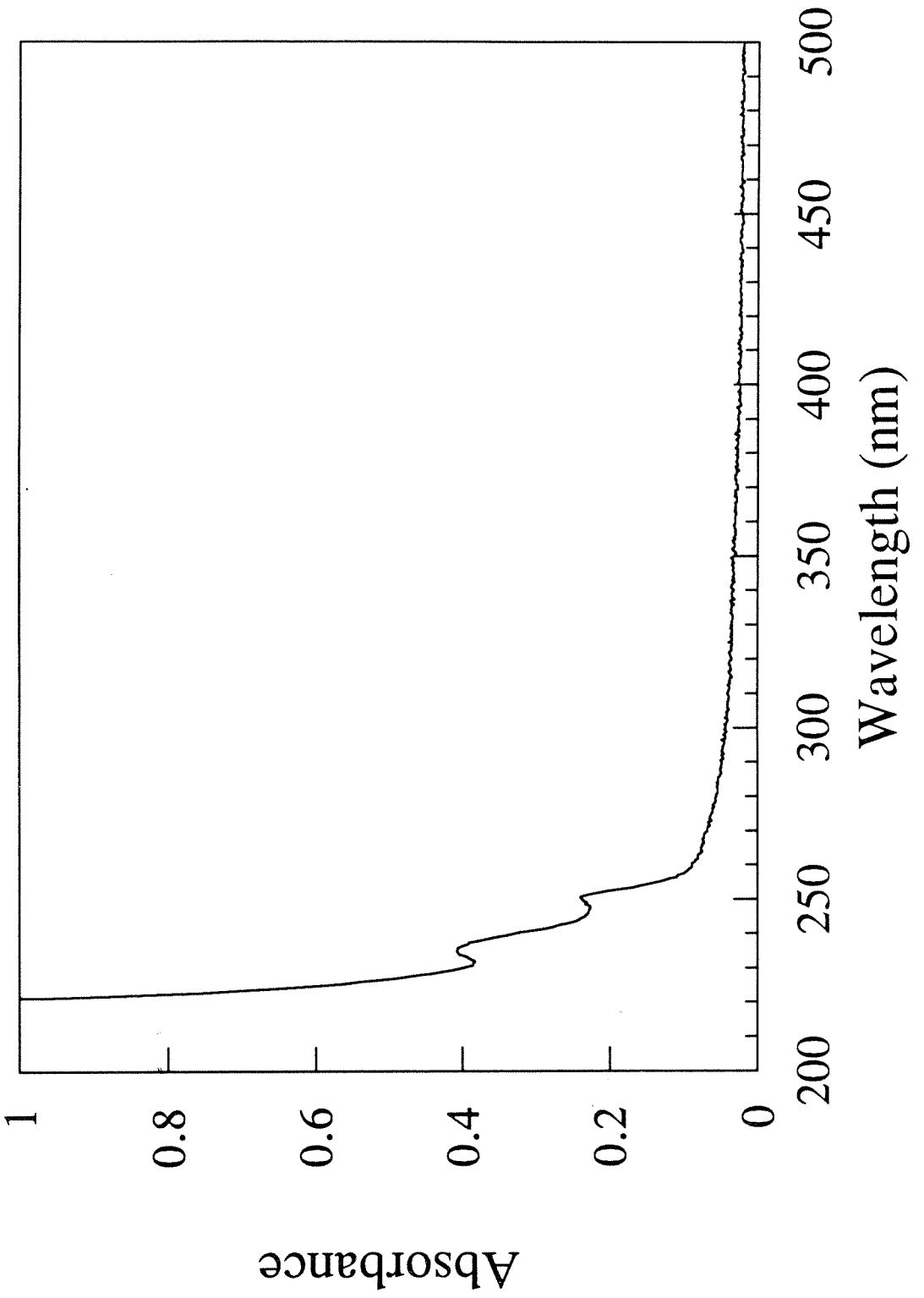


Figure 2.7. Absorption spectra of dppe(---), and Au(dppe)₂ (PF₆), 20 μM.

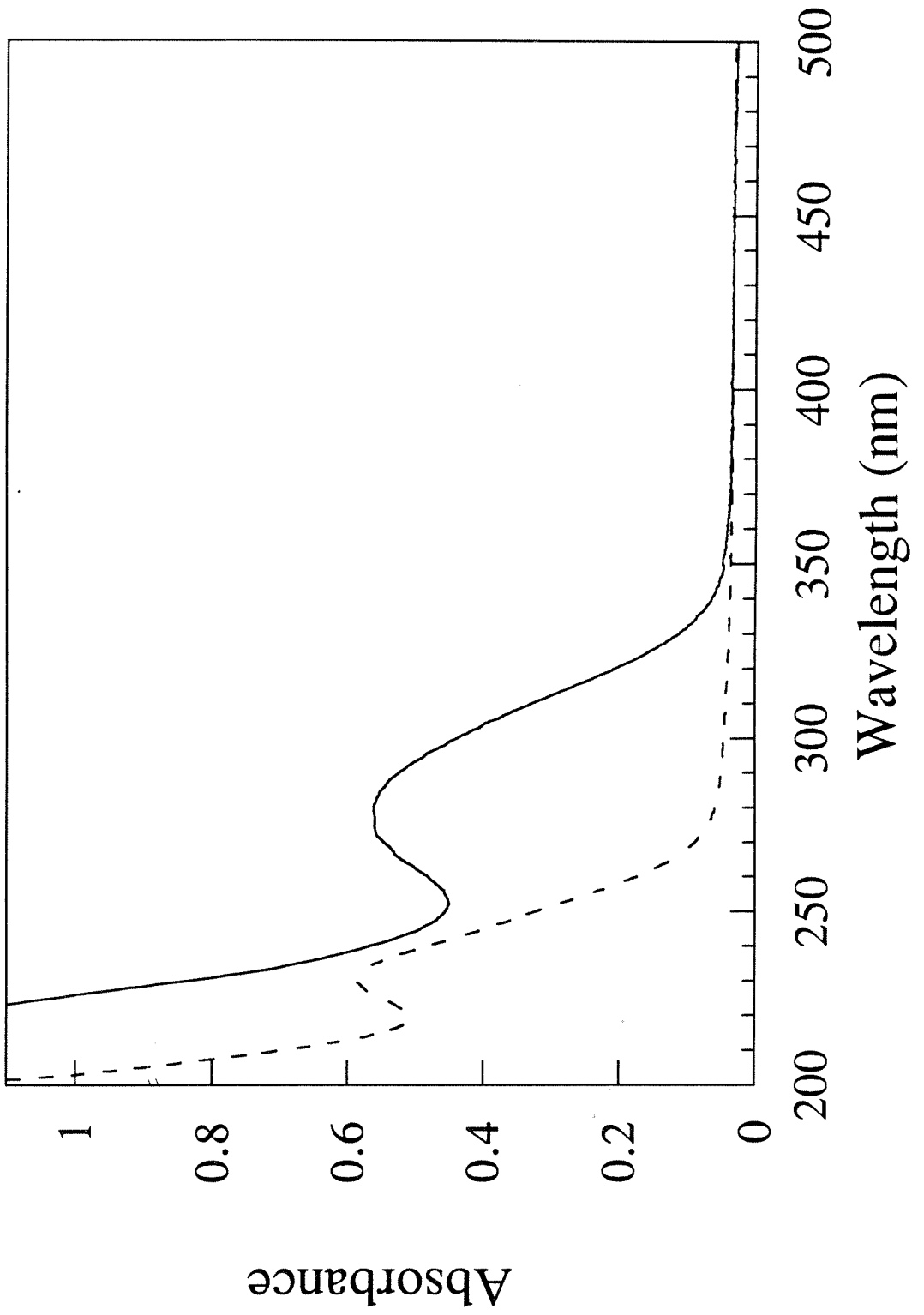
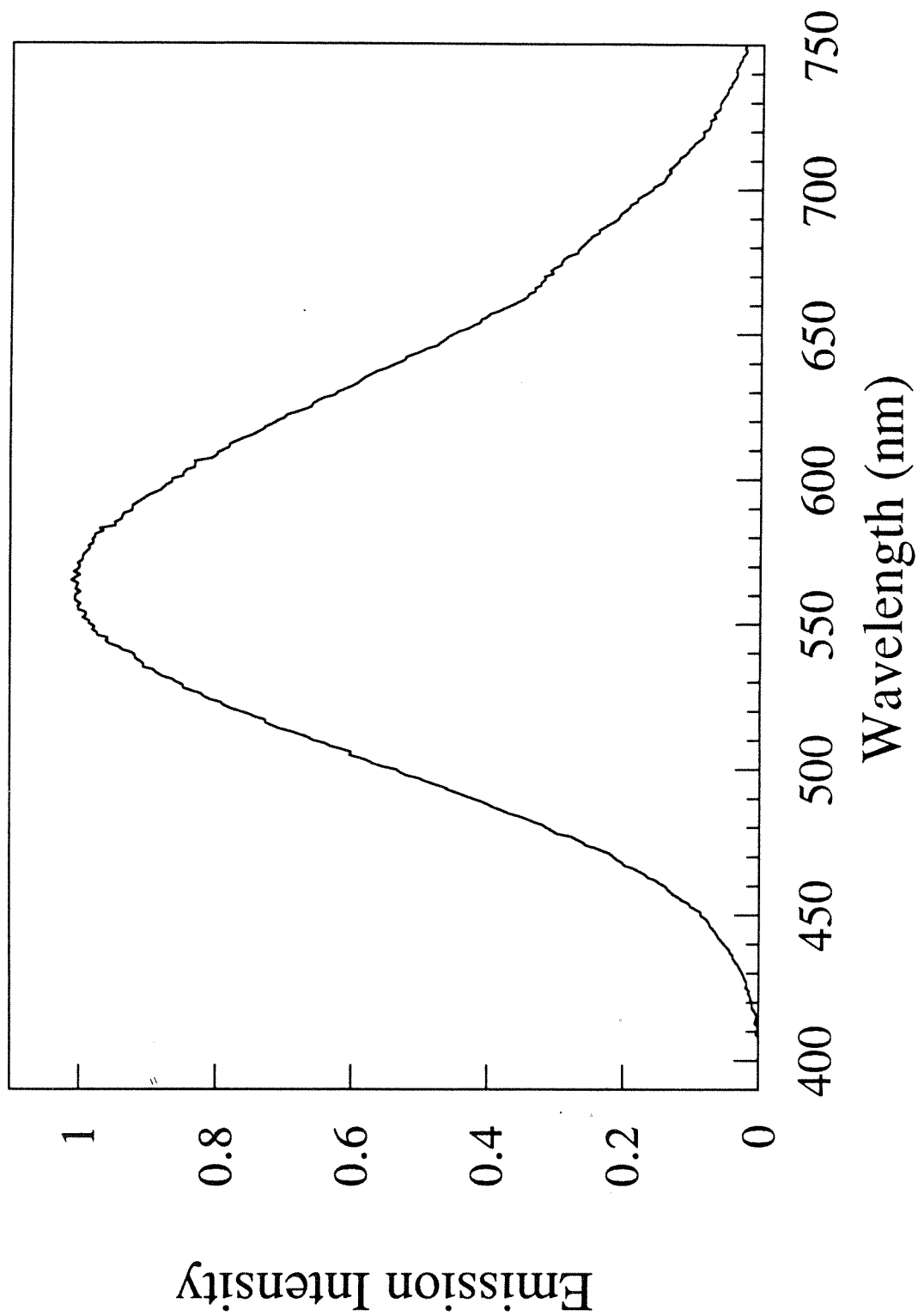


Figure 2.8. Solid-state emission spectrum of $\text{Au}(\text{dppe})_2(\text{PF}_6)$.



absorption band and the emission band identifies the emission as triplet to singlet phosphorescence. The dramatic increase in the intensity of phosphorescence compared to the free ligand is attributed to the heavy atom effect discussed in chapter one.

The electronic absorption spectra for the three dcpe complexes are shown in figures 2.9-2.11. The monomeric $\text{Au}(\text{dcpe})_2^+$ species absorbs only in the UV with the lowest energy absorption band occurring at 234 nm (with a shoulder at 266 nm). This absorption band has been attributed to a metal centered $d \rightarrow p$ transition similar to the 280 nm band in $\text{Au}(\text{dppe})_2^+$. The $^1A_1 \rightarrow ^1B_2$ ($d_{xz}, d_{yz} \rightarrow p_x, p_y$) transition is both dipole allowed and spin allowed ($\epsilon = 35,000 \text{ M}^{-1}\text{cm}^{-1}$). The complex does not emit in solution or as a solid at room temperature.

The dimeric complex $\text{Au}_2(\text{dcpe})_2^{2+}$ has an intense band ($\epsilon = 10,000 \text{ M}^{-1}\text{cm}^{-1}$) at 270 nm and a weaker shoulder at 320 nm. The Au-Au distance of 2.936 Å indicates a significant interaction as mentioned previously. This interaction occurs primarily between the orbitals along the z axis of the D_{2h} complex. The filled d_z^2 orbitals mix to produce a filled $d\sigma$, and a filled $d\sigma^*$ as the HOMO; the empty p_z orbitals also mix to generate an empty $p\sigma$ as the LUMO and a higher lying $p\sigma^*$. The low energy band at 270 nm is assigned as the $^1A_g \rightarrow ^1B_{1u}$ ($d\sigma^* \rightarrow p\sigma$), and the shoulder at 320 nm is ascribed to the corresponding $^1A_g \rightarrow ^3B_{1u}$ ($d\sigma^* \rightarrow p\sigma$). Both transitions are dipole allowed and z polarized. The dimer emits as a solid at 77K (Figure 2.12), but does not emit at room temperature (either as a solid or in solution) upon excitation at 366 nm. The emission spectrum shows two emission bands: a low-energy band at 628 nm and a more intense band at 493 nm. Changing the excitation source to 313 nm leads to emission of the solid at room temperature with a single emission band at 625 nm (Figure 2.13), and emission in an ethanol:methanol glass (4:1) at 77 K, $\lambda_{\text{max}} = 604 \text{ nm}$ (Figure 2.14; no emission is observed at room temperature in solution). The low energy emission of the solid is assigned as the $^1A_g \leftarrow ^3B_{1u}$ ($d\sigma^* \leftarrow p\sigma$) transition. The $E_{\nu_0-\nu_0}$ for the emissive transition in the glass is 418 nm with a Stokes shift of $14,700 \text{ cm}^{-1}$.

Figure 2.9. Absorption spectrum of $\text{Au}(\text{dcpe})_2(\text{PF}_6)$, 43 μM .

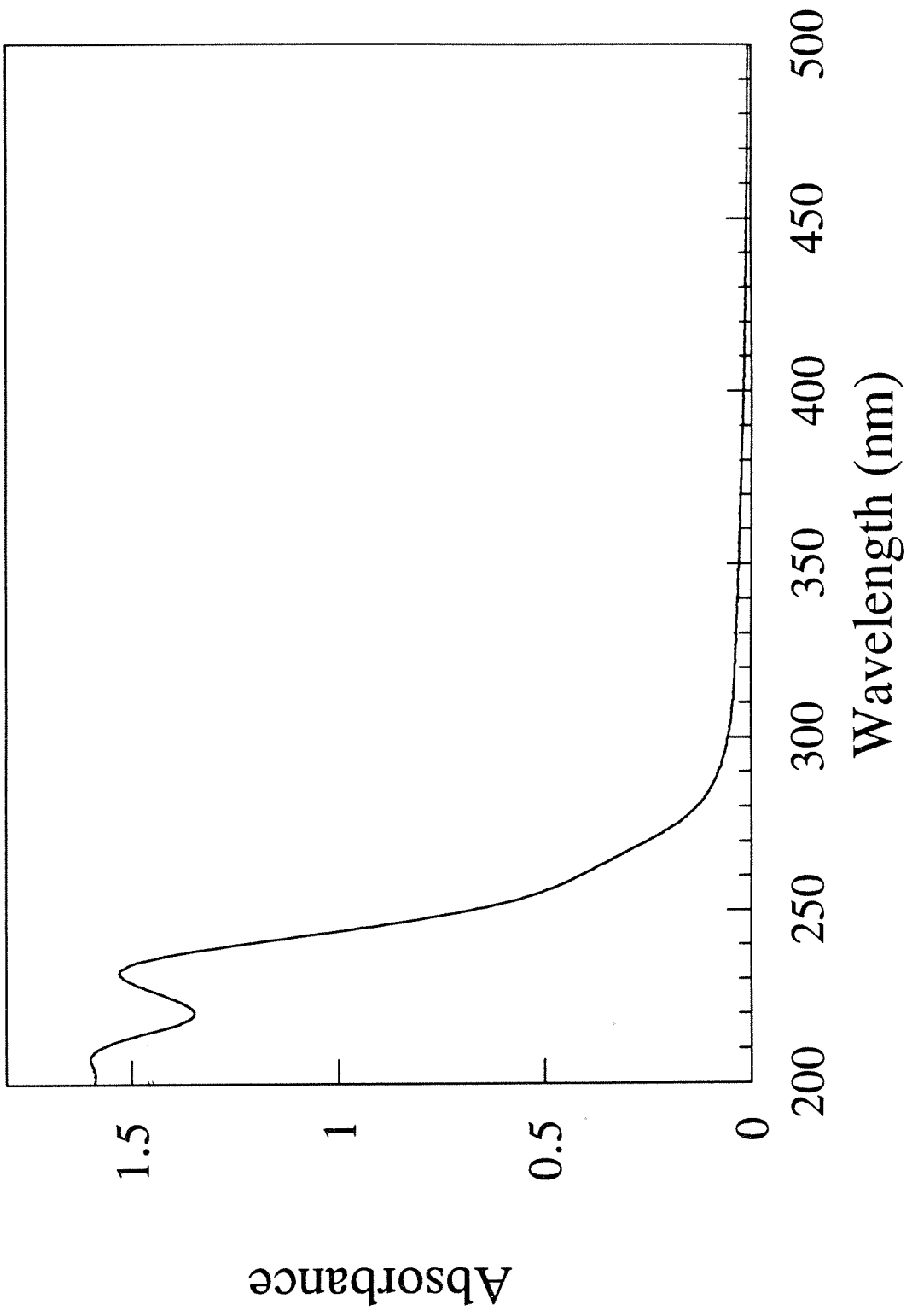


Figure 2.10. Absorption spectrum of $\text{Au}_2(\text{dcpe})_2(\text{PF}_6)_2$, 73 and 730 μM .

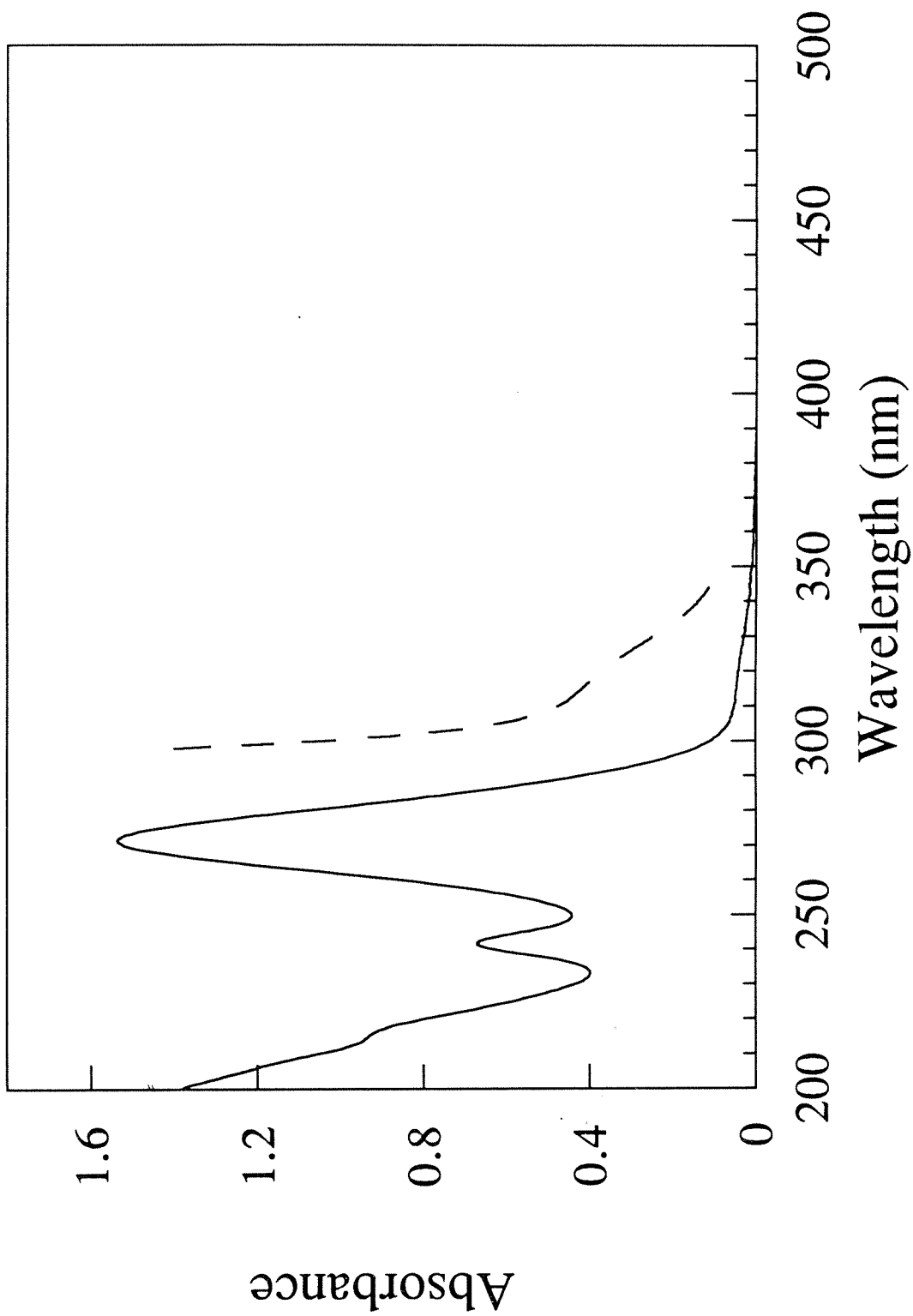


Figure 2.11. Absorption spectrum of $\text{Au}_2(\text{dcpe})_3(\text{PF}_6)_2$, 5, 50, and 500 μM .

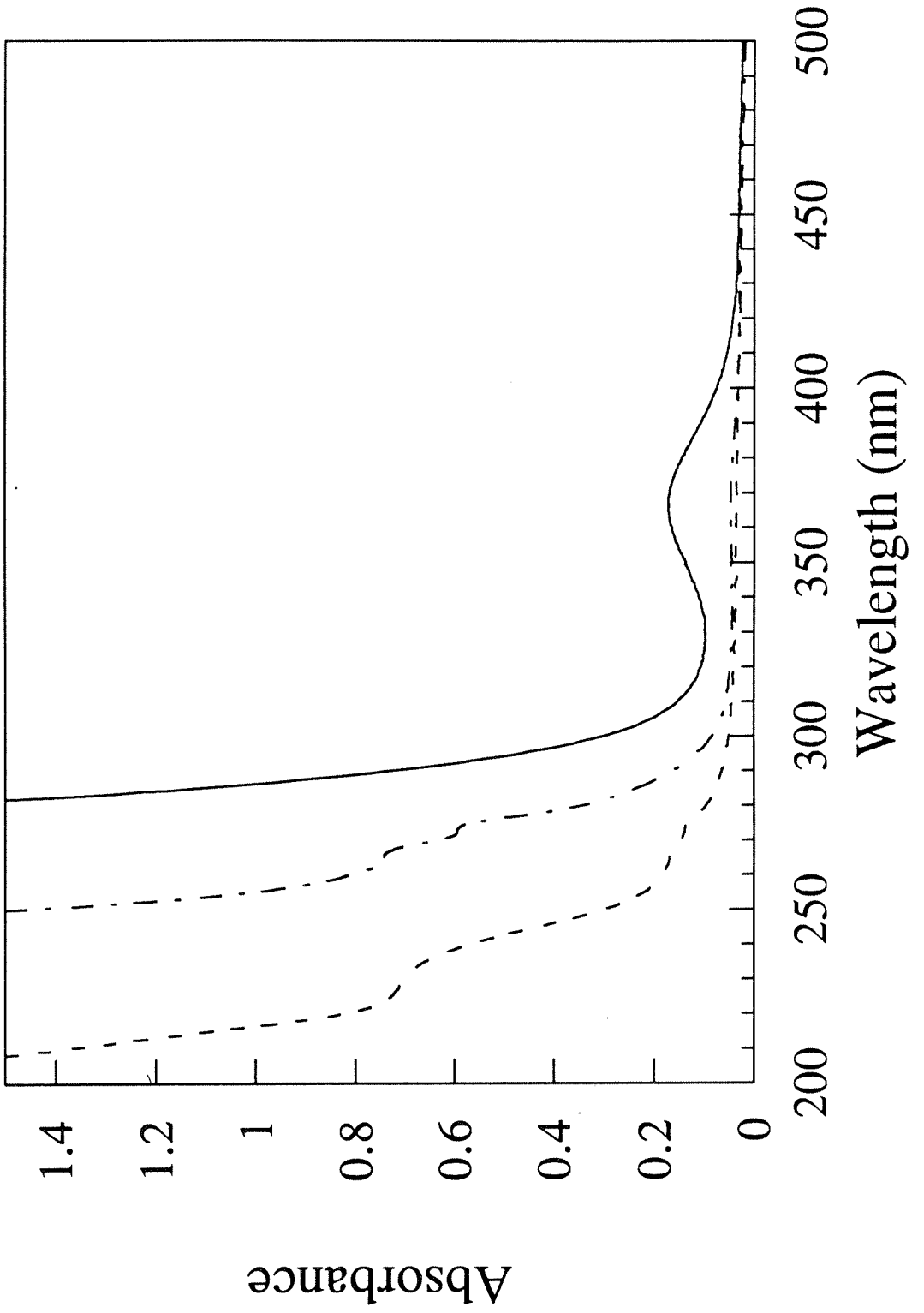


Figure 2.12. Solid-state emission spectrum of $\text{Au}_2(\text{dcpe})_2(\text{PF}_6)_2$ at 77 K, 366 nm excitation.

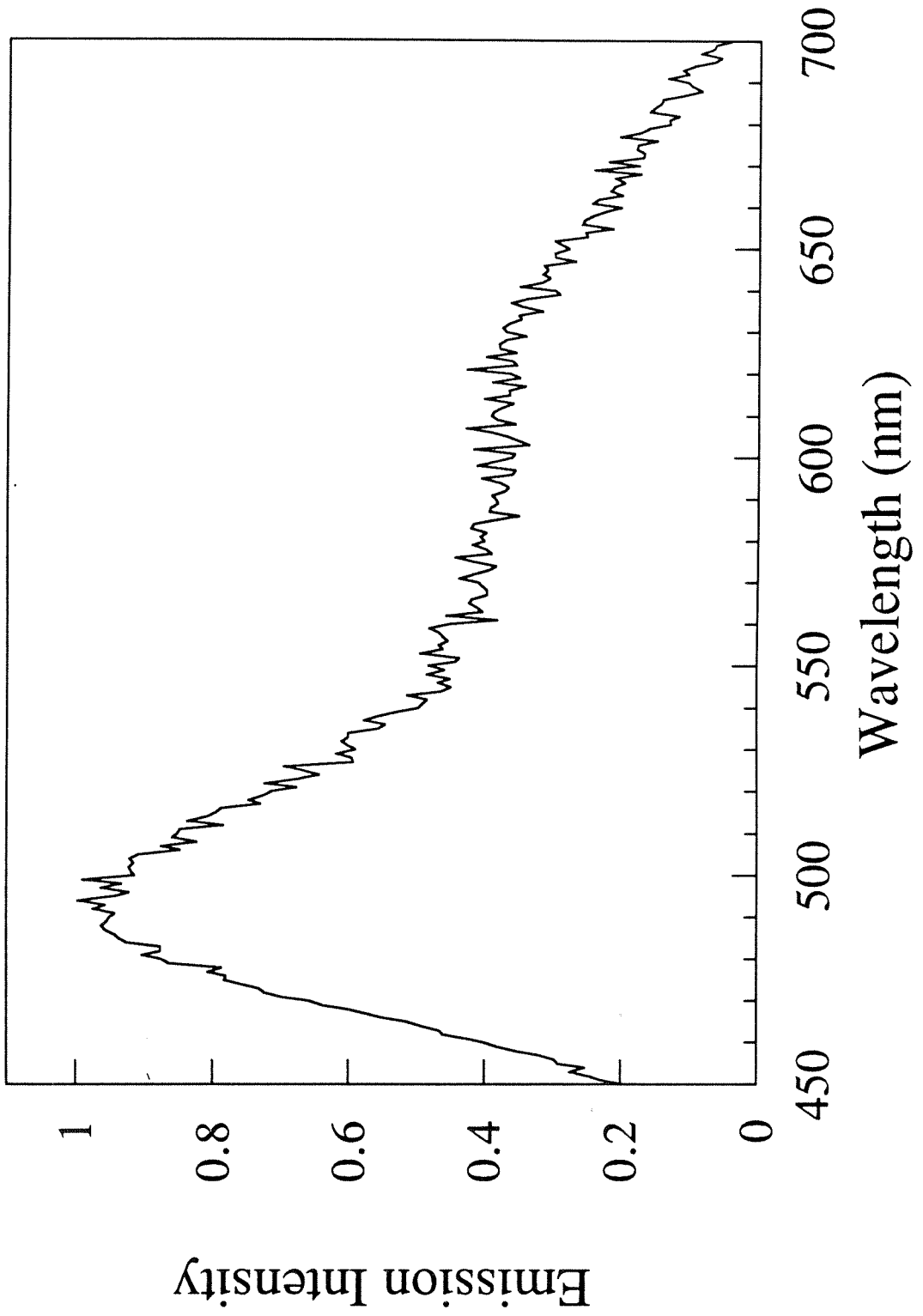


Figure 2.13. Solid-state emission spectrum of $\text{Au}_2(\text{dcpe})_2(\text{PF}_6)_2$ at room temperature, 313 nm excitation.

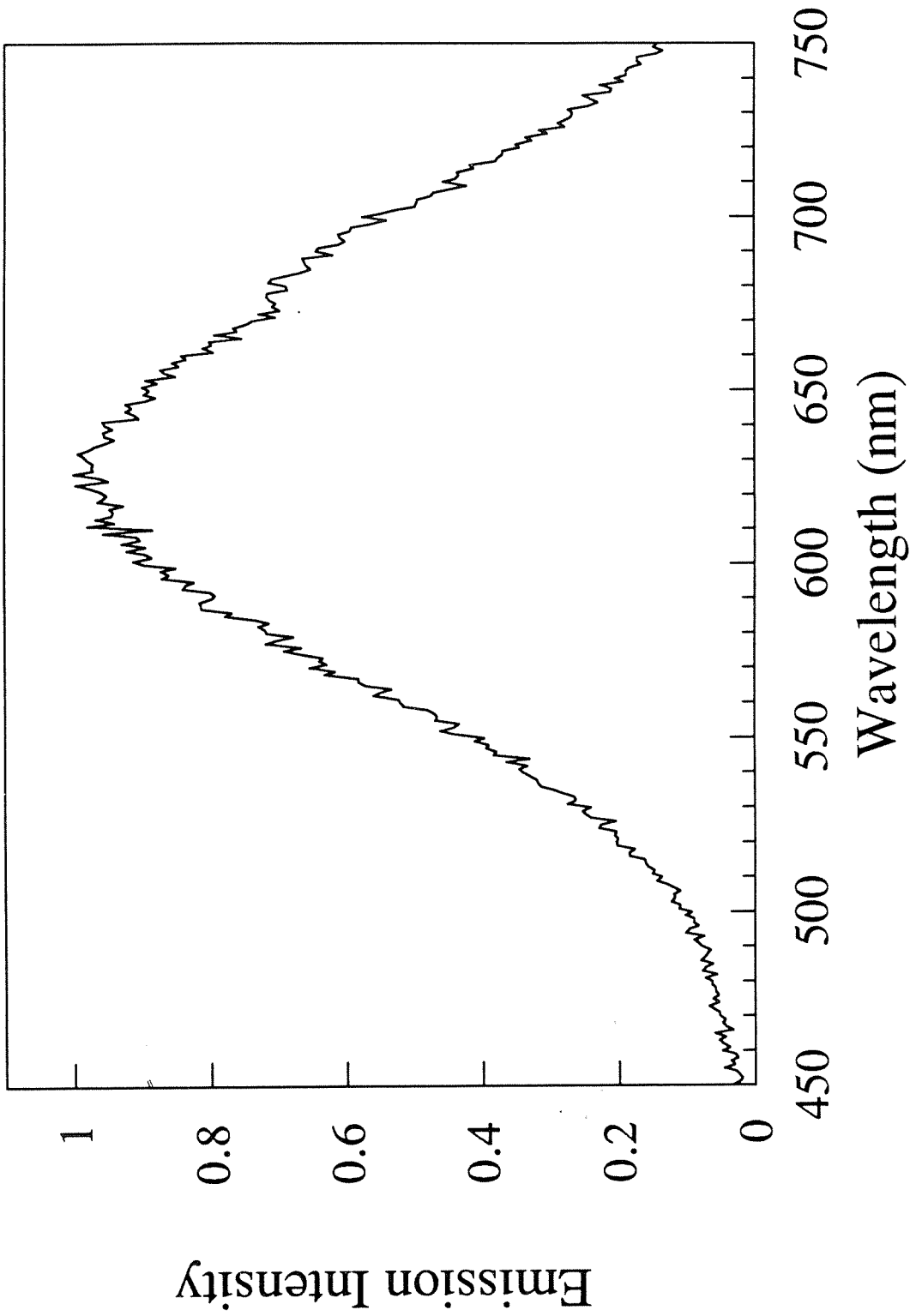


Figure 2.14. Emission spectrum of $\text{Au}_2(\text{dcpe})_2(\text{PF}_6)_2$ at 77 K in a 4:1 ethanol:methanol glass, 313 nm excitation.

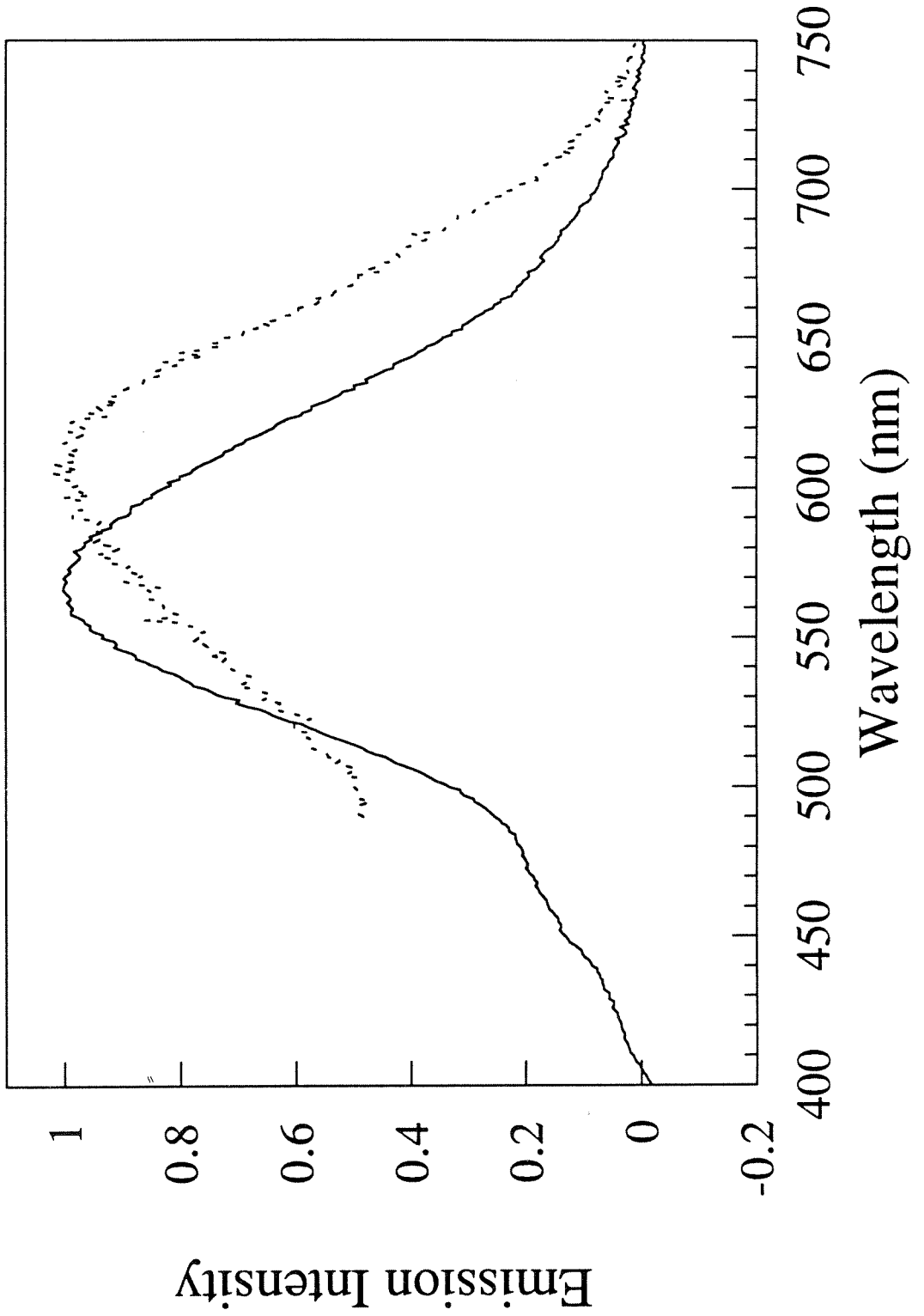


Figure 2.15. Emission spectrum of $\text{Au}_2(\text{dcpe})_3(\text{PF}_6)_2$ in acetonitrile solution at room temperature, 366 nm excitation, 10 μM .

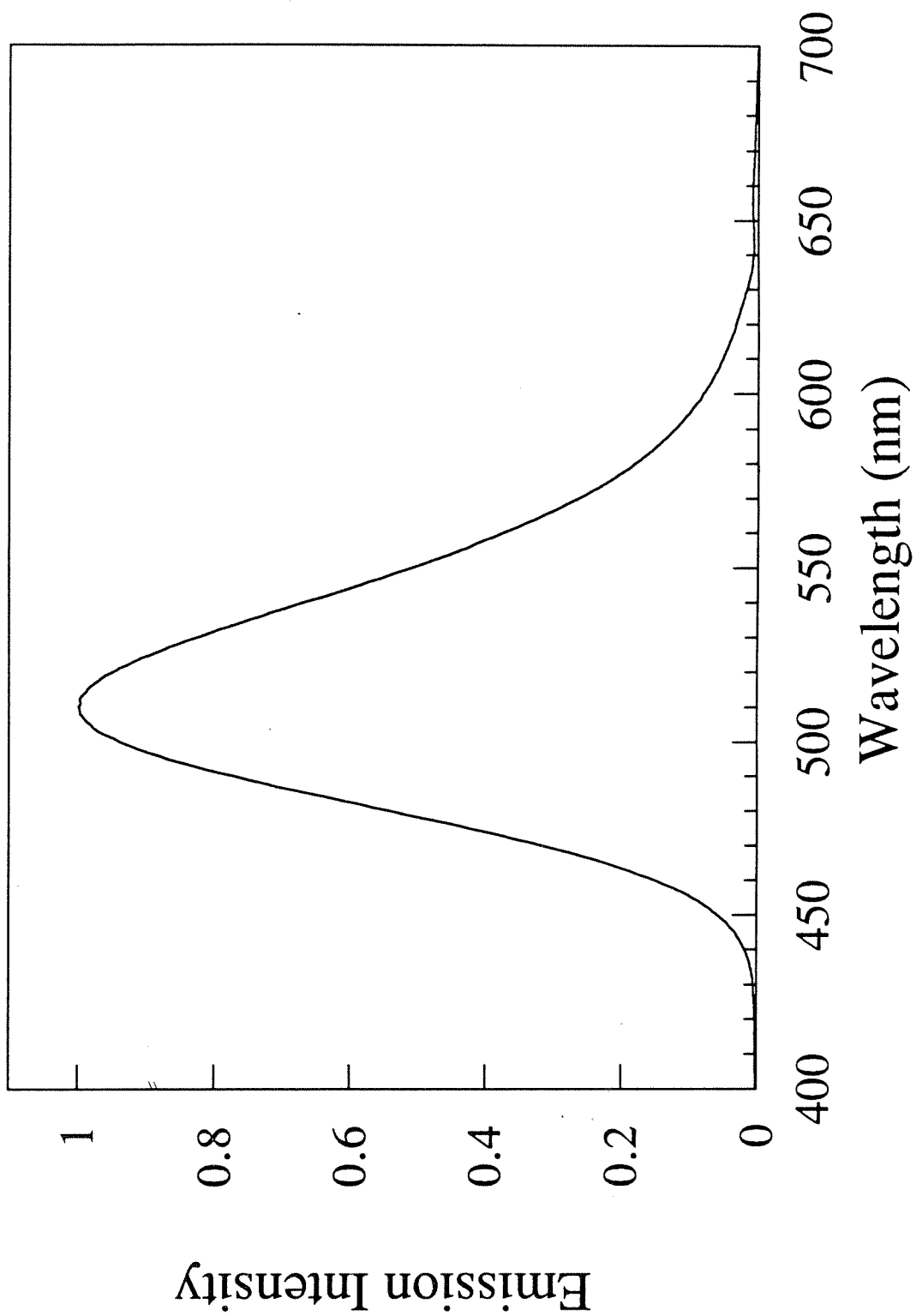
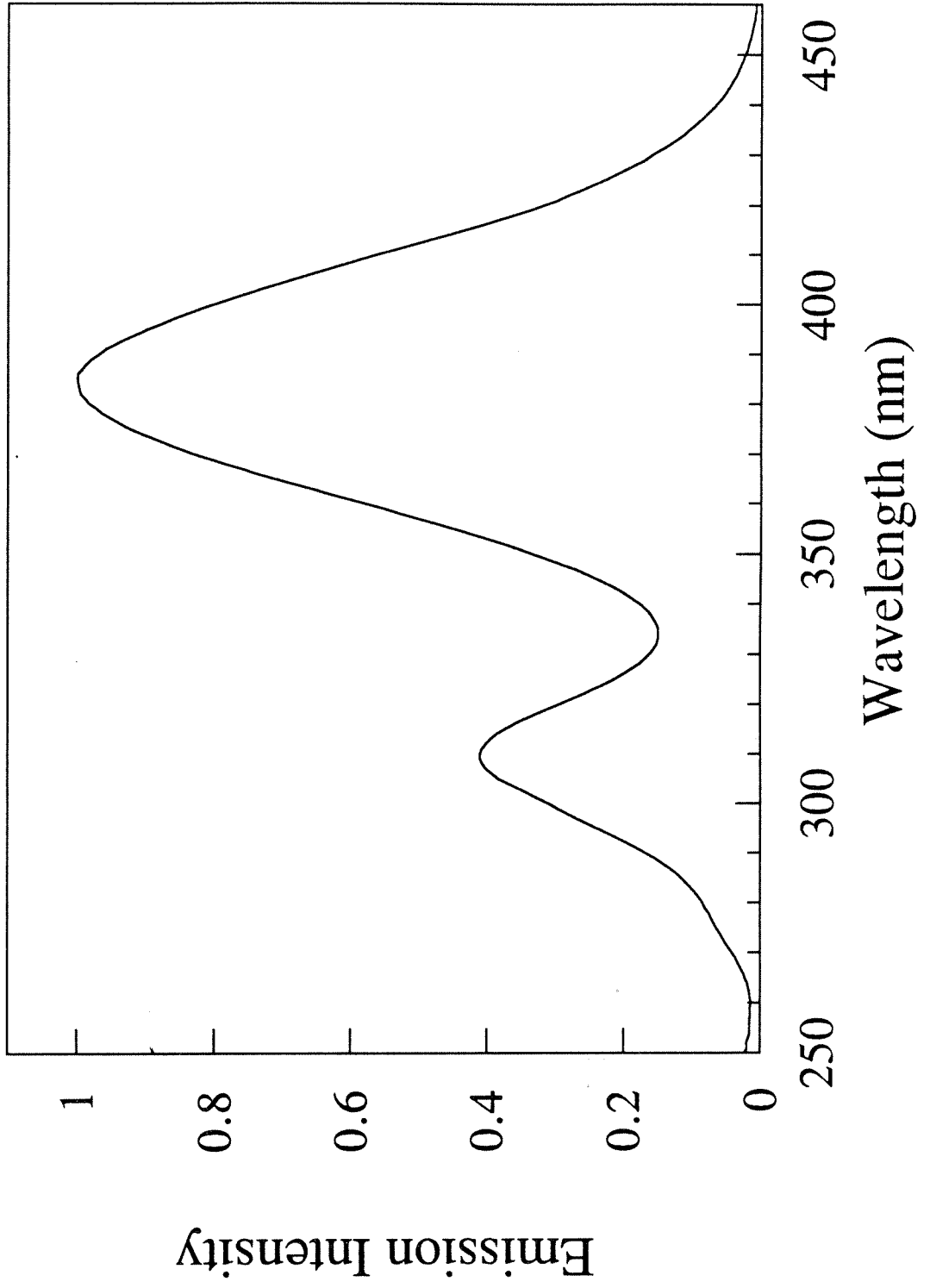


Figure 2.16. Excitation spectrum of $\text{Au}_2(\text{dcpe})_3(\text{PF}_6)_2$ in acetonitrile solution at room temperature, 366 nm excitation, 10 μM .



The compound $\text{Au}_2(\text{dcpe})_3^{2+}$ has a weak low energy absorption at 370 nm ($\epsilon = 300 \text{ M}^{-1}\text{cm}^{-1}$ per AuP_3 unit). Using the approximate D_{3h} symmetry of the AuP_3 unit, this band is attributable to a ${}^1A_1' \rightarrow E' ({}^3E'')$ [$d_{xy}, d_x^2-y^2 (d\sigma^*) \rightarrow p_z$] transition. The $d_{xy}, d_x^2-y^2$ can be assigned as the HOMO since they lie in the plane of the ligands. Lying perpendicular to the plane of the ligands, the p_z is clearly the lowest energy p orbital and can be assigned as the LUMO since there are no low energy orbitals on the ligand. The resulting HOMO to LUMO, ${}^1A_1' \rightarrow {}^3E''$ transition is both spin and dipole forbidden. Spin orbit coupling of the gold splits the ${}^3E''$ state into $A_1', A_2', E',$ and E'' levels; the ${}^1A_1' \rightarrow E' ({}^3E'')$ is the only dipole allowed transition. The corresponding singlet transition will be weak since the ${}^1A_1' \rightarrow {}^1E''$ is dipole forbidden, and is obscured by the allowed bands at 265 nm and 274 nm ($\epsilon = 32,500 \text{ M}^{-1}\text{cm}^{-1}$ to $26,000 \text{ M}^{-1}\text{cm}^{-1}$ per AuP_3 unit respectively). The two higher energy allowed transitions are assigned as allowed $d \rightarrow p$ transitions, but exact orbital assignment is difficult. Both the ${}^1A_1' \rightarrow {}^1E'$ ($d_{xz}, d_{yz} \rightarrow p_z$) and the ${}^1A_1' \rightarrow {}^1A_2''$ ($d_z^2 \rightarrow p_z$) are dipole allowed transitions. This complex luminesces intensely both as a solid ($\lambda_{\text{max}} = 501 \text{ nm}$) and in acetonitrile solution at room temperature ($\lambda_{\text{max}} = 508 \text{ nm}$; $\tau = 21.1 \mu\text{s}$ (5); $\phi = 0.80$ (5); Figure 2.15). The emission corresponds to the ${}^1A_1' \leftarrow E' ({}^3E'')$ transition. The excitation spectrum (Figure 2.16) has one very intense low energy band at 383 nm and a weaker band at 310 nm. The strong band at 383 nm confirms the emission assignment as being complementary to the assignment for the absorption at 370 nm. The large quantum yield ($\phi = 0.8$ for 366 nm excitation) supports the assignment of the absorption at 370 nm as a direct singlet to triplet transition, and the extremely long lifetime provides further evidence that the emission occurs from a triplet state. The $E_{\nu_0-\nu_0}$ for the emissive transition in acetonitrile solution is 432 nm with a Stokes shift of $7,800 \text{ cm}^{-1}$.

The dipe complexes of gold are structurally similar to the dcpe complexes and the assignments for the absorption bands (Figures 2.17-2.19) are as follows: $\text{Au}(\text{dipe})_2^+$, ${}^1A_1 \rightarrow {}^1B_2$ ($d_{xz}, d_{yz} \rightarrow p_x, p_y$) at 233 nm with a shoulder at 255 nm; $\text{Au}_2(\text{dipe})_2^{2+}$,

$^1A_g \rightarrow ^1B_{1u}$ ($d\sigma^* \rightarrow p\sigma$) at 269 nm, $^1A_g \rightarrow ^3B_{1u}$ ($d\sigma^* \rightarrow p\sigma$) at 315 nm; $Au_2(dipe)_3^{2+}$, $^1A_{1'} \rightarrow E'$ ($^3E''$) [d_{xy} , $d_{x^2-y^2}$ ($d\sigma^*$) $\rightarrow p_z$] at 368 nm, $^1A_{1'} \rightarrow ^1E'$ [d_{xy} , $d_{x^2-y^2}$ ($d\sigma^*$) $\rightarrow p_z$] obscured by the higher energy $d \rightarrow p$ bands at 268 nm and 227 nm. The $Au_2(dipe)_2^{2+}$ complex emits as a solid at room temperature ($\lambda_{max} = 630$ nm) upon 313 nm excitation and in a ethanol:methanol (4:1) glass at 77K ($\lambda_{max} = 566$ nm), but shows no emission at room temperature with 366 nm excitation (Figure 2.20). Only the $Au_2(dipe)_3^{2+}$ complex emits in acetonitrile solution at room temperature ($\lambda_{max} = 510$ nm; Figure 2.21). The excitation spectrum of $Au_2(dipe)_3^{2+}$ has an intense low energy band at 383 nm and a second band at 308 nm (Figure 2.22).

The complex $Au_2(dppb)_3^{2+}$ is only sparingly soluble in any solvent so the absorption spectrum could only be obtained for low concentrations in ethanol. The lowest energy observable absorption band occurs at 270 nm (Figure 2.23). The compound emits both as a solid and in ethanol solution at room temperature ($\lambda_{max} = 534$ nm; Figure 2.24) The emission is assigned as a $^1A_{1'} \leftarrow E'(^3E'')$ transition analogous to the emissive transition observed for $Au_2(dcpe)_3^{2+}$. The excitation spectrum shows two bands at 359 nm and 320 nm (Figure 2.25). The 359 nm band presumably corresponds to the $^1A_{1'} \rightarrow E'(^3E'')$ transition which is not observable in the absorption spectrum due to solubility limitations. The higher energy band falls on the tail of the 270 nm absorption band and is assigned as the $^1A_{1'} \rightarrow ^1E''$ transition.

Low Temperature Spectra To confirm the assignment of the low energy absorption band and emission of $Au_2(dcpe)_3^{2+}$ low temperature (77 K) absorption and emission spectra were measured. The d_{xy} , $d_{x^2-y^2} \rightarrow p_z$ transition assigned to the absorption band involves removing an electron from the Au-P σ^* orbital and placing it into the non-bonding p_z orbital; therefore, the excited state should have stronger Au-P bonds and a narrower potential well. Cooling the sample reduces the number of thermally accessible vibrational levels in the ground state and in the case of a more

Figure 2.17. Absorption spectrum of $\text{Au}(\text{dipe})_2(\text{PF}_6)$, 67 μM .

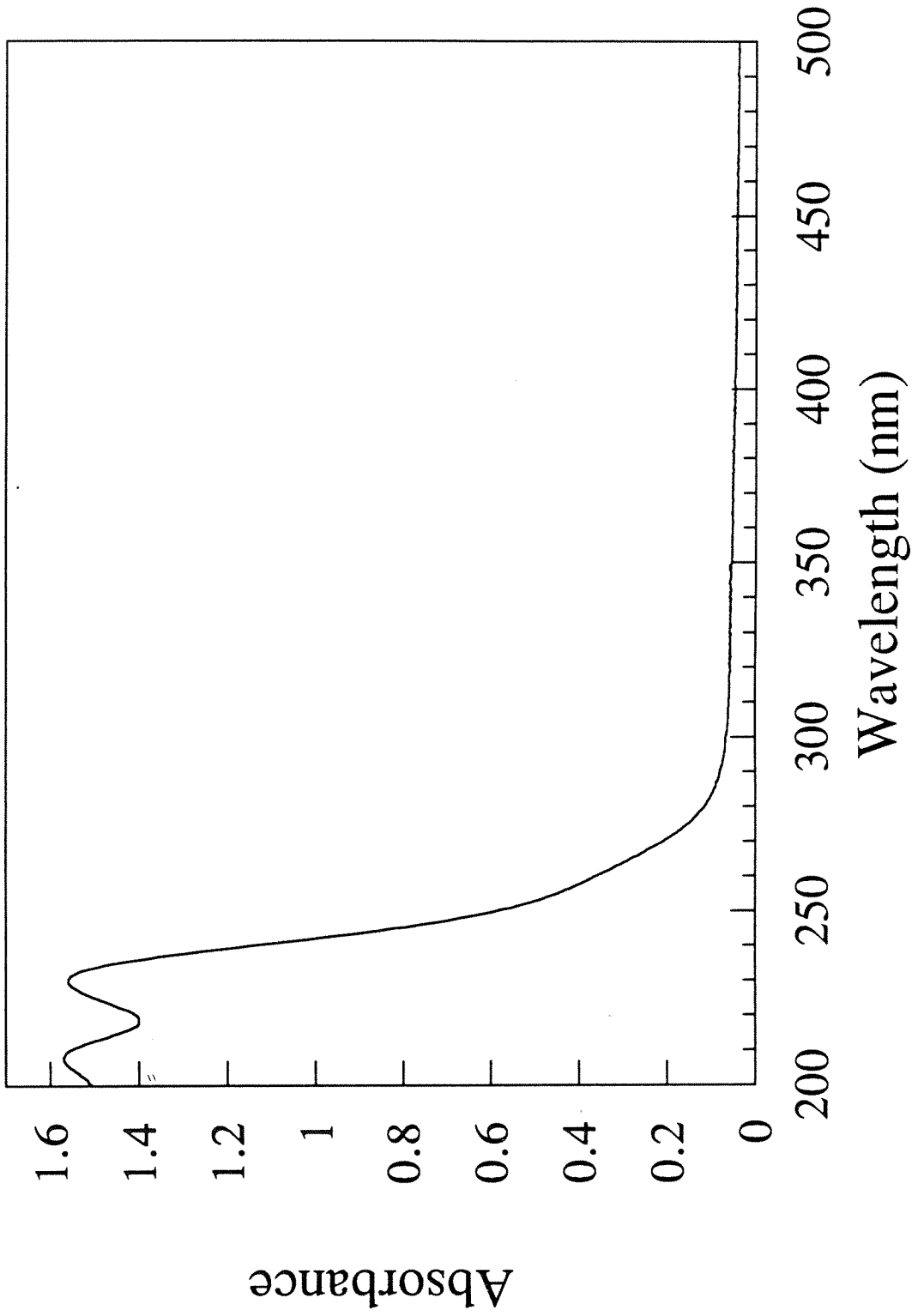


Figure 2.18. Absorption spectrum of $\text{Au}_2(\text{dipe})_2(\text{PF}_6)_2$, 85 μM .

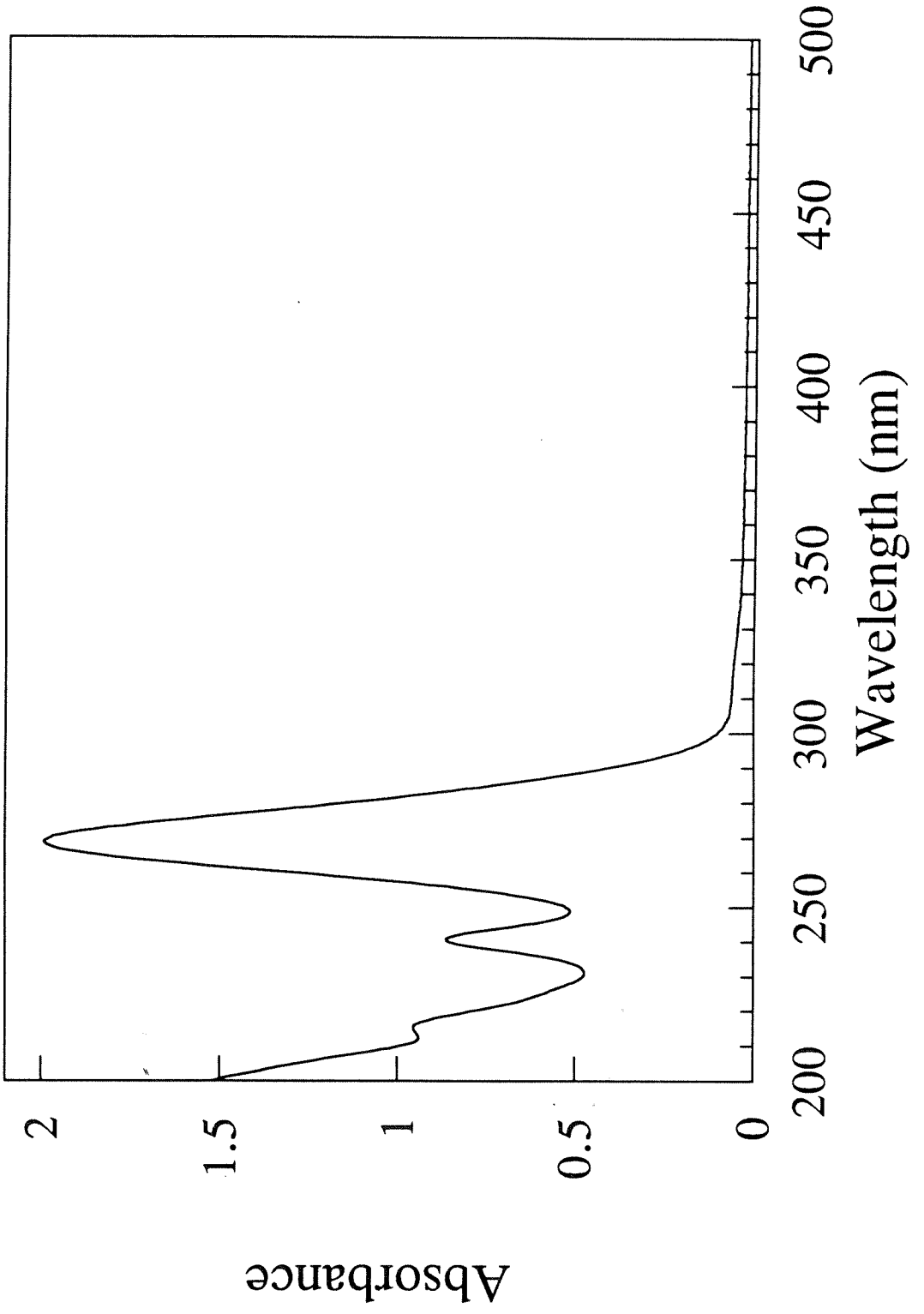


Figure 2.19. Absorption spectrum of $\text{Au}_2(\text{dipe})_3(\text{PF}_6)_2$, 8 and 800 μM .

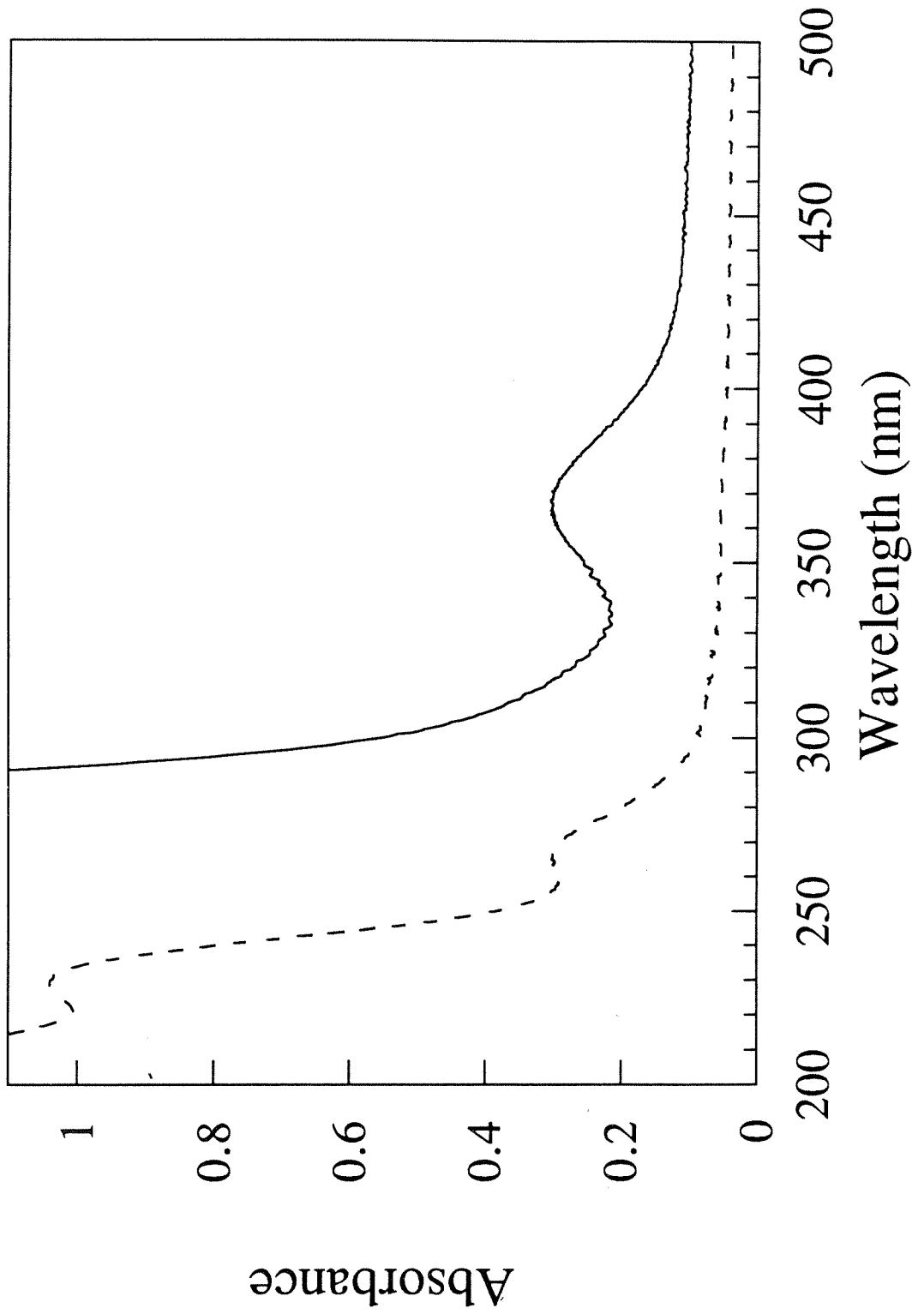


Figure 2.20. Solid-state emission spectrum of $\text{Au}_2(\text{dipe})_2(\text{PF}_6)_2$ at room temperature, 313 nm excitation.

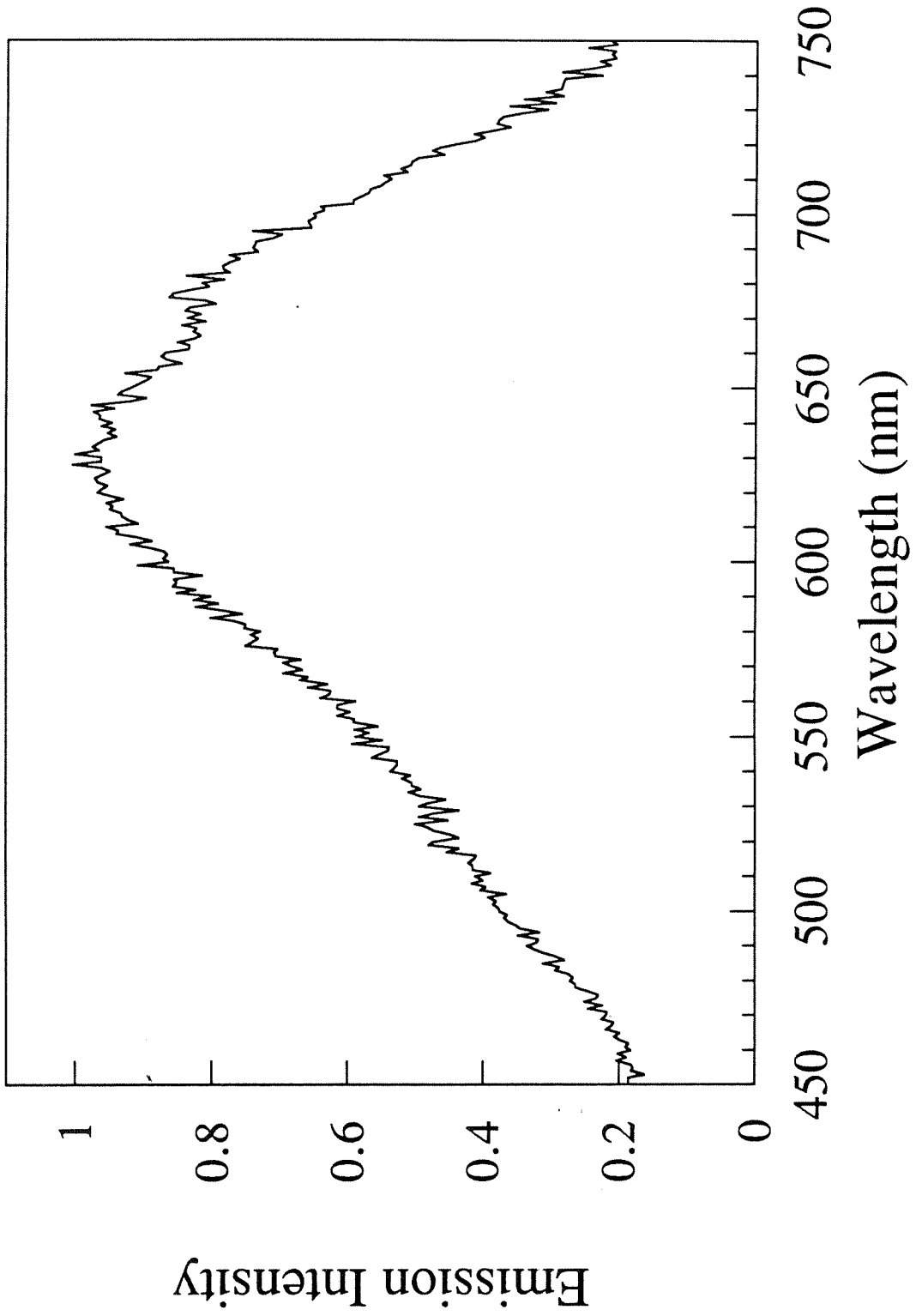


Figure 2.21. Emission spectrum of $\text{Au}_2(\text{dipe})_3(\text{PF}_6)_2$ in acetonitrile solution at room temperature, 366 nm excitation, 10 μM .

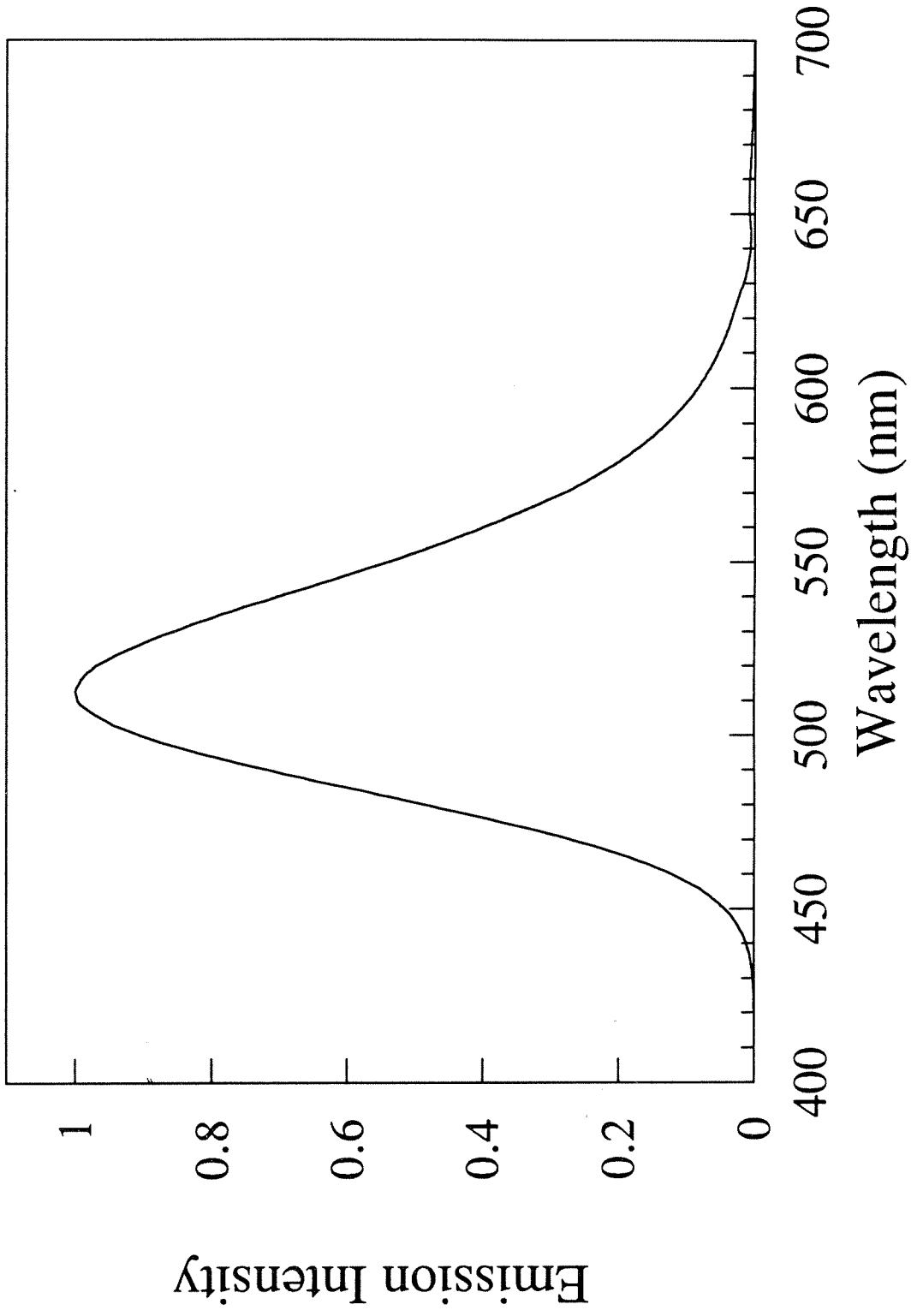


Figure 2.22. Excitation spectrum of $\text{Au}_2(\text{dipe})_3(\text{PF}_6)_2$ in acetonitrile solution at room temperature, 366 nm excitation, 10 μM .

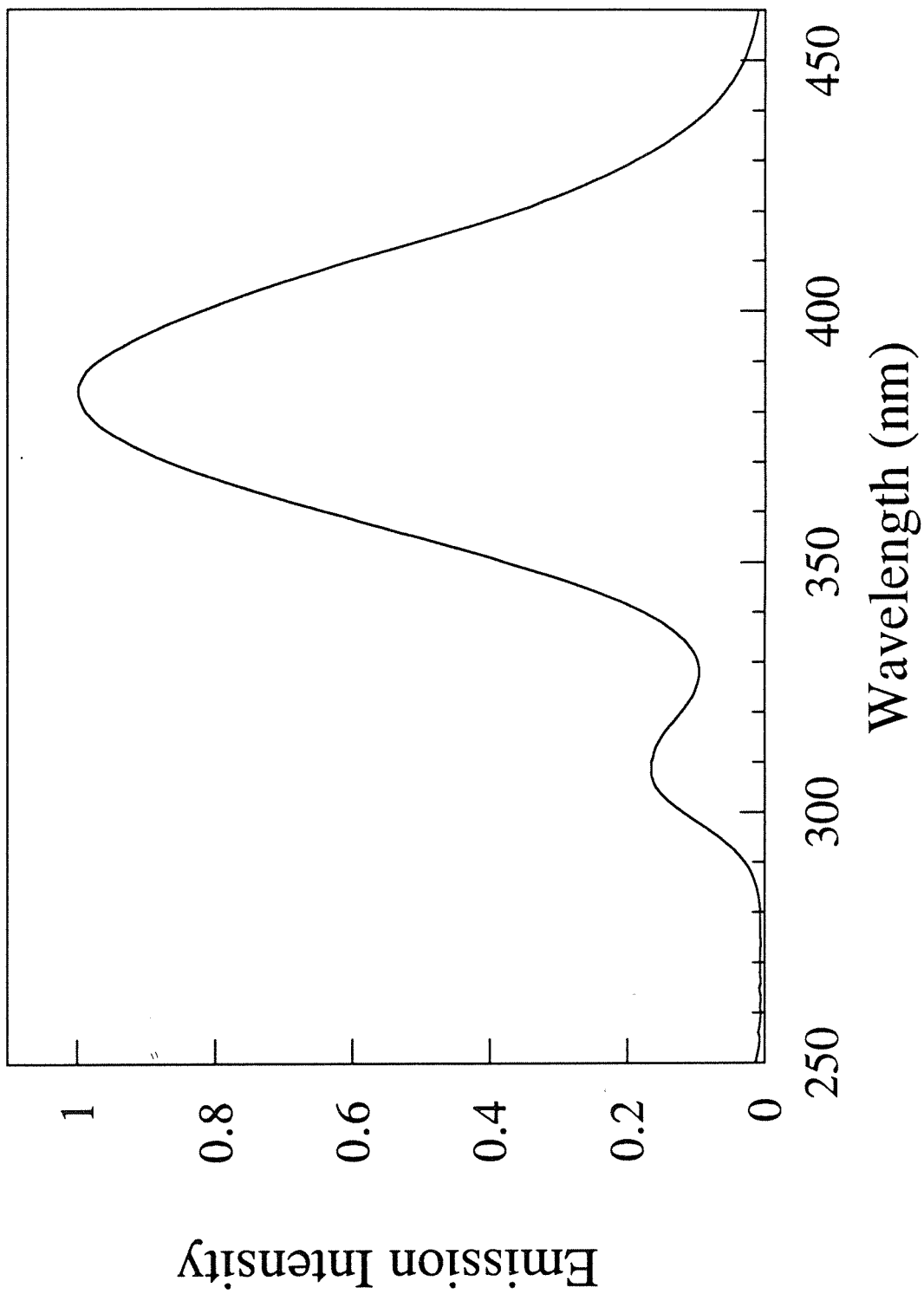


Figure 2.23. Absorption spectrum of $\text{Au}_2(\text{dppb})_3(\text{PF}_6)_2$ in ethanol, 3 μM .

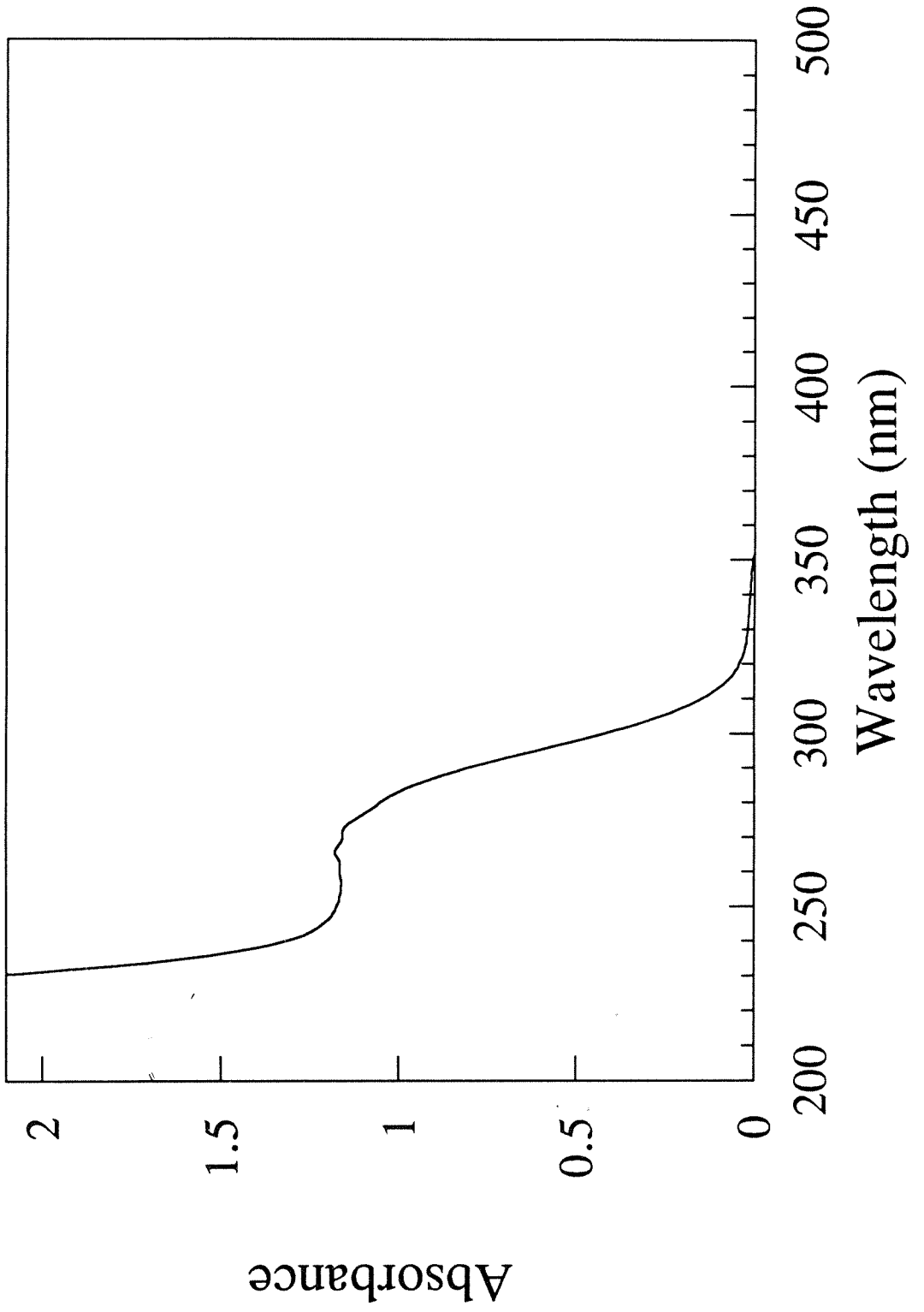


Figure 2.24. Emission spectrum of $\text{Au}_2(\text{dppb})_3(\text{PF}_6)_2$ in ethanol solution at room temperature, 366 nm excitation, 2 μM .

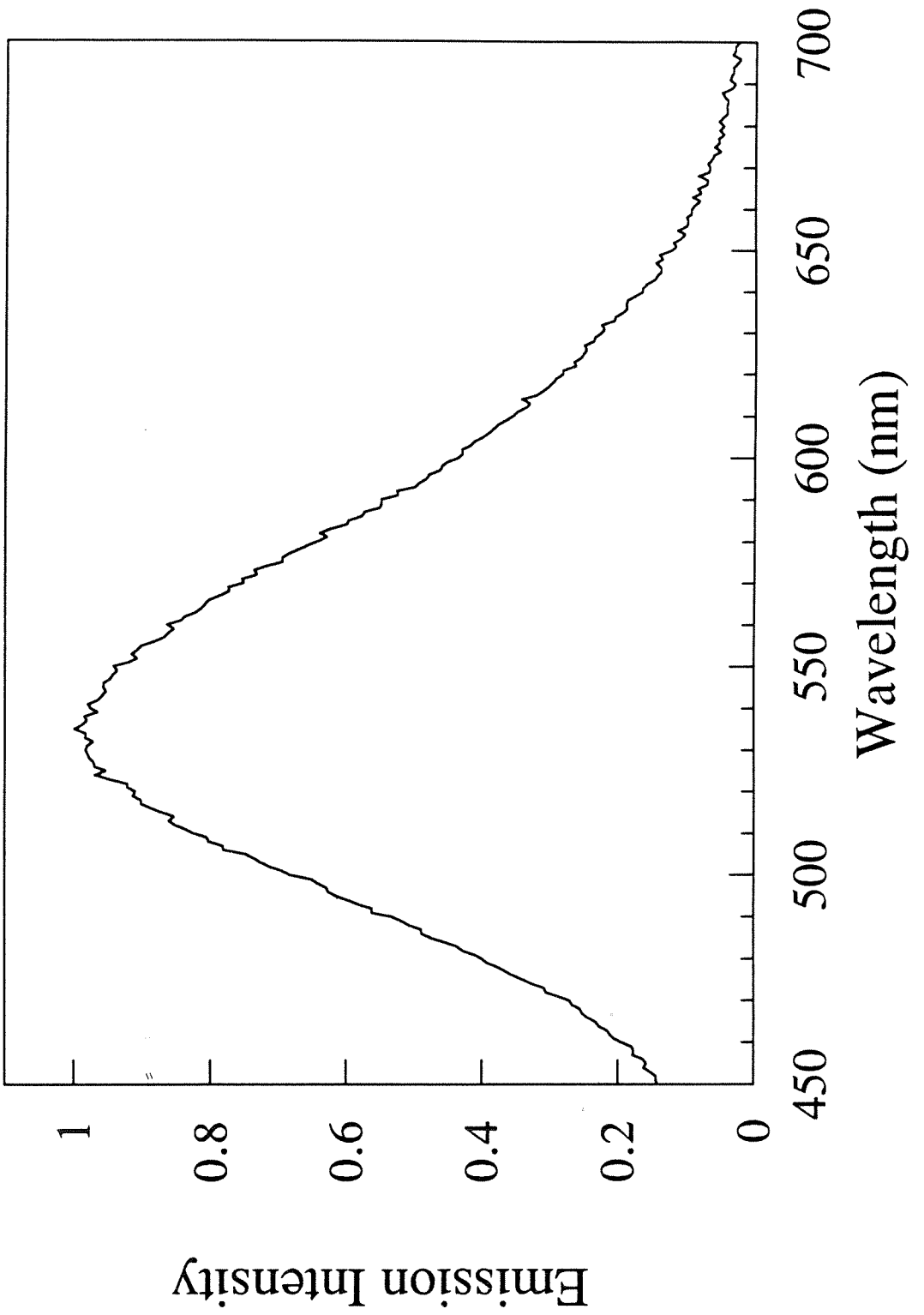
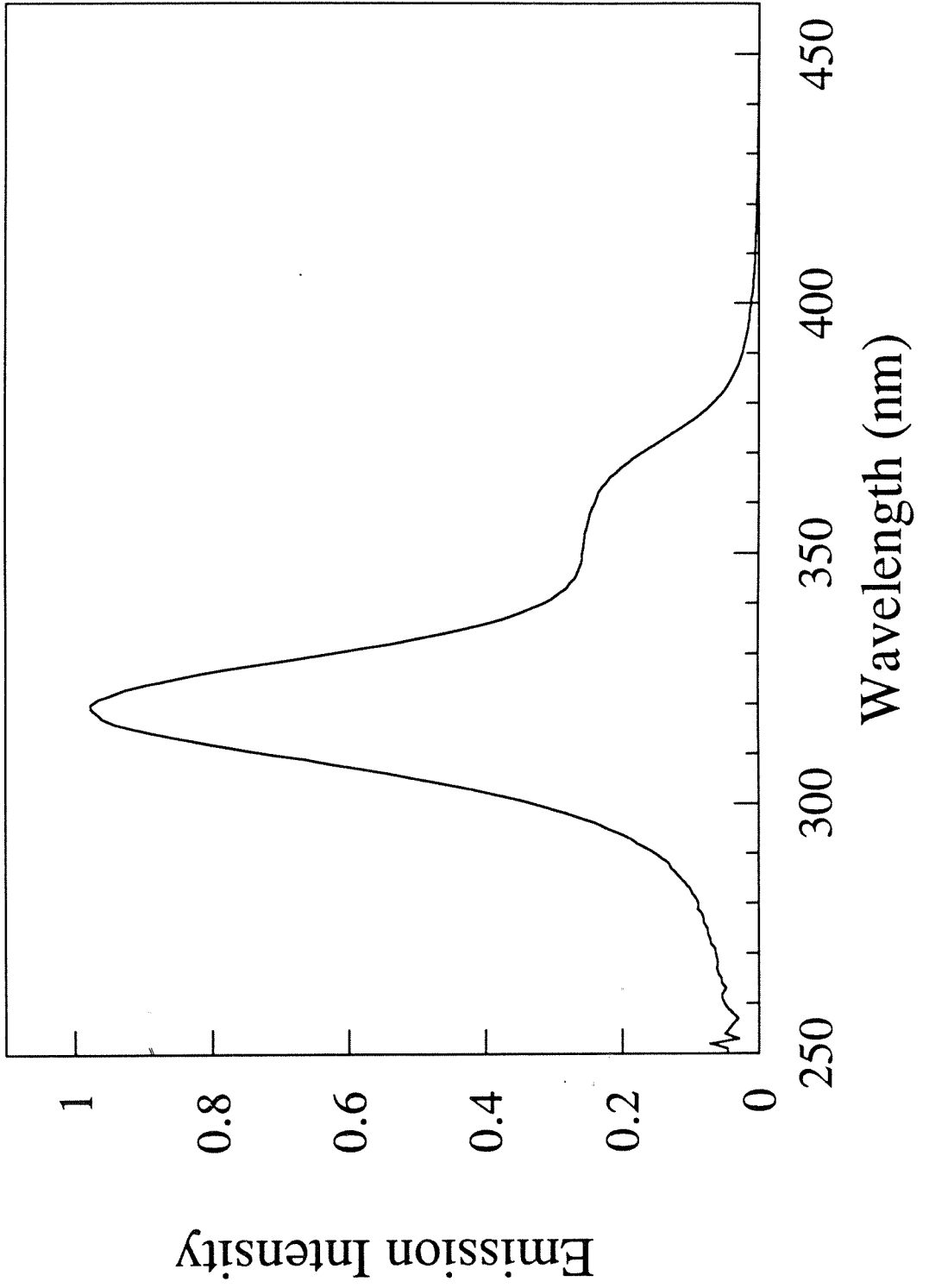


Figure 2.25. Excitation spectrum of $\text{Au}_2(\text{dppb})_3(\text{PF}_6)_2$ in ethanol solution at room temperature, 366 nm excitation, 2 μM .



strongly bound excited state will lead to a narrowing of the absorption band concomitant with a red shift of the maximum. Figure 2.26 depicts an idealized situation with the excited state directly above the ground state. At temperature T_1 , ν_0 and ν_1 vibrational levels are occupied in the ground state. The allowed vertical Frank-Condon transitions are $\nu_0 \rightarrow \nu_0$, $\nu_1 \rightarrow \nu_1$, and $\nu_1 \rightarrow \nu_2$. As the material is cooled only the ν_0 level is occupied in the ground state and the only allowed transition is $\nu_0 \rightarrow \nu_0$. Losing the higher energy $\nu_1 \rightarrow \nu_2$ transition causes the absorption band to narrow and red shift. Most excited states involve occupation of σ^* orbitals as opposed to bonding or non-bonding orbitals, in which case the bond strength of the excited state is lower than the ground state and a blue shift in the maximum of the absorption band would be expected on cooling. The 7 nm red shift in the absorption band (Figure 2.27) and a 3 nm blue shift of the emission observed for $\text{Au}_2(\text{dcpe})_3^{2+}$ demonstrate that the excited state is more strongly bound than the ground state.

Titration with Triphenylphosphine The compound $\text{ClAu}(\text{PPh}_3)$ was placed into a solution of acetonitrile and degassed. The emission of the solution was then monitored as PPh_3 was added to the solution. The resulting titration (Figure 2.28) shows that the solution begins to emit ($\lambda_{\text{max}} = 520 \text{ nm}$) as soon as half an equivalent of PPh_3 is added; emission continues to increase even up to the addition of nine equivalents. This emission is assigned as a $^1\text{A}_1' \leftarrow \text{E}'(^3\text{E}'')$ transition, analogous to that observed for $\text{Au}_2(\text{dcpe})_3^{2+}$. The emission is believed to originate from a three coordinate $\text{Au}(\text{PPh}_3)_3^+$ complex which is in equilibrium with $\text{Au}(\text{PPh}_3)_2^+$, $\text{Au}(\text{PPh}_3)_4^+$ and free PPh_3 . The broad ^{31}P NMR signal at room temperature supports the suggestion of an equilibrium between different species.

Photochemistry The emissive complex $\text{Au}_2(\text{dcpe})_3^{2+}$ is a potent photo-reductant capable of reducing a variety of haloalkanes and aryl halides. Emission of $\text{Au}_2(\text{dcpe})_3^+$ is completely quenched by 1,2-dibromoethane, bromobenzene, carbontetrachloride, and chloroform (control experiments in the dark showed no change

Figure 2.26. Energy surface diagram: a, b, and c represent the allowed vertical Frank-Condon transitions of v_0-v_0 , v_1-v_1 and v_1-v_2 .

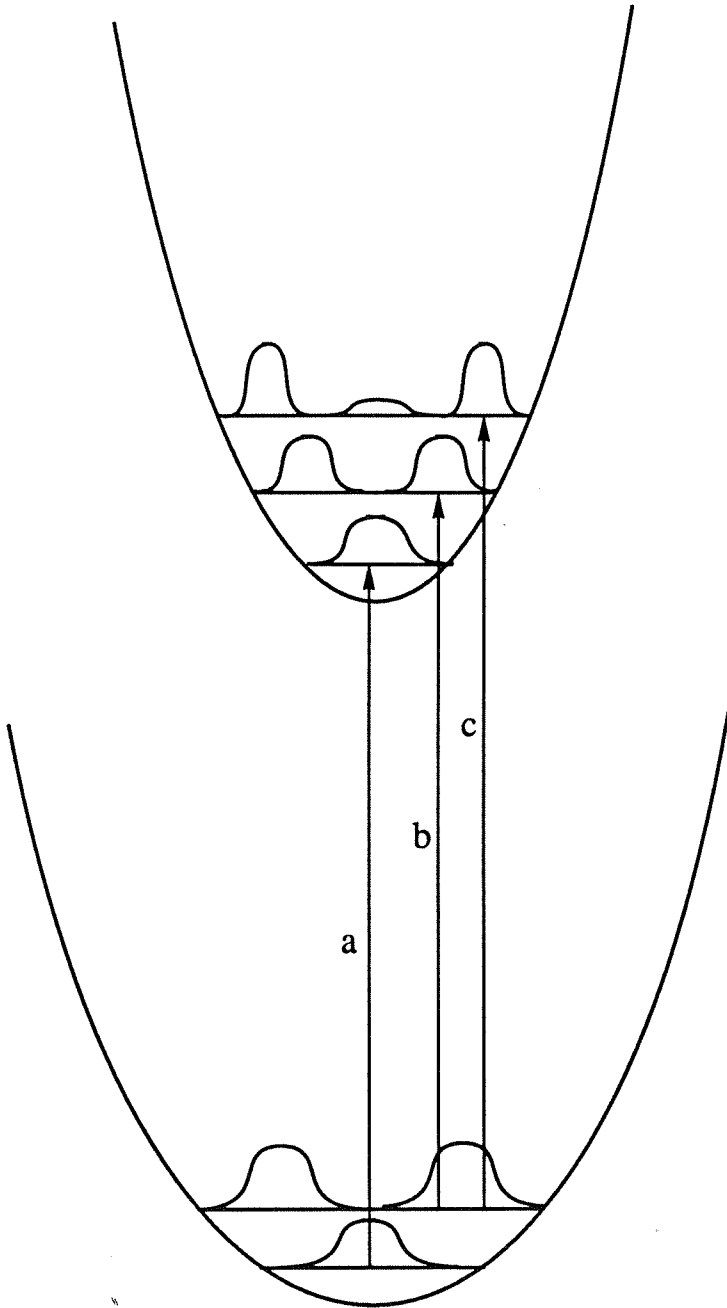


Figure 2.27. Absorption spectra of $[\text{Au}_2(\text{dcpe})_3] (\text{PF}_6)_2$ at 298 K (lower trace) and 77 K (upper trace).

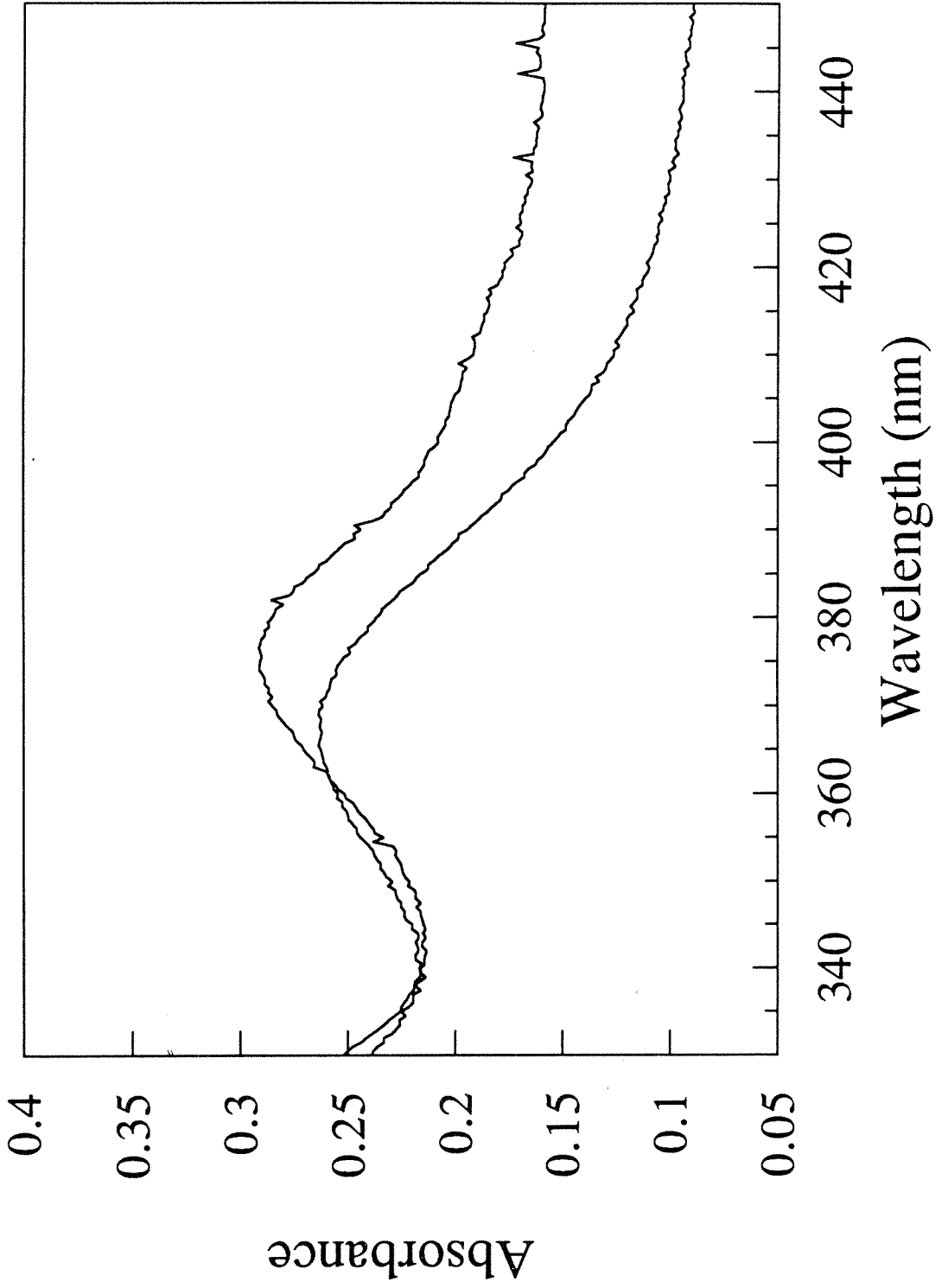
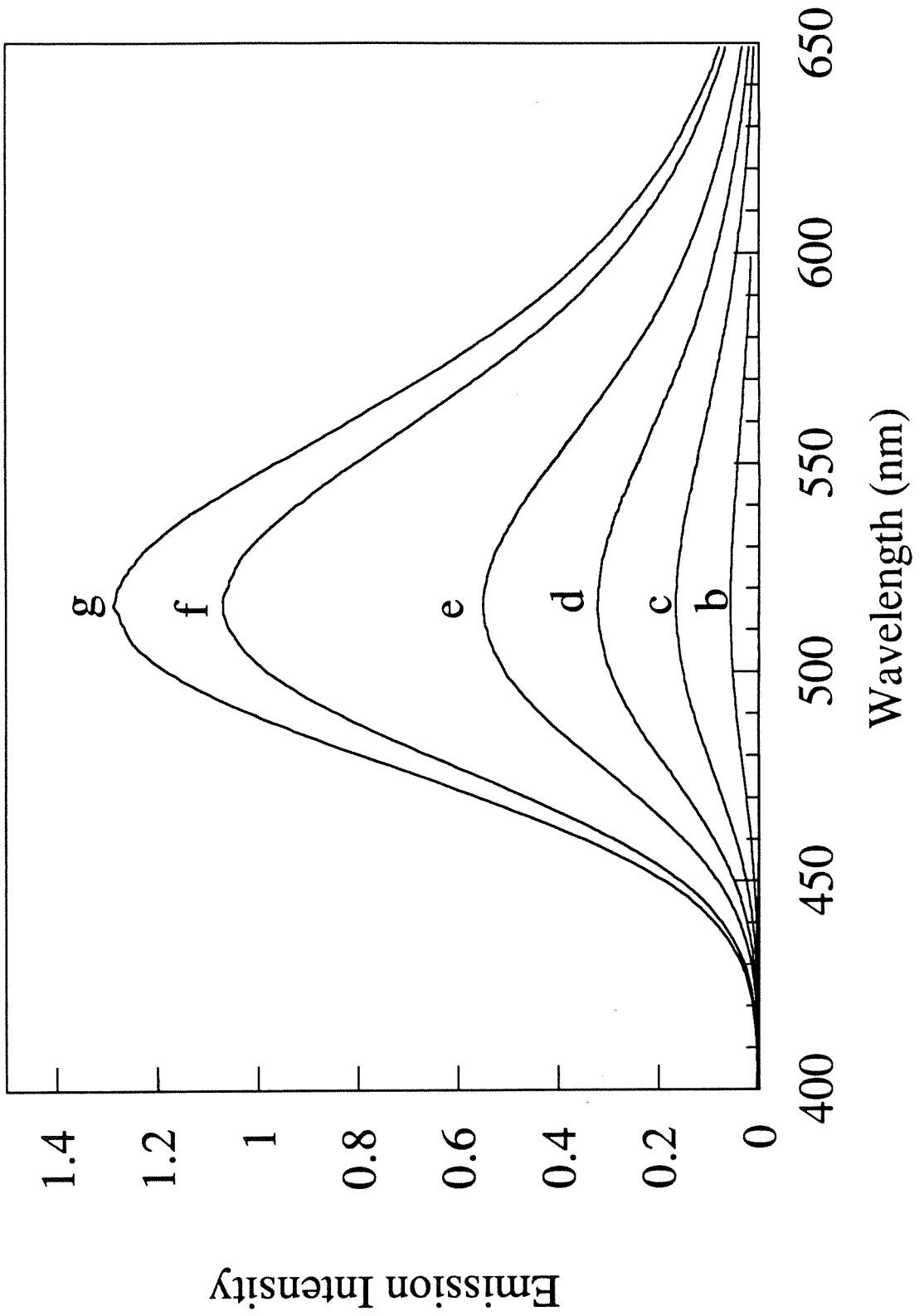
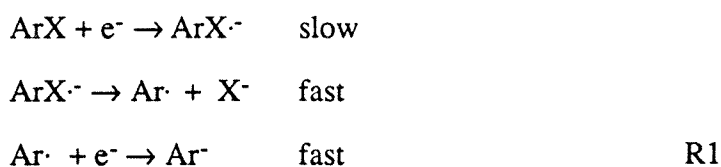


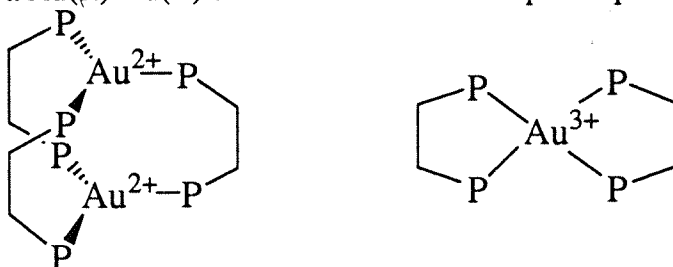
Figure 2.28. Emission spectra of $\text{ClAu}(\text{PPh}_3)$ with a, 0 (coincides with the baseline); b, 0.5; c, 1.0; d, 1.5; e, 2.0; f, 5.0; g, 9.0 equivalents of PPh_3 added.



in the electronic absorption spectrum of $\text{Au}_3(\text{dcpe})_3^{2+}$ in the presence of the halogenated compounds). No quenching of the emission was observed in the presence of chlorobenzene. The photoreactions with 1,2-dibromobenzene, bromo-benzene and chloroform have been followed by ^{31}P NMR; after photolysis for 15 minutes with a 366 nm Hg hand held lamp, the $\text{Au}_2(\text{dcpe})_3^{2+}$ phosphorous signal diminished completely and was replaced by a singlet (1,2-dibromobenzene, 61.1 ppm; bromobenzene, 61.1 ppm; chloroform, 60.7 ppm). Quenching rates were obtained by monitoring the luminescence as a function of the concentration of the quencher as described in chapter 3 (Table 2.3). In general reduction of haloaromatic compounds is an irreversible two electron process¹⁹ in which the halocarbon is reduced by one electron, dissociates X^- , and the remaining aromatic radical is quickly reduced to Ar^- . The reaction with $\text{Au}_2(\text{dcpe})_3^{2+}$ is irreversible and most likely proceeds in this manner with the



formation of Au(II) as the Cl^- transfers to the gold center; the Au(II) may then disproportionate or transfer a second electron to form Au(III). The nature of the Au product is intriguing. The appearance of a lone singlet shows that there is only one phosphorous product and that all of the phosphorous atoms in the product are equivalent. The signals observed near 60 ppm do not correspond to either the free dcpe ligand (3.0 ppm) or the oxide of the ligand (51.4 ppm). Since all phosphorous atoms must be equivalent there are only a few choices for possible gold complexes. Two possible complexes are a Au(II)-Au(II) dimer similar to the complex reported by Fackler,²⁰ and a



four coordinate Au(III) complex with two chelating dcpe units. Crystals that diffract have been grown, but lost solvent and cracked before the structure was solved.

Excited State Potential The potential of the excited state can be estimated from the $\nu_0 \rightarrow \nu_0$ energy and the oxidation potential of the metal center. The $\nu_0 \rightarrow \nu_0$ energy of $\text{Au}(\text{dcpe})_3^{2+}$ was approximated at 1% of the maximum intensity assuming a Gaussian absorption band (Equation 1).²¹ As a check the same procedure was employed with the

$$\nu_{1\%} = \nu_{\text{max}} \pm 1.29 (\Delta\nu_{1/2}) \quad 1.$$

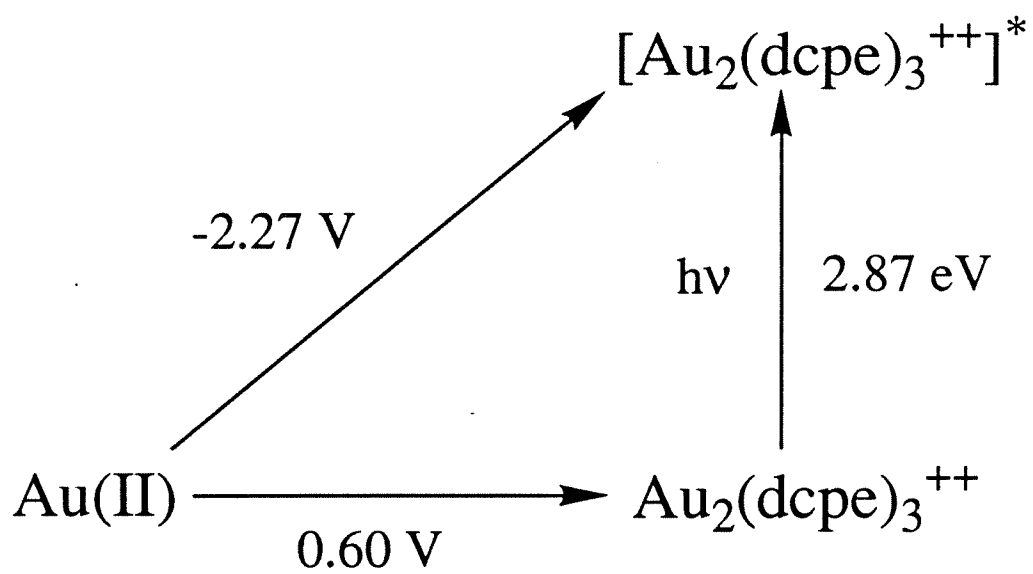
emission band, which gave a value of $23,420 \text{ cm}^{-1}$ compared to $22,850 \text{ cm}^{-1}$ from the absorption band. The average value of $23,130 \text{ cm}^{-1}$ (432 nm) corresponds to 2.9 eV. The ground state electrochemistry shows that the oxidation of the Au(I) center is completely irreversible with E_{pc} at 0.6 V. Using the E_{pc} as a maximum limit on $E_{1/2}$, the $\nu_0 \rightarrow \nu_0$ energy gives an excited state potential of 2.3 V vs SSCE (Figure 2.29). The value 2.3 eV for the ΔG of excited state oxidation fits in well with the observed rate of atom abstraction from bromobenzene. Saveant has studied the reduction of bromobenzene with a series of strong reducing agents and made an experimental plot of the rate of electron transfer vs. the potential of the catalyst.¹⁹ The rate of $8.68 \times 10^7 \text{ M}^{-1}\text{s}^{-1}$ for reduction by the excited $\text{Au}(\text{dcpe})_3^{2+}$ (see chapter 3) corresponds to a potential of 2.5 V vs. SCE.

General Synthesis of Three Coordinate Gold Complexes Several attempts were made to design a general synthetic procedure for three coordinate gold(I) complexes. The first strategy was to make a gold complex with one monodentate phosphine and then add one equivalent of a bidentate chelating phosphine. The ClAuPR_3 are readily prepared and isolated by adding one equivalent of PR_3 to compound 3 in acetonitrile. After four hours of stirring, the product precipitates as a white powder. Addition of the bidentate phosphine dcpe lead to a mixture of products which included $\text{Au}_2(\text{dcpe})_2^{2+}$. There was no evidence for the desired three coordinate complex $\text{PR}_3\text{Au}(\text{dcpe})^+$ in the ^{31}P NMR.

Table 2.3 Excited state quenching rates of $[\text{Au}_2(\text{dcpe})_3] (\text{PF}_6)_2$ with aryl and alkyl halides; the quenching rate with $\text{C}_6\text{H}_5\text{Cl}$ was too slow to measure.

Quencher	$k_q(\text{M}^{-1}\text{s}^{-1})$	$E_{1/2}$ (V vs SCE)
CCl_4	1.8×10^9	
CHCl_3	4.7×10^8	
$\text{BrCH}_2\text{CH}_2\text{Br}$	4.7×10^8	
$\text{C}_6\text{H}_5\text{Br}$	8.8×10^7	-2.44
$\text{C}_6\text{H}_5\text{Cl}$	$< 1 \times 10^5$	-2.78

Figure 2.29 Modified Latimer diagram for $[\text{Au}_2(\text{dcpe})_3] (\text{PF}_6)_2$.



Attempts to synthesize three coordinate complexes of the type $\text{CNAu}(\text{dcpe})$ from AuCN and dcpe were unsuccessful due to the formation of $\text{Au}(\text{CN})_2^-$. Most recently, the complex $\text{ClAu}(\text{dcpp})$ has been isolated in an effort to take advantage of the poor bridging capabilities of the dcpp bidentate ligand. The propyl bridge between the phosphines adopts a chelating conformation much more readily than a bridging conformation, so that unwanted products such as $\text{Au}_2(\text{dcpp})_2^{2+}$ may be avoided. The next step will be to add one equivalent of PR_3 and determine if the compounds $\text{PR}_3\text{Au}(\text{dcpp})^+$ are stable on the NMR time scale (products should give one doublet and one triplet signal in the ^{31}P NMR spectra).

Conclusions

A series of three coordinate gold complexes which luminesce in solution at room temperature has been synthesized. The novel emission transition in these complexes is a metal centered $d \leftarrow p$ transition. The lifetime ($\tau = 21.1 \mu\text{s}$) in solution is long enough for the gold moiety to interact with other compounds and act as a potent photo-reductant with a $(\text{Au}(\text{I})^*/\text{Au}(\text{II}))$ potential of 2.4 V. The excited gold complex is capable of reducing halo aromatics such as bromobenzene. Photo-reactions with haloaromatics and haloalkanes results in halo abstraction of X^- and a total transfer of two electrons to the substrate.

The only complexes which display the long-lived luminescence in solution are $\text{Au}_2(\text{dcpe})_3^{2+}$, $\text{Au}_2(\text{dipe})_3^{2+}$, $\text{Au}(\text{PPh}_3)_3^+$, and $\text{Au}_2(\text{dppb})_3^{2+}$. In all four of these cases the emission is ascribed to a $^1\text{A}_1 \leftarrow \text{E}'$ ($^3\text{E}''$) emission. The corresponding absorption transition has also been identified as the lowest energy absorption band in $\text{Au}_2(\text{dcpe})_3^{2+}$, and $\text{Au}_2(\text{dipe})_3^{2+}$. It is clear that the Au-Au interaction is not crucial for solution emission as suggested by previous literature since none of solution emissive complexes have a significant Au-Au interaction.

The crucial aspect for emission from an isolated $\text{Au}(\text{I})$ monomer unit is the coordination environment of the metal center. Three coordinate complexes are the only

type of monomers observed to emit. In comparison to the two and four coordinate complexes, the three coordinate species have the greatest electron density on the Au(I) atom while still preserving a non-bonding p orbital as the LUMO. Two coordinate complexes have no low energy $d \rightarrow p$ transitions, because the reduced electron density on the Au(I) center stabilizes the d_{xy} , $d_{x^2-y^2}$ orbitals relative to the p_z orbital. Four coordinate compounds have more electron density on the Au(I) center, but the LUMO is a high energy σ^* p orbital so the $d \rightarrow p$ transitions are high in energy.

The three coordinate environment also leads to solution emission not observed for the two coordinate gold dimers. Emission is observed for the two coordinate dimers $\text{Au}_2(\text{dcpe})_2^{2+}$ and $\text{Au}_2(\text{dipe})_2^{2+}$ in methanol:ethanol glass at 77 K, with an $E_{\nu_0-\nu_0}$ of 404 nm for the $^1A_g \rightarrow ^3B_{1u}$ ($d\sigma^* \rightarrow p\sigma$) transition. The $E_{\nu_0-\nu_0}$ of 418 nm is similar to the $E_{\nu_0-\nu_0}$ of 432 nm for the $^1A_1 \rightarrow E'$ ($^3E''$) transition of the three coordinate complexes, yet only the three coordinate complexes emit in solution. The sterics of the three coordinate environment reduce the non-radiative decay rate by protecting the metal center from solvent collisions. The two coordinate dimers have open areas for solvent interactions, which may deactivate the excited state by energy transfer.

There is a great deal of distortion in the excited state of the three coordinate gold complexes as evidenced by the large Stokes shift of $7,800 \text{ cm}^{-1}$ for $\text{Au}_2(\text{dcpe})_3^{2+}$. The corresponding reorganization energy of the excited state, λ_{ex} , is 11 kcal/mol.²² This energy reflects the increase in bonding to the phosphines due to the removal of an electron from a d M-L σ^* orbital. The Stokes shift for the two coordinate dimers observed in the 77 K glass is nearly twice as large ($14,700 \text{ cm}^{-1}$), with $\lambda_{\text{ex}} = 21 \text{ kcal/mol}$. The increase in the excited state reorganization energy evinces the large increase in the strength of the Au-Au bond due to the removal of an electron from the d σ^* orbital and occupation of the p σ orbital.

The compounds $\text{Au}_2(\text{dcpe})_3^{2+}$ and $\text{Au}_2(\text{dipe})_3^{2+}$ are the only compounds to my knowledge that have isolated AuP_3 units which are stable in solution. The other three

coordinate gold complexes reported are solids which undergo equilibria in solution (such as $\text{Au}(\text{PPh}_3)_3^+$ mentioned earlier) to form two coordinate and four coordinate complexes. The equilibria are evident by broad ^{31}P NMR signals which split into multiple signals upon cooling. Both $\text{Au}_2(\text{dcpe})_3^{2+}$ and $\text{Au}_2(\text{dipe})_3^{2+}$ show one distinct triplet signal for the bridging phosphines and one distinct doublet signal for the chelating phosphines with the appropriate 1:2 integration ratio. These patterns would be severely broadened if ligands were labile on the NMR time scale. Solution equilibria may be responsible for some of the emission observed in previous literature. For example, $\text{Au}_2(\text{dmpm})_3^{2+}$ displays the same strong emission as $\text{Au}_2(\text{dcpe})_3^{2+}$, so trace amounts of $\text{Au}_2(\text{dmpm})_3^{2+}$ in a solution of $\text{Au}_2(\text{dmpm})_2^{2+}$ will lead to emission. These stable three coordinate complexes offer a unique opportunity for studying the potential photochemistry of gold(I) complexes.

References

- (1) King, C.; Wang, J.C.; Khan, Md. N. I.; Fackler, J.P. Jr. *Inorg. Chem.* **1989**, *28*, 2145.
- (2) (a) Che, C.M.; Wong, W.T.; Lai, T.F.; Kwong, H.L. *J. Chem. Soc., Chem. Commun.* **1989**, 243. (b) Che, C.M.; Kwong H.L.; Yam, V.W.W.; Cho, K.C. *J. Chem. Soc., Chem. Commun.* **1989**, 885.
- (3) (a) Che, C.M.; Kwong, H.L.; Poon, C.K.; Yam, V.W.W. *J. Chem. Soc., Dalton Trans.* **1990**, 3215. (b) Yam, V.W.W.; Che, C.M. *J. Chem. Soc., Dalton Trans.* **1990**, 3747.
- (4) Miskowski, V.M. unpublished results.
- (5) Roundhill, D.M.; Gray, H.B.; Che, C.M. *Accts. Chem. Res.* **1989**, *22*, 55.
- (6) Fordyce, W.A.; Brummer, J.G.; Crosby, G.A. *J. Am. Chem. Soc.* **1981**, *103*, 7061.
- (7) Harvey, P.D.; Gray, H.B. *J. Am. Chem. Soc.* **1988**, *110*, 2145.
- (8) The singlet triplet crossover must be competitive with fluorescence and non-radiative decay from the singlet state, for the excitation spectrum to match the absorption spectrum.
- (9) Bailey, J.B.; Hill, M.H.; Miskowski, V.M.; Gray, H.B. manuscript in preparation.
- (10) Sweeney, R.J. Ph.D. Thesis, California Institute of Technology, 1990.
- (11) Cloke, F.G.N.; Gibson, C.G.; Green, M.L.H.; Mtetwa, V.S.B.; Prout, K. *J. Chem. Soc., Dalton Trans.* **1988**, 2227-2229.
- (12) Grim, S.O.; Barth, R.C.; Mitchell, J.D.; Del Guadio, J. *Inorg. Chem.* **1977**, *16*, 1776-1779.
- (13) Glemser, O.; Sauer, H. *Handbook of Preparative Inorganic Chemistry: Vol II, second edition*, **1965**, Academic Press, New York, New York.
- (14) Parish, R.V.; Parry, W.; McAuliffe, C.A. *J. Chem. Soc., Dalton Trans.* **1981**, 2098-2194.

- (15) Jones, G.C.H.; Jones, P.G.; Maddock, A.G.; Mays, M.J.; Verganao, P.A.; Williams, A.F. *J. Chem. Soc., Dalton Trans.* **1977**, 1440-1443.
- (16) U'son, R.; Laguna, A.; Vicente, J.; Garcia, J.; Jones, P.G.; Sheldrick, G.M. *J. Chem. Soc., Dalton Trans.* **1981**, 655-657.
- (17) Savas, M.M.; Mason, W.R. *Inorg. Chem.* **1987**, *26*, 301-307.
- (18) Fenske Jr., G.P.; Mason, W.R. *Inorg. Chem.* **1974**, *13*, 1783-1786.
- (19) Andrieux, C.P.; Blocman, C.; Dumas-Bouchiat, J-M; Saveant, J-M. *J. Am. Chem. Soc.* **1979**, *101*, 3431-3441.
- (20) (a) Murray, H.H.; Fackler, J.P.; Porter, L.C.; Briggs, D.A.; Guerra, M.AA.; and Lagow, R.J. *Inorg. Chem.* **1987**, *26*, 357-363. (b) Khan, N.I.; Fackler Jr., J.P.; King, C.; Wang, J.C.; Wang, S. *Inorg. Chem.* **1988**, *27*, 1672-1673.
- (21) Strickler, S.J.; Berg, R.A. *J. Chem.. Phys.*, **1962**, *37*, 814.

Chapter 3

Electron Transfer at High Driving Forces

Background.

The semi-classical Marcus expression (Equation 1) predicts that ET rates, k_{ET} , are governed by three factors: the matrix coupling element, H_{ab} , the driving force, $-\Delta G^0$,

$$k_{ET} = \left\{ \frac{2(H_{ab}^2)}{h} \sqrt{\frac{\pi^3}{\lambda RT}} \right\} e^{-\left(\frac{(\Delta G^0 + \lambda)^2}{4RT(\lambda)}\right)} \quad 1.$$

and the reorganization energy, λ .¹ The Marcus expression is derived from transition state theory, with the barrier to ET defined as the difference in energy between the minimum of the reactant potential surface and the point where the reactant potential surface crosses the product potential surface. All of the parameters in the Marcus equation can be readily identified by looking at a plot of the potential surfaces for the reactants and the products: the free energy change for the reaction, $-\Delta G^0$, is the difference between the minima of the reactant and product potential wells; λ is the vertical energy difference between the reactant and product surfaces at the reactant surface minimum when $-\Delta G^0 = 0$; H_{ab} is represented by one half of the separation between the potential surfaces at the crossing avoidance point (Figure 3.1).

Marcus theory predicts that for a given H_{ab} and λ , k_{ET} will increase as the driving force ($-\Delta G^0$) increases until a maximum rate is reached at $-\Delta G^0 = \lambda$; the domain where $-\Delta G^0 < \lambda$ is known as the "normal region." When $-\Delta G^0 = \lambda$ there is no barrier to electron transfer, because the product potential surface intersects the minimum of the reactant potential surface (Figure 3.2). At higher driving forces ($-\Delta G^0 > \lambda$) a new barrier to ET arises as the reactant and product potential surfaces become nested (Figure 3.3). The new barrier to ET causes k_{ET} rates to decrease as the driving force increases; the domain where $-\Delta G^0 > \lambda$ is referred to as the "inverted region." A plot of $\ln(k_{ET})$ vs. $-\Delta G^0$ results in a parabola with a maximum rate at $-\Delta G^0 = \lambda$ (Figure 3.4). The matrix coupling element, H_{ab} , is a function of the electronic coupling between the donor and the acceptor. Since H_{ab} only appears in the pre-exponential term, a change in H_{ab} simply moves the entire parabola vertically (Figure 3.5); as the

Figure 3.1. Reactant and product energy surfaces for $\Delta G^0 = 0$ (self exchange ET)

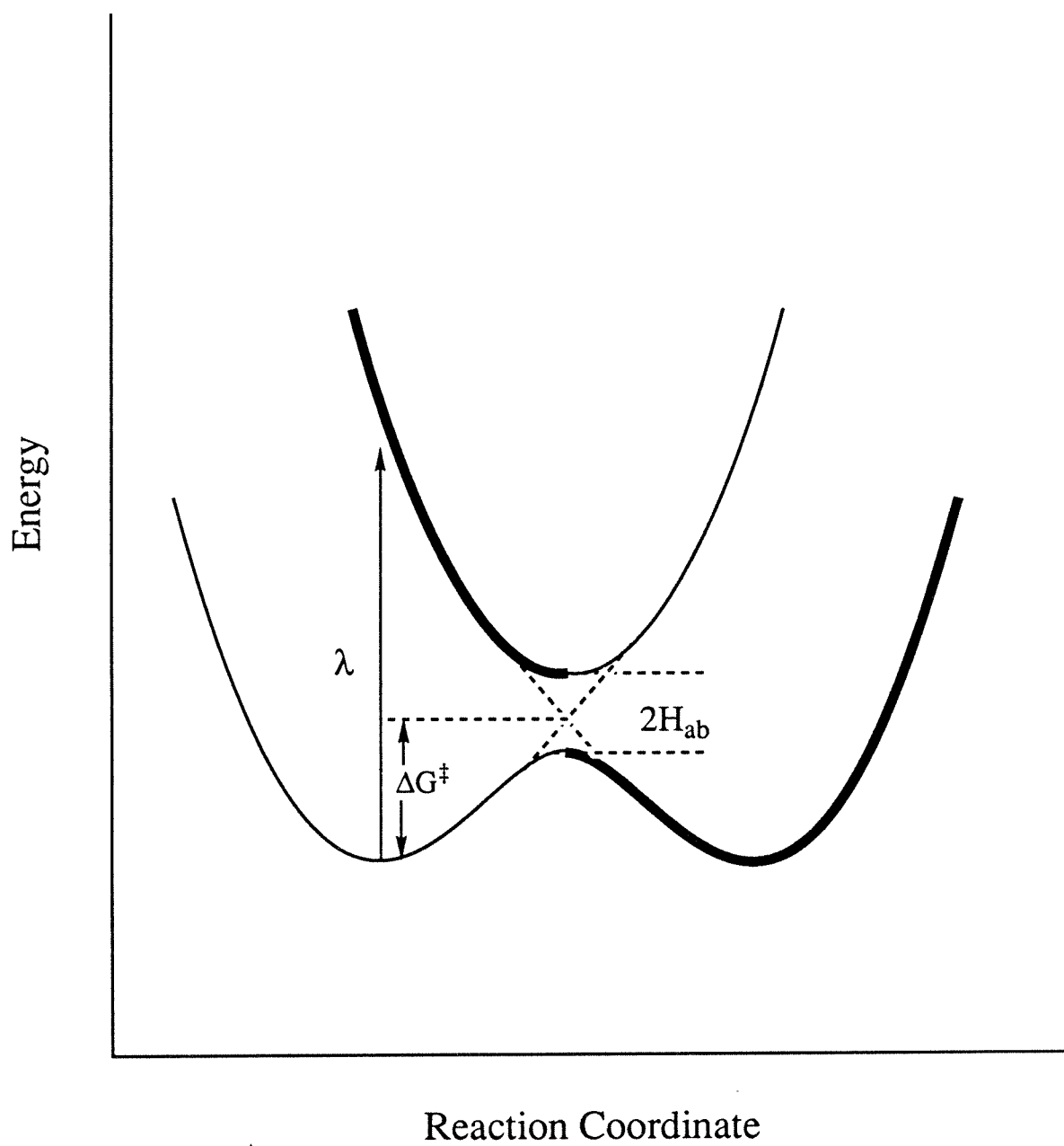


Figure 3.2. Reactant and product energy surfaces for $\Delta G^0 \approx \lambda$.

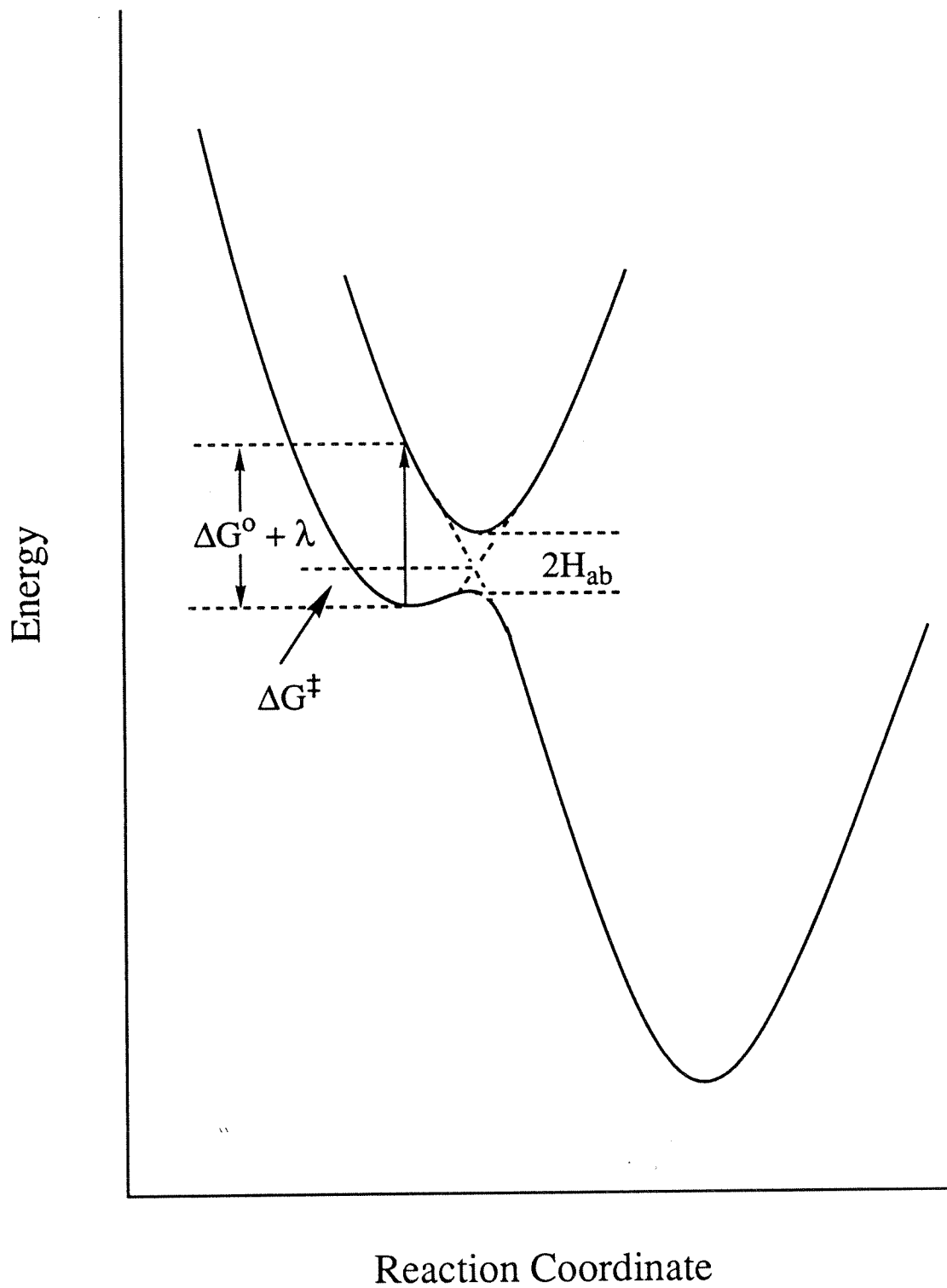


Figure 3.3. Reactant and product energy surfaces for $\Delta G^0 > \lambda$.

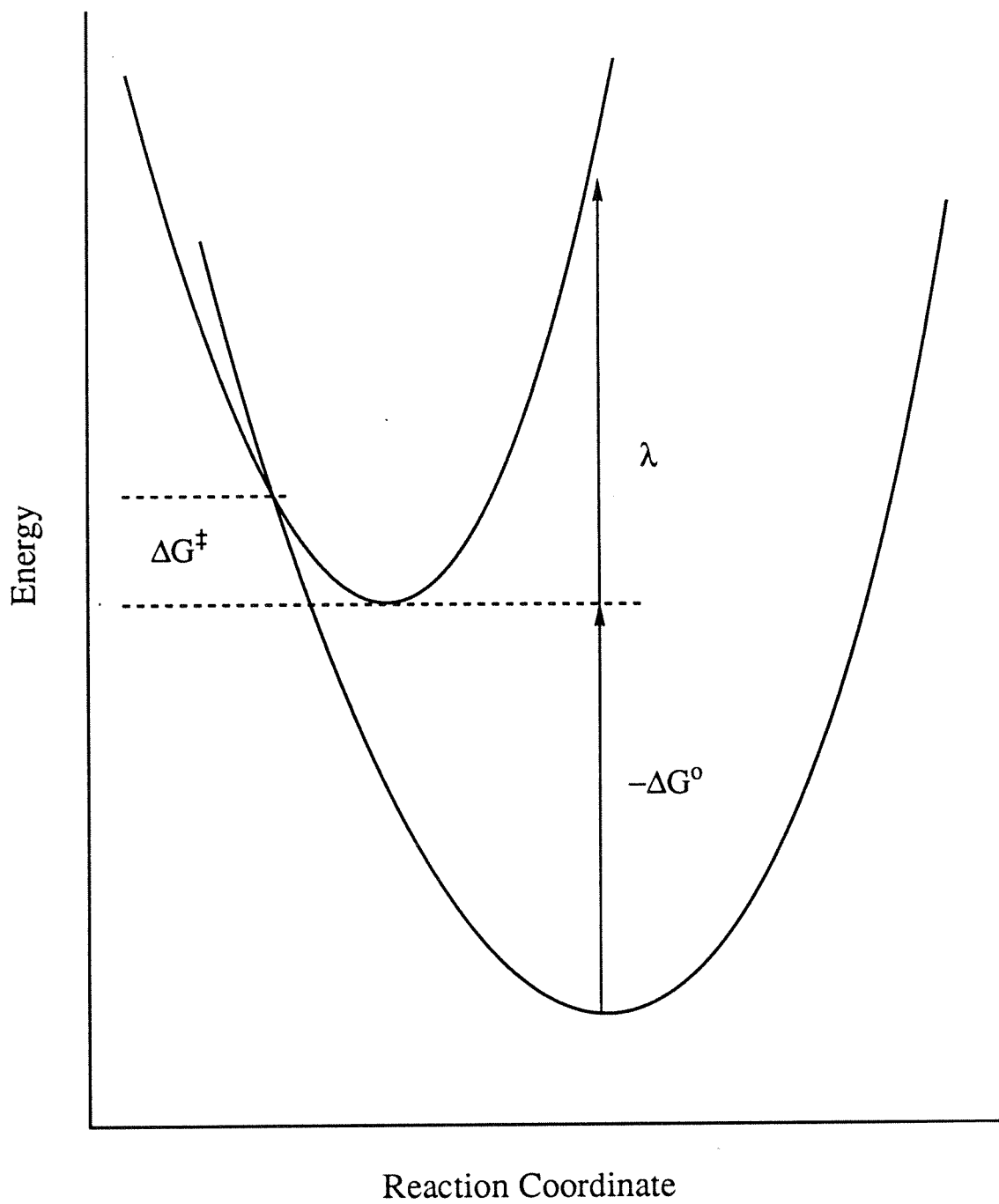


Figure 3.4 Theoretical Marcus plot of $\ln(k_{ET})$ vs $-\Delta G^0$.

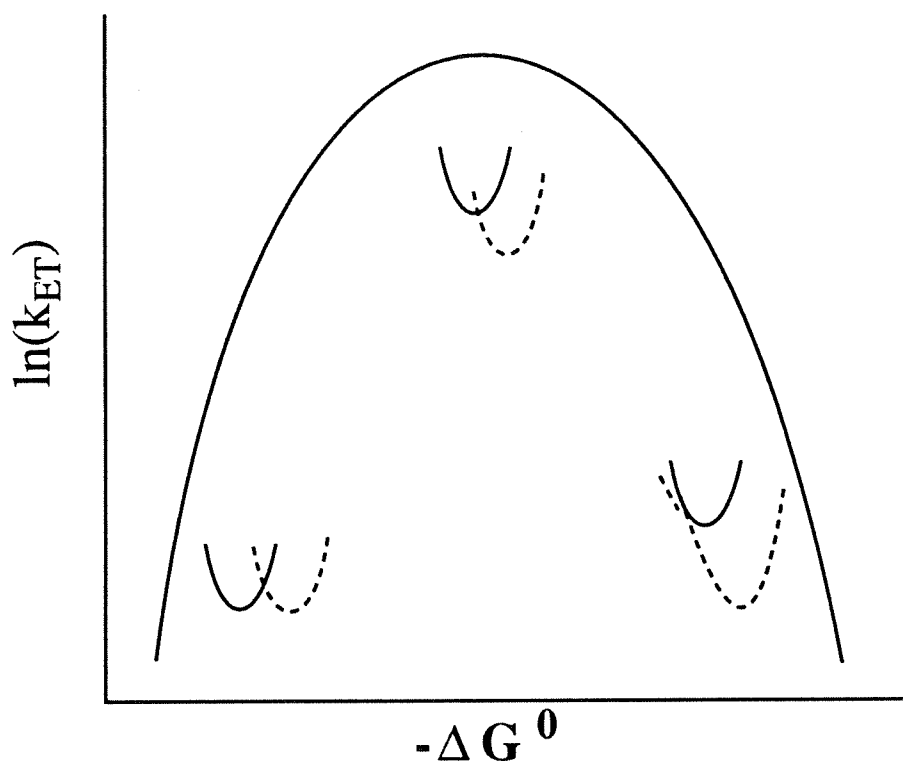


Figure 3.5. Coupling effects on the theoretical Marcus curve; $H_{ab}(a) > H_{ab}(b)$.

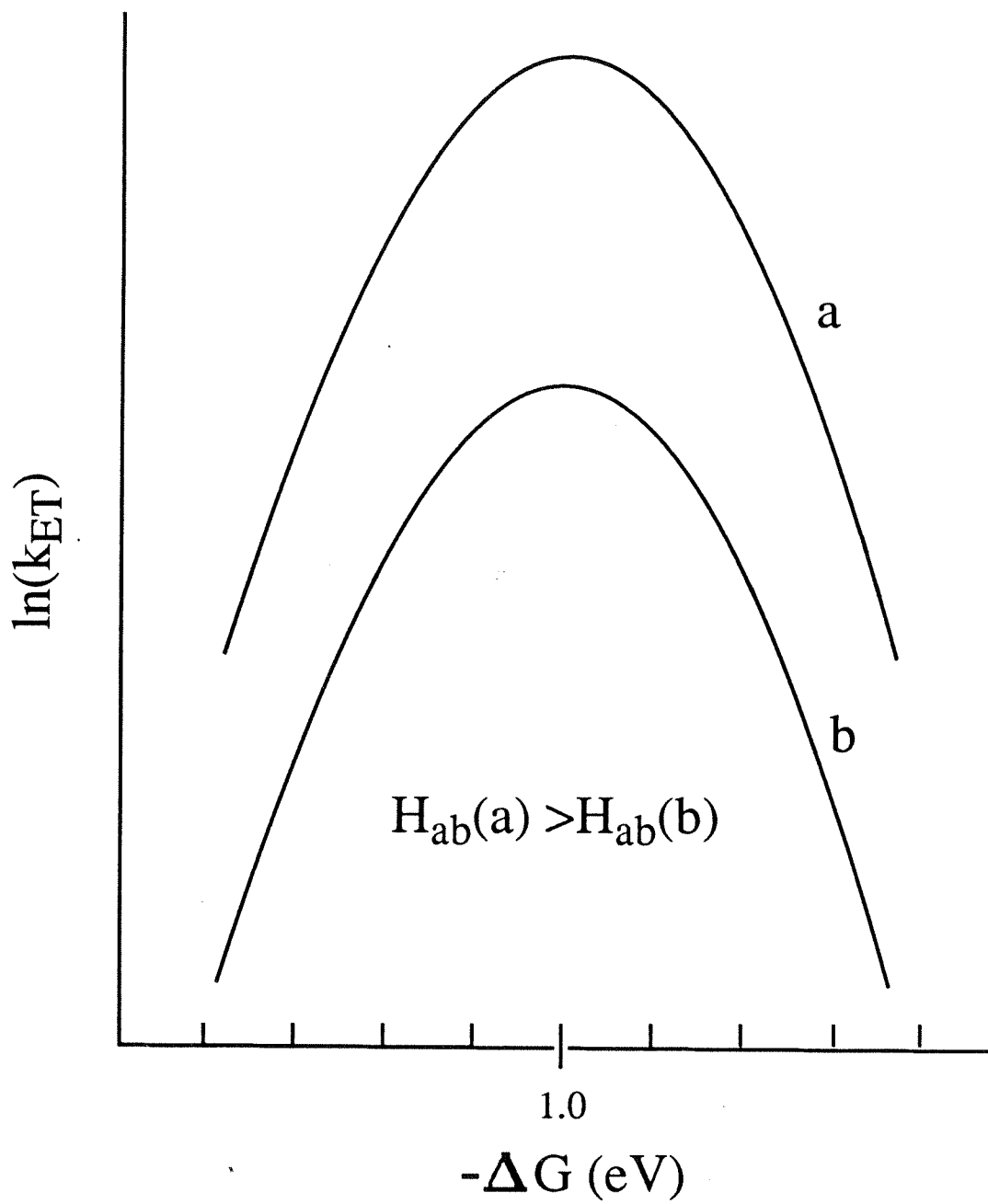
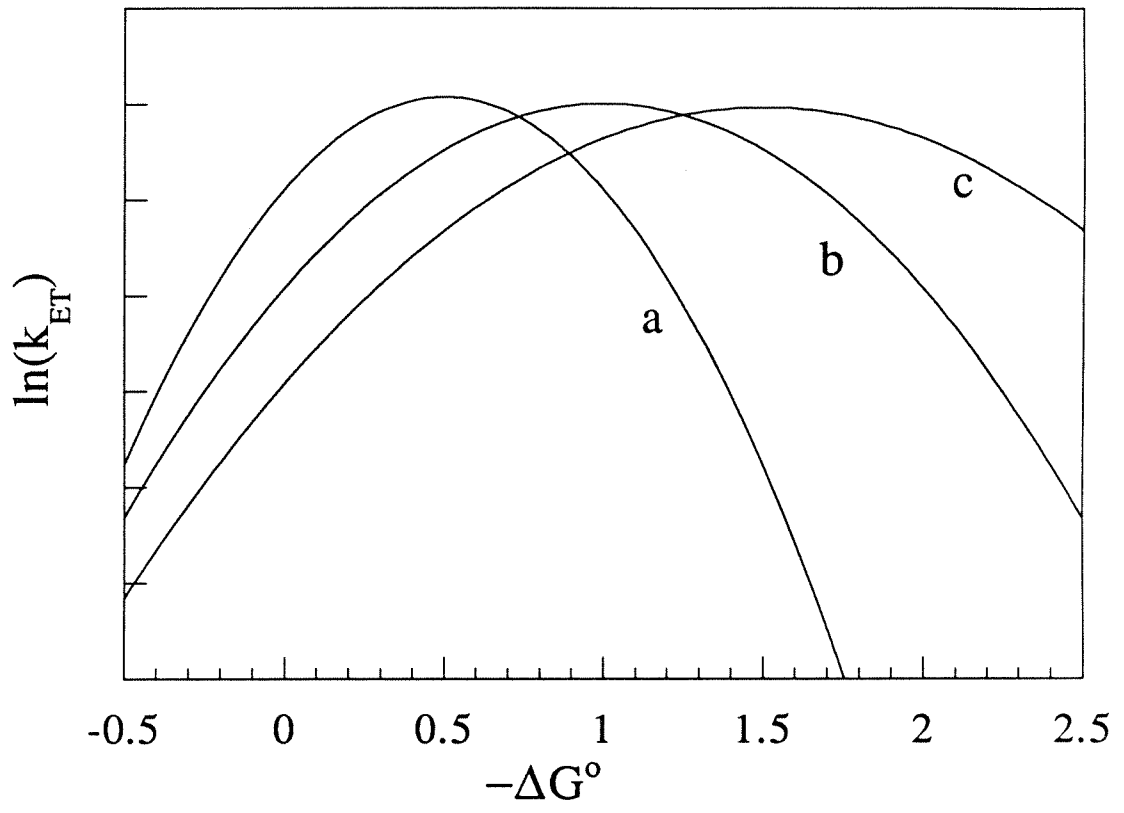
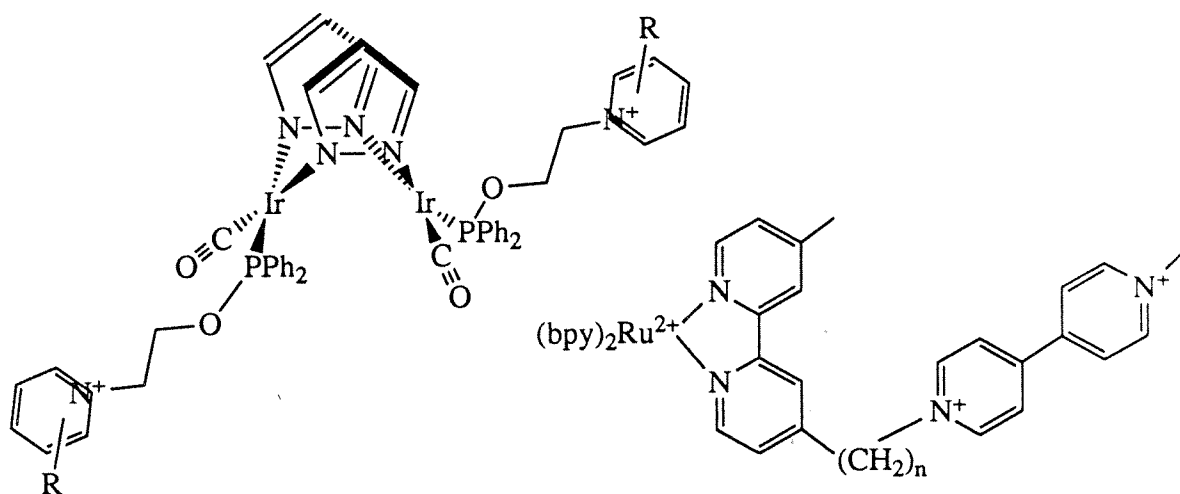


Figure 3.6. Reorganization energy effects on the theoretical Marcus curve; $\lambda(a) = 0.5 \text{ eV}$, $\lambda(b) = 1.0 \text{ eV}$, $\lambda(c) = 1.5 \text{ eV}$.



coupling increases all of the ET rates increase. The reorganization energy, λ , represents a combination of the energy required for the solvent dipoles to reorient, λ_s , and the energy required for any bond length or bond angle changes within the molecule, λ_i , during the ET reaction. Changing λ affects both the position of the maximum and the shape of the curve; as λ increases the maximum rate occurs at a higher driving force and the parabola becomes broader (Figure 3.6). It has been suggested that the back ET rate in the initial charge separation step of photosynthesis is slow because the driving force for the recombination reaction, $-\Delta G_b$, is much greater than λ so the rate is in the "inverted region" of the parabola, while the forward photo-induced ET reaction has a driving force, $-\Delta G_f$, near λ to give an ET rate close to the maximum of the Marcus curve.

There is a plethora of experimental evidence that supports Marcus theory at low driving forces ($-\Delta G^0 < \lambda$), and in the last several years there have also been many reports of recombination ET rates that are inverted at high driving forces ($-\Delta G^0 > \lambda$).^{2a-h} One of the earliest reports of the inverted region came from the pulse radiolysis experiments of Closs and Miller, who reported inverted behavior for an intramolecular charge shift reaction.^{2a} Mallouk et al. have recently attached a methyl viologen acceptor to the



Intramolecular Donor - Acceptor Complexes

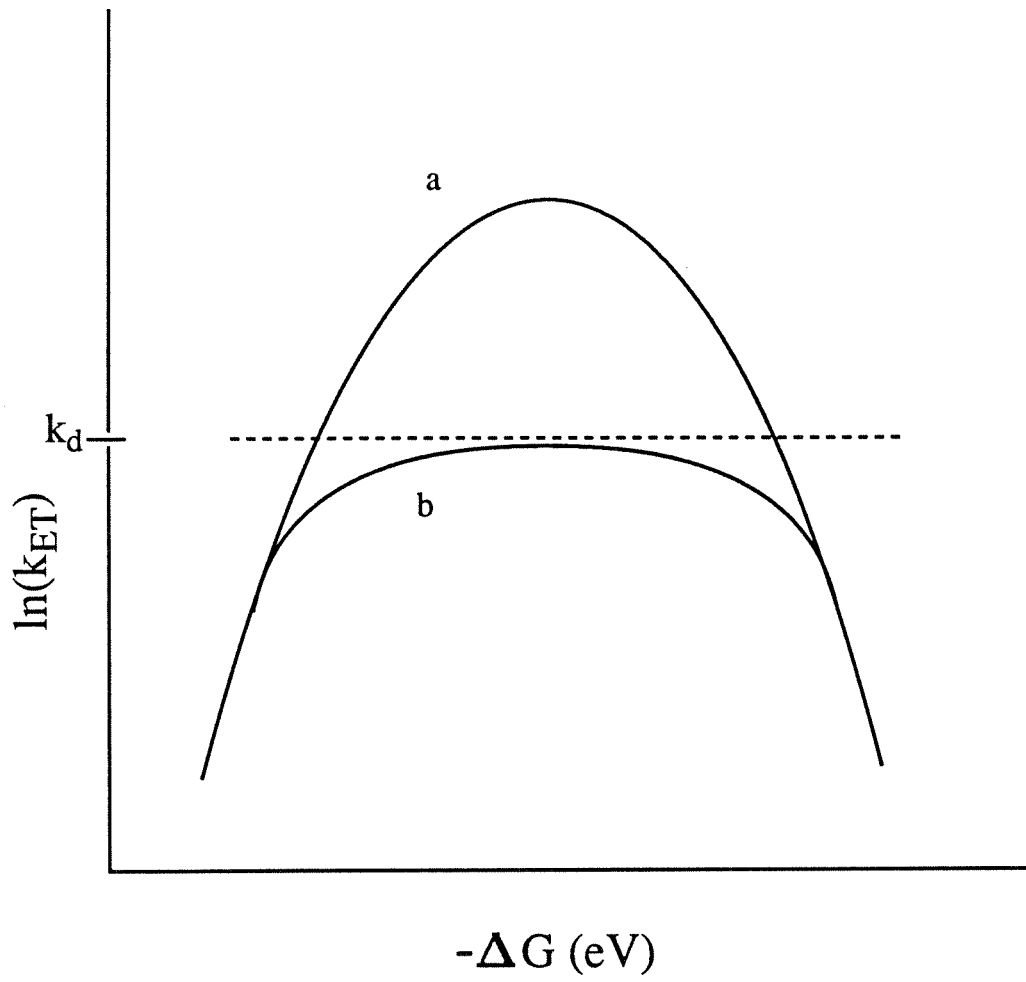
4' position of a bipyridine (bpy) ligand of $\text{Ru}(\text{bpy})_3^{2+}$ and studied the photo-induced ET rates as a function of the driving force.^{2h} Forward rates from the ruthenium excited state to the methyl viologen acceptor reach a maximum value of $1.4 \times 10^{11} \text{ s}^{-1}$, while the recombination rates show inverted behavior with driving forces greater than 1 eV. Inverted behavior has also been observed by Gray et al. with a series of pyridinium phosphinites attached to an iridium dimer, where it is possible to distinguish forward ET rates from the singlet and triplet excited states of the iridium center independently.^{2g} They observed forward ET rates from the singlet excited state as fast as $1 \times 10^{11} \text{ s}^{-1}$, and inverted recombination rates when $-\Delta G_b > 1.0 \text{ eV}$. One of the iridium complexes has a fairly long-lived charge separated state with a forward ET rate of $2.7 \times 10^{10} \text{ s}^{-1}$ and a slower (inverted) back ET rate of $6.7 \times 10^7 \text{ s}^{-1}$.

Although there have been several reports of inverted behavior for recombination and charge shift reactions in intramolecular systems, there have been no observations of inverted behavior for a bimolecular system. Rhem and Weller reported bimolecular ET rates with a series of organic complexes for driving forces ranging from -0.25 eV to 2.65 eV. Their observed rates reached the diffusion limit at 0.25 eV and remained pegged at the diffusion limit all the way out to 2.65 eV, with no sign of inverted behavior.³

Introduction.

All of the reported "inverted" rates have involved the charge shift or recombination ET reactions of intramolecular systems. The lack of any experimental inverted rates for the bimolecular systems is curious, especially in the case of Rhem and Weller who monitored ET rates for driving forces up to 2.65 eV. Inverted behavior may be more difficult to observe in bimolecular systems because ET rates faster than the diffusion rate in the solution cannot be measured. This diffusion limit caps the top of any Marcus curve which exceeds the diffusion rate (Figure 3.7); a strongly coupled system will have ET rates at the diffusion limit over a wide driving force range. However, the ET rates observed by Rhem and Weller cover such

Figure 3.7. Marcus plots for bimolecular ET; (a) shows the theoretical first order k_{ET} , and (b) shows the theoretical curve corrected for the diffusion limiting rate k_d .



a vast range that it is difficult to believe the diffusion limit alone can account for the lack of inverted behavior.

High driving force ET rates were investigated in two different bimolecular systems. First, ET from the excited state donor, $\text{Au}_2(\text{dcpe})_3^{2+*}$, to a series of pyridinium acceptors (py^+) was examined. The $E_{\text{V}_0-\text{V}_0}$ of 2.3 eV for the emissive state makes it possible to study forward ET rates with high driving forces. High driving force recombination ET rates from pyridinyl radicals ($\text{py}\cdot$) to the iridium dimer $[\text{Ir}(\text{cod})(\text{pz})]_2^+$ (Ir_2^+) were also examined (cod = cyclooctadiene, pz = pyrazole). Forward ET rates from $[\text{Ir}(\text{cod})(\text{pz})]_2$ (Ir_2) to py^+ acceptors have been shown to increase as the driving force increases until they reach the diffusion limit and then remain diffusion limited out to a driving force of 1.03 eV.⁴ No inverted behavior was observed for these forward rates.

The recombination ET rates for the bimolecular system were investigated, because inverted behavior was reported for intramolecular recombination rates in a system with a similar donor and acceptor.^{2g} The donor for the bimolecular recombination rates is the pyridinyl radical and the acceptor is Ir_2^+ . In the intramolecular system the cod ligand is replaced by a CO and a phosphinite; the pyridium is linked to the iridium dimer center via the phosphinite. Electron-transfer rates of the intramolecular system show classical Marcus behavior, in which the forward ET rates fall in the normal region and the recombination ET rates are in the inverted region. The best fit Marcus curve has a λ of 0.85 eV, and an H_{ab} of 35 cm^{-1} . The bimolecular system should have a smaller value for H_{ab} , since the donor and acceptor are not covalently linked to one another. The Ir_2 donor and py^+ acceptor undergo identical charge changes during ET for both systems, so the reorganization energy should be close to 0.85 eV for the bimolecular system. Recombination rates for the bimolecular system have driving forces as high as 1.82 eV, so they should be deeply inverted.

Experimental Section.

Materials. The iridium(III) chloride was a loan from the Johnson Mathey heavy metals program. All other chemicals were reagent grade or better and purchased from the

Aldrich Chemical Company. The synthesis of $\text{Au}_2(\text{dcpe})_3^{2+}$ has been described in chapter two.

Lifetime and Transient Absorption Measurements. The basic layout of the time resolved emission and absorption experiments is as follows: the excitation source was either the second ($\lambda_{\text{max}} = 532 \text{ nm}$; used for Ir_2) or third ($\lambda_{\text{max}} = 355 \text{ nm}$; used for $\text{Au}_2(\text{dcpe})_3^{2+}$) harmonic of a Quanta-Ray Nd-YAG laser with 20 ns pulse width ; a PTi arc lamp supplied the white light source, a DH 10 SA Inc. monochrometer was placed before the detector; a R955 Hamamatsu PMT functioned as the detector; a RTD 710A digitizer digitized the analog signal; a 386 PC was used to work up the data (Figure 3.8). The arc lamp power was 68 W, and in the case of weak signals the arc lamp was pulsed at 6 Hz. The laser power was < 10 mJ at the sample to avoid multiphoton reactions. The focusing mirrors (labeled c in Figure 3.8) are designed with a 1 cm radius hole for the laser pulse to pass through. For time bases less than 1 ms the signal was amplified with a fast amplifier designed at Brookhaven National Laboratories, and for time bases greater than 1 ms the signal was amplified with a commercial slow amplifier. All solutions for ET studies with $\text{Au}_2(\text{dcpe})_3^{2+}$ were 0.1 M in TBA PF_6 to ensure that the ionic strength remained constant.

Spectroelectrochemistry. The thin layer cell used for the spectroelectro-chemistry has been described previously.⁵ For determining the spectrum of the reduced methyl viologen radical $\text{MeV}^{\cdot+}$ in acetonitrile, a new cell was constructed out of Ultem, which does not degrade in organic solvents. A Princeton 174A polarographic analyzer was used to apply a constant potential and a Varian Cary 219 spectrophotometer was used to record the spectrum. A sample of $[\text{MeV}](\text{PF}_6)_2$ was weighed out in a dry box with a nitrogen atmosphere and diluted to a concentration of 375 μM . The solution was placed into the thin layer cell and both the reference and auxiliary electrodes were put in place prior to removal from the dry box. A constant potential of -550 mV vs NHE was applied and the absorbance at 395 nm was monitored as a function of time. Absorbance increased dramatically as the radical was formed and then plateaued once the bulk electrolysis reached completion. When

Figure 3.8. Laser arrangement for time resolved emission and absorption; (a) indicates a laser mirror, (b) is a 50% reflecting mirror for the 308 nm fundamental line of the excimer laser, (c) and (d) indicate a broad band focussing mirror with a focal length of 50 cm, (e) indicates a broad band mirror.

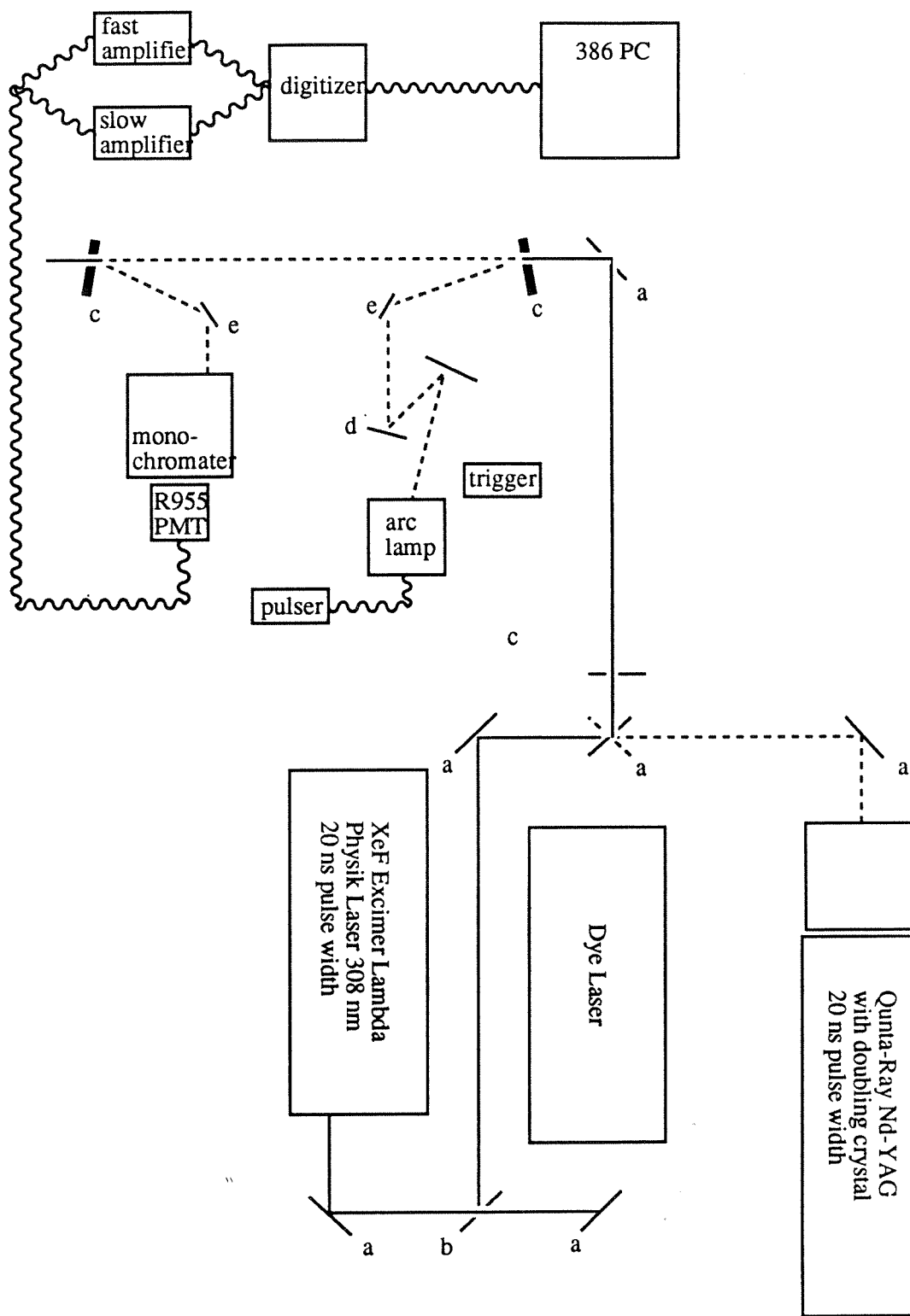


Figure 3.9. Absorption spectrum of MeV.

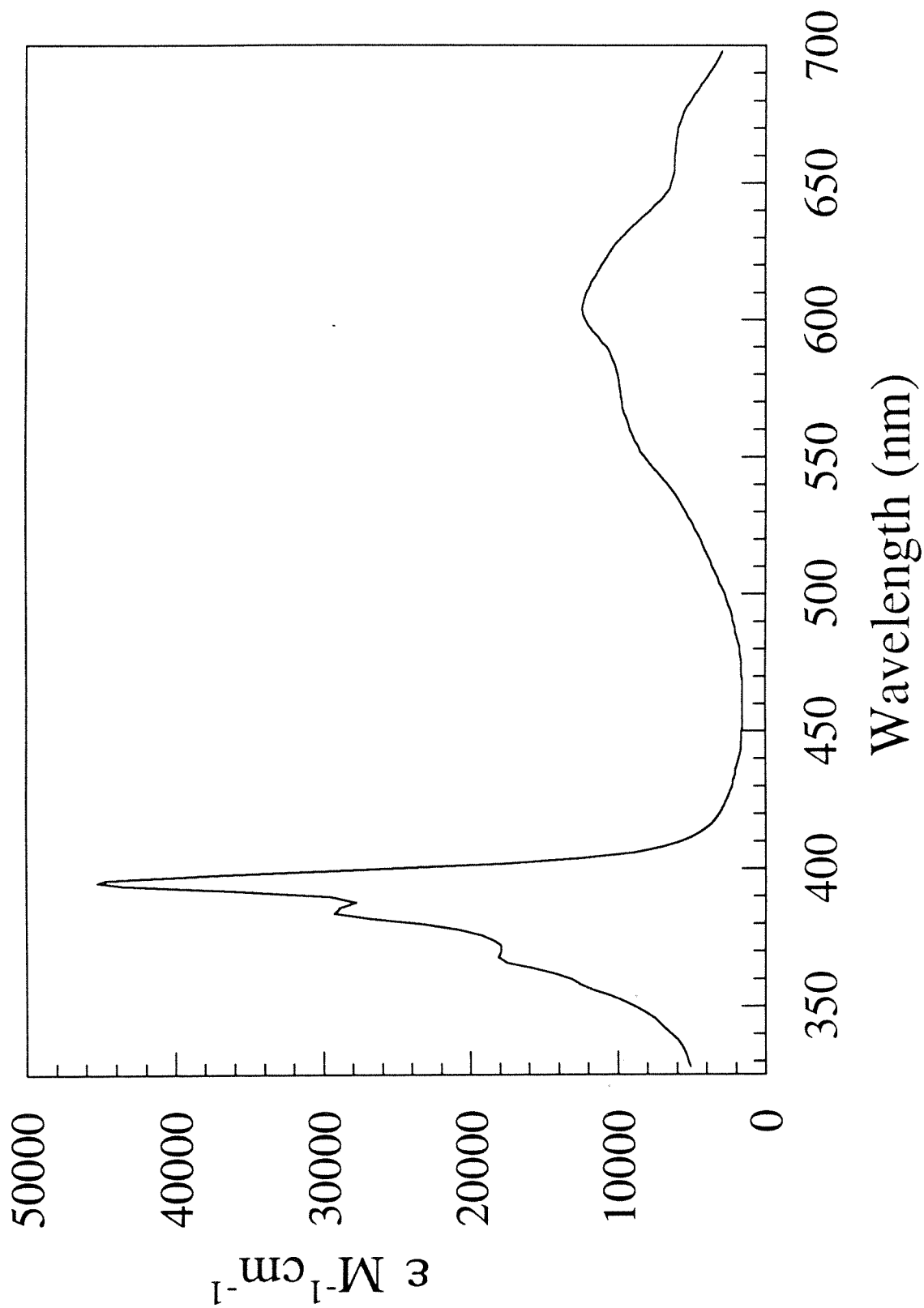


Figure 3.10. Transient absorption spectrum of a solution containing MeV^{2+} (380 μM) and Ir_2 (160 μM) at 390 nm, excitation at 532 nm.

----> FIXED PARAMETER; ! ----> FIXED SIGN

$$y(t) = 1/(C0+C1*t)$$

C0 = 7.544E+00

C1 = 7.156E+04

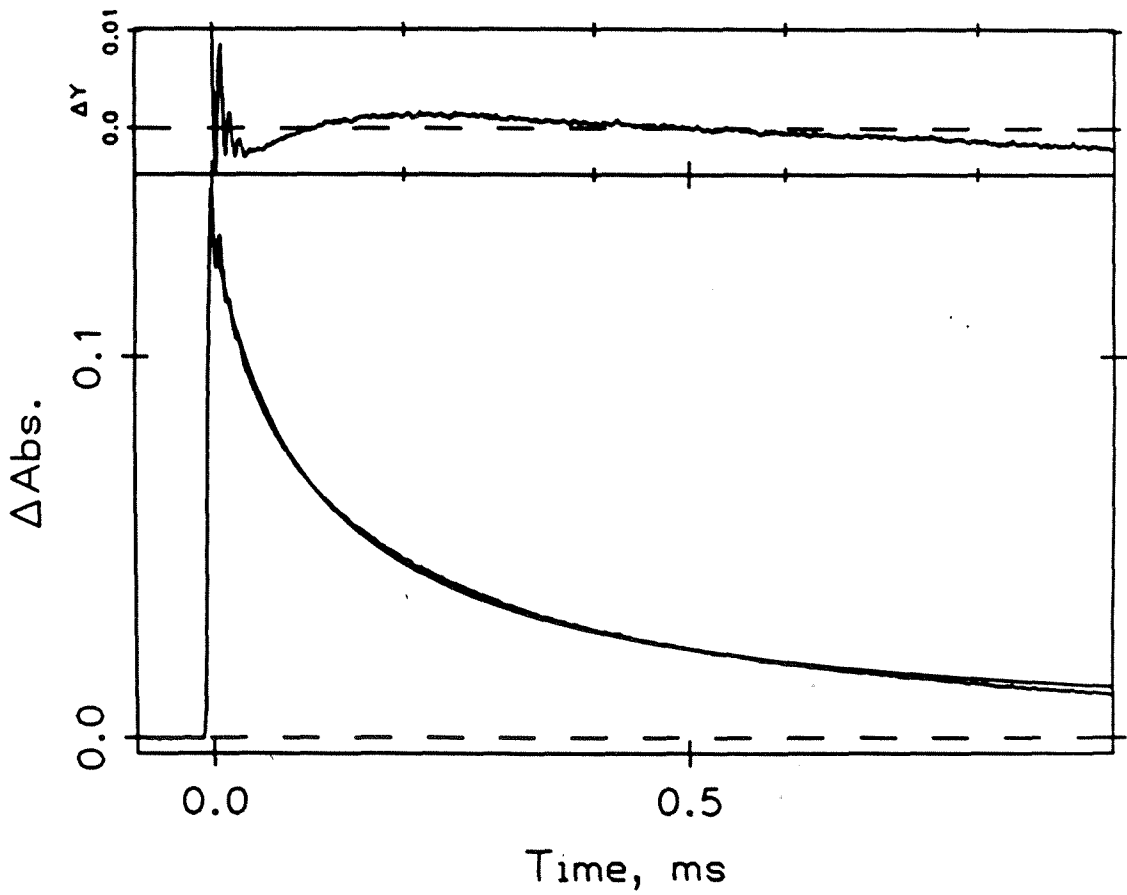


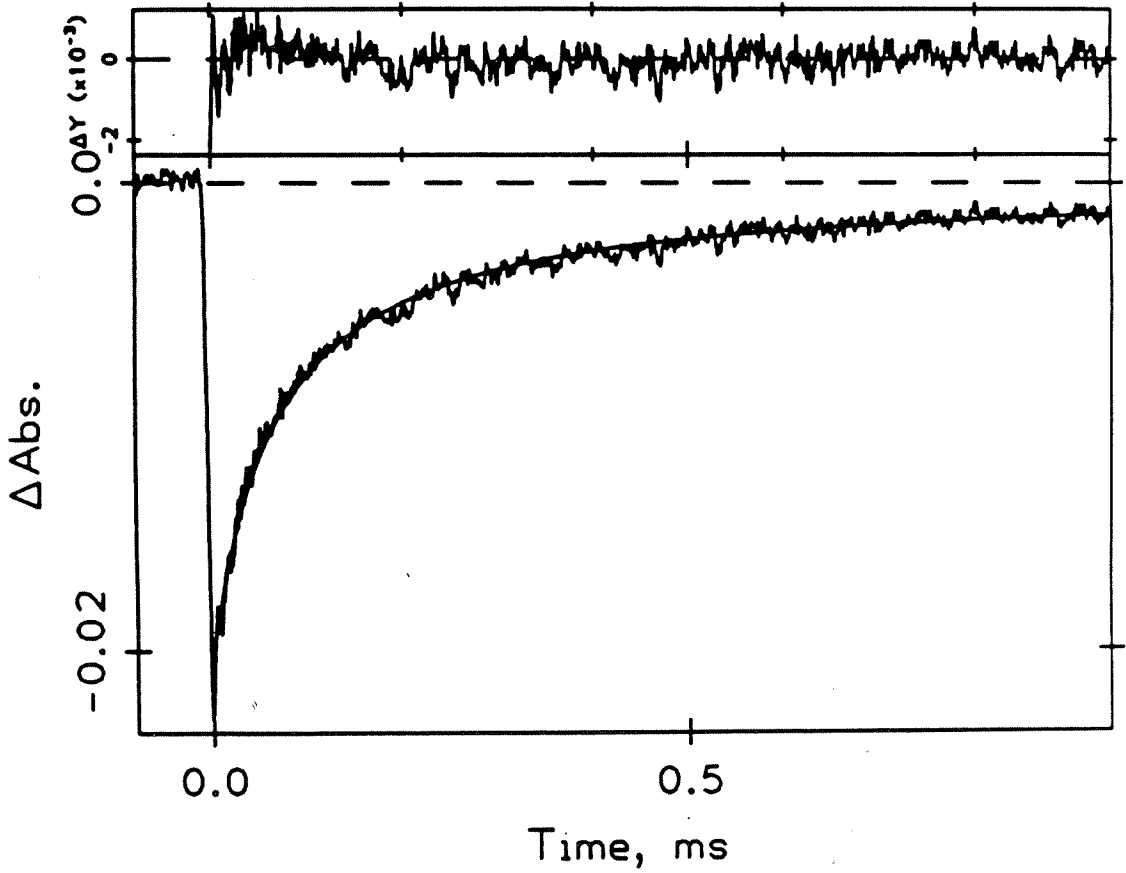
Figure 3.11. Transient absorption spectrum of a solution containing MeV^{2+} and Ir_2 at 500 nm, excitation at 532 nm.

---> FIXED PARAMETER; ! ---> FIXED SIGN

$$y(t) = 1/(C0+C1*t)$$

$$C0 = -4.930E+01$$

$$C1 = -7.363E+05$$



the absorbance remained unchanged for one minute, a spectrum of the $\text{MeV}^{\cdot+}$ was taken from 700 nm to 250 nm (Figure 3.9). The potential was then changed to -350 mV vs. NHE to regenerate MeV^{2+} . Absorbance at 390 nm was monitored as a function of time and when the absorbance remained unchanged for one minute a spectrum of MeV^{2+} was taken from 700 nm to 250 nm. The spectrum of MeV^{2+} was taken to ensure no degradation had occurred which could affect the $\text{MeV}^{\cdot+}$ spectrum. The ϵ for $\text{MeV}^{\cdot+}$ at 605 nm agreed well with the published value.⁶

Determination of $\Delta\epsilon$. The $\Delta\epsilon$ at 500 nm between Ir_2 and Ir_2^+ was necessary to convert the measured ΔOD values in the transient absorption spectra to concentrations. The ϵ for Ir_2 was easily determined by measuring the absorption spectrum. Unfortunately, the electrochemistry of Ir_2 is not completely reversible, so the ϵ for Ir_2^+ could not easily be determined by spectroelectrochemistry. Instead, the ϵ of Ir_2^+ was determined from transient absorption spectra taken in the presence of 380 μM MeV^{2+} . The MeV^{2+} quenches the excited state of Ir_2 by ET, leading to the formation of Ir_2^+ and $\text{MeV}^{\cdot+}$. The spectra of MeV^{2+} , $\text{MeV}^{\cdot+}$, and Ir_2 are all known, and the $\text{MeV}^{\cdot+}$ radical is the only one of the three species which absorbs appreciably at 390 nm. A transient absorbance trace of Ir_2 with N-methylpyridinium was taken at 390 nm to verify that Ir_2^+ has no absorbance at 390 nm (the transient absorbance trace showed no ΔOD). For the solution of Ir_2 and MeV^{2+} the ΔOD at 390 nm depends solely on the concentration of $\text{MeV}^{\cdot+}$ (Equation 2).

$$\Delta\text{OD}_{390}(t) = \Delta\epsilon_{390}(\text{MeV}^{\cdot+}) * b * [\text{MeV}^{\cdot+}]_t \quad 2.$$

A transient absorbance trace at 390 nm can be used to determine the concentration of $\text{MeV}^{\cdot+}$ at any time ($[\text{MeV}^{\cdot+}]_t$; Figure 3.10). The ET reaction which leads to the formation of $\text{MeV}^{\cdot+}$ must also produce an equal amount of Ir_2^+ . Since the back ET reaction has a one to one stoichiometry for $\text{MeV}^{\cdot+}$ and Ir_2^+ , the concentration of the two species will be equal at all times and the ΔOD at any wavelength (ΔOD_n) can simply be expressed according to

$$\Delta\text{OD}_n(t) = \{\Delta\epsilon_n(\text{MeV}^{2+}/\text{MeV}^{\cdot+}) + \Delta\epsilon_n(\text{Ir}_2/\text{Ir}_2^+)\} * b * [\text{MeV}^{\cdot+}]_t \quad 3.$$

Equation 3. The $\Delta\epsilon_n$ (MeV²⁺/MeV⁺) is known for all wavelengths and $[\text{MeV}^{+}]_t$ can be determined from the transient absorbance trace at 390 nm, so that $\Delta\epsilon_n$ (Ir₂/Ir₂⁺) is readily

$$\frac{\Delta\text{OD}_n(t)}{\Delta\text{OD}_{390}(t)} = \frac{\Delta\epsilon_n(\text{MeV}^{2+}/\text{MeV}^{+}) + \Delta\epsilon_n(\text{Ir}_2/\text{Ir}_2^{+})}{\Delta\epsilon_{390}(\text{MeV}^{2+}/\text{MeV}^{+})} \quad 4.$$

obtained from a transient absorbance trace at the appropriate wavelength using Equation 4.

The transient absorbance trace at 500 nm shows a sharp bleach as Ir₂⁺ is produced by the forward ET and then a slow decay back to zero as the recombinant ET occurs (Figure 3.11).⁷

The $\Delta\epsilon_{500}$ (Ir₂/Ir₂⁺) was determined to be 7,000 cm⁻¹M⁻¹.⁸

[Ir(cod)(pz)]₂ The synthesis of the iridium dimer was adapted from the procedure described by Marshall.^{4,9} An excess of cod (12.0 mL) was added to a stirring solution of IrCl₃·3H₂O (5.0 g) and 100 mL of a 2:1 ethanol:water mixture in a 250 round-bottom Schlenk flask. The flask was equipped with a condenser and a bubbler, and then heated to reflux. After refluxing for 48 hours, a red product had precipitated. The solution was cooled to room temperature and the product, [Ir(cod)(Cl)₂]₂, was collected by vacuum filtration. If too much cod is used, or the ethanol:water ration is not quite right the cod will separate out and the product will remain dissolved in the cod layer. In this event the product can be precipitated by adding just enough isopropanol to solubilize the cod layer. The isolated red product was then added to 50 mL of freshly distilled, Ar purged THF in a 100 mL round-bottom Schlenk flask. The solution was stirred under Ar as a solution of pyrazole and excess triethylamine in 10 mL of THF was added dropwise. The solvent was removed from the resulting deep red solution under vacuum. The residue was chromatographed on a Florisil column under an Ar atmosphere with benzene as the eluant. Evaporation of the benzene produced deep red crystals which were dried under vacuum. The solid product is air stable and need not be stored under Ar, but solutions of the iridium dimer are air sensitive and must be prepared using degassed or Ar purged solvents. Analysis Calculated: C: 35.95; H: 4.11; N: 7.62. Found C: 36.13; H: 4.06; N: 7.32.

N-methyl pyridinium hexafluorophosphate⁴ The following method was used to prepare all of the hexafluoro phosphate salts. A three fold excess of the alkylating agent (iodomethane) was added to a solution of the pyridine or substituted pyridine (4 g) and 100 mL of a 1:1 acetone:ethanol mixture. The solution was refluxed for 24 hours. If the iodide salt precipitated upon cooling then it was collected by vacuum filtration, otherwise the solvent was removed by rotary evaporation under reduced pressure. The solid iodide salt, or the residue remaining after evaporation was dissolved in a minimum of water. Addition of a slight excess of ammonium hexafluorophosphate in 2 mL of water resulted in the precipitation of the hexafluorophosphate salt as a white powder. The white powder was collected by vacuum filtration, recrystallized from a 2:1:1 water:acetone:ethanol solution and dried under vacuum.

N-methyl 3,4-dicyanopyridinium tetrafluoroborate¹⁰ One equivalent of trimethyloxonium tetrafluoroborate was added to a stirring mixture of 3,4-dicyanopyridine and 40 mL of acetonitrile under nitrogen at room temperature. After stirring for four hours the solvent was removed by rotary evaporation. The residue was recrystallized from methanol/ether to give clear plates of the desired product. Analysis calculated for C₈H₆N₃BF₄: C, 41.60; H, 2.62; N, 18.19. Found: C, 41.91; H, 2.98; N, 18.45.

Results and Discussion.

ET Rates with Au₂(dcpe)₃^{2+*}. The rate of ET can be measured by monitoring the lifetime of a luminescent species as a function of the concentration of quencher; the quencher in the ET studies discussed here is a pyridinium or substituted pyridinium (py⁺). In the absence of a quencher, there are two intramolecular processes the excited molecule can undergo. The excited state may radiate light to go back to the ground state, k_r , or it may decay to the ground state by some non-radiative process, k_{nr} . The lifetime of the excited state with no acceptor present, τ_0 , is given by Equation 5.

$$\tau_0 = (k_r + k_{nr})^{-1} \quad 5.$$

Adding a quencher provides another possible route for decay to the ground state. The new non-radiative, bimolecular process shortens the lifetime, τ , according to Equation 6.

$$\tau = (k_r + k_{nr} + k_q [Q])^{-1} \quad 6.$$

The Stern-Volmer equation can be derived from Equations 5 and 6 (Equation 7). A plot

$$\tau_0/\tau = 1 + \tau_0[Q]k_q \quad 7.$$

of τ_0/τ vs. [quencher] will yield a straight line with a slope of $\tau_0(k_q)$.¹¹

The luminescent complex $Au_2(dcpe)_3^{2+*}$ acts as the electron donor and py^+ performs the role of the acceptor. Electron-transfer rates were studied as a function of the driving force for the reaction by monitoring the quenching with a series of different pyridiniums. Altering the substituents on the pyridinium changes $E_{1/2}$ for the acceptor which in turn changes the driving force according to Equation 8 (W_r is the work required to bring the reactants together and W_p is the work required to bring the products together).¹² The

$$-\Delta G^0 = [E_{1/2}(py^+/py\cdot) - E_p^a(Au_2(dcpe)_3^{2+}) + E_{v_0-v_0} + W_r - W_p] \quad 8.$$

work terms were derived from the electrostatic equation W (eV) = $(0.395 \cdot Z_a Z_b / d) [1 / (1 + 0.48d \cdot \mu^{1/2})]$; Z_a and Z_b are the charges on the donor and acceptor; d is the center to center distance when ET occurs; μ is the ionic strength (since one of the products is neutral $W_p = 0$). The values for $E_p^a(Au_2(dcpe)_3^{2+})$ and the $E_{v_0-v_0}$ of the emissive transition were reported in chapter two

All luminescence decays for the quenching studies fit well to single exponential functions. A sample of the transient decay of the excited state is given in Figure 3.12. A representative example of a Stern-Volmer plot is shown in Figure 3.13. All of the Stern Volmer plots yielded lines with correlation factors > 0.99 . A summary of the data for the rates obtained with the gold complex and the pyridiniums is provided in Table 3.1.

The quenching rates with the entire series of pyridiniums are then used to generate a Marcus plot of $\log(k_q)$ vs. driving force (see Figure 3.14). The rates increase as the driving force increases until they reach the diffusion limit of 1×10^{10} in acetonitrile. The rates continue to remain at the diffusion limit as the driving force increases from 1.2 eV to 1.9 eV.

In order to fit the data to the Marcus expression it is necessary to note that the measured quenching rates are bimolecular rates and the ET rates predicted by the Marcus expression are unimolecular rates. The true kinetic scheme for the bimolecular electron transfer involves the formation of a donor-acceptor contact pair followed by unimolecular ET and diffusion away of the oxidized donor and the reduced substrate (see Figure 3.15). The k_{23} in this scheme is now the same unimolecular ET rate predicted by Marcus theory. By assuming a steady-state approximation for $[D^*A]$, and $[D^+A^-]$ one can derive an expression for the

$$k_q = \frac{k_{12}}{1 + \frac{k_{21}}{k_{23}} \left(1 + \frac{k_{32}}{k_{30}}\right)} \quad 9.$$

quenching rate k_q (Equation 3.9). As long as the association and dissociation rates for the D^*A contact pair are both equal to the diffusion rate ($k_{12} = k_{21} = k_d$), and the rate of back electron transfer to regenerate the excited state, $[D^*A]$, is negligible compared to the combined rates of dissociation to $[D^+]$ and $[A^-]$ and back electron transfer to the ground state $[DA]$ ($k_{32} \ll (k_{30} + k_{34})$), k_q can be related to the electron transfer rate, k_{ET} ($k_{ET} = k_{23}$), and the diffusion rate, k_d , as seen in Equation 3.10.¹¹

$$1/k_q = 1/k_d + 1/k_{ET} \quad 10.$$

Equation 3.10 was used along with the Marcus expression to obtain theoretical values for k_q . Figure 3.14 shows the data and the best theoretical fit. The results give a value of 10.5 cm^{-1} for H_{ab} and 1.66 eV for λ . The large value for λ can be divided into two components: λ_i refers to reorganization within the molecule such as bond length and bond angle changes, and λ_o refers to the reorganization energy of the solvent as the solvent dipoles align to the new charge distribution. Based on the bimolecular electron transfer study with Ir_2 and the same pyridiniums performed in acetonitrile, the solvent contribution can be estimated as $\approx 0.75 \text{ eV}$. The resulting λ_i of 0.91 eV (21 kcal/mol), indicates that a large amount of reorganization is involved during the first electron transfer to make Au(II) . This result is not entirely surprising in light of the large Stokes shift associated with the emission

Figure 3.12. Luminescence decay of $\text{Au}_2(\text{dcpe})_3^{2+}$, excitation 355 nm.

---> FIXED PARAMETER; ! ---> FIXED SIGN

$$y(t) = C0 + C1 \exp(-k1 * t)$$

#C0 = 0.000E+00

!C1 = 3.959E-02

!k1 = 5.131E+04 s⁻¹

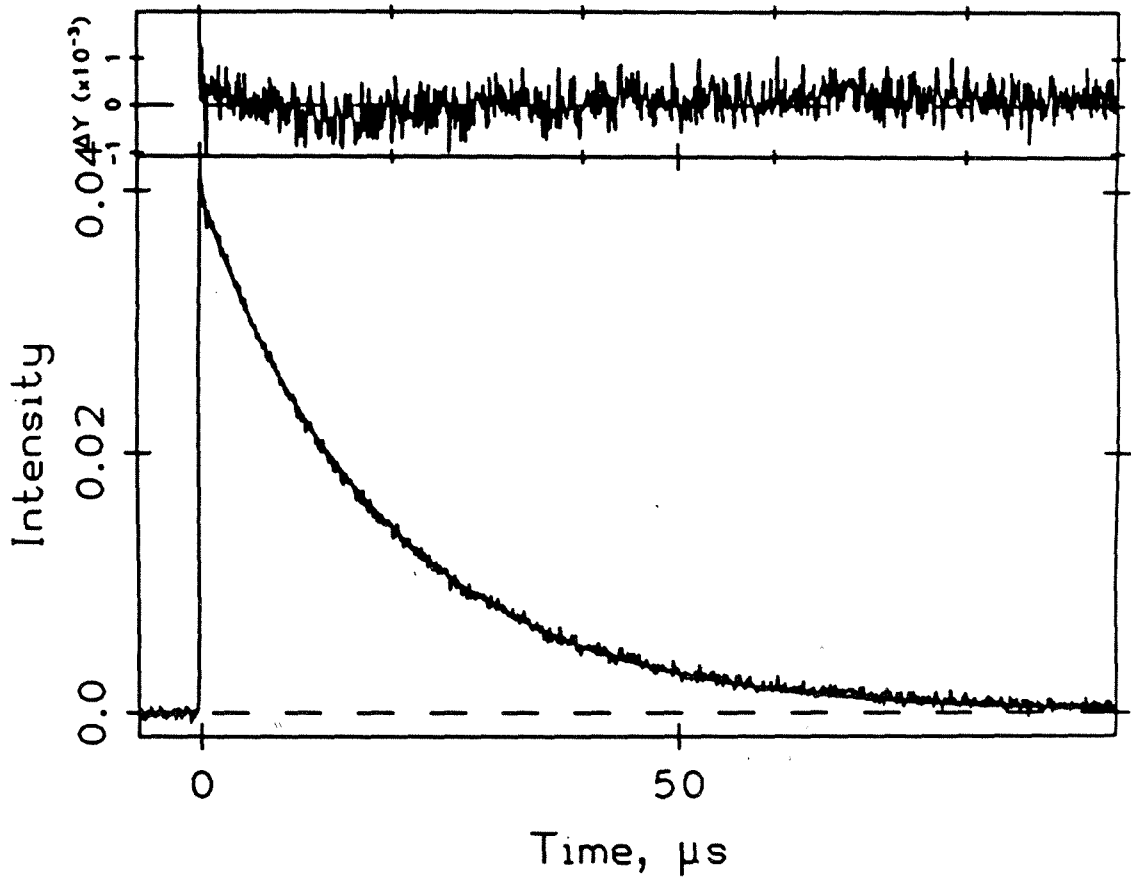


Figure 3.13. Sample Stern Volmer plot with 3,4-dicyanopyridinium as the quencher.

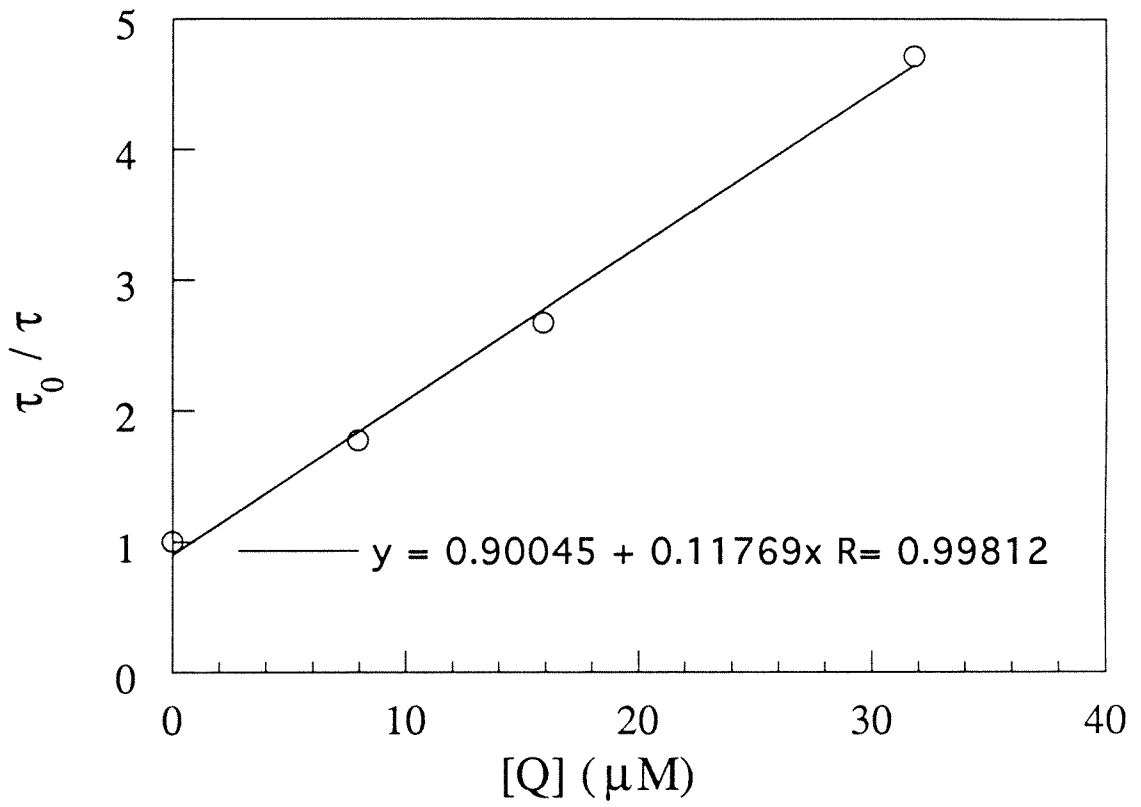


Figure 3.14. Marcus plot for the forward ET reactions between $\text{Au}_2(\text{dcpe})_3^{2+}$ and a series of substituted pyridiniums; each point represents a quenching rate with a different pyridinium. The solid line represents a the theoretical best fit curve.

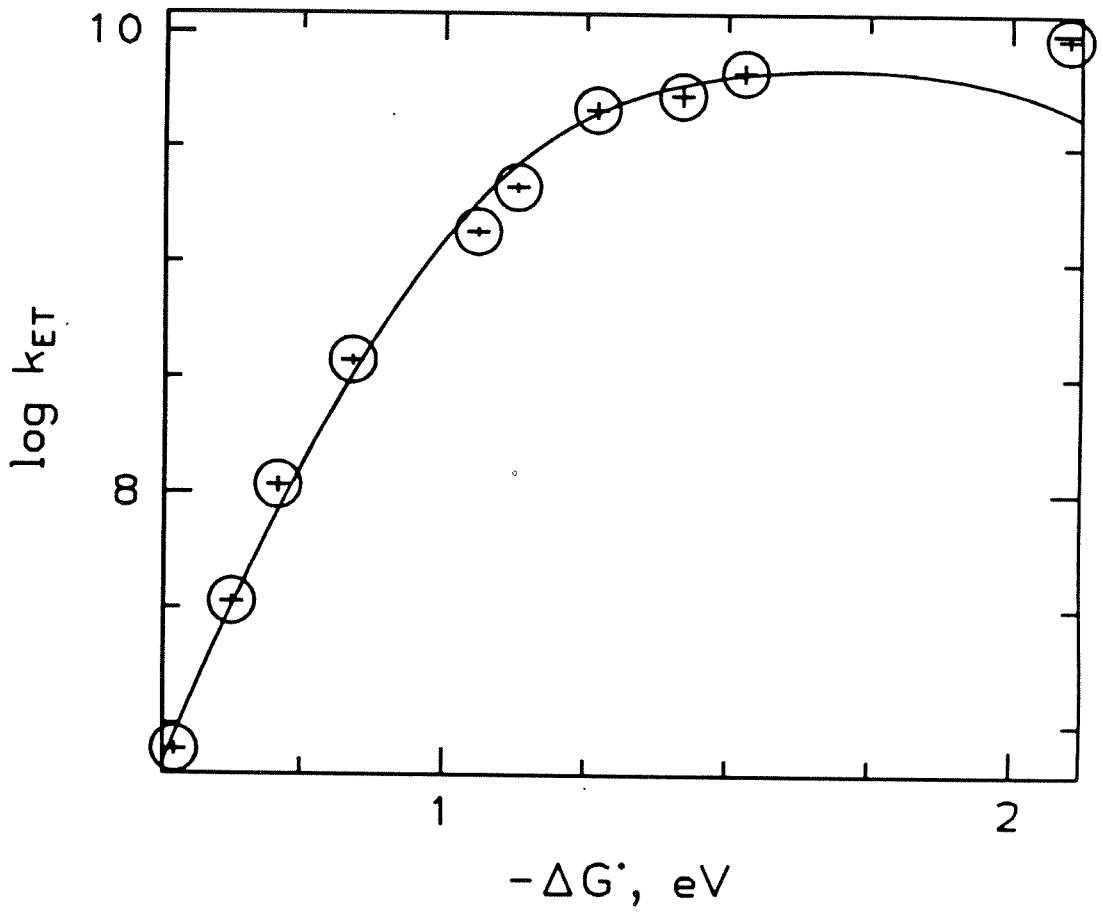


Table 3.1. Quenching rates and driving forces for the forward ET reactions between $\text{Au}_2(\text{dcpe})_3^{2+}$ and a series of substituted pyridiniums.

R	R'	$E_{1/2}$ (V vs SCE)	$-\Delta G^{\circ}$ (eV)	k_q ($M^{-1}s^{-1}$)
CH ₃	3,4-CN	-0.10	2.10	9.46×10^9
CH ₃	4-CN	-0.67	1.53	6.72×10^9
CH ₃	4-CO ₂ NH ₃	-0.78	1.42	5.10×10^9
C ₂ H ₅	4-CONH ₂	-0.93	1.27	4.59×10^9
C ₆ H ₅ CH ₂	3-CONH ₂	-1.07	1.13	2.10×10^9
CH ₃	3-CONH ₂	-1.14	1.06	1.35×10^9
CH ₂ CH ₃		-1.36	0.84	3.75×10^8
CH ₃	2-OCH ₃	-1.48	0.72	1.08×10^8
CH ₃	2,3,6-CH ₃	-1.57	0.63	3.38×10^7
CH ₃	2,4,6-CH ₃	-1.67	0.53	7.74×10^6

Figure 3.15. Kinetic scheme for bimolecular ET.

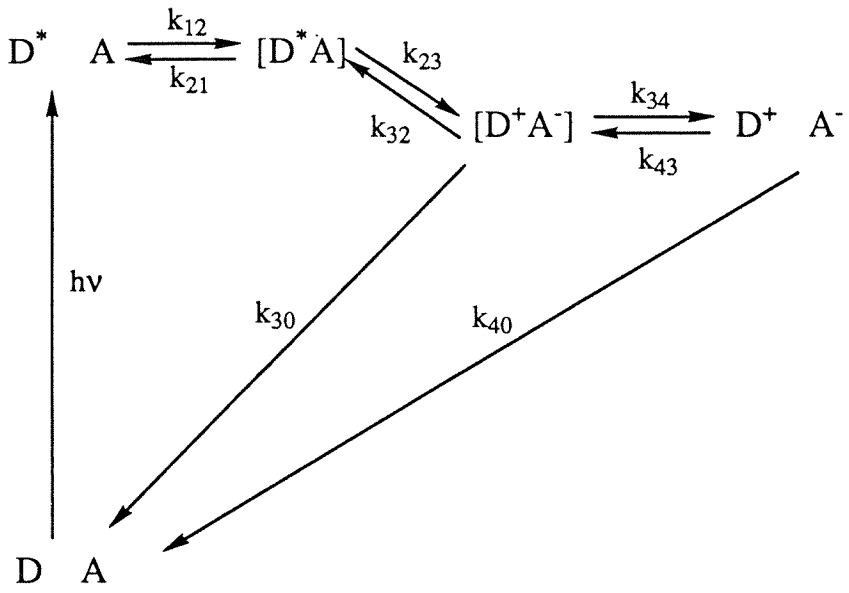
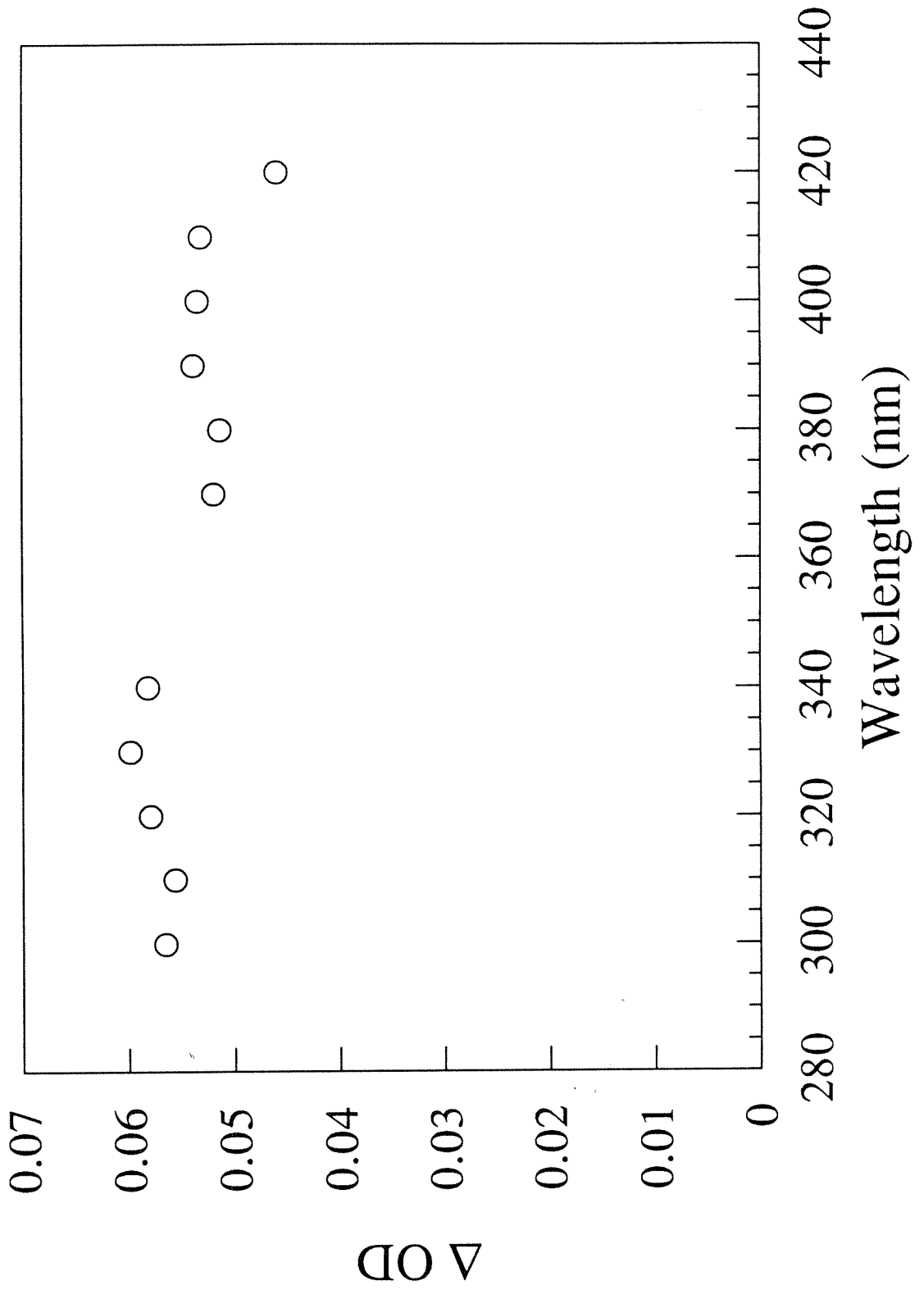


Figure 3.16. Transient absorption spectrum of $\text{Au}_2(\text{dcpe})_3^{2+}$.



of $\text{Au}_2(\text{dcpe})_3^{2+}$ ($7,800 \text{ cm}^{-1}$), which demonstrates a substantial distortion of 11 kcal/mol even in the excited state. In fitting the data to Marcus theory, the diffusion limited high driving force points were discarded based on results with the iridium system (*vide infra*). Recombination rates could not be studied because changes in the absorption spectrum were not intense enough in the visible region. The excited state transient absorption spectrum (Figure 3.16) shows only moderate increase in absorption in the UV area.

Forward ET Rates with $[\text{Ir}(\text{cod})(\text{pz})]_2$. The photophysics of the iridium dimer, Ir_2 , have been well characterized. The lowest energy absorption band (Figure 3.17) is at 500 nm and has been assigned as a $d\sigma^* \rightarrow p\sigma$ absorption. Emission of the complex at 680 nm (Figure 3.18) has been assigned as the corresponding $d\sigma^* \leftarrow p\sigma$ transition and has a lifetime of 240 ns in acetonitrile at room temperature.¹³ Forward electron transfer rates were determined in the same manner as described above for the gold complex. The resulting rates are given in Table 3.2, and correlate well with those measured by Marshall.⁴ Driving forces were calculated according to Equation 11 in the same manner as described for the gold

$$-\Delta G^0 = E_{1/2}(\text{py}^+/\text{py}\cdot) - E_{1/2}(\text{Ir}_2^+/\text{Ir}_2) + E_{\nu_0-\nu_0} + W_r - W_p \quad 11.$$

system (*vide supra*) Although the driving force for ET has been extended to 1.6 eV, the rates continue to be diffusion limited. To verify that all of the observed quenching was due to electron transfer, quantum yields for the electron transfer were measured by monitoring the absorption spectrum at 500 nm during the lifetime of the excited state with quencher present. The excited state transient absorption spectrum shows a strong bleach at 500 nm.⁴ With no quencher present the bleach recovers back to zero with an exponential rate equal to the rate of the luminescence decay. When an ET quencher is present the recovery of the bleach consists of two components: a fast step corresponding to the lifetime of the excited state and proportional to the amount of unquenched excited state, and a second, slower component due to the formation of Ir_2^+ which decays according to the recombination ET rate. Quenching by energy transfer leads to the ground state, Ir_2 , directly, as opposed to Ir_2^+ , so the bleach will

Figure 3.17. Absorption spectrum of Ir₂.

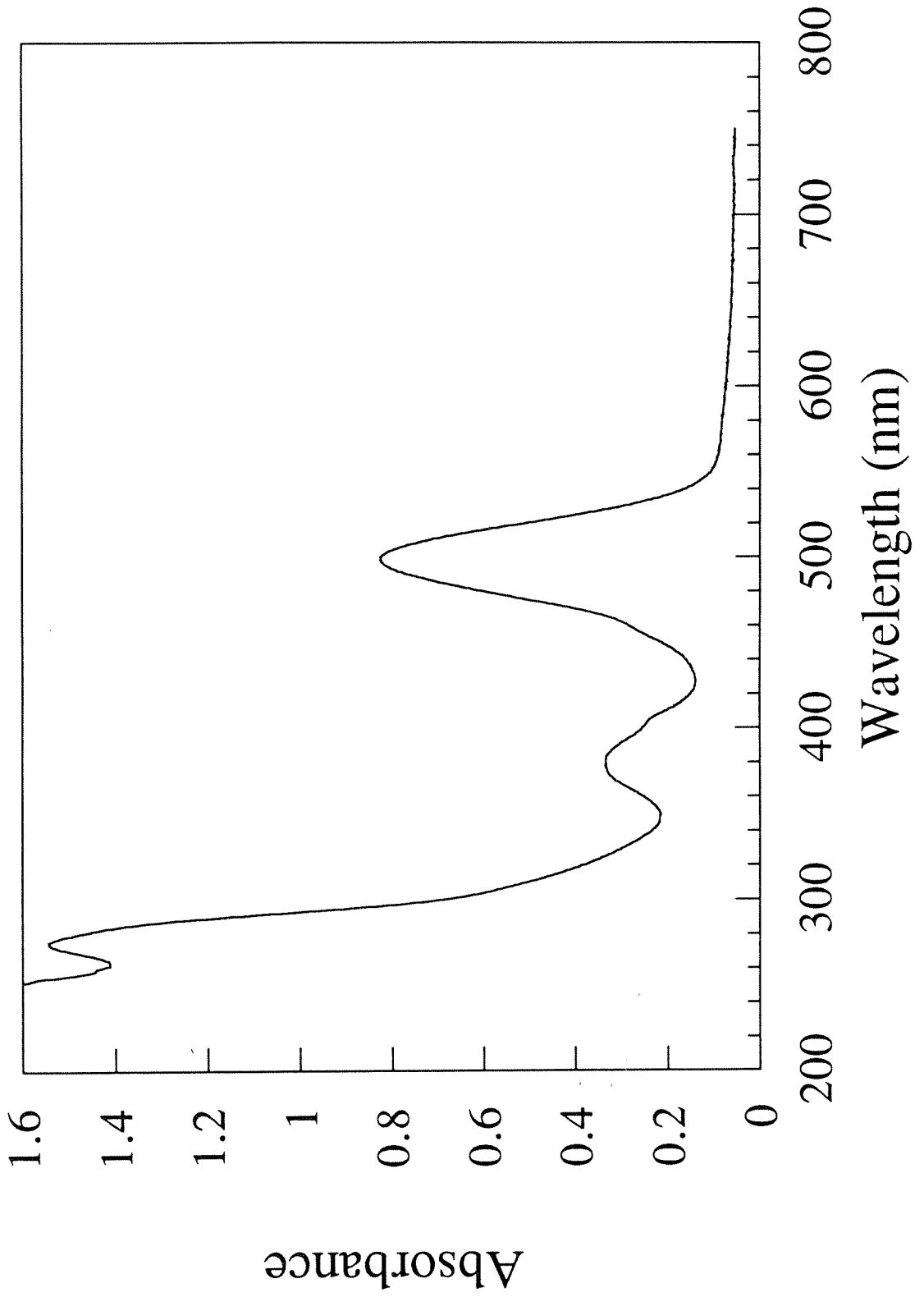


Figure 3.18. Emission spectrum of Ir₂.

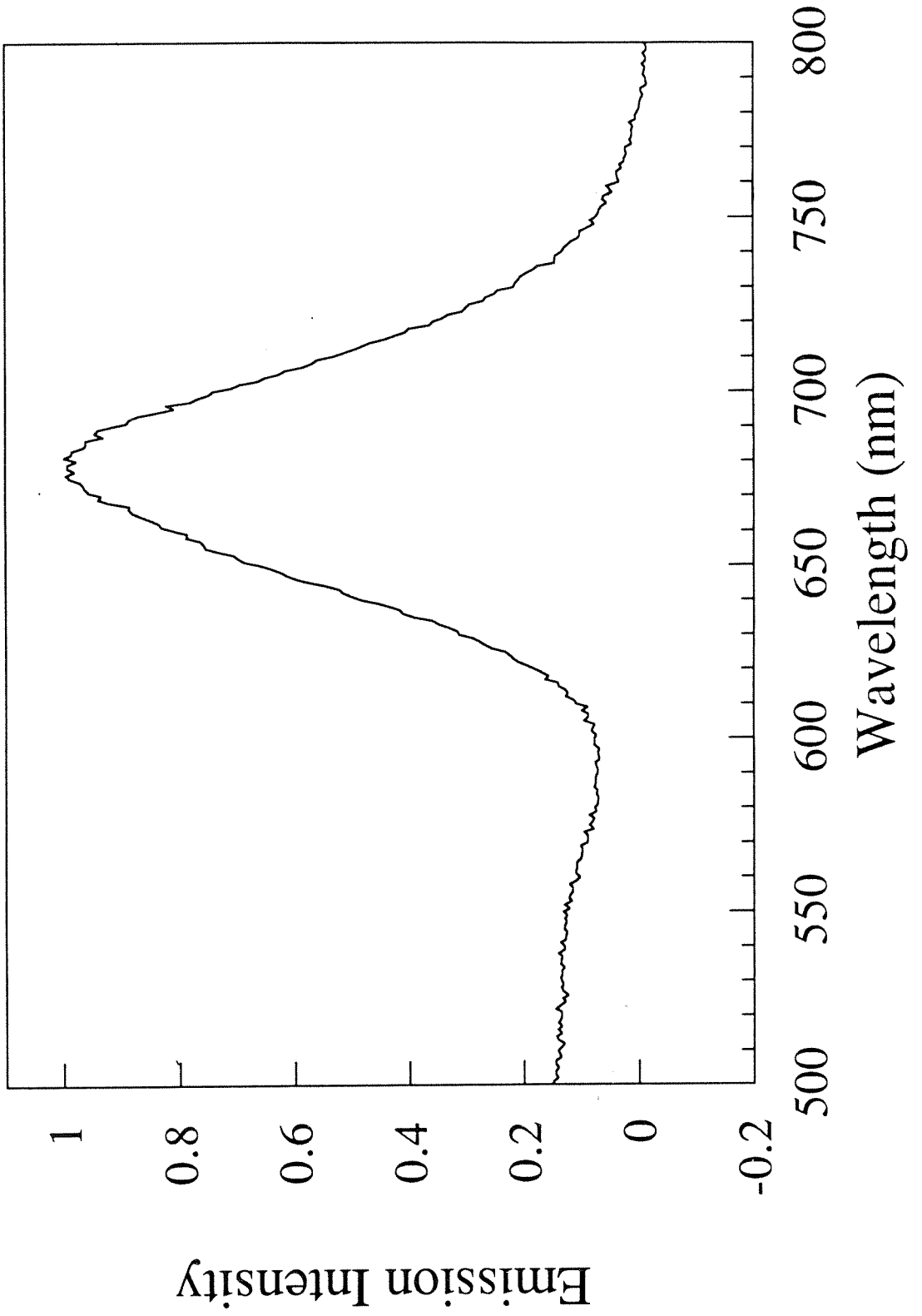


Figure 3.19. Transient absorbance trace used for the quantum yield determination with 3,4-dicyano-N-methylpyridinium.

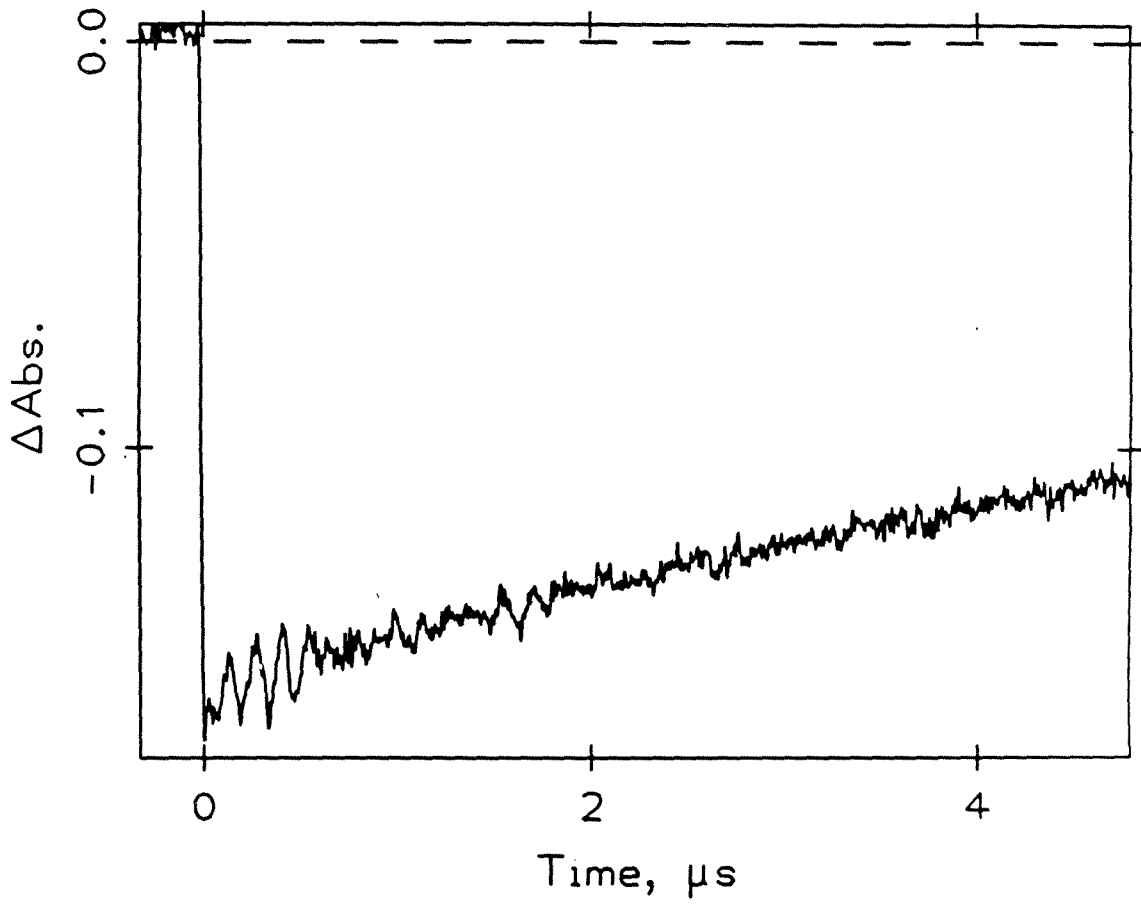


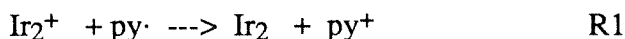
Table 3.2. Quenching rates and driving forces for the forward (k_q) ET reactions and the recombination (k_b) reactions between Ir₂ and a series of pyridiniums.

R	R'	$E_{1/2}$ (V vs SCE)	$-\Delta G_f^\circ$ (eV)	k_q ($M^{-1}s^{-1}$)	$-\Delta G_b^\circ$ (eV)	k_b ($M^{-1}s^{-1}$)	ϕ_{ET}
CH ₃	3,4-CN	-0.10	1.60	1.26×10^{10}	0.40	2.52×10^9	1.00
CH ₃	4-CN	-0.67	1.03	1.30×10^{10}	0.97	7.77×10^9	0.78
CH ₃	4-CO ₂ NH ₃	-0.78	0.92	9.27×10^9	1.08	5.95×10^9	0.69
C ₂ H ₅	4-CONH ₂	-0.93	0.77	8.81×10^9	1.23	3.36×10^9	0.53
C ₆ H ₅ CH ₂	3-CONH ₂	-1.07	0.63	6.12×10^9			
C ₂ H ₅		-1.36	0.34	2.47×10^9	1.66	9.52×10^8	0.36
CH ₃	2-OCH ₃	-1.48	0.22	7.83×10^8	1.78	8.61×10^8	0.19
CH ₃	2,6-CH ₃	-1.52	0.18	6.27×10^8	1.82	6.86×10^8	
CH ₃	2,3,6-CH ₃	-1.57	0.13	2.80×10^8			
CH ₃	2,4,6-CH ₃	-1.67	0.03	2.80×10^7			

recover with a time constant equal to the luminescent decay time constant. The decay trace used in the quantum yield determination for ET to 3,4-bis-dicyanopyridinium is shown in Figure 3.19 and all of the measured quantum yields are listed in Table 3.2. The measured quantum yields increase as the ET rate increases and reach unity for the highest driving force point, confirming the fact that the quenching is solely due to ET.

Recombination Rates with $[\text{Ir}(\text{cod})(\text{pz})]_2$.

The bleach at 500 nm observed in the transient absorption spectrum provides a means to study the recombination ET rates. In the recombination reaction (R1) an electron is transferred from the $\text{py}\cdot$ donor to the Ir_2^+



acceptor resulting in the formation of the original ground states of py^+ and Ir_2 . The time traces of the change in absorption at 500 nm show a strong negative ΔOD followed by a recovery back to zero (Figure 3.20). The recovery back to zero indicates that all of the Ir_2^+ goes back to Ir_2 . The rate of the reaction is expressed as $\partial[\text{Ir}_2^+]/\partial t = -k_b [\text{Ir}_2^+] [\text{py}\cdot]$. For every molecule of Ir_2^+ produced by the forward ET, one molecule of $\text{py}\cdot$ is also produced, so one can make the substitution $[\text{py}\cdot] = [\text{Ir}_2^+]$ to generate the second-order rate law: $\partial[\text{Ir}_2^+]/\partial t = -k_b [\text{Ir}_2^+]^2$. The second-order rate constant k_b (analogous to the quenching rate k_q measured for the forward ET rates) was determined by two methods. The traces of ΔOD vs. time were first fit to second-order kinetics, $y = 1/(C_0 - kt)$, using a non-linear fitting routine (Figure 3.20).¹⁴ The k_b was then obtained according to: $k_b = k (\Delta\epsilon)b$ where b is the path length in cm (1 cm) and $\Delta\epsilon$ for the $\text{Ir}_2^+ / \text{py}\cdot$ system was determined to be $7000 \text{ M}^{-1}\text{cm}^{-1}$ as described earlier. Back ET rates were also determined using the relationship $(-\Delta\text{OD})^{-1} = C_0 + (k_b / b\Delta\epsilon)t$. A plot of $(-\Delta\text{OD})^{-1}$ vs. time gives a straight line with a slope of $k_b / b\Delta\epsilon$ (Figure 3.21). The resulting rates presented in Table 3.2 are the average of applying both rate determination methods to at least two measurements. Driving forces for the recombination rates were calculated according to Equation 12. The recombination ET rates represent the

$$-\Delta G^0 = E_{1/2}(\text{Ir}_2^+/\text{Ir}_2) - E_{1/2}(\text{py}^+/\text{py}\cdot) - W_p + W_r \quad 12.$$

first observation of inverted behavior for a bimolecular system. The decrease in the recombination ET rate as the driving force increases can be seen in Figure 3.21, where the slope of the lines decreases dramatically as the pyridinyl radicals become better donors (slope $\propto k'_{ET}$).

Although the recombination rates display inverted behavior, the rates do not decrease as fast as classical Marcus theory predicts. The plot of $\log(k'_{ET})$ vs. driving force (Figure 3.22) depicts both the forward and recombination rates. Most of the literature reports on the inverted region in unimolecular systems also demonstrate this rate enhancement in the inverted region. Incorporating quantum mechanics into the Marcus theory can explain the asymmetry of the experimental results. Addition of quantum mechanics lead to the modified Marcus expression in Equation 13.¹⁵ The pre-exponential term remains unchanged, but the

$$\begin{aligned}
 k = & \frac{2H^2_{ab}}{h} \sqrt{\frac{\pi^3}{\lambda_s RT}} \exp \left\{ -S_f - S_c \coth \left(\frac{h\omega_c}{4\pi KT} \right) \right\} \\
 & \times \sum_{m_f=0}^{\infty} \sum_{m_c=-\infty}^{\infty} \frac{S_f^{m_f}}{m_f!} \exp \left(\frac{m_c \omega_c}{4\pi KT} \right) I_{m_c} \left\{ S_c \operatorname{csch} \left(\frac{\omega_c}{4\pi KT} \right) \right\} \\
 & \times \exp \left\{ -\frac{(\Delta G^0 + m_f h \omega_f / 2\pi + m_c h \omega_c / 2\pi + \lambda_s)^2}{4 \lambda_s RT} \right\} \quad 13.
 \end{aligned}$$

exponential term involves a summation over the vibrational levels of a high frequency vibration, ω_f , and a moderate frequency vibration, ω_c ; the low frequency vibrational modes, ω_s , (which include the solvent interactions) are treated classically; $S_i = 2\pi\lambda_i/h\omega_i$. In the limit that only low frequency vibrational modes are coupled to the ET, Equation 13 reduces to the classical Marcus expression in Equation 1. Coupling to high energy modes has no effect in the normal region of the Marcus plot, but leads to a substantial increase in the ET rates which lie in the inverted region.

Enhanced tunneling in the inverted region can be best understood by looking at the potential wells of the reactants and products. In the normal region the reactant and product curves are separated below the crossing point, so that there is little or no overlap between v_0

Figure 3.20. Transient absorbance trace at 500 nm with Ir₂ and 3,4-dicyano-N-methylpyridinium, excitation at 532 nm; solid line is the best fit to bimolecular kinetics.

---> FIXED PARAMETER; ! ---> FIXED SIGN

$$y(t) = 1/(C0+C1*t)$$

C0 = -3.686E+01

C1 = -4.257E+05

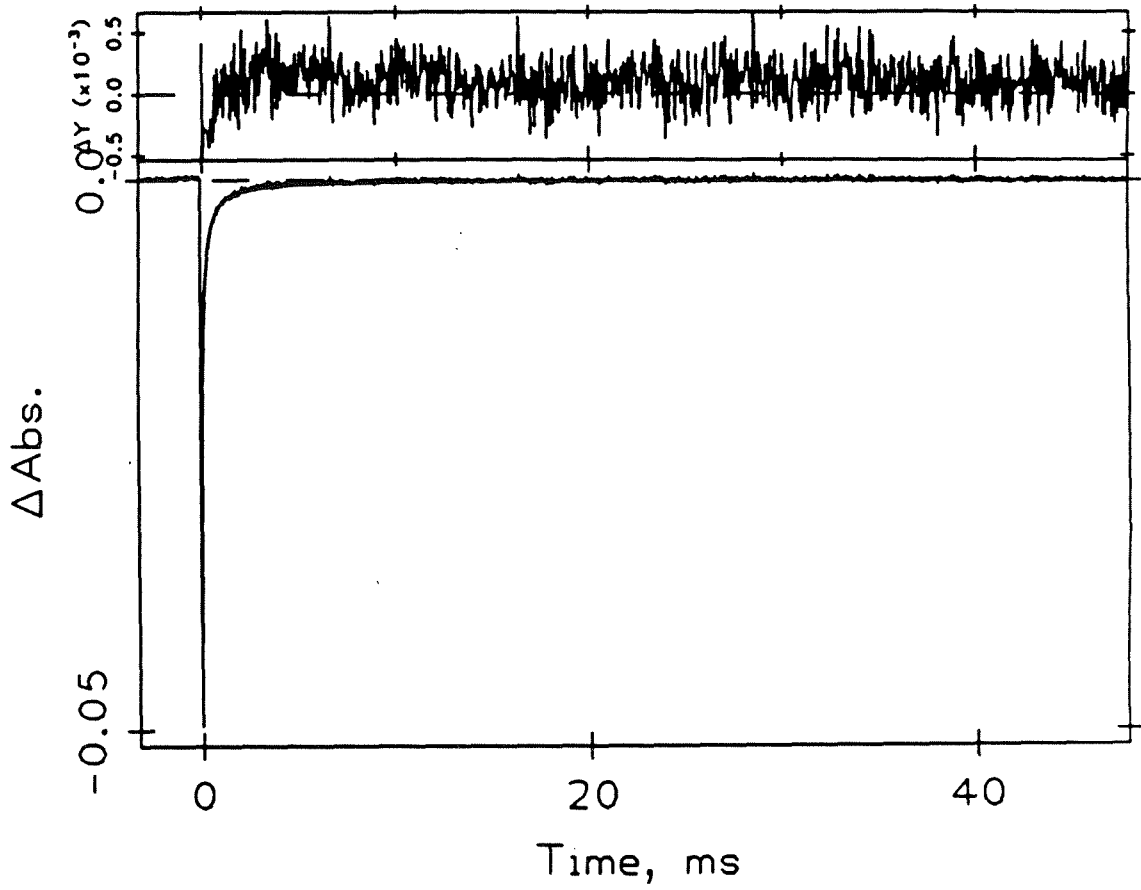


Figure 3.21. Plot of $1/\Delta\text{absorbance}$ vs time for the recombination reaction with 4-cyano-N-methylpyridinium (squares), N-ethylisonicotinamide (triangles), N-ethylpyridinium (circles), and 2,6-dimethyl-N-methylpyridinium (asterisks).

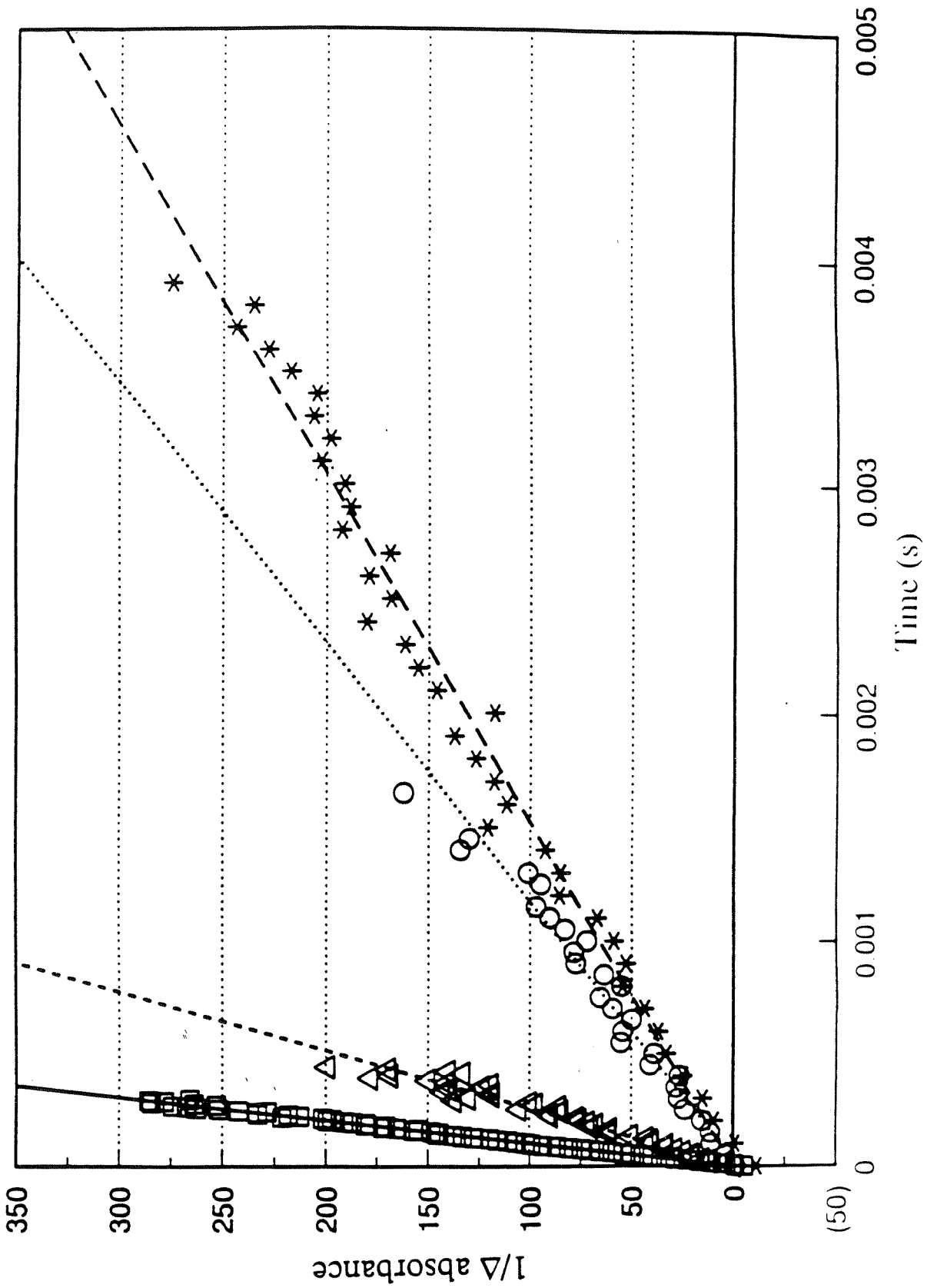
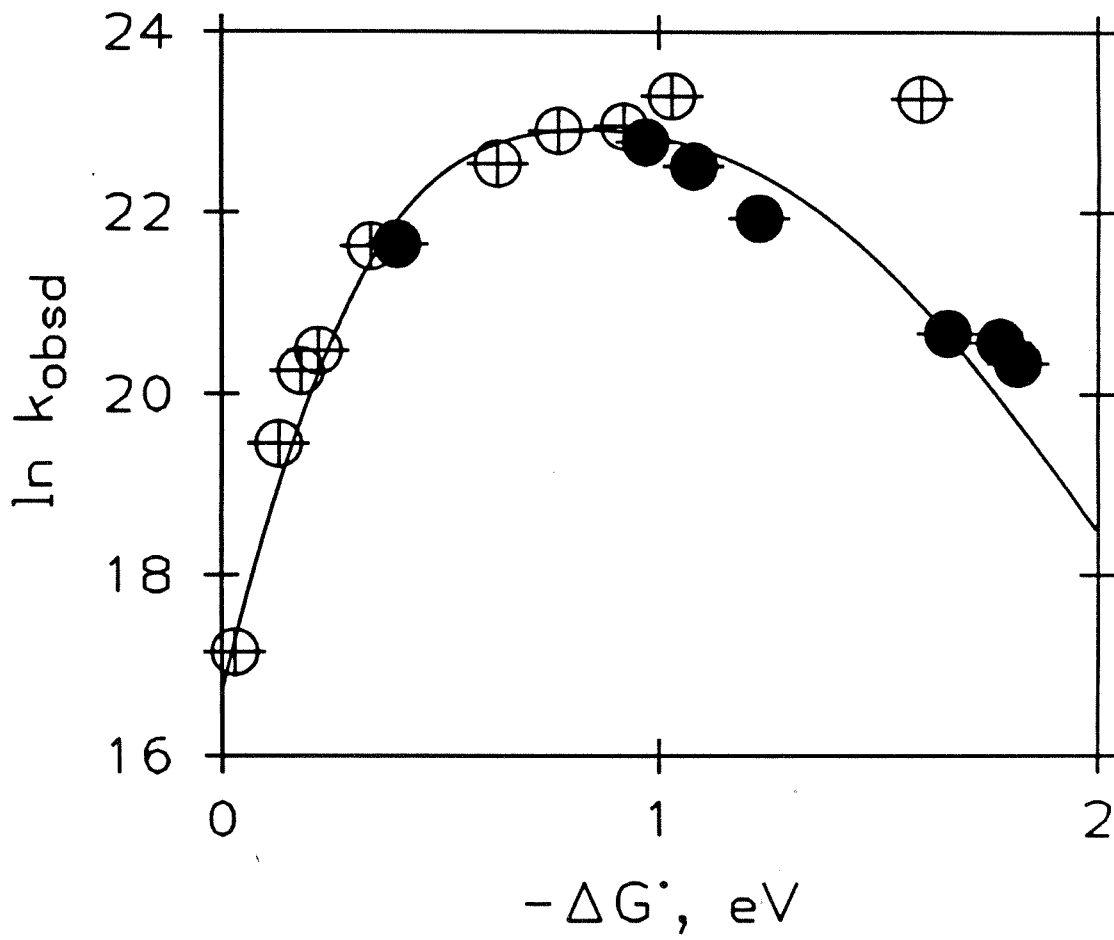


Figure 3.22. Marcus plot of forward (open circles) and recombination (filled circles) ET rates. The solid line is the best fit theoretical curve excluding the diffusion limited forward rates; $H_{ab} = 10 \text{ cm}^{-1}$, $\lambda = 0.85 \text{ eV}$.



wave function of the reactants and any v_n wave function for the products. The lack of any overlap prohibits tunneling to excited vibrational states of the product. In the inverted region the reactant and product potential wells become nested and it is possible for the reactant wave function to have considerable overlap with one of the vibrationally excited wave functions for the product. In order to have reasonable overlap the product wave function must have the same energy as the reactant wave function. For low energy vibrations the vibrational level where $\Delta E_{v_0-v_0} = \Delta G^0$ will be large; therefore, the electron density will be primarily at the classical turning points. This situation generates very little overlap with the v_0 wave function of the reactant since the turning points lie outside of the reactant potential well. For high energy vibrations the vibrational level required to match the energy of the reactant v_0 level will be considerably smaller, and the wave function will show more quantum mechanical effects with significant electron density between the turning points. Electron density between the turning points will have a large overlap with the v_0 wave function of the reactant, resulting in a significant amount of tunneling to the excited vibrational state (Figure 3.23). Tunneling through the reaction barrier will enhance the observed ET rates. Rate enhancement will only be significant ET in the inverted region when there is coupling to high frequency vibrations.

The quantum modified Marcus expression provides a very good fit for the bimolecular data with $\lambda = 0.85$ eV and $H_{ab} = 10$ cm⁻¹. The values obtained for λ and H_{ab} are very similar to those reported by Gray et al. for the intramolecular system of iridium phosphinites; however, the intramolecular system shows classical behavior in the inverted region. The discrepancy between the bimolecular and the unimolecular results in the inverted region can be explained if the bimolecular ET is coupled to a high frequency vibration and the unimolecular system is only coupled to low frequency vibrations. It is difficult to imagine why the vibrational coupling would change drastically, since the two systems are so similar chemically.

Part of the discrepancy at high driving forces can be explained by taking into account the fact that bimolecular ET can occur at a variety of distances, where as the donor - acceptor distance is relatively fixed in the unimolecular system. As the donor and acceptor approach one another in a bimolecular system both the coupling and the reorganization energy change as a function of distance. The coupling, H_{ab} , represents the overlap between the donor and acceptor orbitals and falls off exponentially as the distance increases (Equation 14; r is the donor acceptor distance; σ is the sum of the hard sphere radii of the donor and acceptor;

$$H_{ab}^2 = (H_{ab}^0)^2 \exp[-\beta(r-\sigma)] \quad 14.$$

β is the decay constant). The other distance dependent factor is the reorganization energy of the solvent, λ_s . As the charge separation distance for ET becomes greater more solvent dipoles are affected by the ET and λ_s increases as seen in Equation 15 (a_1 and a_2 are the radii

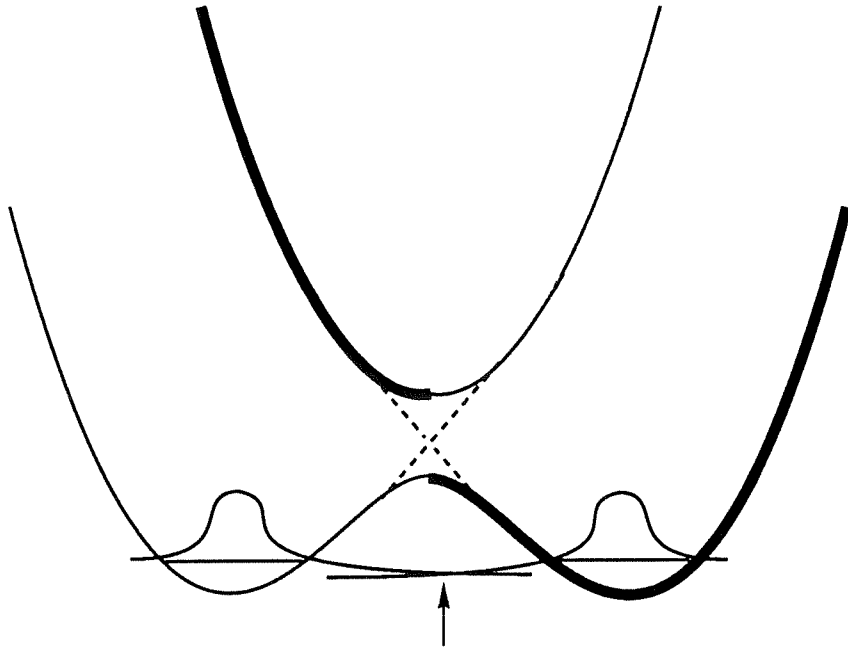
$$\lambda_s = (\Delta e)^2 \left[\frac{1}{2a_1} + \frac{1}{2a_2} - \frac{1}{r} \right] \left[\frac{1}{D_{op}} - \frac{1}{D_s} \right] \quad 15.$$

of the donor and acceptor; D_{op} and D_s are the optical and static dielectric constants).¹⁶

In the normal region of a bimolecular system, both the increase in H_{ab} and the increase in λ_s as the donor and acceptor approach lead to a greater ET rate at shorter distances; ET will take place almost exclusively at the point of contact between the donor and acceptor for all points in the normal region. As long as the ET occurs at the fixed contact distance (cd) both H_{ab} and λ_s will remain constant at H_{ab-cd} and λ_{s-cd} . A Marcus curve using H_{ab-cd} and λ_{s-cd} should fit all of the observed rates with $-\Delta G^0 < \lambda_{s-cd}$. In the inverted region, the decrease of H_{ab} with increasing distance still reduces the ET rate, but the increase in λ_s causes the ET rate to increase as the distance increases. Increasing λ_s shifts the maximum of the Marcus curve to a higher driving force so that a point which used to lie in the inverted region for the curve with H_{ab-cd} and λ_{s-cd} moves closer to the maximum for the new curve with $\lambda_s > \lambda_{s-cd}$ (Figure 3.24). At large donor acceptor separations the exponential drop in H_{ab} will predominate and the ET rate will decrease. Since the ET rate is no longer a maximum at the contact distance, a significant amount of ET will occur at distances greater

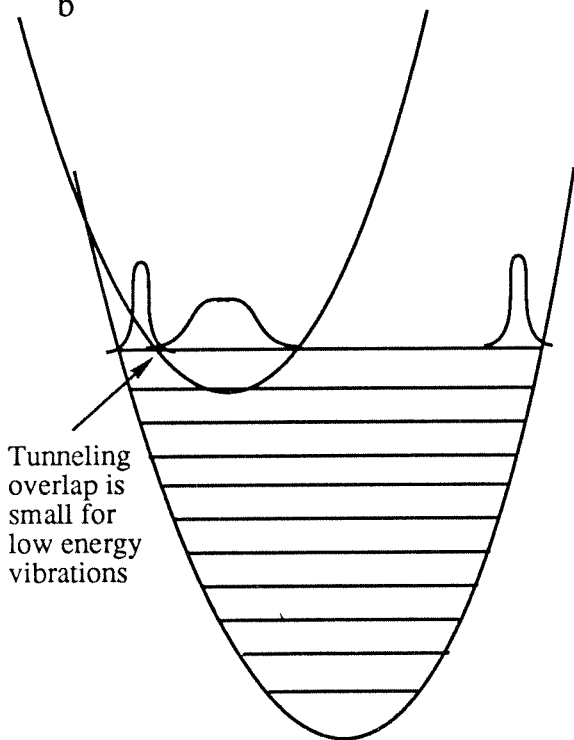
Figure 3.23. Tunneling effects; (a) in the normal region, (b) in the inverted region coupled to a low energy vibration, and (c) in the inverted region coupled to a high energy vibration.

a



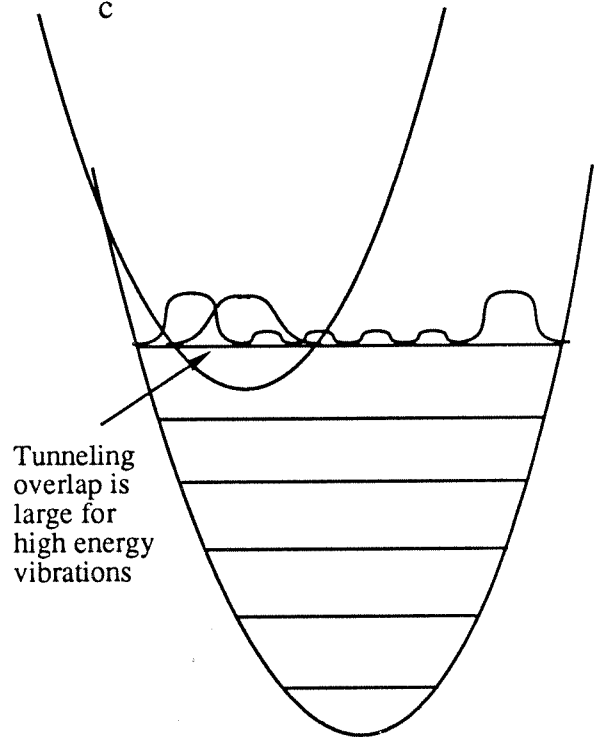
Tunneling overlap is negligible in the normal region

b



Tunneling overlap is small for low energy vibrations

c



Tunneling overlap is large for high energy vibrations

Figure 3.24. Distance effect on ET rates in the inverted region; (a) Marcus plot for the λ at the contact distance and (b) Marcus plot for the slightly larger λ at some distance d ($d >$ the contact distance).

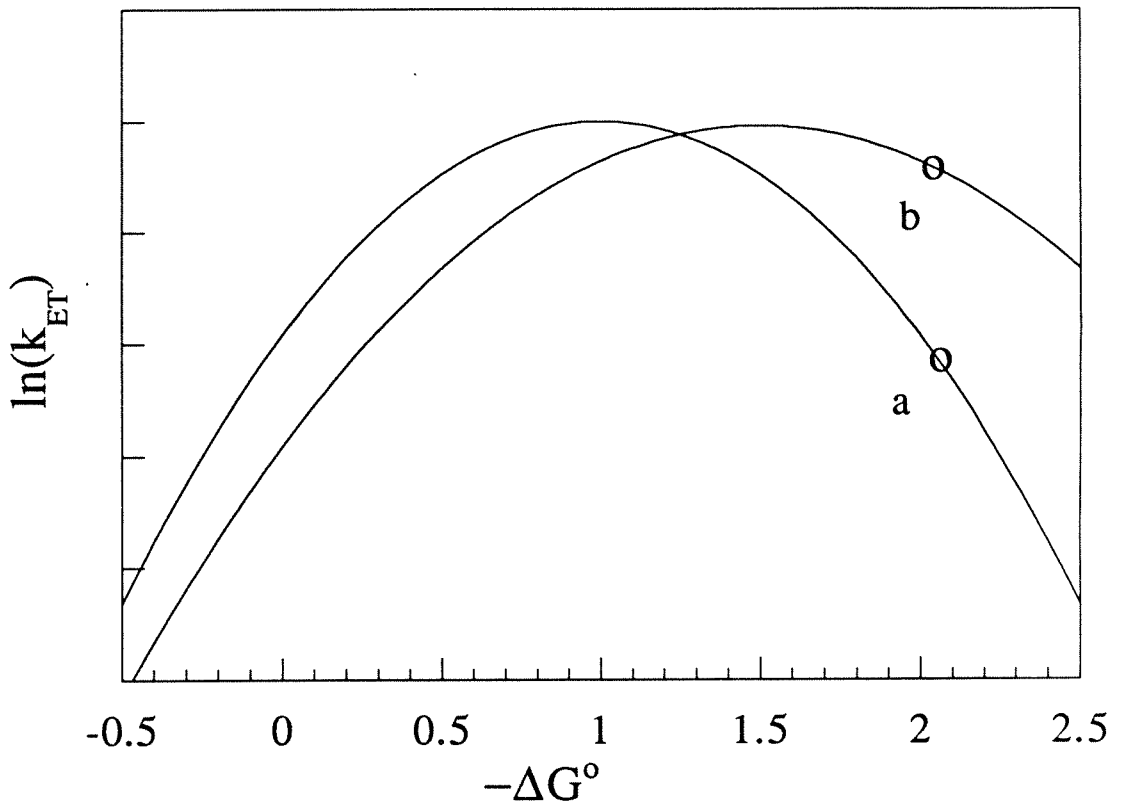
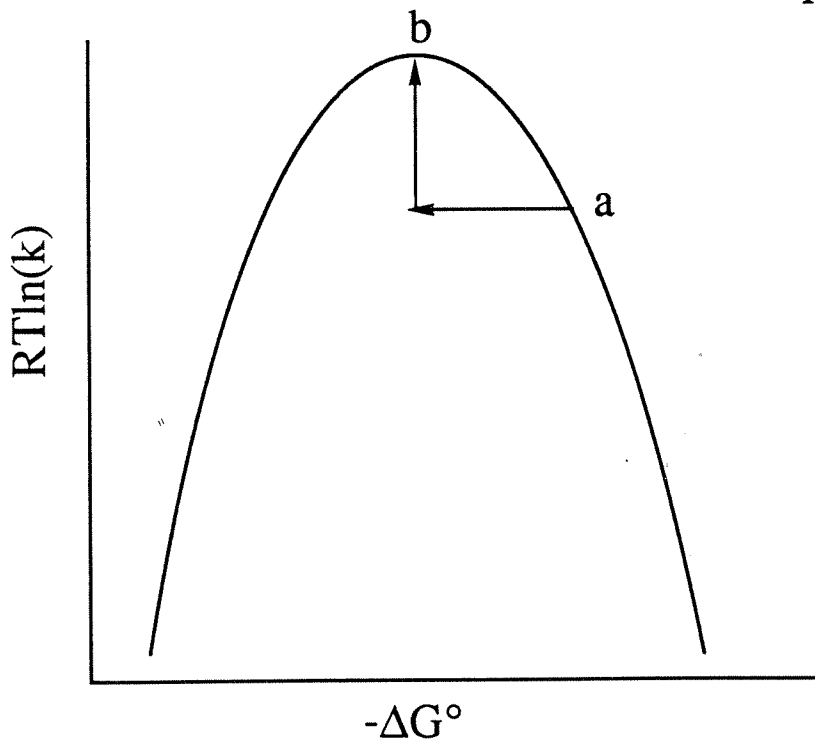
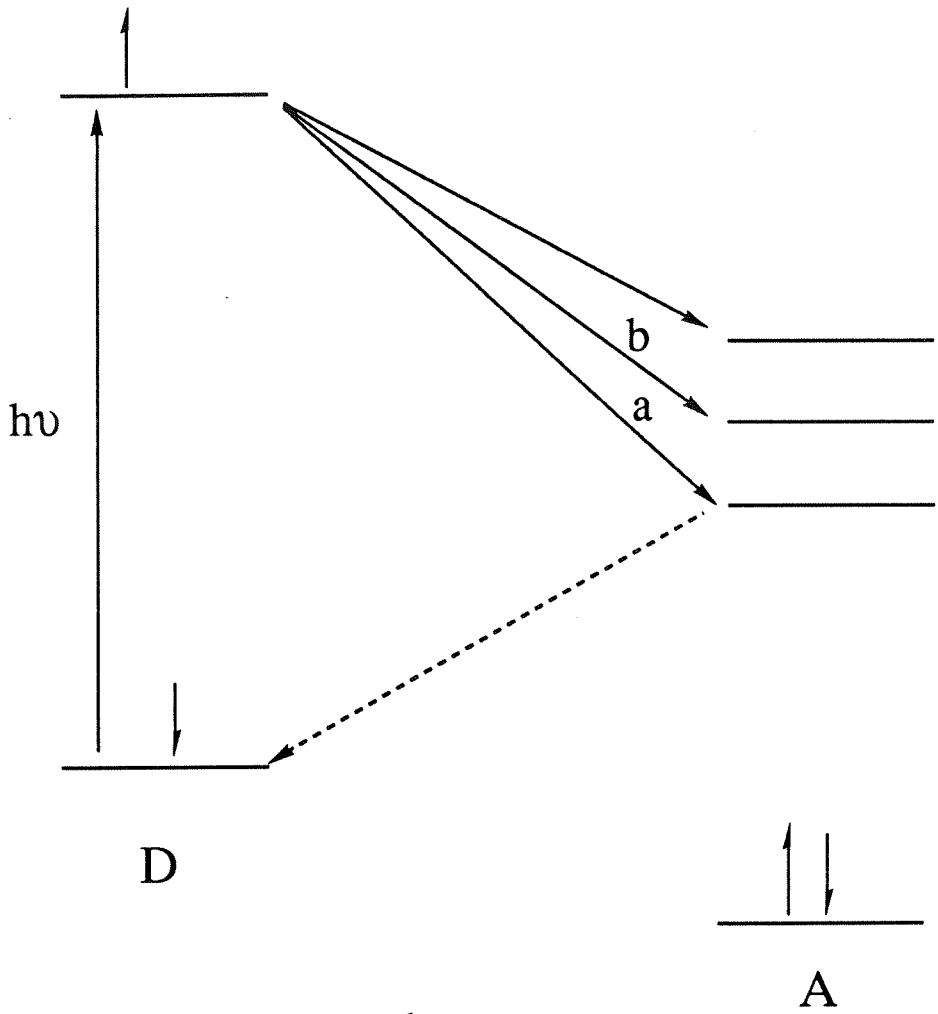


Figure 3.25. Enhancement of ET rates in the inverted region by low lying excited states; (a) ET to the LUMO on the acceptor, and (b) ET to a low lying excited state. Lower Marcus curves shows the rates for paths (a) and (b).



than the contact distance. The parameters H_{ab} and λ_s will differ from H_{ab-cd} and λ_{s-cd} for the reactions with $-\Delta G^0 > \lambda_{s-cd}$ so the classical Marcus curve will not fit the experimental data. The faster ET rates at distances slightly greater than the contact distance will lead to faster observed rates than those predicted from theory. Sutin et al. have calculated that the magnitude of this effect for a hypothetical system at a driving force of 2.0 eV can be as large as an order of magnitude. A correction of this type to the observed back ET rates for the bimolecular Ir_2 system would compensate for a large amount of the discrepancy with the unimolecular system, but the correction is not enough to fit completely classical behavior. Some tunneling must be occurring.

Conclusions.

We have made the first observation of inverted behavior for a bimolecular system. The observed rates are extremely interesting, because the high driving force recombination ET rates show clear inverted behavior even in the region where the forward ET rates are diffusion limited (Figure 3.22). This is the first system where both forward photo-induced ET and recombination ET rates have been observed at high driving forces. The difference in behavior between the forward and recombination rates can be explained by postulating that the electron can transfer to low lying excited states in the forward ET reaction which are not accessible for the back ET.

In the photo-induced reaction the electron transfers from the $d\sigma^*$ of the Ir_2^+ to a π^* orbital on the pyridinium. There exists a manifold of π^* orbitals to which the electron can transfer. At low driving forces the electron will transfer exclusively to the lowest lying π^* orbital; ET to higher excited states will be substantially slower since the driving force would be lower. At high driving forces $-\Delta G^0 > \lambda$, lowering the driving force will increase the ET rate if the new driving force is closer to λ (Figure 3.25). In order to explain the diffusion limited forward ET rates it is necessary to have excited states available that are within 0.3 eV of the lowest energy ET state. Reports in literature estimate that the pyridinyl radical has excited states 0.5 eV above the ground state.¹⁷ The PES spectrum of the Ir_2 complex shows

that there are also low energy states in Ir_2^+ which are only 0.4 eV above its ground state.¹⁸ Electron transfer to produce either Ir_2^+ or pyridinyl excited states could account for the fast rates observed at high driving forces for the photo-induced ET. The back reaction produces the ground state Ir_2 and pyridinium complexes. From their UV/VIS spectra it is known that the lowest excited state in the Ir_2 complex is 2.5 eV above the ground state and the lowest excited state for the pyridiniums is > 3.0 eV, so that ET to an excited state would be an endoergonic reaction. With the excited states inaccessible the back rates display the expected inverted behavior at high driving force.

The results reported here have intriguing implications for the initial charge separation step of photosynthesis. As mentioned in chapter 1, the photosynthetic center is contained within a membrane. The lack of a mobile solvent leads to a small value for λ , estimated λ to be 0.3 eV.¹⁹ The initial long-lived, charge-separated state in photosynthesis could be explained if the forward ET reaction falls on the top of the Marcus curve and the back reaction at higher driving force falls in the inverted region. One drawback to this hypothesis is that it places a very strict requirement on the driving force for the forward ET, since the small value of λ will cause the ET rates to drop off precipitously as the driving force changes from the optimal value of $\Delta G^0 = \lambda$.

The results presented here suggest an alternative possibility. If low lying excited states are accessible on either the donor chlorophyll or the acceptor pheophiton then the forward ET rate would be fast for any driving force greater than λ . The back ET to form the ground state complexes will still remain inverted for driving forces greater than λ because no low lying excited states are accessible.

References.

- (1) Marcus, R.A.; Sutin, N. *Biochim. Biophys. Acta* **1985**, *811*, 265-322.
- (2) (a) Calcaterra, L.T.; Closs, G.L.; Miller, J.R. *J. Am. Chem. Soc.* **1983**, *105*, 670-671.
(b) Wasielewski, M.R.; Niemczyk, M.P.; Svec, W.A.; Pewitt, E.B. *J. Am. Chem. Soc.* **1985**, *107*, 1080-1082. (c) McLendon, G.; Miller, J.R. *J. Am. Chem. Soc.* **1985**, *107*, 7811-7816. (d) Gould, I.R.; Ege, D; Mattes, S.L.; Farid, S.J.; *J. Am. Chem. Soc.* **1987**, *109*, 3794-3796. (e) Ohno, T.; Yoshimura, A.; Shioyama, H.; Mataga, N.J.. *Phys. Chem.* **1987**, *91*, 4365-4370.
(f) Macqueen, D.B.; Schanze, K.S. *J. Am. Chem. Soc.* **1992**, *114*, 1897-1898. (g) Fox, L.S.; Kozik, M.; Winkler, J.R.; Gray, H.B. *Science* **1990**, *247*, 1069-1071. (h) Mallouk, T.E.; Schmehl, R.H.; Atherton, S.J.; Kim, Y.I.; Riley, R.L.; Yonemoto, E.H. *J. Am. Chem. Soc.*, **1992**, *114*, 8081-8087.
- (3) Rehm, D.; Weller, A. *Israel J. Chem.* **1970**, *8*, 259-271.
- (4) Marshall, J.M. Ph.D. Thesis, California Institute of Technology, **1987**.
- (5) Ellis, W. Ph.D. Thesis, California Institute of Technology,
- (6) Steckham, E.; Kuwana, T.; *Ber. Buns. Gesell.*, **1974**, *78*, 253-258.
- (7) The time chosen for the ΔOD values at 395 nm and 500 nm corresponded to when the largest signals were observed.
- (8) Ph.D. Thesis, University of Minnesota, Boyd, D.C. **1987**.
- (9) Bushnell, G.W.; Fjeldsted, D.O.K.; Stobart, S.R.; Zaworotko, M.J.; Knox, S.A.R.; Macpherson, K.A. *Organometallics*, **1985**, *4*, 1107-1114.
- (10) Burke, M.R.; Brown, T.L. *J. Am. Chem. Soc.* **1989**, *111*, 5105.
- (11) (a) Balzani, V.; Moggi, L.; Manfrin, M.F.; Bolletta, F. *Coord. Chem. Rev.* **1975**, *15*, 321-433. (b) Sutin, N.; Creutz, C. *Pure and Appl. Chem.* **1980**, *52*, 2717-2738.
- (12) Bock, C.R.; Connor, J.A.; Gutierrez, A.R.; Meyer, T.J.; Whitten, D.G.; Sullivan, B.P.; Nagle, J.K. *J. Am. Chem. Soc.* **1979**, *101*, 4815-4824.
- (13) Marshall, J.L.; Hopkins, M.D.; Miskowski, V.M.; Gray, H.B. *Inorg. Chem.* **1992**, *31*, 5034-5040.

- (14) The fitting program was written by J.R. Winkler and modified by T. M. McCleskey.
- (15) Brunshwig, B.S.; Sutin, N. *Comments Inorg. Chem.* **1987**, *6*, 209-235.
- (16) Brunshwig, B.S.; Ehrenson, S.; Sutin, N. *J. Am. Chem. Soc.* **1984**, *106*, 6858-6859.
- (17) Itoh, M.; Nagakura, S. *Bull. Chem. Soc. Jpn.* **1966**, *39*, 369-375.
- (18) Lichtenberger, D.L.; Copenhaver, A.S.; Gray, H.B.; Marshall, J.L.; Hopkins, M.D. *Inorg. Chem.* **1988**, *27*, 4488-4493.
- (19) Parson, W.W.; Ke, B. *Photosynthesis: Energy Conversion by Plants and Bacteria*, Vol. I. **1982**, Academic Press, New York, New York.

Chapter Four:
Gold as a Luminescent Probe
for the
Coordination Environment of the Active Site in Azurin

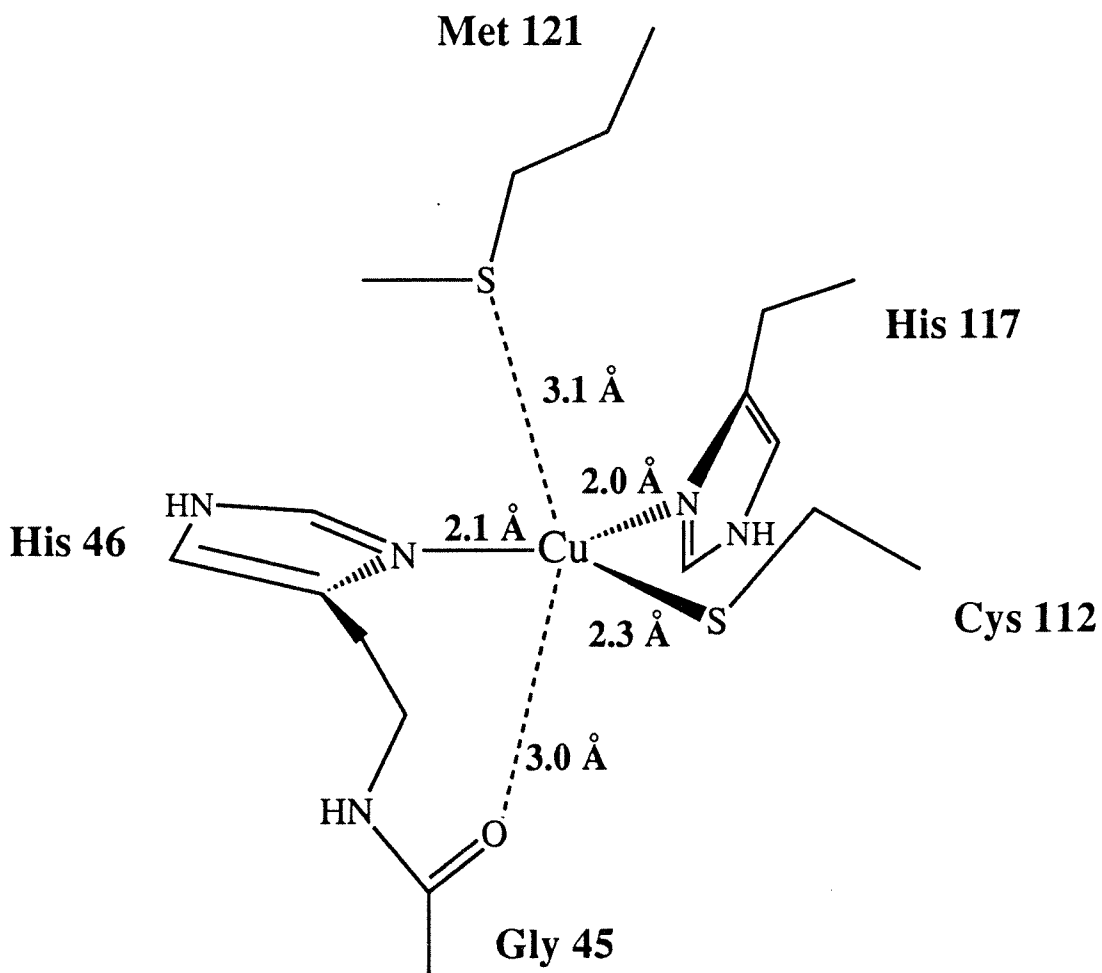
Background

There has been a great deal of discussion in literature concerning the coordination chemistry of the active site in the blue copper protein azurin.^{1,2} It is agreed that the site is a type I copper site with three essential features: the Cu(II) is strongly bound to two histidines and a cysteine with an intense band ($\lambda_{\max} = 630 \text{ nm}$) due to a ligand to metal charge transfer from the cysteine to the Cu(II); the epr spectrum has a small hyperfine splitting of $58 \times 10^{-4} \text{ cm}^{-1}$; the copper reduction potential ($E_{1/2} = 288 \text{ mV}$, pH 8.5) is high compared to aqueous Cu(II). The question under discussion is the strength of the interaction between the copper center and the methionine at position 121. The crystal structure of the oxidized form of *Pseudomonas aeruginosa* has been determined, yielding copper-ligand distances of: Cu(II)-His117, 2.0 Å; Cu(II)-His46, 2.1 Å; Cu(II)-Cys112, 2.3 Å; Cu(II)-Met121, 3.1 Å (Figure 4.1).³ The distance of 3.1 Å between the Cu(II) and the methionine is clearly longer than a normal copper thioether bond, but there is still the possibility of some interaction. Solomon et al. have used these crystal coordinates to perform SCF-X α -SW calculations to determine that a 30 % bond exists between the copper and the methionine.⁴ Recent NMR experiments on the Co(II) and Ni(II) substituted azurins have shown paramagnetic shifts of the methyl proton resonances of the methionine is observed; these observations have been interpreted as an indication that the methionine is bound to the copper center.⁵

Introduction

In chapter two it was shown that three-coordinate Au(I) complexes emit, where as four-coordinate Au(I) complexes show no emissive properties. This feature was exploited by using gold as luminescent probe for the coordination geometry of the active site in *Pseudomonas aeruginosa* azurin. The Au(I) center is known to bind thiols strongly, so the cysteine will be a good ligand. The Au(I) is a more appropriate substitution for the Cu(I) center than the Ni(II) and Co(II), since Au(I) is isoelectronic with Cu(I), and is found in similar coordination environments. In terms of the

Figure 4.1 Active site of *Pseudomonas aeruginosa*.



methionine interaction, Au(I) is a softer metal than Cu(I), so one would expect any metal-methionine interaction in the reduced wild-type (WT) holo azurin to increase upon Au(I) substitution. If the Au(I) azurin has a significant interaction with the methionine to generate a distorted tetrahedral geometry, then no emission will be observed. No interaction with the methionine would place the Au(I) in a trigonal planar environment, and strong luminescence should be observed from the Au(I) center.

A previous attempt to make Au(I) substituted azurin has been published, using gold thiomalate as the starting material. The initial thiomalate starting material already has a fairly strong gold-thiolate bond, so one would expect surface binding to form a two coordinate gold complex with the gold-thiolate bond remaining intact. The report shows only a portion of the ^1H spectrum, and offers no evidence for whether or not the gold atom is bound to the active site.

A mutant azurin was also prepared, in which the methionine at position 121 (Met 121) is replaced with a leucine residue. The Met121 to Leu121 mutant has been made previously and is known to retain a type I blue copper site.⁶ The mutant Au(I) azurin will serve as a good control since it has no possible fourth ligand for the Au(I) center. Luminescence from the gold(I) center should be readily observed in this gold substituted protein. Comparison between the WT-Au(I) and Met121 \rightarrow Leu121 -Au(I) azurins will show even subtle bonding interactions by a shift in the emission maximum. Any bonding interaction will raise the energy of the p_z orbital and lead to higher energy emission.

Experimental

Materials All enzymes and buffers for DNA manipulations were purchased from New England BioLabs or Mannheim Boehringer Biochemicals unless otherwise specified. Most techniques were standard biological techniques.⁷ Sequencing was performed with a Sequenase version 2.0 kit purchased from the United States Biochemical Corp. Oligonucleotides were synthesized at the Caltech microchemical

facility. Electroporation was induced with a Bio-Rad Gene-Pulser set at 2.5 kV and 200 ohms. Cells were centrifuged with a RC2-B Sorvall Superspeed centrifuge. Ultracentrifugation for DNA isolation was carried out with a Beckman L2-75B ultracentrifuge. The Muta-Gene Kit was purchased from Bio-Rad. The QIAX-Gel Extraction kit and the Plasmid Maxi-kit were purchased from Qiagen. The pET System was purchased from Novagen. The FPLC purifications were done with a Pharmacia FPLC System using a Mono Q column. The loading buffer, A, is a solution of 10 mM Diethanolamine (DEA) at pH = 8.8, and the eluant buffer, B, is a solution of 100 mM NaCl, and 10 mM DEA at pH = 8.8. All media was autoclaved for 20 minutes and allowed to cool prior to use.

Protein Preparation *Pseudomonas aeruginosa* azurin was expressed from a synthetic gene in *Escherichia coli* with a frozen cell culture previously prepared.⁸ An aliquot (200 μ L) of frozen (-70°C) cells which had been transformed with a pET 9-A plasmid containing the azurin gene was suspended in 20 mL of 2xYT media with 50 μ g/mL kanamycin and shaken for 14 to 20 hours at 30 °C. The 20 mL of suspended cells were then added to a 6 L flask containing 4 L of 2xYT media with 50 μ g/mL kanamycin. The solution was shaken at 30 °C for 5 hours. The absorbance was measured at 1 hour intervals at 550 nm and 650 nm. When the absorbance at 550 nm was greater than 2.0 and the absorbance at 650 nm was greater than 1.5, 3mL of a 20% aqueous solution of IPTG was added, and the cell mixture was shaken for \approx 5 hours at 30°C. The cell paste was then isolated by centrifugation at 5000 rpm. The cells were then resuspended in 360 mL of a 20% sucrose, 30 mM Tris, and 1mM EDTA at pH = 8.0 by shaking at room temperature. The cell paste was isolated by centrifugation at 8000 rpm and resuspended in 360 mL of a 4 mM NaCl, ice-cold, aqueous solution causing osmotic shock. The azurin produced by the *E. coli* is transported to the periplasm between the inner and outer cell membranes. The mild lysing conditions cause only the outer membrane to lyse so that the contents of the periplasm are released into solution,

but the rest of the cell remains intact. The solution was shaken in a cold room at 4°C overnight. The cell paste was removed by centrifugation at 5000 rpm, and the supernate was stirred gently 4°C. Addition of 36 mL of a 0.5 M aqueous solution of ammonium acetate (pH = 4.1; note initial addition of the solution should be made slowly to avoid fast pH changes) resulted in the precipitation of some unwanted proteins. The precipitate was removed by centrifugation at 7000 rpm, and the supernate was reduced in volume to 35 mL by ultrafiltration at . The buffer system was the exchanged to pH = 8.8 with 10 mM DEA by adding three aliquots of the new buffer and reducing the volume by ultrafiltration between additions. The apo-azurin was further purified by FPLC. The FPLC trace shows two peaks at 15% buffer B; the first peak is due to Zn²⁺-azurin and the second peak corresponds to apo-azurin.

Site-Directed Mutagenesis The site-directed mutagenesis involves taking an oligonucleotide of ≈ 20 base pairs with the desired mutation and annealing it to a single stranded plasmid containing the WT-azurin gene. The oligonucleotide was synthesized to match with the Met121 area of the azurin gene. The uracil containing plasmid and the oligonucleotide were combined with annealing buffer and water. The solution was then placed in a water bath at 80°C. The water bath was allowed to cool to 30°C, at which point the annealed plasmid was placed on ice. The plasmid was ligated by addition of synthesis buffer, 5 fold diluted polymerase, and T4 ligase. The resulting solution was kept at 37°C for 90 minutes. The ligase was stopped with the addition of 90 μL TE. The plasmid was then transformed into MV1190 cells: 45 μL of frozen MV1190 cells were placed on ice for 30 minutes; 10 μL of the plasmid solution were added; the mixture was shocked with 2.5 KV at 100 ohms; shocked cells were promptly treated with 900 μL SOC. The transformed cells were placed at 37°C for 1 hour and then centrifuged for 1 minute. The supernate was discarded to leave 100 μL of solution. The cells were resuspended and plated out onto LB culture plates containing ampicillin. The plates were incubated at 30°C for 14 hours. One of the resulting cell colonies was placed into 10 mL

of 2xYT media containing 30 µg/mL of ampicillin and shaken overnight at 30°C. The 10 mL of suspended cells was placed into a flask containing 500 mL of 2xYT and shaken for 12 hours at 30°C. The cells were isolated by centrifugation at 5000 rpm and the DNA was isolated using a Quiagen DNA kit. An aliquot of DNA was sequenced by standard procedures. Another aliquot of the DNA was cleaved with Bagel II and NDE I. The DNA was separated on a gel and the resulting small fragment containing the mutant azurin gene was isolated. A kanamycin resistant pET 9-A plasmid was cleaved with NDE I and BamHI. The DNA from the cleavage reaction was separated on an agar gel. The large fragment was isolated from the gel. The DNA was extracted from the gel according to the procedure for the Quiagen DNA extraction. Next the Pet-9A DNA (3 µL) and the mutant azurin DNA (6 µL) were combined and ligated with T4-ligase (1 µL T4-ligase with 2 µL ligase buffer and 8 µL water). The Pet 9A plasmid was transformed into BL21(DE3) *E. coli* cells by a heat shock procedure: competent BL21(DE3) cells (20 µL) and an aliquot of the Pet-9A plasmid solution (5 µL) were mixed together and placed on ice for 30 minutes; the solution was placed in a 42°C bath for 45 seconds; 80 µL of SOC were added and the solution was iced for 2 minutes and then incubated at 37°C for 1 hour. The cells were plated out onto LB plates containing 30 µg/mL kanamycin and incubated at 30°C overnight. One colony from the cell culture was placed into 20 mL of 2xYT containing 30 µg/mL kanamycin and shaken for 12 hours at 30°C. The 20 mL of suspended cells were then added to 1 L of 2xYT containing 30 µg/mL kanamycin and shaken at 30°C for 14 hours. Twenty aliquots of 100 µL were diluted with 100 µL of 50% glucose and frozen for protein preparations and the remaining cells were isolated by centrifugation at 5000 rpm. The DNA was extracted according to the Quiagen procedure and the entire gene was sequenced. The protein was expressed and purified in the same manner as described for WT-azurin except that prior to high pressure ultra filtration the solution was made 1mM EDTA and stirred at room

temperature for 24 hours. The addition of EDTA removes a large percentage of the zinc from the Zn-azurin. The FPLC trace shows two peaks just as the WT-azurin.

Incorporation of Gold(I) The Au(I) starting material, $\text{ClAuS}(\text{CH}_2\text{CH}_2\text{OH})_2$, was prepared by adding a two-fold excess of $\text{S}(\text{CH}_2\text{CH}_2\text{OH})_2$ to a stirring solution of 1g auric acid (HAuCl_4) in 50 mL of nanopure water. After stirring for three hours, the water was removed by rotary evaporation under reduced pressure. The resulting oil was dissolved in 15 mL of ethanol followed by the addition of ether to precipitate the product. The $\text{ClAuS}(\text{CH}_2\text{CH}_2\text{OH})_2$ can be stored for months under ether, but will decompose in less than twelve hours if one tries to isolate the solid. A threefold excess of $\text{ClAuS}(\text{CH}_2\text{CH}_2\text{OH})_2$ in 1 mL of water was added to a solution of 10 mg of apo-azurin in 8 mL of 10mM DEA at pH = 8.8 and the solution was allowed to sit for forty-eight hours. Surface bound gold was removed reducing the volume in a centricon and exchanging the buffer with a 100 mM NaCl, 10mM DEA solution at pH = 8.8. After sitting for three hours the buffer was exchanged back to 10 mM DEA at pH = 8.8. The gold substituted protein was purified by FPLC. The FPLC trace shows a major peak for the gold substituted protein followed by a small peak for the apo-protein (Figure 4.2).

Results and Discussion

Electronic Absorption Spectra The Au(I)-WT-azurin has an absorption spectrum similar to that of apo-WT-azurin (Figures 4.3 -4.4). Both proteins have a strong UV absorption band at 260 nm and the characteristic spike, due to the tryptophan residue, at 292 nm. The Au(I) -WT-azurin spectrum differs from that of apo-WT-azurin spectrum with a low energy shoulder at 308 nm and a large increase in the absorbance at 250 nm. The two new features must be due to transitions which involve the metal orbitals. The band at 308 nm is tentatively assigned as the metal centered $^1A_1 \rightarrow E'$ ($^3E''$) transition in analogy with the three coordinate gold complexes discussed in chapter two. The low energy shoulder observed in the Au(I)-WT-azurin spectrum is also observed in the isoelectronic reduced-holo-WT-azurin spectrum. The only difference between the

Figure 4.2. FPLC trace for Au(I)-WT-azurin purification.

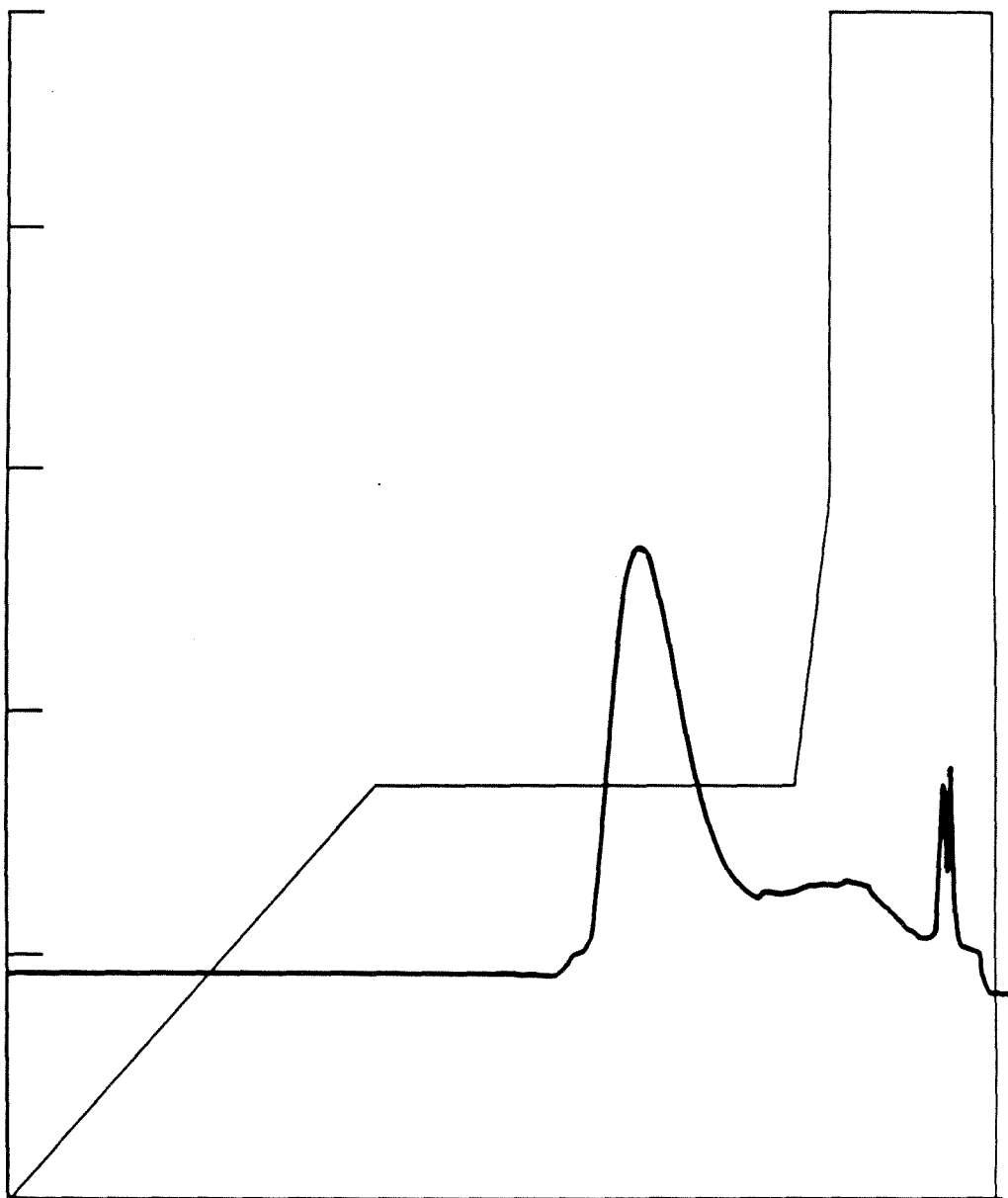


Figure 4.3. Absorption spectrum of apo-WT-azurin.

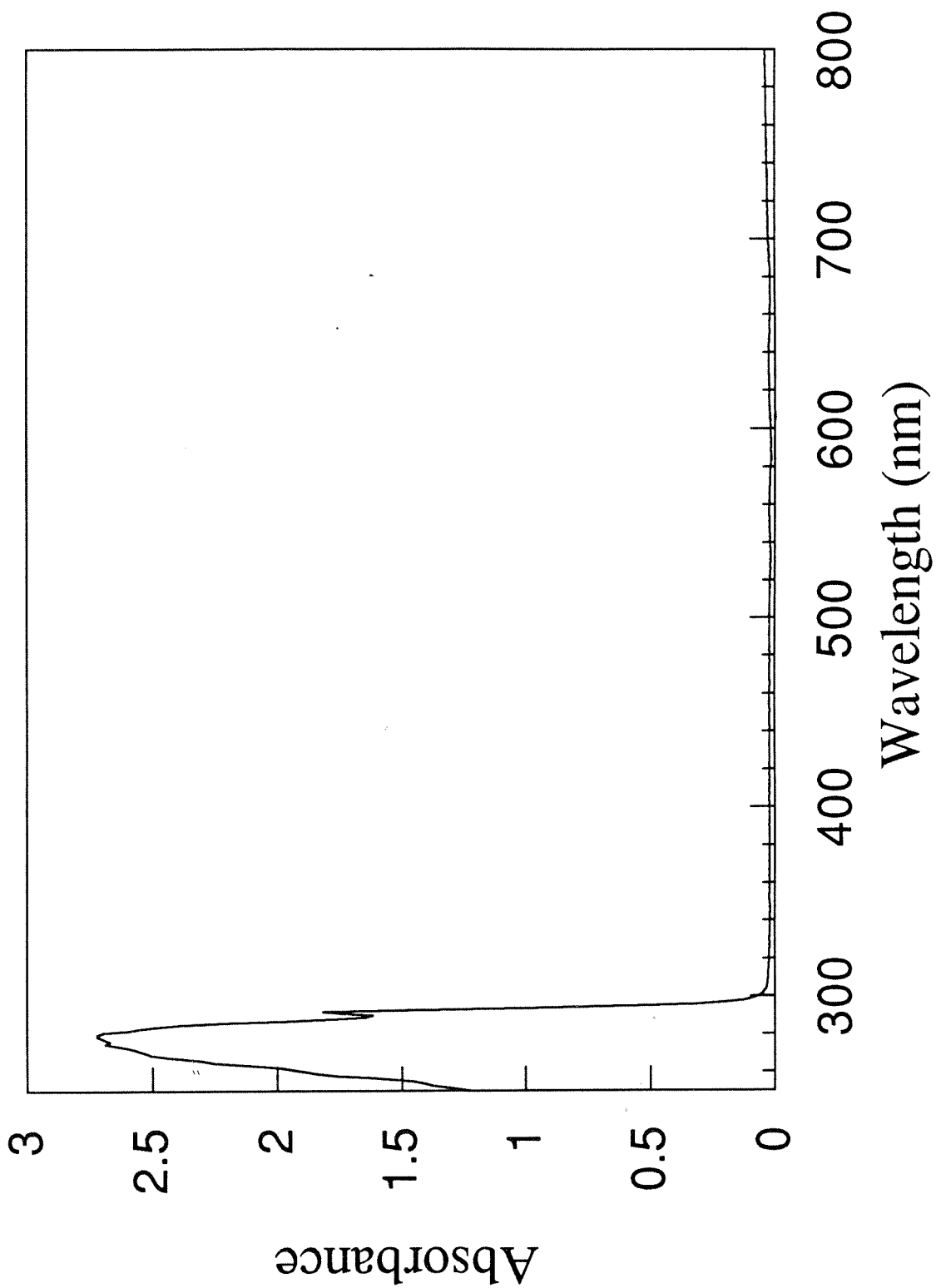


Figure 4.4 Absorption spectrum of Au(I)-WT-azurin.

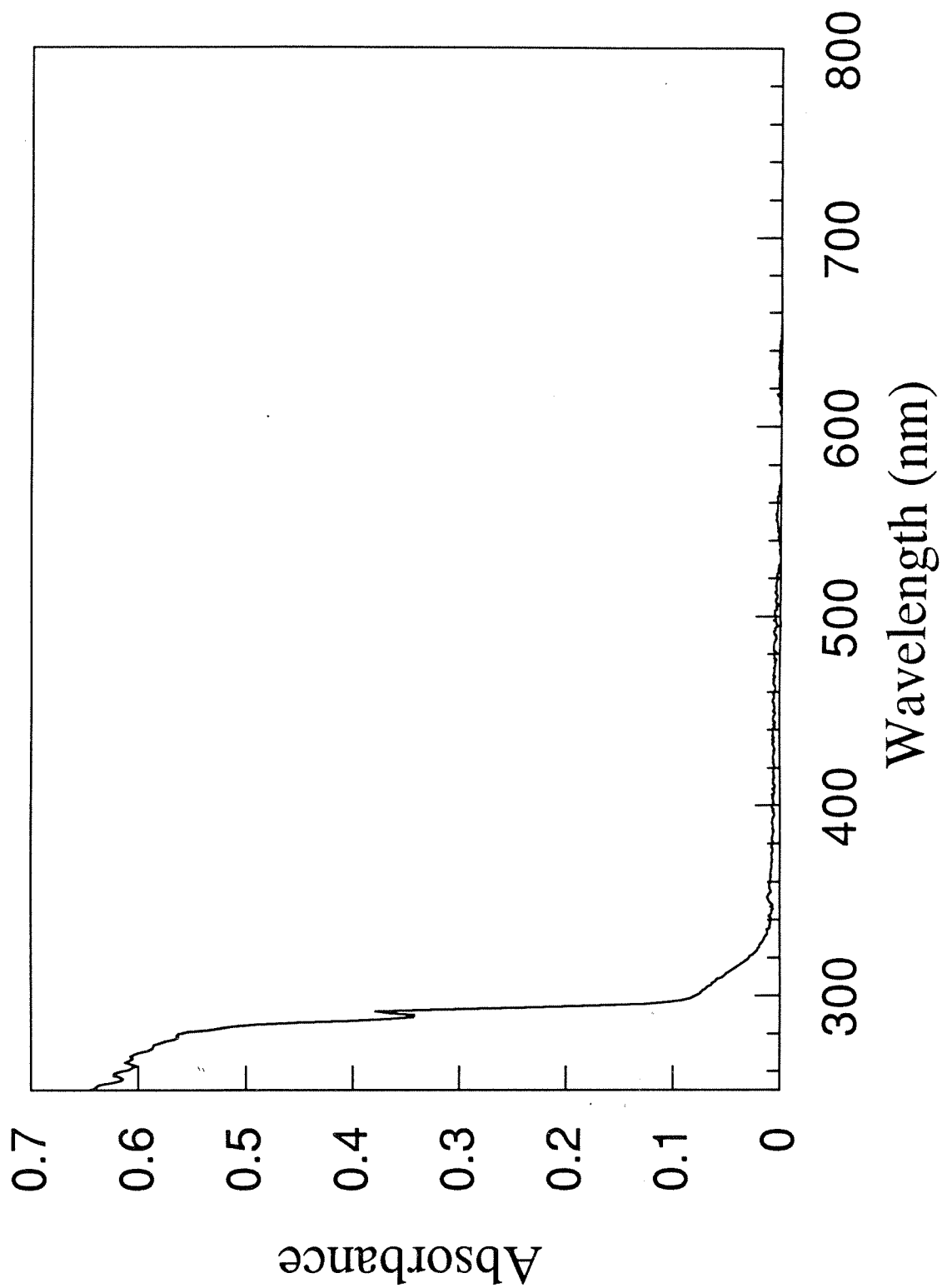


Figure 4.5. Emission spectrum of apo-WT-azurin, 77 K glycerol:water glass.

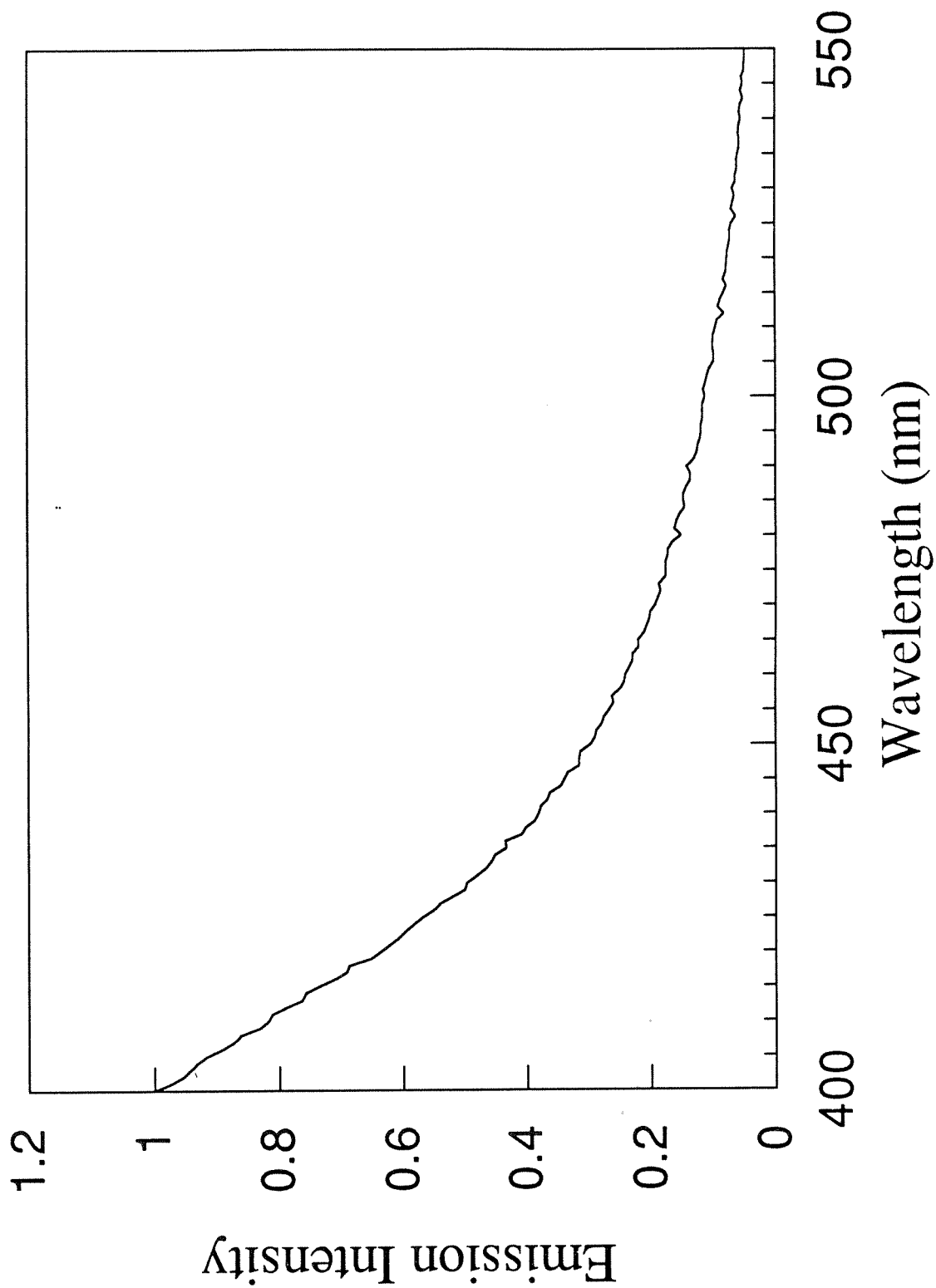


Figure 4.6. Emission spectrum of reduced-holo-WT-azurin, 77 K glycerol:water glass.

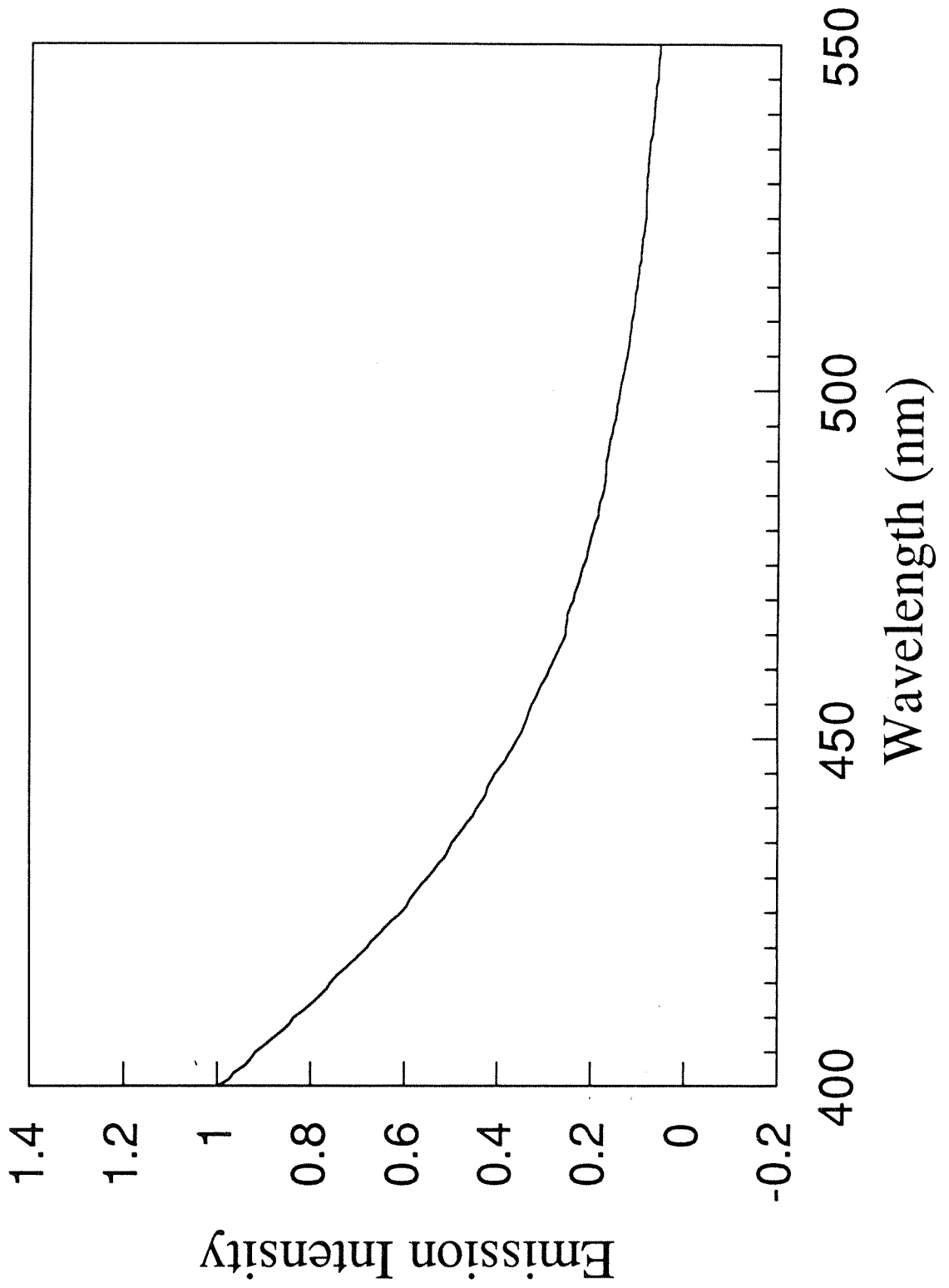


Figure 4.7. Emission spectrum of holo-WT-azurin, 77 K glycerol:water glass.

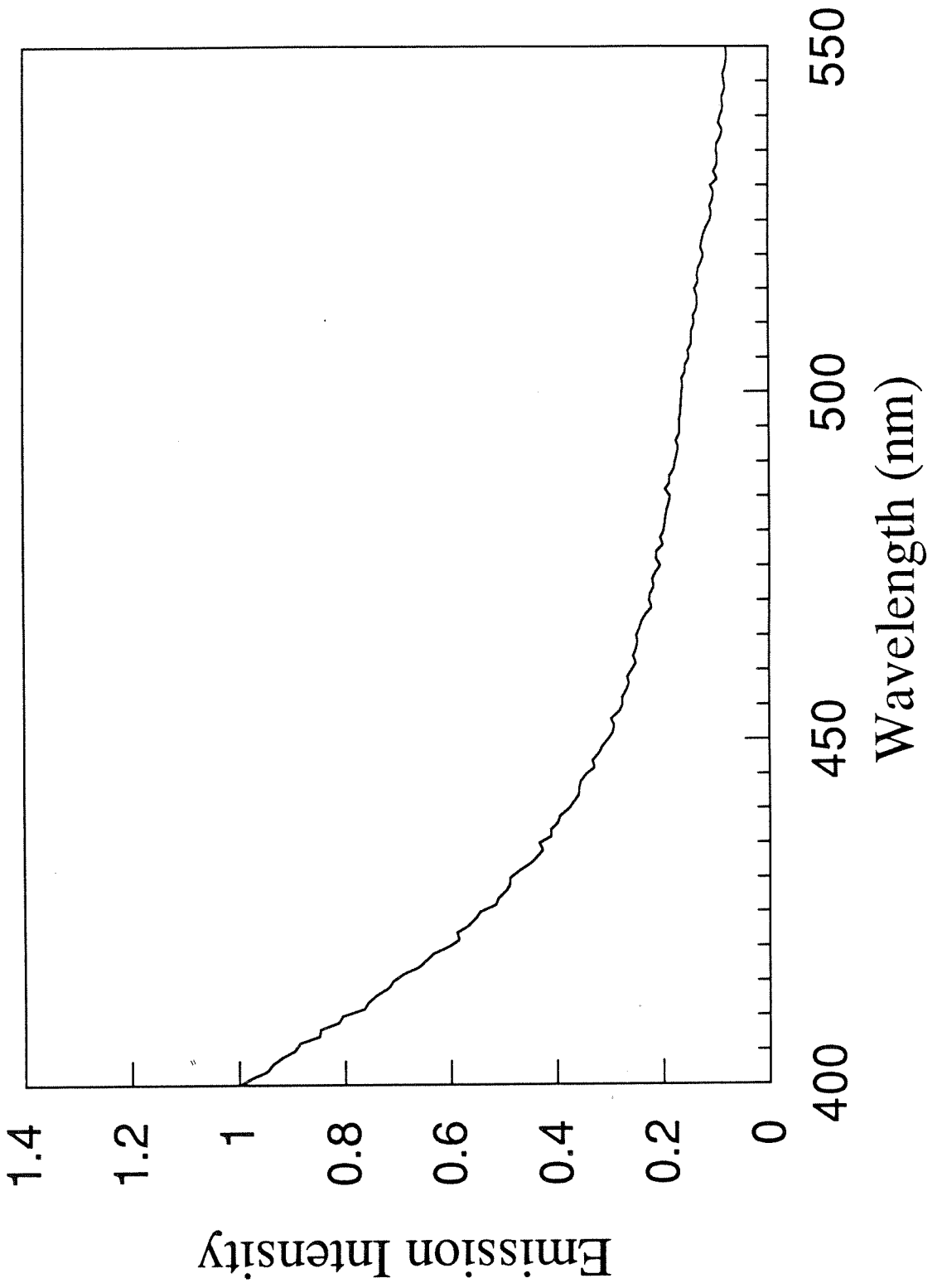


Figure 4.8. Emission spectrum of Au(I)-WT-azurin, 77 K glycerol:water glass.

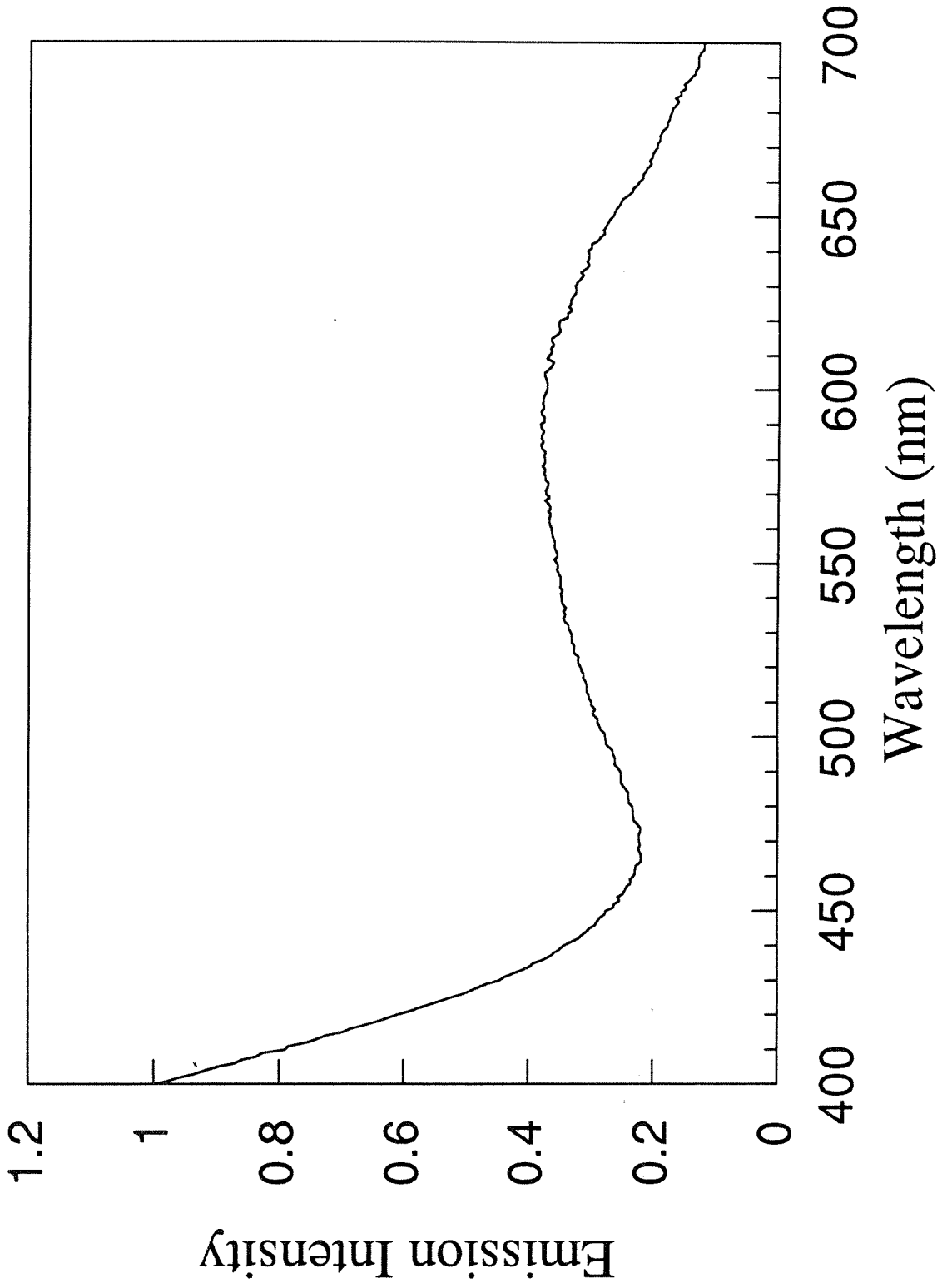


Figure 4.9. Luminescence decay of Au(I)-WT-azurin, 77 K glycerol:water glass.

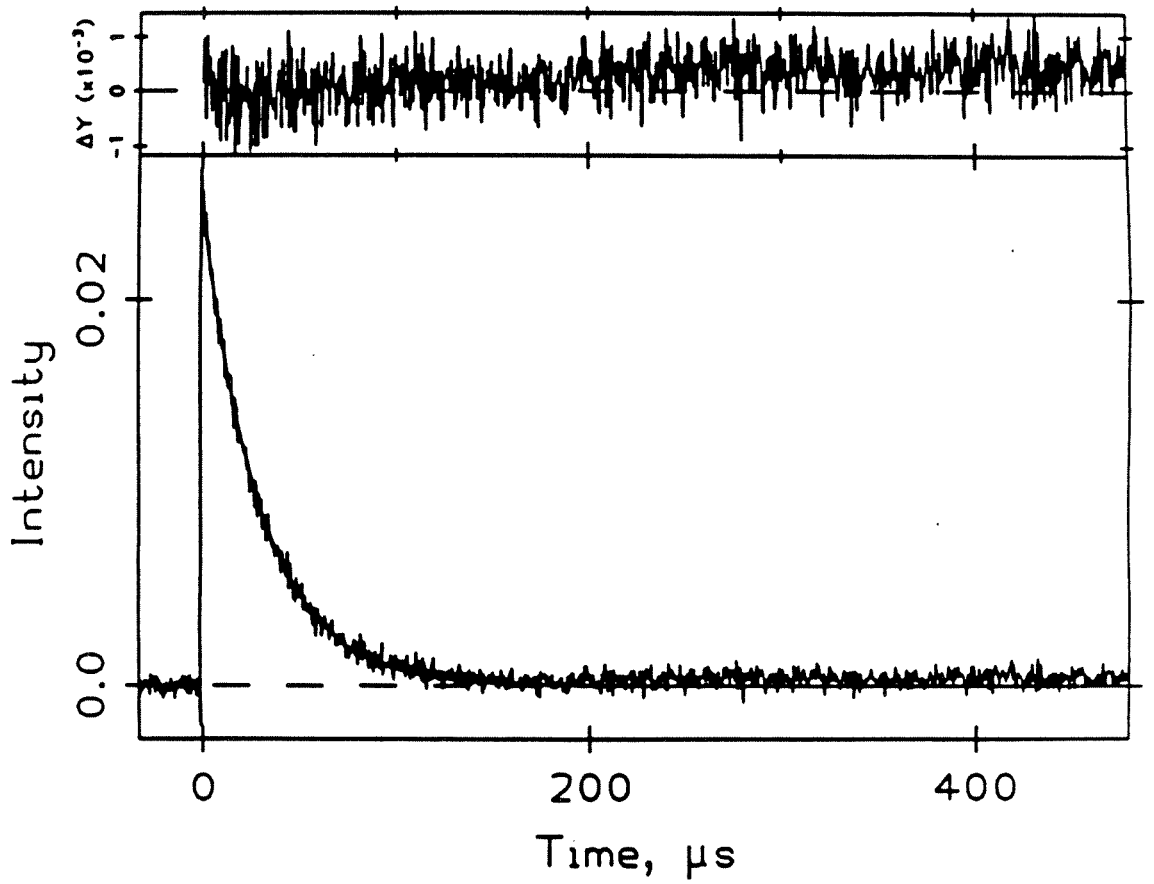
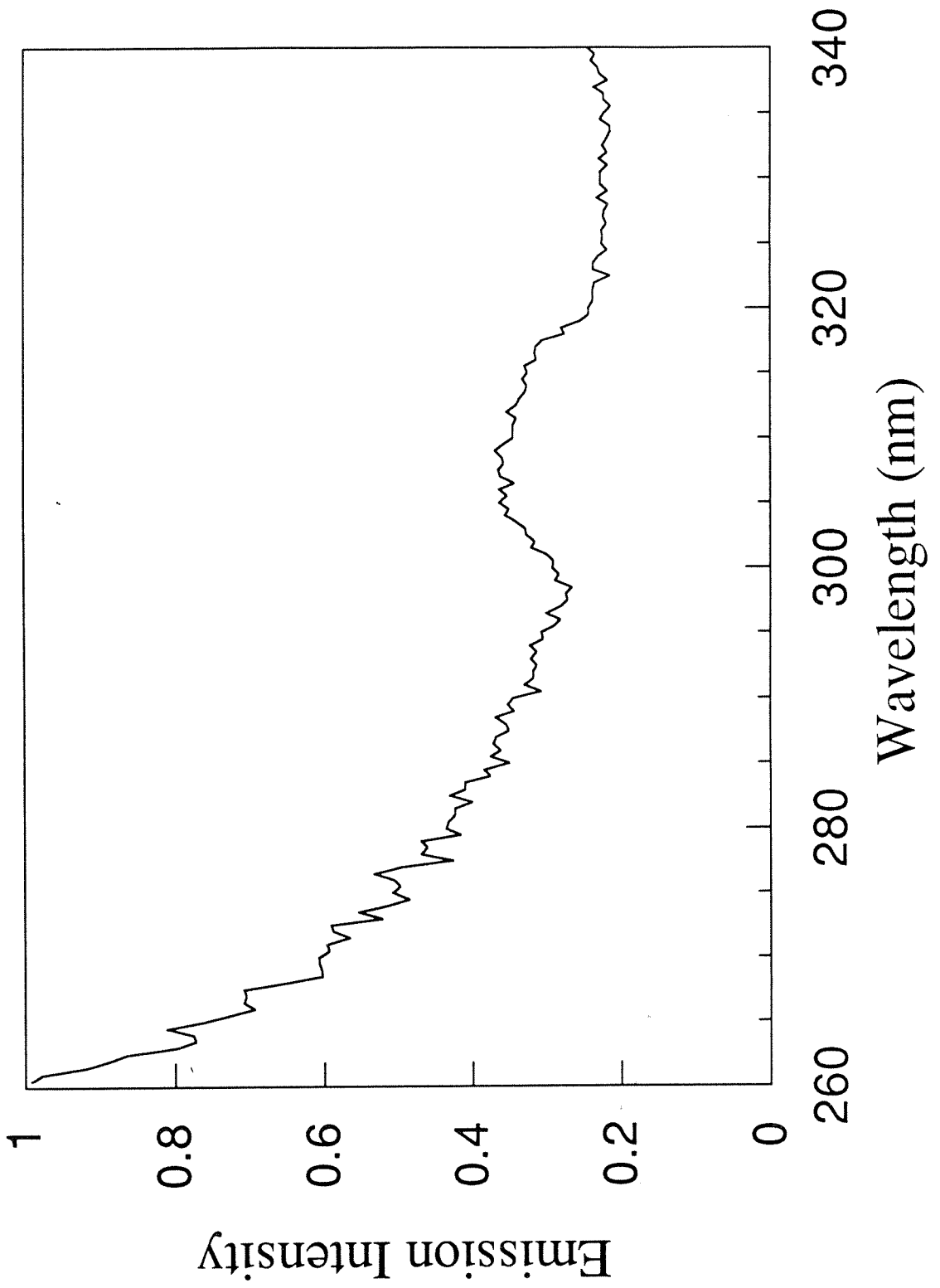


Figure 4.10. Excitation spectrum of Au(I)-WT-azurin.



Au(I)-WT-azurin spectrum and that of reduced-holo- WT-azurin is that the Au(I)-WT-azurin has greater absorbance at 250 nm.⁹

Emission and Excitation Spectra

The emission spectra of holo-, reduced-holo-, and apo- azurins at 77 K in a 50:50 water:glycerol glass are nearly identical (excitation at 313 nm; Figures 4.5 to 4.7). The emission spectra consist of a combination of fluorescence and phosphorescence from the tryptophan residue. The tryptophan emission has been observed previously: the fluorescence maximum occurs at 310 nm with a lifetime of 12 ns and the phosphorescence maximum occurs at 445 nm with a lifetime of 210 ms (lifetimes measured at room temperature).^{10,11} The emission spectrum of the Au(I)-WT-azurin shows the tryptophan emission as well as a new low energy emission band at 580 nm (Figure 4.8). This low energy emission has a lifetime of 30 μ s, which corresponds well with the lifetime observed for the three coordinate gold(I) complexes discussed in chapter two (Figure 4.9). The excitation spectrum of the Au(I)-WT-azurin has a band at 308 nm (Figure 4.10). The fact that the band at 308 nm leads to emission with a lifetime of 30 μ s supports the assignment of the band as the $^1A_1 \rightarrow E' (^3E'')$ transition.

Control Experiments for Active Site Binding

An excess of CuSO_4 was added to a solution of Au(I)-WT-azurin (100 μ M) and the solution was left standing at 4 $^\circ$ for one day. The solution was then repeatedly (3 times) reduced in volume by centrifuge filtration and diluted with buffer A to remove the CuSO_4 . The absorption spectrum remain unchanged from the initial Au(I)-WT azurin spectrum indicating that the gold does indeed bind to the active site. If gold were not bound to the active site then a band at 628 nm would have appeared as the Cu^{2+} bound to the active site. The fact that Cu^{2+} does not displace the Au^+ demonstrates that the gold is tightly bound to the active site.

A further test of active site binding was accomplished with a Cys112 to Asp112 mutant. The mutant is known to bind Cu(II) in the active site through Cu(II)-oxygen

binding.¹² The Au(I) soft metal center does not tend to bind oxygen, and would not be expected to bind the active site of the Asp112 mutant. The mutant azurin was placed in solution with two equivalents of $\text{ClAuS}(\text{CH}_2\text{CH}_2\text{OH})_2$ for one day at 4 °C and then purified by FPLC. The purified protein showed no indication of binding Au(I) and readily bound Cu(II) upon addition of CuSO_4 . The lack of Au(I) binding indicates that the cysteine of the active site is needed to bind Au(I) in the WT-azurin.

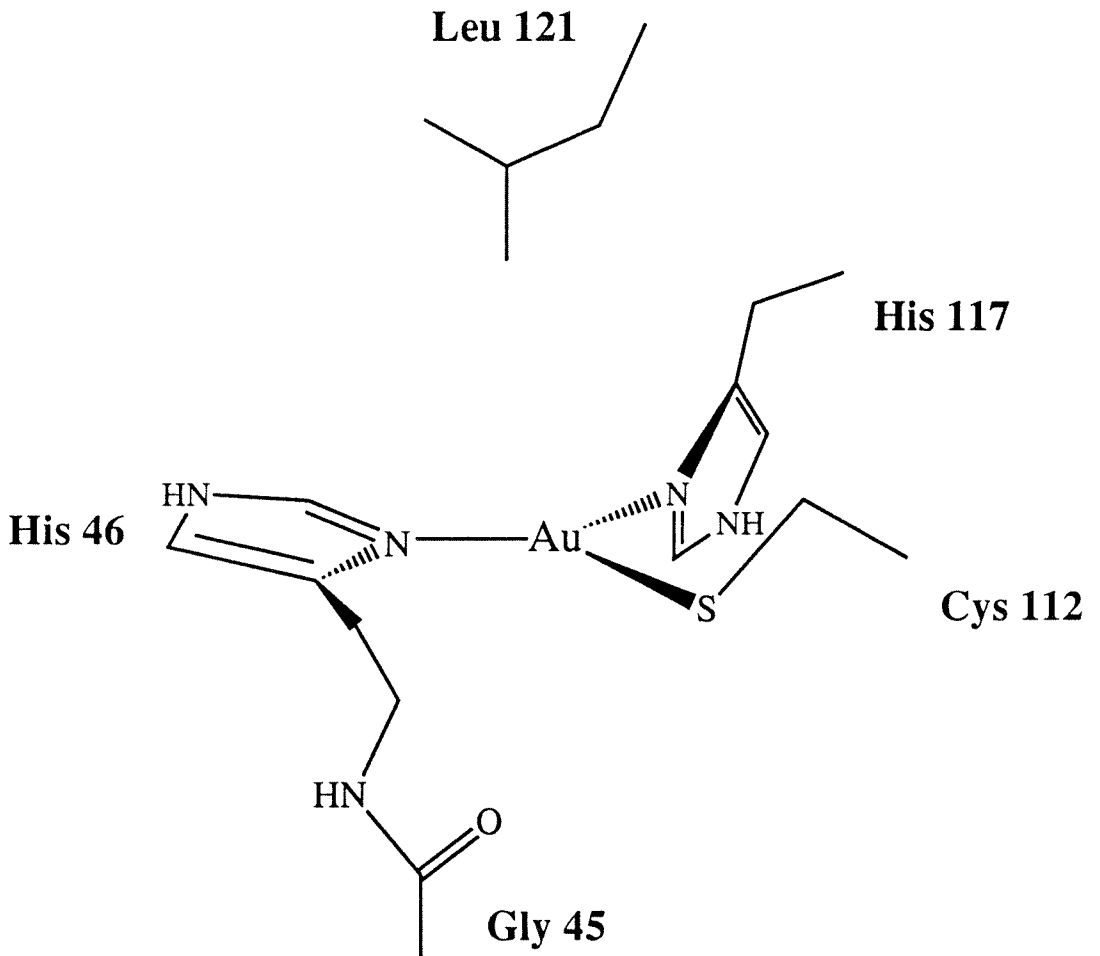
To ensure that surface binding is not present, the $\text{ClAuS}(\text{CH}_2\text{CH}_2\text{OH})_2$ was added to a solution of holo-WT-azurin and the solution was allowed to stand for one day at 4 °C. After washing with buffer B, FPLC purification showed only one peak. The absorption spectra of the purified protein is identical to holo-WT-azurin, and the emission spectrum shows only tryptophan emission. The absence of any low energy emission demonstrates that the 580 nm emission of Au(I)-WT-azurin is not due to surface bound Au(I).

Conclusions

We have synthesized a Au(I)-WT-azurin where the Au(I) center is bound to the active site. The Au(I)-WT-azurin has an emission band not present in holo, reduced-holo, or apo-azurins. As discussed in chapter two, isolated two coordinate Au(I) complexes such as $\text{Au}(\text{PCy}_3)_2^+$ and four coordinate complexes such as $\text{Au}(\text{dcpe})_2^+$ do not emit, but three coordinate gold complexes are highly emissive. The low energy ($\lambda_{\text{max}} = 580 \text{ nm}$) emission of the Au(I)-WT-azurin has been assigned as the $^1\text{A}_1 \leftarrow \text{E}'$ ($^3\text{E}''$) transition associated with the three coordinate Au(I). The corresponding absorption band appears as a shoulder at 308 nm. The large Stokes shift of $15,400 \text{ cm}^{-1}$ for the Au(I)-WT-azurin is nearly twice that observed for the three coordinate model complexes, indicating a substantial amount of reorganizational energy in the excited state.

Based on the 580 nm emission of Au(I)-WT-azurin the geometry of the Au(I) site in azurin is believed to be three coordinate with the Au(I) bound to Cys112, His46, and His117. The Au(I) center is isoelectronic with Cu(I), so the Cu(I) site is also believed to

Figure 4.11. Theoretical active site for the Au(I)-Leu121 mutant.



be three coordinate with no bonding interaction between the Cu(I) center and the Met121. If there were any bonding interaction between the Cu(I) and Met121, one would expect the interaction to be even greater for the larger, softer Au(I) center since methionine is a soft ligand. Even a small amount of bonding interaction would move the $E_{\nu_0-\nu_0}$ energy to higher energy than the 430 nm $E_{\nu_0-\nu_0}$ energy observed for the three coordinate complexes in chapter two and any significant bonding interaction would shut off the emission completely. The partial bond suggested by Solomon for the 2.9 Å Cu(I) - methionine corresponds to bond energy of 7 kcal/mol. This interaction should shift the $E_{\nu_0-\nu_0}$ energy from 430 nm to 390 nm. The $E_{\nu_0-\nu_0}$ does shift 20 nm to higher energy for the Au(I)-WT-azurin ($E_{\nu_0-\nu_0} = 410$ nm), but this is much smaller than the predicted shift and could also be explained by less electron density donation from the ligands. The cysteine and two histidines in Au(I)-WT-azurin would be expected to be less donating than three phosphines, so that the d orbitals of Au(I)-WT-azurin will be slightly lower in energy. The $E_{\nu_0-\nu_0}$ of the Au(I) substituted Leu121 mutant (Figure 4.11) will provide a better reference point than the model complexes and is in the process of being prepared.

References

- (1) Adman, E.T. *Advances in Protein Chemistry*, **1991**, *42*, Academic Press, New York, New York. 155-197.
- (2) Sykes, A.G. *Advances in Inorganic Chemistry*, **1992**, *36*, Academic Press, New York, New York. 377-408.
- (3) Adman, E.T.; Stenkamp, R.E.; Sieker, L.C.; Jensen, L.H. *J. Mol. Bio.* **1978**, *123*, 35.
- (4) Lowery, M.D.; Solomon, E.I. *Inorganica Chimica Acta*, **1992**, *198*, 233-243.
- (5) Moratal, J-M.; Salgado, J.; Donaire, A.; Jimenez, H.R.; Castells, J.J. *Chem. Soc., Chem. Commun.*, **1993**, 110-112.
- (6) Otiko, G.; Sadler, P.J. *Biochem. Soc. Trans.*, **1981**, *9*, 445-446.
- (7) Karlsson, B.G.; Nordling, M; Pascher, T.; Tsai, L-C.; Sjolín, L.; Lundberg, L.G. *Protein Engineering*, **1991**, *4*, 343-349.
- (8) Maniatis, T.; Fritsch, E.F.; Sambrook, J. *Molecular Cloning: A Laboratory Manual, second edition*. **1982**, Spring Harbor Laboratory, Cold Spring Harbor, New York.
- (9) Chang, T. Ph.D. Thesis, California Institute of Technology, .
- (10) Glusker, J.P. *Advances in Protein Chemistry*, **1991**, *28*, 3935-3939.
- (11) Hutnik, C.M.; Szabo, A.G. *Biochemistry*, **1991**, *28*, 3935-3939.
- (12) Klemens, F.K.; McMillin, D.R. *Photochem. and Photobiol.*, **1992**, *55*, 671-676.
- (13) Mizoguchi, T.J.; Di Bilio, A.J.; Gray, H.B.; Richards, J.H. *J. Am. Chem. Soc.*, **1992**, *114*, 10076-10078.

Appendix 1 X-ray data for $[\text{Au}_2(\text{dcpe})_2](\text{PF}_6)_2$.

Table 1. Final Refined Parameters for
Bis(μ -DHPE) Digold bis-Hexafluorophosphate

x, y, z and $U_{eq}^a \times 10^4$				
Atom	x	y	z	U_{eq}
Au	652(.3)	5652	2500	439(1)
P1	1058(1)	5593(1)	717(1)	481(4)
C1	458(4)	4959(5)	-262(5)	681(20)
C10	2116(6)	5166(6)	635(8)	533(24)
C11	2128(7)	4273(5)	1132(7)	810(27)
C12	3017(9)	3932(6)	1106(9)	1030(35)
C13	3626(7)	4503(8)	1673(9)	1052(35)
C14	3624(6)	5342(8)	1209(9)	951(33)
C15	2746(5)	5736(6)	1198(8)	768(26)
C20	1107(5)	6670(5)	219(6)	597(20)
C21	300(9)	7167(7)	439(10)	894(37)
C22	407(6)	8091(6)	119(9)	1006(34)
C23	697(8)	8193(6)	-994(9)	1077(36)
C24	1465(9)	7702(8)	-1196(11)	1442(48)
C25	1372(6)	6772(6)	-934(7)	907(27)
P2	3292(3)	8292	2500	899(8)
F1	3128(8)	8509(8)	1366(5)	2497(54)
F2	3924(9)	8924	2500	3533(72)
F3	2639(8)	7639	2500	2385(44)
F4	3854(8)	7670	2050(8)	2838(63)

$$^a U_{eq} = \frac{1}{3} \sum_i \sum_j [U_{ij}(a_i^* a_j^*)(\bar{a}_i \cdot \bar{a}_j)]$$

Table S2. Complete Distances and Angles for Bis(μ -DHPE) Digold bis-Hexafluorophosphate

Distance(Å)		Distance(Å)	
Au -Au	2.935(1)	C23 -H23A	0.953
Au -P1	2.314(2)	C23 -H23B	0.951
P1 -C1	1.848(7)	C24 -H24A	0.943
P1 -C10	1.819(10)	C24 -H24B	0.955
P1 -C20	1.825(8)	C25 -H25A	0.948
C1 -C1	1.463(9)	C25 -H25B	0.948
C10 -C11	1.550(13)		
C10 -C15	1.522(13)		
C11 -C12	1.516(15)		
C12 -C13	1.504(16)		
C13 -C14	1.456(16)		
C14 -C15	1.532(14)		
C20 -C21	1.534(14)		
C20 -C25	1.505(11)		
C21 -C22	1.535(16)		
C22 -C23	1.470(15)		
C23 -C24	1.472(17)		
C24 -C25	1.524(16)		
P2 -F1	1.477(14)		
P2 -F2	1.424(31)		
P2 -F3	1.469(27)		
P2 -F4	1.448(16)		
C1 -H1A	0.950		
C1 -H1B	0.950		
C10 -H10	0.951		
C11 -H11A	0.949		
C11 -H11B	0.949		
C12 -H12A	0.949		
C12 -H12B	0.952		
C13 -H13A	0.951		
C13 -H13B	0.948		
C14 -H14A	0.952		
C14 -H14B	0.950		
C15 -H15A	0.950		
C15 -H15B	0.950		
C20 -H20	0.952		
C21 -H21A	0.949		
C21 -H21B	0.949		
C22 -H22A	0.947		
C22 -H22B	0.954		

Table S2. (Cont.)

			Angle(°)				Angle(°)
P1	-Au	-P1	160.6(1)	H11B	-C11	-C10	109.5
Au	-P1	-C1	120.7(2)	H11A	-C11	-C12	109.4
Au	-P1	-C10	109.1(3)	H11B	-C11	-C12	109.3
Au	-P1	-C20	107.4(2)	H11B	-C11	-H11A	109.6
C10	-P1	-C1	103.8(4)	H12A	-C12	-C11	108.6
C20	-P1	-C1	108.2(3)	H12B	-C12	-C11	108.4
C20	-P1	-C10	107.0(4)	H12A	-C12	-C13	109.4
C1	-C1	-P1	117.8(5)	H12B	-C12	-C13	109.0
C11	-C10	-P1	109.4(6)	H12B	-C12	-H12A	109.4
C15	-C10	-P1	111.2(6)	H13A	-C13	-C12	109.0
C15	-C10	-C11	110.7(8)	H13B	-C13	-C12	109.4
C12	-C11	-C10	109.3(8)	H13A	-C13	-C14	108.6
C13	-C12	-C11	112.0(9)	H13B	-C13	-C14	108.7
C14	-C13	-C12	111.5(10)	H13B	-C13	-H13A	109.6
C15	-C14	-C13	112.4(9)	H14A	-C14	-C13	108.9
C14	-C15	-C10	111.2(8)	H14B	-C14	-C13	109.0
C21	-C20	-P1	112.8(6)	H14A	-C14	-C15	108.5
C25	-C20	-P1	115.9(6)	H14B	-C14	-C15	108.7
C25	-C20	-C21	110.4(7)	H14B	-C14	-H14A	109.3
C22	-C21	-C20	110.8(9)	H15A	-C15	-C10	109.1
C23	-C22	-C21	112.6(9)	H15B	-C15	-C10	109.1
C24	-C23	-C22	111.4(10)	H15A	-C15	-C14	109.1
C25	-C24	-C23	113.4(10)	H15B	-C15	-C14	108.9
C24	-C25	-C20	109.6(8)	H15B	-C15	-H15A	109.5
H1A	-C1	-P1	107.3	H20	-C20	-P1	102.3
H1B	-C1	-P1	107.4	H20	-C20	-C21	109.3
H1B	-C1	-H1A	109.5	H20	-C20	-C25	105.3
C1	-C1	-H1A	107.4	H21A	-C21	-C20	109.0
C1	-C1	-H1B	107.4	H21B	-C21	-C20	108.9
F2	-P2	-F1	87.7	H21A	-C21	-C22	109.2
F3	-P2	-F1	92.3	H21B	-C21	-C22	109.3
F4	-P2	-F1	84.2	H21B	-C21	-H21A	109.7
F1	-P2	-F1	175.3	H22A	-C22	-C21	108.9
F3	-P2	-F2	180.0	H22B	-C22	-C21	108.3
F4	-P2	-F2	92.6	H22A	-C22	-C23	109.0
F4	-P2	-F3	87.4	H22B	-C22	-C23	108.6
H10	-C10	-P1	108.5	H22B	-C22	-H22A	109.4
H10	-C10	-C11	109.3	H23A	-C23	-C22	108.9
H10	-C10	-C15	107.7	H23B	-C23	-C22	109.2
H11A	-C11	-C10	109.7	H23A	-C23	-C24	108.8

Table S2. (Cont.)

	Angle(°)
H23B -C23 -C24	109.4
H23B -C23 -H23A	109.1
H24A -C24 -C23	109.1
H24B -C24 -C23	108.4
H24A -C24 -C25	108.5
H24B -C24 -C25	107.7
H24B -C24 -H24A	109.7
H25A -C25 -C20	109.4
H25B -C25 -C20	109.2
H25A -C25 -C24	109.3
H25B -C25 -C24	109.4
H25B -C25 -H25A	109.8

Bis(mu-DHPE) Digold (PF0)2				Page		1											
1	k	0	0	877	867	9	1	677	696	-14	3	411	391	7			
			1	369	419	-47	2	250	232	7	4	-183	50	-19			
1	3549	3731	-49	2	346	355	-7	3	239	216	9	5	311	290	6		
			2	1251	1280	-22	4	151	171	-5	6	128	46	7			
			3	317	305	8	5	398	380	9							
2	k	0	4	1016	1027	-9	6	-86	48	-7	0	k	1				
			5	619	617	2	7	579	592	-8	1	2409	2441	-14			
0	1410	1418	-8	6	114	140	-8	8	-61	163	-22	3	2887	2861	9		
1	831	843	-15	7	374	363	7	9	383	381	1	5	1415	1484	-54		
2	570	529	52	8	451	438	8	10	170	142	6	7	2579	2657	-34		
			9	-157	39	-17	11	-43	47	-2	9	1265	1353	-82			
			10				12	-71	73	-6	11	309	290	13			
1	669	639	44	11	k	0	13	147	179	-5	13	562	576	-11			
2	2276	2324	-30				14	-36	15	0	15	784	804	-15			
3	1583	1554	17	1	156	143	5					17	493	487	3		
			2	848	891	-41	16	k	0	19	-17	80	-4				
			3	187	189	-1	0	742	731	7	1	k	1				
4	k	0	4	1410	1424	-10	1	44	67	-2	0	2484	2511	-11			
			5	241	235	3	2	424	440	-8	1	1555	1429	88			
0	739	743	-5	6	233	233	0	3	169	32	22	2	1934	1841	53		
1	2116	2177	-40	7	253	225	14	4	109	123	-2	3	1456	1391	49		
2	149	132	14	8	251	259	-4	5	193	147	12	4	630	640	-14		
3	2808	2816	-3	9	187	120	19	6	513	499	8	5	960	940	20		
4	186	100	40	10	633	617	11	7	231	137	24	6	1968	2010	-24		
			5	k	0			8	424	445	-10	7	565	553	13		
			6					9	52	4	1	8	1533	1602	-49		
1	1016	1048	-33	12	k	0	10	197	204	-1	9	280	284	-3			
2	1682	1705	-15	0	226	182	22	11	149	67	11	10	699	742	-45		
3	367	367	0	1	455	466	-9	12	143	80	8	11	589	577	11		
4	2211	2150	30	2	100	35	10	13	92	104	-1	12	155	188	-13		
5	939	925	11	3	1090	1133	-35					13	268	288	-10		
			6	k	0			1	508	521	-7	14	763	806	-35		
			7					2	196	177	4	15	76	80	0		
0	1786	1788	0	4	29	21	0	3	41	64	-1	16	583	598	-10		
1	761	760	1	5	809	816	-6	4	235	285	-17	17	120	124	0		
2	1174	1224	-46	6	145	104	10	5	313	307	2	18	225	238	-3		
3	924	914	9	7	112	86	5	6	181	221	-10	19	152	194	-9		
4	132	77	24	8	274	289	-7	7	318	354	-14	20	93	100	0		
5	885	877	8	9	477	462	9	8	146	29	13						
6	1363	1366	-14	10	206	199	2	9	273	237	11	2	k	1			
			7	k	0			10	146	152	-1	1	1955	1849	60		
			8					11	73	6	3	2	2927	2869	19		
1	2029	2122	-52	1	562	543	15	12	181	172	1	3	180	186	-6		
2	189	176	9	2	677	706	-25					4	1726	1711	9		
3	1218	1260	-35	3	203	207	-1	18	k	0	5	659	670	-14			
4	553	588	-43	4	759	778	-16	0	387	398	-5	6	1246	1222	20		
5	1015	1030	-14	5	139	161	-6	1	210	180	7	7	1431	1446	-11		
6	133	107	10	6	258	267	-4	2	183	196	-3	8	273	280	-6		
7	1377	1380	-1	7	483	455	18	3	428	356	34	9	910	972	-62		
			8	k	0			4	125	143	-3	10	1031	1031	0		
			9					5	307	329	-8	11	181	205	-11		
0	2203	2331	-66	10	440	446	-3	6	205	231	-6	12	806	817	-10		
1	240	221	14	11	81	143	-10	7	107	92	1	13	364	387	-15		
2	1279	1295	-12	12	301	296	2	8	110	179	-11	14	388	387	0		
3	376	402	-28	13	120	28	6	9	173	147	4	15	457	467	-6		
4	629	627	1					10	65	14	2	16	146	32	16		
5	363	352	10	14	k	0					17	332	316	7			
6	1146	1136	8	0	743	762	-16	18	302	312	-3	18	302	312	-3		
7	527	551	-23	1	237	271	-15	19	-130	40	-11	19	-130	40	-11		
8	993	1013	-13	2	563	568	-3	20	271	276	-1						
			9	k	0			1	148	158	-1	3	k	1			
			10					2	375	373	0	0	3031	2905	41		
1	1284	1276	6	3	535	550	-11	3	-77	24	-4	1	1275	1227	41		
2	594	598	-4	4	-40	79	-7	4	445	429	7	2	271	284	-19		
3	-81	67	-18	5	250	249	0	5	198	109	15	3	2663	2615	20		
4	1089	1128	-34	6	537	534	2	6	170	215	-9	4	439	450	-16		
5	835	810	24	7	-47	30	-2	7	131	64	7	5	2098	2072	13		
6	561	554	6	8	494	513	-12	8	126	83	5	6	579	568	14		
7	896	871	22	9	321	309	5					7	699	683	17		
8	143	101	12	10	239	252	-4	20	k	0	8	593	594	-1			
9	479	488	-5	11	290	281	3	0	10	114	-7	9	804	819	-15		
			10	k	0			1	166	192	-5	10	373	331	33		
			11					2	181	52	16						
			12														
			13														
			14														
			15	k	0												

8 133 124 1	18 k 2	6 855 883 -30	13 734 742 -6
9 453 452 0		7 1108 1122 -13	14 278 261 7
10 589 544 15	0 172 139 7	8 274 186 60	15 -68 91 -10
11 240 181 17	1 203 174 7	9 1029 1031 -1	16 253 212 13
12 528 492 19	2 -70 81 -7	10 909 884 22	17 366 356 4
13 57 117 -6	3 445 429 8	11 136 121 4	18 177 101 13
14 102 151 -7	4 -89 51 -6	12 807 824 -14	19 363 311 18
15 266 243 6	5 413 414 0	13 500 517 -12	20 173 52 14
16 14 139 -10	6 150 159 -1	14 257 259 0	
	7 188 160 5	15 529 533 -3	6 k s
14 k 2	8 86 174 -13	16 171 187 -4	
0 835 828 6	9 256 134 26	17 303 277 9	1 1095 1105 -9
1 226 233 -2	10 128 59 7	18 345 307 15	2 836 830 7
2 518 545 -19		19 66 77 0	3 532 506 30
3 375 408 -20	19 k 2	20 246 166 18	4 1325 1323 1
4 164 11 25	1 219 81 27		5 230 225 3
5 387 386 0	2 257 249 2	3 k s	6 808 785 22
6 556 548 5	3 82 60 1	0 1020 1000 20	7 1064 1033 26
7 92 109 -2	4 449 406 19	1 508 493 22	8 142 78 18
8 688 660 18	5 147 49 11	2 1164 1128 33	9 919 923 -3
9 288 260 10	6 277 240 10	3 1573 1529 30	10 869 894 -22
10 401 386 7	7 -116 72 -10	4 232 206 23	11 192 205 -5
11 266 281 -5	8 -71 36 -3	5 1593 1602 -6	12 911 904 5
12 -76 16 -4	20 k 2	6 516 487 34	13 388 367 11
13 176 137 7	0 146 154 -1	7 896 869 27	14 264 265 0
14 292 290 0	1 109 93 1	8 861 864 -2	15 453 439 8
15 116 81 3	2 202 116 15	9 722 736 -14	16 111 201 -19
15 k 2	3 252 264 -3	10 590 408 -14	17 268 290 -7
1 743 743 0	4 34 49 0	11 1093 1090 2	18 315 284 10
2 74 29 4	5 240 241 0	12 299 293 2	19 -23 61 -2
3 288 305 -8	0 k s	13 661 673 -9	7 k s
4 -55 87 -9	1 1117 1118 0	14 288 271 8	0 1361 1382 -15
5 342 339 1	3 1021 1001 19	15 142 92 9	1 128 137 -4
6 -46 103 -9	5 776 819 -52	16 247 271 -8	2 1077 1077 0
7 657 628 19	7 1265 1310 -37	17 436 405 15	3 848 844 4
8 159 140 4	9 1384 1456 -54	18 125 53 8	4 167 145 11
9 548 501 26	11 356 342 10	19 375 335 15	5 569 549 22
10 167 105 11	13 695 681 11	20 -120 71 -10	6 1056 1017 33
11 173 153 4	15 801 827 -20	4 k s	7 369 390 -17
12 76 70 0	17 336 339 -1	1 214 190 23	8 1447 1449 -1
13 153 227 -15	19 -151 92 -19	2 1318 1250 54	9 321 342 -13
14 133 91 5	1 k s	3 215 197 15	10 697 708 -9
16 k 2	0 1566 1555 7	4 1935 1975 -23	11 622 597 20
0 655 657 -1	1 1453 1431 17	5 266 236 25	12 192 158 10
1 166 144 5	2 2074 2017 31	6 1247 1249 -2	13 206 173 10
2 390 439 -27	3 560 561 -1	7 203 157 26	14 672 614 40
3 223 232 -2	4 160 147 10	8 198 244 -29	15 108 43 7
4 -90 60 -9	5 318 299 22	9 209 268 -36	16 546 539 3
5 249 203 15	6 972 1010 -38	10 833 836 -3	17 160 165 -1
6 429 442 -6	7 178 169 5	11 104 62 7	18 89 180 -13
7 211 179 8	8 1494 1527 -23	12 1100 1101 0	19 137 118 2
8 545 495 27	9 434 444 -9	13 61 25 2	
9 140 26 12	10 816 845 -28	14 403 408 -3	8 k s
10 276 247 8	11 644 617 25	15 124 43 11	1 1493 1518 -18
11 76 137 -7	12 322 327 -3	16 226 273 -16	2 317 232 65
12 127 111 2	13 236 276 -18	17 56 42 0	3 904 896 7
13 220 154 13	14 690 702 -9	18 385 407 -9	4 281 279 -14
17 k 2	15 89 47 4	19 63 9 2	5 585 602 -17
1 371 375 -1	16 597 582 10	20 317 271 13	6 -49 99 -16
2 344 306 16	17 128 134 -1	5 k s	7 1440 1453 -8
3 117 134 -3	18 -135 117 -21	0 967 955 11	8 243 253 -5
4 387 404 -8	19 187 136 10	1 391 362 36	9 1141 1123 14
5 237 199 11	20 180 136 7	2 614 616 -2	10 190 181 3
6 222 266 -13	2 k s	3 1543 1556 -7	11 367 377 -6
7 420 371 23	1 2108 2046 33	4 250 230 16	12 179 146 9
8 110 53 5	2 1185 1124 54	5 1605 1631 -17	13 549 524 16
9 288 263 8	3 1190 1173 15	6 353 302 45	14 191 107 18
10 208 193 3	4 1278 1246 26	7 546 526 20	15 731 695 23
11 -85 41 -4	5 625 616 11	8 636 653 -17	16 -44 62 -3
12 258 230 7		9 558 571 -12	17 392 336 23
		10 400 387 10	18 -191 41 -21
		11 1098 1100 -1	19 -134 26 -9
		12 180 127 14	9 k s

Bis(mu-DHPE) Digold (PF6)2							Page		5						
0	1428	1471	-31	15	125	71	6	1	191	128	14	18	173	159	2
1	455	432	21	16	-93	135	-15	2	214	268	-17	19	134	39	9
2	1049	1032	14					3	395	404	-4	20	157	139	2
3	707	720	-13	13	k	s		4	61	18	2				
4	210	240	-18					5	353	354	0		2	k	4
5	596	602	-5	0	645	638	5	6	299	280	7				
6	860	895	-32	1	265	259	2	7	87	154	-10	0	1941	1856	48
7	296	310	-8	2	476	499	-16	8	391	338	21	1	464	447	23
8	1117	1113	3	3	620	643	-18	9	-191	54	-22	2	1496	1443	38
9	168	158	3	4	61	30	2	10	149	149	0	3	1554	1540	9
10	630	603	20	5	731	734	-2	11	290	225	17	4	537	347	-11
11	434	412	13	6	403	384	10					5	1423	1413	7
12	167	178	-3	7	228	168	19	18	k	s		6	1075	1088	-11
13	400	392	4	8	531	527	2					7	536	554	-20
14	617	617	0	9	358	400	-21	1	168	97	13	8	1284	1306	-17
15	138	112	4	10	376	382	-3	2	301	297	1	9	607	625	-18
16	457	438	9	11	598	581	10	3	87	56	2	10	592	601	-8
17	56	55	0	12	108	54	5	4	436	411	12	11	826	856	-26
18	220	78	23	13	407	400	2	5	-59	74	-5	12	219	242	-10
				14	137	186	-8	6	271	280	-3	13	637	672	-27
				15	74	35	2	7	190	176	2	14	601	581	14
				16	186	234	-9	8	119	37	7	15	24	83	-5
10	k	s						9	112	90	2	16	435	435	0
1	805	834	-28					10	270	216	13	17	507	263	16
2	890	849	37	14	k	s						18	61	114	-5
3	444	430	12					19	k	s		19	283	274	2
4	810	819	-8	1	638	662	-18					20	123	89	3
5	342	349	-5	2	214	247	-12	0	89	70	1				
6	867	887	-17	3	200	252	-19	1	132	126	0		s	k	4
7	698	708	-8	4	423	390	20	2	-85	67	-7				
8	138	162	-7	5	250	258	-3	3	296	326	-9	1	729	703	32
9	604	596	5	6	276	266	4	4	-57	21	-2	2	1604	1589	10
10	503	484	12	7	585	604	-12	5	332	306	8	3	344	331	15
11	-133	45	-16	8	-73	98	-10	6	-175	49	-18	4	1694	1664	19
12	713	684	19	9	627	600	17	7	144	124	2	5	271	275	-3
13	358	385	-12	10	275	315	-14	8	-24	16	0	6	1310	1295	12
14	319	325	-2	11	231	218	3					7	496	486	11
15	403	391	5	12	309	292	3	20	k	s		8	362	394	-29
16	90	38	4	13	196	177	3					9	359	400	-34
17	131	143	-1	14	-141	22	-11	1	122	128	0	10	978	1002	-21
18	254	212	9	15	338	280	17	2	89	160	-9	11	158	182	-8
								3	66	68	0	12	1143	1165	-16
11	k	s		15	k	s		4	251	262	-2	13	241	248	-2
0	373	361	8	0	808	815	-5	5	169	46	14	14	367	407	-23
1	628	596	28	1	187	51	26					15	313	341	-13
2	124	149	-7	2	516	530	-8	0	k	4		16	165	170	-1
3	1043	1056	-11	3	84	57	3					17	80	83	0
4	93	41	7	4	158	29	20	0	1770	1743	17	18	367	374	-2
5	1104	1103	0	5	24	90	-6	2	1977	1921	31	19	127	35	8
6	217	186	12	6	471	438	19	4	267	256	11	20	316	275	12
7	587	594	-5	7	-88	26	-6	6	1206	1218	-10				
8	369	383	-8	8	700	681	11	8	1679	1709	-19	4	k	4	
9	445	406	24	9	179	117	12	10	947	973	-23				
10	53	53	0	10	365	391	-10	12	368	346	14	0	319	286	37
11	808	794	10	11	-70	97	-9	14	635	667	-24	1	867	887	-22
12	202	205	0	12	90	62	2	16	630	610	12	2	341	361	-25
13	610	589	12	13	-64	39	-3	18	225	233	-2	3	1603	1591	8
14	255	223	9	14	283	275	2	20	-148	100	-17	4	503	487	19
15	-51	94	-7									5	1719	1686	20
16	145	93	7					1	k	4		6	129	128	0
17	200	230	-6									7	736	767	-32
				16	k	s						8	222	222	0
				1	587	572	10	1	2714	2651	26	9	786	778	6
				2	193	176	4	2	479	454	34	10	168	175	-2
				3	310	265	18	3	800	794	6	11	1209	1202	5
				4	262	274	-4	4	875	896	-23	12	36	50	-1
				5	229	208	6	5	826	810	16	13	719	735	-12
				6	194	187	1	6	709	697	13	14	142	73	13
				7	507	539	-17	7	1592	1623	-21	15	162	123	9
				8	182	65	18	8	356	332	21	16	228	102	31
				9	461	433	12	9	1357	1364	-5	17	361	303	23
				10	137	33	10	10	270	307	-24	18	-17	83	-4
				11	52	87	-2	11	373	400	-21	19	358	349	3
				12	120	122	0	12	517	490	21				
				13	188	238	-11	13	590	598	-6				
								14	189	191	0	5	k	4	
				17	k	s		15	682	661	15				
				0	301	318	-6	16	51	57	0	1	893	877	16
								17	403	396	3	2	1321	1330	-7

Bis(mu-DHPE) Digold (PF6)2 Page 6

Table with multiple columns of numerical data and labels (e.g., 3 k 4, 13 k 4). Each row contains several groups of numbers and letters, likely representing different facets or symmetry elements of the crystal structure.

Bis(mu-DHPE)				Digold (PF6)2				Page 7							
18	278	256	7	6	617	591	26	18	138	48	9	14	195	131	11
19	134	199	-12	7	218	210	4					15	157	79	10
				8	897	901	-3	9	k	5		16	96	104	0
	2	k	5	9	616	607	7								
				10	628	610	12	0	930	963	-30	13	k	5	
1	1376	1394	-13	11	729	743	-11	1	289	262	4				
2	1736	1713	14	12	-105	119	-22	2	800	779	19	0	455	462	-4
3	89	5	16	13	554	554	0	3	808	824	-14	1	259	238	9
4	1813	1793	11	14	241	230	3	4	287	286	0	2	394	403	-5
5	804	815	-11	15	110	12	9	5	605	608	-2	3	726	734	-6
6	952	961	-8	16	367	329	15	6	1057	1065	-6	4	99	38	7
7	1348	1380	-24	17	261	267	-2	7	317	313	2	5	538	562	-16
8	160	175	-6	18	102	179	-11	8	678	647	24	6	304	290	6
9	841	844	-2	19	315	290	7	9	152	153	0	7	110	136	-5
10	861	842	16					10	241	214	10	8	310	314	-1
11	248	256	-3	6	k	5		11	408	405	1	9	260	265	-1
12	757	751	5					12	191	153	9	10	205	212	-2
13	424	419	2	1	1630	1622	5	13	284	289	-2	11	368	344	10
14	340	352	-6	2	938	945	-7	14	387	350	16	12	104	10	7
15	454	449	3	3	471	469	1	15	149	115	5	13	166	178	-2
16	-85	50	-7	4	996	995	0	16	273	287	-4	14	196	148	9
17	252	265	-4	5	587	571	15	17	112	90	2	15	75	45	1
18	333	298	13	6	579	590	-10								
19	106	34	5	7	1085	1091	-5	10	k	5		14	k	5	
				8	373	353	14								
	3	k	5	9	1078	1078	0	1	619	615	3	1	580	588	-5
0	604	628	-30	10	455	462	-4	2	861	822	34	2	323	332	-4
1	1208	1158	42	11	276	262	7	3	109	86	5	3	238	223	5
2	160	138	12	12	412	418	-3	4	865	874	-7	4	404	431	-16
3	2260	2225	17	13	322	326	-1	5	582	598	-13	5	216	218	0
4	174	169	8	14	19	61	-2	6	506	519	-10	6	100	104	0
5	1638	1658	-15	15	457	432	13	7	456	465	-6	7	426	405	11
6	431	437	-5	16	197	164	7	8	-57	113	-14	8	181	133	11
7	548	568	-20	17	382	343	15	9	211	226	-5	9	338	350	-4
8	601	595	5	18	204	221	-3	10	492	483	6	10	256	249	2
9	838	851	-11	19	88	70	1	11	104	11	8	11	55	71	-1
10	81	139	-14					12	488	476	7	12	220	153	14
11	1067	1089	-16	7	k	5		13	248	221	8	13	216	160	12
12	207	170	12					14	262	235	8	14	117	5	7
13	781	766	11	0	1705	1706	0	15	143	195	-10				
14	207	211	-1	1	402	390	11	16	-110	8	-7	15	k	5	
15	204	209	-1	2	1383	1387	-2	17	160	64	11				
16	156	113	8	3	474	482	-8					0	659	696	-25
17	280	245	11	4	282	269	9	11	k	5		1	33	115	-9
18	42	36	0	5	143	156	-5	0	433	418	10	2	423	435	-6
19	352	360	-9	6	1054	1031	19	1	464	479	-11	3	222	215	2
				7	-65	57	-8	2	194	228	-14	4	146	90	10
				8	1208	1194	10	3	1029	1052	-19	5	-119	24	-11
				9	331	301	17	4	161	92	17	6	420	393	13
				10	534	503	22	5	726	704	17	7	-130	82	-16
				11	128	127	0	6	215	222	-2	8	476	463	6
				12	173	184	-3	7	184	147	11	9	19	114	-8
				13	172	94	17	8	136	160	-6	10	196	209	-3
				14	453	444	4	9	427	406	12	11	25	92	-4
				15	87	97	-1	10	67	3	3	12	-111	90	-11
				16	492	459	16	11	599	572	17	13	-145	31	-11
				17	161	87	10	12	140	119	3				
				18	161	167	-1	13	360	342	7	16	k	5	
								14	50	65	-1				
				8	k	5		15	-70	79	-6	1	529	521	4
								16	-83	39	-4	2	112	76	5
				1	1524	1542	-12					3	80	131	-7
				2	220	172	25					4	-72	84	-9
				3	609	604	5	12	k	5		5	352	314	16
				4	536	549	-12					6	-53	142	-15
				5	891	886	4	1	156	155	0	7	466	455	5
				6	345	356	-8	2	707	717	-7	8	133	32	10
				7	1185	1173	9	3	209	166	14	9	313	302	3
				8	152	125	7	4	977	971	4	10	-48	28	-1
				9	672	642	23	5	109	115	-1	11	73	62	0
				10	148	93	12	6	451	436	9	12	-120	91	-12
				11	114	159	-10	7	166	162	1				
				12	238	221	6	8	199	217	-6	17	k	5	
				13	334	332	0	9	141	139	0				
				14	112	145	-6	10	494	454	22	0	436	432	2
				15	473	454	9	11	126	117	1	1	138	101	6
				16	-87	48	-6	12	393	367	12	2	272	273	0
				17	297	276	6	13	106	8	7	3	176	235	-15

Bis(mu-DHPE) Digold (PF6)2				Page		9	
14 k	6					13	109 114 0
0	612 623	-7	1 1461 1489	-19	1 167 158	4	14 452 463 -6
1	189 243	-17	3 1089 1082	6	2 1078 1073	4	15 -97 83 -10
2	447 406	24	5 903 932	-27	3 211 186	13	16 427 401 10
3	443 469	-15	7 1436 1452	-11	4 1761 1795	-20	17 127 115 1
4	160 43	18	9 846 865	-16	5 87 78	1	
5	218 240	-7	11 197 201	-1	6 752 744	6	8 k 7
6	389 371	8	13 418 439	-12	7 96 156	-18	
7	181 73	20	15 664 651	8	8 250 218	15	1 1144 1157 -10
8	448 425	11	17 365 350	6	9 -70 29	-5	3 359 355 2
9	215 219	-1	19 -155 99	-12	10 791 785	4	4 206 159 17
10	240 190	13			11 133 153	-4	5 549 557 -6
11	198 194	0	1 k 7		12 722 714	5	6 -83 13 -7
12	-97 43	-6	0 1472 1504	-23	13 137 11	14	7 1000 1005 -3
13	122 65	5	1 267 255	9	14 366 375	-4	8 34 48 0
			2 1343 1365	-16	15 103 50	5	9 671 678 -5
			3 509 511	-2	16 217 203	3	10 120 68 8
			4 171 138	15	17 94 38	4	11 106 127 -4
			5 497 506	-9	18 380 349	11	12 139 107 5
			6 1211 1231	-15			13 338 347 -3
			7 290 288	1	5 k 7		14 116 141 -4
			8 1074 1076	-2	0 906 912	-4	15 510 461 23
			9 196 220	-10	1 541 590	-51	16 -144 61 -13
			10 577 594	-13	2 295 294	0	17 359 282 24
			11 484 469	10	3 1368 1355	9	
			12 -74 144	-23	4 111 74	9	9 k 7
			13 282 246	14	5 1090 1094	-3	0 921 963 -36
			14 607 590	11	6 397 379	13	1 261 233 14
			15 37 61	-1	7 113 21	14	2 830 821 7
			16 502 462	21	8 458 475	-12	3 449 413 25
			17 -103 107	-14	9 464 456	5	4 -82 35 -8
			18 -35 163	-15	10 273 234	16	5 400 408 -5
					11 755 751	2	6 778 783 -4
			2 k 7		12 95 54	5	7 118 187 -18
			1 1369 1429	-45	13 500 517	-10	8 695 695 0
			2 977 987	-9	14 223 203	6	9 193 160 9
			3 309 324	-11	15 -82 176	-25	10 315 296 8
			4 1028 1029	0	16 224 194	7	11 373 365 3
			5 336 344	-6	17 255 263	-2	12 226 184 12
			6 722 696	25	18 172 111	9	13 290 276 4
			7 714 739	-23			14 408 405 1
			8 113 85	6	6 k 7		15 -45 99 -6
			9 751 746	4	1 1248 1237	8	16 374 314 20
			10 743 732	8	2 807 808	-1	
			11 133 85	9	3 120 109	3	10 k 7
			12 565 571	-4	4 842 812	27	1 692 683 7
			13 296 284	5	5 417 408	7	2 722 764 -34
			14 283 270	5	6 351 412	-45	3 298 245 25
			15 373 374	0	7 795 802	-5	4 812 819 -5
			16 -29 100	-7	8 -57 65	-7	5 309 295 7
			17 198 251	-13	9 743 735	6	6 546 584 -27
			18 182 236	-12	10 573 582	-6	7 478 447 19
					11 -84 114	-16	8 84 46 4
			3 k 7		12 361 400	-20	9 273 300 -11
			0 1142 1150	-7	13 235 252	-5	10 530 507 14
			1 516 503	12	14 116 206	-19	11 118 47 8
			2 357 374	-15	15 435 407	13	12 497 453 23
			3 1739 1739	0	16 171 139	6	13 254 256 0
			4 209 202	3	17 313 271	12	14 148 223 -16
			5 1304 1288	12	18 225 206	4	15 322 258 19
			6 117 156	-13			16 24 64 -1
			7 268 239	17	7 k 7		
			8 359 377	-13	0 1497 1470	18	11 k 7
			9 405 394	7	1 307 327	-14	0 249 249 0
			10 236 208	11	2 790 815	-24	1 506 474 22
			11 842 825	12	3 332 318	10	2 24 106 -9
			12 204 175	8	4 113 187	-26	3 895 903 -5
			13 602 591	7	5 157 119	11	4 175 165 2
			14 166 138	6	6 849 835	11	5 785 792 -5
			15 -108 116	-18	7 167 187	-6	6 165 154 2
			16 167 162	1	8 984 994	-8	7 273 289 -7
			17 255 269	-4	9 173 206	-11	8 62 110 -6
			18 -180 88	-21	10 431 423	4	9 398 367 16
					11 307 310	-1	10 -112 48 -10
0 k	7		4 k 7		12 147 174	-6	

6	400	399	0	2	-56	68	-5
7	270	255	6	3	231	225	1
8	520	525	-3	4	187	124	13
9	244	221	7	5	233	194	10
10	261	231	9	6	153	112	6
11	430	441	-5	7	501	466	16
12	142	139	0	8	-160	76	-17
13	431	396	14	9	441	397	17
14	309	300	3	10	126	95	3
15	161	103	7				
11 k 8							
1	207	171	12	0	478	456	10
2	566	578	-8	1	137	76	8
3	229	191	12	2	304	322	-6
4	963	943	14	3	243	180	16
5	133	132	0	4	-158	36	-16
6	561	547	9	5	168	175	-1
7	285	271	5	6	244	297	-15
8	105	81	3	7	186	94	14
9	74	162	-14	8	352	378	-9
10	465	439	13	17	k	8	
11	138	42	11				
12	546	534	6	1	261	268	-1
13	245	151	20	2	180	196	-3
14	258	273	-3	3	29	100	-5
12 k 8							
0	336	293	20	4	299	320	-6
1	321	328	-3	5	104	95	1
2	183	192	-2	6	276	206	18
3	703	683	14	18	k	8	
4	-53	88	-7	0	180	137	7
5	687	692	-3	1	137	95	5
6	95	83	1	2	172	77	12
7	236	251	-5	3	265	287	-6
8	197	151	11	0	k	9	
9	292	301	-3	1	888	897	-8
10	-90	149	-19	3	627	643	-15
11	540	536	1	5	604	612	-7
12	201	70	20	7	1058	1082	-18
13	444	388	21	9	820	825	-3
13 k 8							
1	437	450	-7	11	238	302	-26
2	420	432	-6	13	400	427	-13
3	210	208	0	15	503	508	-2
4	560	542	10	17	211	265	-13
5	127	117	1	1	k	9	
6	436	393	21	0	862	884	-20
7	390	372	8	1	466	494	-25
8	112	49	6	2	675	670	4
9	323	324	0	3	479	484	-4
10	453	400	24	4	198	220	-11
11	145	153	-1	5	239	242	-1
12	400	384	5	6	727	756	-25
14 k 8							
0	574	577	-1	7	247	281	-17
1	43	163	-17	8	935	936	0
2	411	419	-4	9	174	205	-10
3	269	250	6	10	520	514	3
4	59	48	0	11	344	329	7
5	265	267	0	12	178	216	-11
6	424	418	2	13	240	178	18
7	143	106	5	14	523	489	19
8	520	462	28	15	113	51	6
9	201	209	-1	16	403	367	14
10	316	299	5	17	223	92	23
11	297	267	8	2	k	9	
15 k 8							
1	495	505	-5	1	655	668	-12
				2	793	808	-14
				3	250	214	19
				4	621	623	-1
				5	259	268	-5

6	587	575	9	3	249	255	-2
7	683	713	-25	4	786	811	-21
8	146	129	4	5	91	177	-21
9	657	652	3	6	498	498	0
10	550	576	-17	7	663	675	-8
11	198	153	12	8	78	106	-4
12	474	478	-2	9	670	675	-3
13	319	322	-1	10	457	451	3
14	239	230	2	11	156	181	-6
15	315	349	-12	12	504	488	9
16	-166	113	-23	13	277	250	8
17	109	179	-10	14	171	159	2
3 k 9							
0	613	623	-9	15	339	324	4
1	411	425	-11	16	200	133	12
2	215	198	8	7 k 9			
3	949	969	-17	0	1061	1056	4
4	119	73	10	1	317	296	11
5	916	928	-10	2	675	686	-9
6	276	242	17	3	414	431	-11
7	432	434	-1	4	209	190	7
8	501	511	-7	5	304	299	2
9	457	455	0	6	654	660	-4
10	246	276	-11	7	182	175	2
11	735	722	9	8	911	888	16
12	94	135	-6	9	168	181	-3
13	502	501	0	10	530	509	12
14	253	205	14	11	330	297	14
15	145	133	2	12	122	132	-1
16	-114	142	-18	13	110	166	-9
17	194	255	-14	14	425	403	9
4 k 9							
1	219	245	-14	15	-158	30	-14
2	555	544	9	16	364	340	7
3	30	79	-5	8 k 9			
4	1308	1304	2	1	924	916	6
5	146	123	6	2	128	168	-11
6	829	838	-7	3	503	500	1
7	203	216	-4	4	252	271	-8
8	227	248	-9	5	437	448	-7
9	128	116	2	6	151	148	0
10	681	679	1	7	884	877	5
11	115	75	5	8	198	29	29
12	726	706	13	9	704	704	0
13	-149	20	-15	10	109	139	-5
14	321	311	3	11	163	241	-21
15	148	78	9	12	93	110	-2
16	200	216	-3	13	289	298	-3
17	-117	54	-8	14	55	94	-3
5 k 9							
0	629	660	-27	15	461	434	11
1	236	203	15	9 k 9			
2	305	270	20	0	755	781	-20
3	895	887	7	1	242	217	10
4	157	118	11	2	615	621	-5
5	1077	1058	14	3	484	474	6
6	245	248	-1	4	132	82	9
7	332	320	6	5	466	462	2
8	482	497	-10	6	663	649	9
9	438	420	11	7	212	199	3
10	314	293	9	8	697	699	-1
11	717	705	8	9	82	65	1
12	25	130	-11	10	383	391	-3
13	502	491	5	11	316	296	7
14	185	178	1	12	46	101	-5
15	100	64	3	13	255	244	3
16	237	171	14	14	354	377	-7
6 k 9							
1	727	746	-16	15	155	71	9
2	512	514	-1	10 k 9			
				1	464	476	-7
				2	568	562	4
				3	308	257	22
				4	678	649	21

Bis(mu-DHPE)				Digold (PF6)2				Page 14							
1	868	882	-10	9	240	235	1	9	-94	186	-18	10	353	300	19
2	301	294	3	10	355	377	-9	10	-150	48	-13	11	143	69	8
3	188	202	-4	11	14	91	-4					12	229	273	-11
4	390	405	-8	12	331	334	0	11	k	12					
5	439	449	-5	13	-117	63	-9					3	k	13	
6	190	185	1					1	121	148	-4				
7	680	683	-1	6	k	13		2	423	410	5	0	301	279	9
8	74	81	0					3	100	42	5	1	235	250	-5
9	496	501	-2	0	617	605	7	4	533	505	14	2	31	157	-18
10	204	172	7	1	293	214	30	5	135	120	2	3	598	597	0
11	96	138	-6	2	527	497	19	6	306	279	9	4	-57	53	-4
12	206	220	-3	3	468	458	5	7	113	121	-1	5	547	532	9
13	225	238	-3	4	56	63	0	8	52	96	-3	6	153	114	7
14	148	109	5	5	361	324	16	9	24	49	-1	7	197	167	7
				6	478	465	7					8	222	212	2
				7	132	30	11	12	k	12		9	263	218	13
				8	431	407	11					10	105	108	0
				9	241	240	0	0	159	170	-2	11	420	395	9
0	665	673	-6	10	275	230	14	1	210	228	-4	12	62	81	-1
1	310	296	6	11	276	262	4	2	86	128	-5				
2	460	469	-5	12	-50	38	-2	3	515	490	11	4	k	13	
3	724	717	5	13	250	156	20	4	215	47	25				
4	77	128	-8					5	340	358	-6	1	110	46	7
5	612	597	9	7	k	12		6	-78	47	-4	2	477	484	-4
6	512	505	4					7	106	63	4	3	-93	49	-5
7	128	122	1	1	707	678	19					4	680	674	3
8	414	433	-9	2	236	157	23	13	k	12		5	121	24	10
9	212	250	-11	3	223	224	0					6	390	379	5
10	180	192	-2	4	233	184	14	1	290	260	9	7	-57	31	-2
11	399	376	9	5	394	391	1	2	301	320	-6	8	77	36	3
12	204	117	16	6	106	21	7	3	-149	110	-19	9	132	23	10
13	363	294	23	7	543	536	3	4	370	320	17	10	365	349	5
14	186	214	-5	8	124	87	5	5	158	70	10	11	-118	34	-8
				9	423	385	17	6	99	146	-6	12	431	386	17
				10	53	102	-4								
				11	197	102	16	14	k	12		5	k	13	
				12	98	73	2								
1	227	250	-8					0	402	336	24	0	351	329	10
2	747	727	14	8	k	12		1	148	118	4	1	204	209	-1
3	164	127	8					2	273	236	9	2	214	195	5
4	847	850	-2	0	769	750	12	3	252	235	4	3	560	565	-3
5	255	226	10	1	30	67	-2					4	119	17	10
6	427	422	2	2	462	449	7	0	k	13		5	539	513	14
7	245	235	3	3	-28	108	-9	1	539	571	-20	6	-99	120	-16
8	203	132	17	4	228	162	18	3	238	237	0	7	197	136	13
9	164	96	12	5	52	104	-5	5	377	360	8	8	236	207	7
10	412	412	0	6	441	442	0	7	572	566	3	9	197	222	-5
11	160	42	15	7	42	73	-2	8	462	433	13	10	88	134	-5
12	487	445	19	8	505	470	17	9	106	114	-1	11	399	388	4
13	32	94	-4	9	137	25	10								
14	208	205	0	10	232	235	0	1	k	13		6	k	13	
				11	-130	81	-12								
0	194	177	4	9	k	12		0	544	570	-17	1	449	458	-4
1	421	427	-3					1	-70	110	-13	2	340	328	4
2	79	109	-4	1	565	530	20	2	387	426	-21	3	-86	106	-12
3	866	863	2	2	213	252	-12	3	238	220	6	4	359	402	-19
4	87	18	5	3	-119	103	-16	4	-50	78	-6	5	-148	145	-28
5	683	673	6	4	360	327	13	5	240	182	18	6	276	213	20
6	-157	44	-20	5	260	271	-3	6	477	459	10	7	323	356	-12
7	179	160	4	6	263	219	13	7	-75	73	-7	8	94	52	3
8	203	134	16	7	435	393	19	8	504	492	6	9	365	349	5
9	345	339	2	8	-129	31	-10	9	-27	114	-8	10	285	280	1
10	-134	84	-15	9	326	288	12	10	298	266	10	11	135	94	5
11	480	469	5	10	162	154	1	11	211	191	4				
12	-20	40	-1	11	-87	68	-6	12	79	120	-4	7	k	13	
13	327	286	12												
				10	k	12		2	k	13		0	621	592	17
												1	93	90	0
				0	373	394	-9	1	417	440	-12	2	410	381	13
1	426	429	-1	1	165	181	-3	2	405	394	5	3	204	204	0
2	644	635	6	2	199	216	-4	3	187	143	11	4	85	54	2
3	182	205	-6	3	425	440	-7	4	462	440	12	5	115	166	-9
4	695	680	10	4	157	97	9	5	179	195	-4	6	400	368	13
5	86	152	-11	5	392	382	4	6	275	282	-2	7	-58	64	-4
6	335	318	7	6	237	254	-5	7	358	362	-1	8	509	505	1
7	392	350	19	7	34	114	-6	8	-103	25	-7	9	145	119	3
8	170	133	7	8	223	242	-5	9	383	341	17	10	273	267	1

Bis(mu-DHPE) Digold (PF6)2				Page 15											
8	k	13		2	k	14		7	438	425	5	1	115	104	1
1	573	538	20	0	379	358	10	8	-62	36	-2	2	296	299	0
2	119	35	8	1	220	96	28	8	k	14		3	-51	23	-1
3	279	213	21	2	281	303	-8	0	552	514	19	4	531	511	10
4	-71	47	-4	3	302	322	-7	1	-35	32	-1	5	89	36	3
5	209	239	-8	4	116	55	7	2	342	339	1	6	271	316	-13
6	114	46	6	5	327	333	-2	3	161	85	11	7	81	89	0
7	531	515	8	6	217	239	-6	4	211	48	25	5	k	15	
8	-66	8	-2	7	148	106	6	5	155	107	7	0	211	224	-3
9	416	375	16	8	354	325	11	6	319	327	-2	1	176	144	6
10	-79	41	-4	9	121	142	-3	7	-209	45	-24	2	125	130	0
9	k	13		10	177	192	-2	9	k	14		3	361	397	-13
0	509	492	8	3	k	14		1	432	399	14	4	165	35	15
1	49	111	-6	1	250	205	14	2	-42	139	-11	5	429	395	13
2	370	379	-3	2	360	324	15	3	79	148	-8	6	160	152	1
3	285	220	20	3	207	166	10	4	241	242	0	6	k	15	
4	-157	17	-15	4	490	460	16	5	126	131	0	1	347	339	2
5	176	213	-8	5	169	75	15	6	143	173	-4	2	179	237	-13
6	362	374	-4	6	307	331	-8	10	k	14		3	177	131	8
7	55	118	-6	7	238	202	9	0	230	274	-11	4	276	295	-5
8	417	378	15	8	77	62	1	1	133	122	1	5	207	136	13
9	51	73	-1	9	188	147	7	2	234	193	9	6	209	191	3
10	k	13		10	303	320	-5	3	385	326	20	7	k	15	
1	299	310	-3	4	k	14		4	81	20	3	0	482	453	13
2	374	319	20	0	162	72	15	0	k	15		1	150	107	6
3	-52	121	-10	1	158	203	-11	1	459	478	-9	2	290	303	-4
4	404	381	8	2	67	78	-1	3	326	276	17	3	217	154	12
5	-104	161	-20	3	494	459	18	5	277	207	20	4	119	77	4
6	280	285	-1	4	108	15	7	7	477	467	4	8	k	15	
7	296	278	5	5	451	464	-6	1	k	15		1	412	382	11
8	120	36	7	6	114	64	5	0	471	469	1	2	105	108	0
11	k	13		7	290	237	15	1	138	95	6	3	197	166	6
0	-68	146	-15	8	-160	68	-17	2	381	344	15	0	k	16	
1	186	203	-3	9	195	234	-9	3	170	177	-1	0	591	558	16
2	80	77	0	10	180	36	16	4	55	84	-2	2	377	317	21
3	445	440	2	5	k	14		5	214	170	9	4	192	105	14
4	-146	46	-12	1	212	171	10	6	329	340	-3	1	k	16	
5	447	408	15	2	364	334	13	7	164	107	8	1	449	425	10
6	173	108	9	3	1	79	-4	8	439	408	13	2	207	124	15
12	k	13		4	443	461	-8	2	k	15		3	194	139	10
1	-101	118	-13	5	80	65	1	1	325	326	0	4	280	243	10
2	296	305	-2	6	390	346	17	2	285	263	7	2	k	16	
3	88	83	0	7	198	181	3	3	-78	126	-13	0	300	310	-2
4	413	413	0	8	154	79	10	4	342	326	5	1	103	121	-2
0	k	14		9	169	142	4	5	210	117	18	2	130	195	-11
0	639	597	-27	0	310	330	-7	6	303	256	14	3	402	354	18
2	389	373	7	1	202	109	19	7	278	309	-9	4	-146	79	-14
4	-17	52	-2	2	197	252	-15	8	124	98	3	3	k	16	
6	204	309	-33	3	334	333	0	3	k	15		1	87	117	-3
8	523	497	13	4	-80	47	-5	4	87	21	4	2	379	351	10
10	225	259	-8	5	315	355	-14	5	426	425	0	3	-122	33	-8
1	k	14		6	266	258	2	6	170	118	8	4	k	16	
1	467	459	4	7	176	119	9	7	158	172	-2	0	143	103	5
2	169	102	13	8	301	335	-11	8	225	175	10	1	237	237	0
3	201	207	-1	9	84	165	-10	4	k	15		2	147	75	8
4	239	207	9	7	k	14		4	k	15					
5	131	150	-3	1	416	422	-2								
6	153	115	6	2	132	111	3								
7	409	409	0	3	206	210	0								
8	-74	37	-4	4	269	254	4								
9	450	383	28	5	118	161	-7								
10	166	111	8	6	-44	124	-9								

Appendix 2 X-ray data for $[\text{Au}_2(\text{dcpe})_3][\text{Au}(\text{CN})_2]_2$.

[(Au(dcpe))₂mu-(dcpe)]₂+ 2[Au(CN)₂]₂-

Page 3

9	-172	2	-40	4	855	868	-10	-9	14	1	2	460	429	25	
10	285	317	-18	5	435	446	-8				3	639	635	3	
11	-105	52	-16	6	-105	35	-19	1	481	436	29	4	1059	1030	21
12	358	386	-16	7	413	428	-11				5	473	452	15	
13	570	551	12	8	-94	45	-14			1	6	690	682	5	
14	-130	73	-23	9	471	466	3				7	159	216	-29	
	-9	3	1	10	475	450	15	1	127	140	-5	8	565	568	-2
				11	147	171	-7	2	518	498	16	9	738	748	-7
				12	312	305	3	3	731	745	-11	10	-90	95	-22
1	194	167	13					4	625	617	6	11	209	245	-16
2	400	380	14	-9	8	1		5	835	835	0	12	197	223	-10
3	184	196	-5					6	-81	48	-12	13	366	355	5
4	887	891	-3	1	699	724	-22	7	564	566	0	14	418	419	0
5	957	969	-9	2	641	625	14	8	256	276	-12				
6	515	562	-38	3	149	111	14	9	825	838	-10	-8	6	1	
7	340	366	-17	4	329	335	-4	10	480	498	-13				
8	-106	40	-17	5	58	90	-7	11	108	133	-7	1	568	568	0
9	210	246	-17	6	342	351	-5	12	452	440	8	2	949	930	15
10	608	590	12	7	747	746	0	13	-134	2	-21	3	329	300	20
11	303	333	-17	8	314	289	14	14	377	369	4	4	123	132	-3
12	292	318	-13	9	260	264	-1	15	298	293	2	5	320	317	2
13	353	368	-8	10	-42	93	-12					6	907	890	13
14	202	193	3	11	433	422	6	-8	2	1	7	623	622	0	
	-9	4	1		-9	9	1	1	1074	1052	15	8	56	101	-9
								2	1084	1081	1	9	395	402	-4
1	94	28	13	1	482	474	7	3	219	243	-13	10	85	152	-19
2	470	432	29	2	268	231	23	4	-80	116	-28	11	589	570	13
3	1085	1067	13	3	327	331	-2	5	175	207	-14	12	272	261	5
4	400	401	0	4	602	619	-13	6	749	771	-16	13	196	234	-15
5	793	810	-14	5	137	166	-11	7	941	939	0				
6	133	160	-11	6	76	63	2	8	379	436	-44	-8	7	1	
7	811	816	-4	7	365	367	-1	9	345	363	-12	1	271	266	3
8	283	327	-27	8	34	109	-13	10	140	192	-20	2	274	207	41
9	-90	111	-25	9	477	471	3	11	333	341	-4	3	973	968	4
10	128	201	-25	10	227	242	-6	12	800	798	1	4	477	480	-2
11	-192	1	-45	11	108	151	-11	13	102	128	-6	5	-39	75	-12
12	512	508	2					14	357	334	12	6	364	380	-12
13	490	502	-7		-9	10	1	15	177	193	-5	7	-89	15	-12
14	38	94	-7									8	441	427	10
	-9	5	1	1	799	782	13	-8	3	1	9	722	703	14	
				2	486	469	12				10	-97	36	-13	
1	256	257	0	3	76	3	8	1	172	135	18	11	225	258	-15
2	117	27	20	4	302	295	4	2	463	446	13	12	-132	51	-23
3	310	310	0	5	148	168	-7	3	913	907	4	13	406	405	0
4	906	891	11	6	482	489	-4	4	1083	1073	7				
5	900	920	-15	7	489	496	-5	5	510	499	8	-8	8	1	
6	157	157	0	8	-129	19	-21	6	494	484	7				
7	549	566	-13	9	-119	121	-33	7	350	284	37	1	807	807	0
8	25	120	-17					8	134	211	-34	2	412	393	16
9	329	360	-19		-9	11	1	9	636	632	2	3	509	494	13
10	415	419	-2					10	463	478	-10	4	152	156	-1
11	-80	80	-14	1	376	396	-15	11	-144	21	-27	5	464	473	-7
12	264	318	-26	2	116	96	6	12	466	443	15	6	685	682	2
13	212	182	10	3	214	204	5	13	-152	68	-32	7	357	361	-3
				4	545	526	13	14	540	523	10	8	262	266	-2
				5	54	100	-9	15	313	295	8	9	342	352	-6
				6	364	345	11					10	323	308	8
				7	127	116	2					11	364	383	-11
				8	387	378	5	-8	4	1		12	98	103	-1
1	570	544	21					1	391	353	31				
2	783	771	9					2	1145	1136	6	-8	9	1	
3	642	642	0		-9	12	1	3	262	222	24				
4	453	465	-10					4	492	491	1	1	340	335	3
5	73	113	-11	1	470	491	-16	5	71	89	-4	2	175	155	10
6	316	322	-3	2	207	241	-17	6	1311	1298	8	3	853	860	-5
7	912	898	10	3	153	79	20	7	575	563	9	4	226	224	1
8	435	443	-5	4	242	255	-6	8	120	153	-11	5	-84	19	-11
9	37	121	-16	5	150	145	1	9	321	300	12	6	255	248	4
10	229	279	-25	6	589	564	16	10	-133	72	-29	7	144	158	-5
11	255	282	-13	7	232	230	0	11	375	360	8	8	582	589	-5
12	555	532	14					12	604	594	7	9	457	457	0
13	171	229	-20		-9	13	1	13	-63	2	-4	10	62	53	1
								14	310	313	-1	11	144	177	-10
				1	235	211	11								
				2	136	49	19								
1	191	187	2	3	163	136	8								
2	312	320	-6	4	347	349	-1	-8	5	1		-8	10	1	
3	94	102	-2												
								1	81	79	0	1	593	587	5

(Au(dcp)) 2 mu-(dcp) 2+				2[Au(CN) 2]-				Page 10							
8	411	414	-1	0	126	53	16	12	365	353	9	9	73	48	5
9	369	359	5	1	210	213	-1	13	328	324	2	10	300	270	21
10	45	100	-8	2	196	212	-7	14	410	390	13	11	299	304	-3
				3	186	148	15	15	231	228	1	12	842	840	1
	0	11	1	4	421	460	-29					13	497	493	3
				5	112	128	-5		1	-8	1	14	148	133	5
-13	70	24	5	6	225	195	14					15	482	478	2
-12	365	355	6	7	201	179	9	0	845	843	2	16	31	80	-6
-11	73	103	-7	8	273	229	23	1	1231	1236	-3	17	211	226	-6
-10	105	122	-5	9	221	201	9	2	496	501	-4				
-9	432	412	15	10	176	142	12	3	339	315	20		1	-4	1
-8	59	104	-11					4	100	28	18				
-7	-58	46	-8		1	-12	1	5	1093	1096	-1	0	942	935	6
-6	451	428	17					6	689	684	4	1	1816	1829	-7
-5	393	411	-14	0	234	176	29	7	282	273	6	2	1580	1587	-5
-4	649	665	-13	1	723	731	-6	8	724	741	-14	3	586	604	-21
-3	405	382	18	2	118	89	8	9	220	189	20	4	1357	1360	-1
-2	533	547	-12	3	91	80	2	10	347	351	-2	5	2234	2239	-2
-1	252	246	3	4	282	267	-3	11	578	592	-12	6	512	520	-9
0	303	290	8	5	568	565	1	12	319	330	-7	7	201	182	14
1	698	694	3	6	298	314	-11	13	360	367	-5	8	595	599	-3
2	187	176	5	7	364	342	15	14	245	241	2	9	881	883	-2
3	7	8	0	8	100	98	0	15	400	403	-1	10	507	493	11
4	145	180	-14	9	101	99	0	16	116	132	-4	11	432	435	-2
5	417	437	-14	10	117	0	17					12	613	623	-8
6	278	266	5	11	525	523	1					13	236	245	-5
7	351	343	4	12	128	62	14		1	-7	1	14	39	116	-16
8	209	191	7									15	682	667	11
	0	12	1		1	-11	1	0	399	407	-7	16	84	135	-12
				0	381	379	0	1	564	559	4	17	205	245	-17
				1	570	587	-14	2	1624	1630	-3				
-11	210	147	24	2	232	224	5	3	407	410	-2				
-10	161	147	5	3	515	534	-16	4	688	685	3		1	-3	1
-9	245	199	22	4	521	529	-7	5	922	926	-4				
-8	299	291	5	5	557	559	-1	6	112	54	19	0	83	86	-1
-7	154	136	6	6	73	138	-22	7	500	492	7	1	372	360	15
-6	497	497	0	7	55	48	1	8	1128	1110	13	2	1894	1891	1
-5	207	192	7	8	443	466	-19	9	28	9	1	3	1217	1244	-23
-4	187	172	6	9	214	211	1	10	-80	9	-13	4	319	312	8
-3	91	58	7	10	92	57	7	11	469	467	1	5	1642	1645	-1
-2	639	625	10	11	393	384	6	12	621	626	-4	6	991	999	-7
-1	208	230	-11	12	173	137	12	13	620	620	0	7	1320	1330	-7
0	105	22	14	13	125	147	-7	14	166	177	-5	8	1395	1416	-14
1	445	420	18					15	377	384	-4	9	775	762	10
2	227	204	11					16	-146	23	-27	10	-51	22	-5
3	360	378	-12		1	-10	1	17	77	91	-2	11	158	183	-11
4	350	344	3									12	828	819	7
5	85	51	5	0	255	230	17		1	-6	1	13	321	325	-2
6	-114	10	-15	1	1046	1067	-16					14	-127	72	-31
	0	13	1	2	124	65	20	0	1195	1206	-8	15	576	568	5
				3	138	80	22	1	1303	1294	6	16	-85	2	-5
				4	324	334	-9	2	700	711	-11	17	354	332	12
-9	224	231	-3	5	809	797	10	3	338	321	18	18	331	318	6
-8	147	140	2	6	601	614	-12	4	49	63	-4				
-7	150	88	18	7	260	250	7	5	1976	2008	-17		1	-2	1
-6	148	118	9	8	591	601	-9	6	400	362	36				
-5	476	483	-4	9	97	72	6	7	184	146	23	0	622	584	50
-4	248	213	17	10	315	326	-8	8	775	772	2	1	1008	1016	-8
-3	267	238	15	11	488	493	-3	9	338	312	20	2	1353	1347	5
-2	145	156	-4	12	113	89	6	10	428	418	7	3	1535	1559	-16
-1	185	98	29	13	89	79	2	11	741	734	6	4	931	915	16
0	189	162	10	14	366	368	-1	12	644	642	1	5	1839	1834	3
1	626	603	16	15	217	173	17	13	443	423	16	6	147	121	15
2	96	38	9					14	-55	8	-4	7	696	673	22
3	78	133	-13					15	500	490	7	8	1046	1055	-7
	1	-14	1		1	-9	1	16	-78	91	-17	9	1421	1420	0
				0	146	104	17	17	85	133	-11	10	510	518	-6
0	25	26	0	1	520	501	16					11	131	117	4
1	351	326	15	2	893	889	3		1	-5	1	12	609	615	-4
2	51	25	2	3	319	322	-2	0	-14	68	-13	13	-163	61	-51
3	90	47	7	4	700	705	-4	1	637	638	0	14	258	279	-12
4	307	317	-5	5	466	453	11	2	1985	1995	-5	15	598	570	20
5	197	128	25	6	388	404	-13	3	796	795	0	16	-66	24	-6
6	263	247	8	7	123	54	22	4	126	89	20	17	236	234	1
				8	983	1002	-16	5	898	913	-13		1	-1	1
				9	26	39	-1	6	704	731	-27				
	1	-13	1	10	221	222	0	7	399	392	6	0	182	2	90
				11	397	388	7	8	1358	1366	-5	1	1201	1230	-26

[(Au(dcpo))₂ mu-(dcpo)]₂₊ 2[Au(CN)₂]-

2	2264	2233	15	3	1364	1395	-24	4	49	63	-3	9	676	690	-12
3	751	777	-31	4	596	599	-3	5	-83	32	-18	10	455	460	-3
4	385	394	-10	5	52	4	5	6	1672	1677	-2	11	473	471	1
5	616	641	-27	6	2140	2132	3	7	682	703	-18	12	268	303	-19
6	1787	1816	-16	7	732	741	-7	8	163	227	-38	13	357	365	-4
7	1373	1348	17	8	236	236	0	9	831	802	21	14	146	154	-2
8	1568	1547	12	9	640	658	-15	10	203	254	-27	15	-133	2	-18
9	827	841	-11	10	149	187	-17	11	489	464	19				
10	202	220	-10	11	248	245	1	12	469	494	-19	1	6	1	
11	282	316	-23	12	910	899	8	13	366	388	-14				
12	1139	1122	12	13	-124	53	-27	14	247	248	0	-17	280	285	-2
13	-50	106	-20	14	515	497	13	15	180	223	-17	-16	91	174	-25
14	337	370	-23	15	324	329	-3	16	385	324	32	-15	116	116	0
15	389	391	-1	16	314	294	10					-14	589	575	10
16	273	296	-12	17	255	259	-1	1	4	1		-13	490	493	-2
17	209	239	-13									-12	657	661	-3
												-11	554	553	0
	1	0	1		1	2	1	-17	459	459	0	-10	305	310	-3
								-16	127	140	-4	-9	71	84	-3
-17	48	127	-15	-18	169	190	-7	-15	153	194	-16	-8	245	240	3
-16	342	340	0	-17	380	368	7	-14	516	501	11	-7	1523	1513	6
-15	302	281	11	-16	286	299	-7	-13	-127	6	-26	-6	364	369	-4
-14	704	683	16	-15	-98	69	-19	-12	636	617	16	-5	99	24	21
-13	389	398	-6	-14	620	608	9	-11	881	872	7	-4	979	982	-2
-12	284	277	3	-13	57	72	-2	-10	430	437	-6	-3	529	530	0
-11	1003	990	9	-12	201	197	1	-9	34	60	-5	-2	802	821	-17
-10	-102	92	-32	-11	1130	1087	29	-8	128	110	9	-1	1447	1461	-9
-9	-89	83	-28	-10	255	276	-14	-7	1305	1325	-14	0	555	563	-7
-8	1106	1117	-7	-9	672	658	12	-6	1337	1327	7	1	59	68	-2
-7	1529	1545	-10	-8	265	269	-2	-5	672	680	-8	2	82	92	-3
-6	1628	1612	10	-7	1747	1740	4	-4	1499	1512	-9	3	1665	1649	9
-5	1773	1794	-12	-6	1104	1108	-3	-3	1259	1257	-1	4	318	343	-21
-4	353	361	-8	-5	1420	1429	-6	-2	907	914	-7	5	337	355	-14
-3	237	268	-29	-4	674	654	22	-1	1910	1903	4	6	445	431	10
-2	268	285	-17	-3	63	61	0	0	314	319	-5	7	240	230	5
-1	2851	2903	-21	-2	1023	1023	0	1	247	233	13	8	635	632	2
0	934	921	14	-1	3154	3123	11	2	609	615	-6	9	884	898	-10
1	341	325	18	0	471	473	-1	3	1821	1793	15	10	63	124	-15
2	942	907	34	1	1201	1203	-1	4	723	750	-26	11	91	147	-16
3	1215	1213	2	2	1059	1063	-4	5	325	343	-15	12	-81	28	-8
4	1028	1049	-19	3	1016	990	23	6	701	716	-13	13	571	551	13
5	1057	1064	-6	4	1519	1511	5	7	167	192	-13	14	282	292	-5
6	591	604	-12	5	1485	1483	1	8	473	468	3				
7	-39	43	-6	6	1600	1582	11	9	1312	1290	13	1	7	1	
8	379	396	-15	7	-69	0	-9	10	29	49	-2				
9	1312	1319	-4	8	468	463	3	11	228	241	-7				
10	554	543	8	9	1272	1253	12	12	-84	94	-21	-16	-45	69	-8
11	235	260	-15	10	114	186	-28	13	550	556	-4	-15	243	240	1
12	746	729	14	11	-123	0	-24	14	336	330	3	-14	449	462	-9
13	-92	91	-25	12	501	492	6	15	222	213	3	-13	219	273	-32
14	676	635	30	13	497	497	0					-12	428	418	7
15	596	552	31	14	572	583	-8					-11	251	245	4
16	231	229	0	15	448	433	10					-10	694	706	-10
17	-126	114	-33	16	129	170	-12	-17	327	329	0	-9	386	364	19
								-16	-164	21	-35	-8	119	129	-4
								-15	146	173	-10	-7	790	797	-5
								-14	818	771	35	-6	396	368	24
								-13	-89	44	-15	-5	510	524	-13
-18	228	227	0	-18	219	238	-8	-12	539	530	8	-4	1042	1056	-11
-17	128	138	-2	-17	416	362	31	-11	224	245	-14	-3	103	69	12
-16	176	217	-17	-16	123	174	-17	-10	715	721	-4	-2	149	99	24
-15	-78	32	-9	-15	379	369	6	-9	381	381	0	-1	675	668	5
-14	824	816	6	-14	748	726	17	-8	438	454	-15	0	1298	1300	-1
-13	383	401	-13	-13	-57	64	-11	-7	981	1004	-19	1	811	814	-1
-12	-72	18	-8	-12	-99	62	-23	-6	439	453	-14	2	559	563	-3
-11	590	578	9	-11	780	762	14	-5	364	363	1	3	714	699	13
-10	78	99	-5	-10	584	588	-3	-4	1693	1737	-27	4	432	440	-6
-9	987	984	2	-9	977	975	1	-3	361	375	-15	5	425	426	-1
-8	1264	1255	6	-8	590	627	-36	-2	54	29	5	6	801	827	-21
-7	1235	1232	2	-7	1023	1030	-5	-1	591	598	-7	7	-76	21	-10
-6	261	216	37	-6	64	45	5	0	1696	1664	19	8	200	216	-8
-5	495	524	-33	-5	272	259	13	1	1082	1071	9	9	267	284	-10
-4	2239	2282	-21	-4	2338	2305	15	2	1405	1418	-8	10	346	345	1
-3	729	720	10	-3	550	553	-3	3	740	732	7	11	177	212	-14
-2	1461	1493	-24	-2	144	144	0	4	274	288	-11	12	181	189	-3
-1	1400	1404	-2	-1	577	564	17	5	283	286	-2	13	419	406	7
0	818	793	29	0	1485	1462	16	6	1254	1220	23				
1	1033	1018	14	1	830	821	10	7	381	398	-13	1	8	1	
2	2372	2344	13	2	1916	1912	2	8	51	121	-17				
				3	211	207	3								

[(Au(dcp)) ₂ mu-(dcp)] ₂ + 2[Au(CN) ₂]-														Page 12	
-16	-74	36	-8	3	760	769	-7	3	569	581	-9	14	251	234	9
-15	214	239	-11	4	119	149	-10	4	127	131	-1	15	199	217	-7
-14	156	183	-10	5	71	80	-1	5	154	184	-13				
-13	399	390	6	6	136	204	-27	6	240	214	13	2	-8	1	
-12	411	413	-1	7	460	456	2	7	297	292	3				
-11	445	415	23	8	389	392	-2	8	145	122	7	0	1456	1476	-12
-10	445	455	-9	9	214	202	4	9	274	271	1	1	355	349	5
-9	76	53	5					10	365	349	10	2	172	128	24
-8	502	497	4		1	11	1					3	98	42	16
-7	1166	1180	-9					2	-12	1		4	1085	1101	-12
-6	102	65	11	-12	218	151	26					5	534	520	12
-5	126	124	1	-11	98	85	2	0	627	635	-7	6	434	430	4
-4	297	287	7	-10	477	487	-7	1	357	356	1	7	928	945	-14
-3	640	620	17	-9	-21	59	-5	2	82	1	10	8	186	155	16
-2	591	594	-2	-8	-56	30	-6	3	338	346	-5	9	350	338	10
-1	821	832	-9	-7	261	272	-6	4	598	585	11	10	728	744	-14
0	782	779	2	-6	347	344	2	5	419	419	0	11	239	225	8
1	47	49	0	-5	521	535	-11	6	332	354	-16	12	313	339	-18
2	159	135	10	-4	556	540	12	7	199	207	-4	13	339	310	-19
3	1233	1230	2	-3	427	438	-8	8	71	50	3	14	458	487	22
4	348	365	-14	-2	144	10	29	9	165	144	8	15	248	247	0
5	-67	4	-7	-1	277	265	8	10	477	490	-9	16	46	59	-1
6	324	316	5	0	723	720	2	11	82	98	-3				
7	679	670	6	1	98	70	6	12	185	127	21	2	-7	1	
8	653	650	2	2	145	125	7								
9	388	408	-13	3	313	305	4	2	-11	1		0	640	658	-17
10	-79	13	-7	4	291	285	3					1	1350	1341	6
11	-154	22	-29	5	359	363	-2	0	499	516	-15	2	643	635	7
12	-90	0	-8	6	260	265	-2	1	104	38	15	3	780	769	11
				7	40	116	-13	2	410	417	-6	4	800	805	-4
								3	740	782	-37	5	131	71	25
								4	396	395	1	6	435	425	9
								5	161	148	6	7	1347	1354	-5
								6	126	103	8	8	85	55	8
								7	614	618	-3	9	112	11	21
								8	206	234	-16	10	673	675	-2
								9	109	91	5	11	549	563	-13
								10	485	488	-2	12	675	665	8
								11	148	126	7	13	386	396	-8
								12	201	174	11	14	454	467	-9
								13	397	370	17	15	107	94	3
								14	-25	48	-3	16	-49	46	-5
												17	348	352	-1
												2	-6	1	
								0	978	995	-13				
								1	136	102	14	0	1462	1464	-1
								2	17	18	0	1	509	513	-4
								3	318	322	-3	2	62	52	3
								4	782	799	-14	3	266	159	85
								5	613	648	-33	4	1893	1916	-13
								6	652	671	-17	5	196	201	-4
								7	603	611	-7	6	123	73	22
								8	-40	33	-5	7	715	717	-1
								9	246	266	-13	8	411	398	11
								10	661	651	7	9	336	324	9
								11	177	160	7	10	827	833	-4
								12	71	93	-5	11	541	537	3
								13	361	364	-2	12	500	506	-5
								14	151	122	9	13	184	192	-4
								15	305	295	5	14	705	714	-6
												15	193	203	-4
								2	-9	1		16	-160	8	-32
												17	304	297	3
								0	741	743	-1				
								1	617	604	11	2	-5	1	
								2	416	410	5				
								3	484	472	10	0	444	437	7
								4	467	472	-4	1	1784	1757	15
								5	277	272	4	2	1126	1134	-6
								6	221	226	-2	3	849	844	4
								7	1112	1158	-36	4	1300	1319	-14
								8	289	301	-10	5	815	816	-1
								9	96	89	2	6	782	798	-15
								10	507	499	7	7	1468	1459	6
								11	366	367	0	8	123	78	17
								12	347	342	4	9	105	110	-2
								13	484	481	2	10	415	421	-5

((Au(dcpe)) 2 mu-(dcpe)) 2+ 2[Au(CN)2]-

Page 13

11	864	855	6	5	1624	1637	-8	7	492	508	-15	10	516	514	2	
12	537	523	12	6	845	863	-16	8	825	829	-3	11	754	754	0	
13	180	178	0	7	1348	1359	-8	9	-47	35	-5	12	273	300	-16	
14	722	703	14	8	411	417	-5	10	115	142	-9	13	170	171	0	
15	145	149	-1	9	160	204	-24	11	1007	949	39	14	71	168	-26	
16	88	121	-7	10	206	203	1	12	-169	16	-47	15	293	306	-6	
17	456	445	7	11	1237	1219	12	13	327	352	-16	16	348	343	2	
				12	313	311	1	14	503	483	14					
				13	326	346	-14	15	339	365	-16	2	4	1		
				14	748	737	8	16	344	336	4					
				15	308	329	-12	17	221	209	4	-17	294	280	7	
0	1423	1434	-7	16	228	263	-17					-16	-54	139	-26	
1	953	972	-19	17	124	160	-10	2	2	1		-15	431	420	7	
2	105	21	30									-14	-83	64	-15	
3	165	151	11	2	0	1		-17	392	359	19	-13	559	536	18	
4	2460	2442	7					-16	-117	7	-17	-12	851	835	13	
5	-49	29	-9	-17	243	242	0	-15	517	500	11	-11	261	268	-4	
6	229	223	5	-16	203	237	-15	-14	-111	85	-27	-10	81	116	-11	
7	776	785	-8	-15	366	362	3	-13	312	326	-9	-9	97	57	11	
8	806	810	-3	-14	431	424	5	-12	756	743	10	-8	1144	1138	3	
9	752	750	2	-13	158	177	-8	-11	334	347	-9	-7	750	748	1	
10	733	726	5	-12	1003	985	13	-10	318	301	12	-6	841	869	-26	
11	639	649	-7	-11	510	483	20	-9	860	858	1	-5	989	991	-1	
12	138	173	-16	-10	70	36	5	-8	1430	1449	-12	-4	264	259	5	
13	-113	2	-20	-9	586	593	-5	-7	983	996	-11	-3	921	933	-11	
14	790	794	-3	-8	983	990	-5	-6	1173	1191	-15	-2	1217	1241	-19	
15	321	326	-3	-7	1103	1126	-18	-5	876	870	5	-1	705	705	0	
16	-63	86	-14	-6	1234	1253	-14	-4	250	250	0	0	272	272	0	
17	464	457	4	-5	868	870	-1	-3	520	513	8	1	778	777	0	
				-4	486	485	0	-2	2111	2114	-1	2	1425	1428	-1	
				-3	-87	30	-20	-1	276	263	15	3	852	854	-2	
				-2	1991	2045	-30	0	231	224	7	4	867	867	0	
0	131	142	-8	-1	426	416	12	1	997	986	10	5	671	649	19	
1	2251	2242	4	0	101	97	2	2	1726	1701	15	6	91	128	-13	
2	91	58	14	0	2056	2040	8	3	1155	1150	3	7	317	334	-12	
3	894	898	-3	1	1289	1314	-20	4	1678	1697	-11	8	1420	1381	23	
4	1271	1263	6	2	177	103	39	5	1122	1109	10	9	158	177	-9	
5	1029	1040	-10	3	1890	1915	-14	6	-36	80	-15	10	260	258	1	
6	913	914	-1	4	887	880	6	7	531	527	3	11	285	278	4	
7	1460	1476	-10	5	236	226	7	8	1327	1318	5	12	603	608	-3	
8	676	666	8	6	7	105	121	-6	9	376	397	-16	13	343	367	-13
9	341	359	-15	7	1358	1356	1	10	-49	156	-37	14	236	262	-11	
10	76	111	-10	8	368	359	6	11	442	461	-15	15	263	257	2	
11	1005	990	10	9	371	401	-22	12	395	413	-13					
12	-46	53	-8	10	557	558	0	13	511	498	9	2	5	1		
13	-45	112	-22	11	12	-63	115	-26	14	382	381	0				
14	600	589	8	12	671	646	19	15	169	182	-4	-17	56	120	-11	
15	108	119	-3	13	834	811	16	16	269	264	2	-16	127	156	-8	
16	238	239	0	14	294	313	-11					-15	513	509	2	
17	451	457	-3	15	160	231	-29	2	3	1		-14	134	142	-2	
				16	-50	71	-8					-13	578	591	-10	
				17				-17	260	291	-16	-12	592	589	2	
								-16	217	245	-13	-11	666	661	4	
								-15	614	623	-7	-10	594	581	11	
								-14	-89	61	-16	-9	437	421	13	
								-13	135	161	-10	-8	512	506	5	
								-12	526	530	-3	-7	277	251	20	
								-11	138	112	9	-6	246	239	5	
								-10	794	784	7	-5	2176	2184	-4	
								-9	893	896	-2	-4	683	703	-20	
								-8	634	626	7	-3	177	157	14	
								-7	250	253	-2	-2	331	339	-8	
								-6	154	166	-8	-1	1456	1454	1	
								-5	1886	1915	-17	0	1204	1199	4	
								-4	743	752	-9	1	1389	1393	-2	
								-3	-21	56	-10	2	828	832	-3	
								-2	1270	1271	-1	3	179	184	-3	
								-1	801	807	-7	4	160	135	12	
								0	1307	1287	15	5	1197	1175	15	
								1	2135	2108	13	6	254	270	-10	
								2	301	284	17	7	18	75	-8	
								3	111	122	-6	8	722	756	-29	
								4	701	666	32	9	277	272	2	
								5	1840	1830	5	10	485	492	-5	
								6	650	642	7	11	436	457	-14	
								7	96	85	3	12	311	334	-13	
								8	983	965	13	13	190	206	-6	
								9	245	248	-2	14	-71	32	-6	
0	1048	1030	17	2	302	292	10	5	1840	1830	5	10	485	492	-5	
1	3034	2976	21	3	-76	34	-16	6	650	642	7	11	436	457	-14	
2	1305	1334	-23	4	966	968	-1	7	96	85	3	12	311	334	-13	
3	936	954	-18	5	1782	1795	-7	8	983	965	13	13	190	206	-6	
4	1098	1100	-2	6	947	960	-11	9	245	248	-2	14	-71	32	-6	

[(Au(dcpe)) 2 mu-(dcpe)] 2+ 2[Au(CN) 2] -

Page 14

2	6	1	-5	475	465	8	-6	360	345	10	3	180	166	7	
			-4	588	590	-1	-5	513	508	3	4	191	181	5	
			-3	418	407	9	-4	246	209	20	5	237	223	9	
-16	-137	12	-23	889	883	5	-3	215	183	16	6	648	661	-11	
-15	365	355	5	-1	397	402	-4	-2	126	125	0	7	314	311	-2
-14	43	83	-6	0	51	80	-6	-1	672	679	-5	8	232	237	-3
-13	666	657	6	1	164	166	-1	0	49	32	1	9	549	563	-12
-12	510	508	1	2	1224	1260	-27	1	91	26	10	10	112	54	13
-11	527	519	6	3	488	502	-12	2	340	360	-14	11	287	261	15
-10	402	391	9	4	250	279	-20	3	172	148	9	12	381	399	-12
-9	177	158	9	5	355	342	9	4	246	242	1	13	112	35	14
-8	827	814	10	6	544	554	-7	5	301	299	0	14	109	105	0
-7	378	380	-1	7	505	574	-7	6	49	99	-8				
-6	57	39	3	8	478	464	10					3	-10	1	
-5	826	845	-16	9	217	196	8	2	12	1					
-4	544	536	7	10	-151	47	-30				0	278	282	-2	
-3	574	569	4	11	85	111	-5	-9	234	218	7	1	155	123	13
-2	1237	1262	-18					-8	225	217	3	2	178	171	3
-1	332	351	-18	2	9	1		-7	159	97	18	3	879	860	15
0	276	270	5					-6	136	103	10	4	427	449	-21
1	181	180	0	-14	322	319	1	-5	220	190	14	5	712	722	-8
2	1650	1644	3	-13	157	162	-1	-4	537	518	13	6	630	621	8
3	599	589	9	-12	126	9	20	-3	318	296	13	7	251	231	13
4	350	371	-16	-11	447	446	0	-2	147	119	9	8	103	89	4
5	428	409	15	-10	300	303	-1	-1	231	234	-1	9	715	729	-12
6	373	374	0	-9	105	89	4	0	195	178	7	10	97	76	5
7	471	466	4	-8	482	506	-20	1	324	304	11	11	232	198	18
8	1017	1017	0	-7	305	270	25	2	522	534	-8	12	293	294	0
9	44	61	-2	-6	563	576	-11	3	-92	64	-15	13	180	146	13
10	42	75	-4	-5	756	750	5					14	228	266	-19
11	49	155	-25	-4	187	178	5	3	-14	1		15	337	332	2
12	465	470	-3	-3	107	68	12								
13	312	333	-10	-2	105	71	10	0	302	292	5				
				-1	865	868	-2	1	128	104	6	3	-9	1	
				0	182	179	-2	2	178	179	0	0	369	352	13
				1	268	245	15	3	215	193	10	1	635	644	-7
-16	104	168	-19	2	434	462	-23	4	301	255	25	2	712	715	-2
-15	426	410	10	3	47	0	3	5	405	398	4	3	400	399	0
-14	-60	98	-17	4	344	342	1	6	144	101	12	4	303	279	18
-13	297	291	3	5	724	731	-5	7	111	87	5	5	307	287	14
-12	147	175	-12	6	202	200	0	8	205	196	3	6	1287	1260	18
-11	642	651	-7	7	210	197	5					7	481	491	-9
-10	503	498	4	8	-99	14	-12	3	-13	1		8	131	38	28
-9	299	273	19	9	427	425	1					9	650	678	-25
-8	759	754	4	10	208	171	13	0	61	32	3	10	378	359	15
-7	184	134	24					1	103	81	5	11	301	304	-2
-6	605	592	11	2	10	1		2	557	574	-13	12	461	466	-4
-5	1000	1030	-24	3	69	36	5	3	69	36	5	13	251	246	3
-4	87	28	13	-13	284	242	21	4	215	201	7	14	323	323	0
-3	231	206	17	-12	39	74	-5	5	256	261	-2	15	163	171	-3
-2	332	334	-2	-11	430	414	11	6	444	456	-9				
-1	1036	1041	-3	-10	106	57	10	7	161	172	-4				
0	857	847	8	-9	211	215	-1	8	215	257	-23				
1	618	614	3	-8	454	468	-11	9	187	121	-23	0	144	124	10
2	859	864	-3	-7	97	73	6	10	133	129	1	1	376	379	-2
3	283	257	17	-6	193	206	-7	11	173	67	28	2	160	146	7
4	347	342	3	-5	372	380	-6					3	1061	1066	-3
5	838	831	5	-4	563	569	-5	3	-12	1		4	396	395	0
6	86	8	11	-3	523	531	-6					5	672	662	8
7	252	287	-23	-2	335	320	11	0	322	336	-10	6	932	954	-17
8	429	429	0	-1	504	523	-16	1	175	138	16	7	97	68	8
9	451	453	-1	0	278	271	4	2	490	484	5	8	354	339	12
10	283	275	4	1	229	214	8	3	382	352	22	9	885	913	-24
11	366	345	12	2	678	683	-3	4	437	435	1	10	108	92	5
12	249	218	13	3	272	264	4	5	434	436	-1	11	173	212	-22
				4	126	73	13	6	518	536	-15	12	414	416	-1
				5	288	254	18	7	-78	70	-17	13	625	634	-7
				6	472	470	1	8	216	174	20	14	378	369	6
-15	150	157	-2	7	457	454	1	9	447	452	-3	15	123	130	-2
-14	373	369	2	8	283	277	3	10	204	185	9	16	317	308	4
-13	368	347	14					11	84	67	3				
-12	335	326	5	2	11	1		12	377	357	12				
-11	294	299	-3									3	-7	1	
-10	273	259	9	-11	567	548	14					0	1172	1177	-4
-9	106	82	7	-10	159	140	6					1	944	957	-11
-8	1024	1056	-25	-9	121	81	10	0	127	91	12	2	957	961	-3
-7	148	122	12	-8	176	179	-1	1	371	359	10	3	744	737	7
-6	309	313	-3	-7	282	277	3	2	902	931	-24	4	135	119	9

[(Au(dcpe))₂ mu-(dcpe)]₂₊ 2[Au(CN)₂]-

6	156	166	-4					5	84	46	6	5	499	478	16
7	1593	1559	19	-15	-40	29	-3	6	135	165	-10	6	316	328	-7
8	357	378	-16	-14	307	286	12	7	94	155	-17	7	258	253	2
9	230	237	-4	-13	255	236	10	8	457	475	-11	8	202	212	-5
10	418	412	4	-12	413	417	-3	9	276	268	3	9	-39	17	-2
11	542	536	4	-11	476	446	23					10	172	112	19
12	363	351	6	-10	384	394	-7		3	10	1	11	493	479	9
13	137	211	-26	-9	384	397	-10								
14	274	313	-19	-8	136	102	14	-12	361	332	17		4	-12	1
				-7	664	677	-12	-11	194	200	-2				
	3	5	1	-6	1425	1430	-3	-10	154	126	9	0	135	116	7
				-5	166	119	22	-9	437	439	-1	1	463	482	-15
-17	35	90	-7	-4	-75	21	-12	-8	65	34	4	2	176	144	14
-16	343	342	0	-3	204	214	-6	-7	176	99	27	3	407	415	-6
-15	152	167	-5	-2	589	585	3	-6	310	301	6	4	550	573	-20
-14	263	278	-8	-1	815	804	9	-5	422	435	-10	5	352	352	0
-13	609	598	8	0	725	732	-6	-4	508	515	-6	6	174	176	0
-12	525	540	-12	1	750	742	6	-3	483	476	5	7	92	49	9
-11	782	785	-2	2	145	28	32	-2	372	370	1	8	453	443	7
-10	432	426	5	3	165	108	25	-1	110	45	15	9	196	179	8
-9	397	402	-4	4	1122	1114	5	0	297	293	2	10	116	43	15
-8	325	298	20	5	38	44	0	1	602	635	-27	11	438	427	7
-7	273	273	0	6	126	106	6	2	202	211	-4	12	156	100	16
-6	1256	1257	0	7	380	374	3	3	178	137	15				
-5	736	754	-17	8	512	510	1	4	321	314	4		4	-11	1
-4	268	259	7	9	336	381	-28	5	350	355	-2				
-3	1062	1050	9	10	390	412	-14	6	365	355	6	0	248	211	23
-2	573	564	9	11	51	75	-3	7	298	295	1	1	923	951	-22
-1	921	940	-16									2	86	14	12
0	1129	1118	8		3	8	1		3	11	1	3	215	207	5
1	473	490	-16									4	371	367	3
2	25	26	0	-15	196	218	-9	-10	162	142	7	5	846	853	-5
3	53	39	2	-14	341	326	8	-9	252	206	21	6	352	368	-13
4	1086	1073	9	-13	133	142	-3	-8	255	250	2	7	374	389	-12
5	142	136	2	-12	273	295	-14	-7	170	203	-15	8	422	423	0
6	199	255	-33	-11	209	211	-1	-6	468	444	17	9	33	14	1
7	792	795	-2	-10	191	173	8	-5	227	192	17	10	234	257	-13
8	190	205	-7	-9	580	588	-6	-4	183	197	-6	11	508	519	-8
9	550	552	-1	-8	254	245	6	-3	-42	24	-3	12	201	157	18
10	666	679	-10	-7	220	208	7	-2	559	562	-2	13	134	78	14
11	154	197	-17	-6	539	545	-5	-1	147	120	9	14	356	354	1
12	-96	127	-29	-5	506	529	-22	0	67	5	6				
13	-85	13	-7	-4	453	447	5	1	296	291	3		4	-10	1
				-3	855	862	-6	2	198	160	15				
	3	6	1	-2	311	301	8	3	265	256	4	0	113	17	23
				-1	120	47	22	4	392	394	-1	1	541	541	0
-16	170	226	-23	0	256	259	-2					2	352	343	6
-15	-125	69	-26	1	854	859	-4		3	12	1	3	484	481	2
-14	363	344	12	2	489	480	7					4	484	473	10
-13	521	510	8	3	397	375	17	-7	95	80	3	5	616	618	-2
-12	369	373	-2	4	546	561	-12	-6	187	165	8	6	296	274	16
-11	449	444	4	5	324	341	-11	-5	430	432	-1	7	252	255	-2
-10	139	115	9	6	402	401	0	-4	301	307	-3	8	931	943	-9
-9	986	989	-2	7	484	473	7	-3	147	168	-7	9	96	39	12
-8	394	374	15	8	236	264	-14	-2	246	210	17	10	181	188	-4
-7	154	114	17	9	-31	88	-9	-1	74	75	0	11	374	365	6
-6	753	734	16	10	-132	82	-27	0	289	247	21	12	321	309	8
-5	545	538	6					1	533	502	21	13	194	188	2
-4	495	482	11		3	9	1					14	429	444	-10
-3	1041	1046	-3						4	-14	1	15	259	233	12
-2	127	97	13	-13	63	64	0								
-1	196	164	20	-12	396	392	2	0	17	99	-12		4	-9	1
0	503	499	3	-11	306	326	-13	1	276	291	-8				
1	1551	1539	7	-10	160	111	17	2	70	72	0	0	933	927	4
2	733	743	-9	-9	405	407	-1	3	195	197	-1	1	1255	1237	13
3	336	325	8	-8	192	222	-16	4	380	396	-10	2	483	476	6
4	445	420	19	-7	459	471	-9	5	157	134	8	3	337	290	36
5	499	499	0	-6	703	696	6	6	-10	82	-9	4	93	35	14
6	357	329	20	-5	127	137	-4	7	275	248	14	5	750	732	15
7	898	912	-10	-4	186	190	-2	8	251	247	2	6	757	764	-6
8	-52	57	-8	-3	280	270	7					7	279	268	8
9	148	200	-22	-2	784	818	-30		4	-13	1	8	923	928	-4
10	195	212	-7	-1	313	329	-12					9	261	234	18
11	355	342	7	0	98	116	-5	0	188	150	16	10	310	307	2
12	325	321	2	1	381	388	-5	1	520	541	-17	11	500	513	-10
13	-92	75	-14	2	146	139	3	2	163	146	6	12	285	266	11
				3	244	252	-5	3	94	97	0	13	274	288	-8
	3	7	1	4	805	811	-5	4	311	316	-3	14	298	304	-3

[(Au(dcpe))₂mu-(dcpe)]₂+ 2[Au(CN)₂]-

Page 17

15	385	384	0	13	119	188	-28	7	441	437	2	11	-128	58	-30	
	4	-8	1	14	29	11	0	8	613	600	11	12	610	611	-1	
				15	573	573	0	9	1177	1177	0	13	445	438	4	
				16	102	147	-12	10	186	166	9	14	431	440	-5	
0	507	518	-10	17	126	142	-4	11	-113	26	-22	15	305	355	-28	
1	360	354	6					12	679	685	-4	16	258	265	-3	
2	1404	1425	-14		4	-4	1	13	-166	81	-50					
3	244	213	22	0	67	8	12	14	577	559	13	4	2	1		
4	729	735	-5	1	105	98	4	15	537	518	12					
5	834	867	-29	2	1925	1928	-1	16	190	205	-6	-17	326	298	14	
6	136	9	33	3	607	610	-2					-16	175	162	4	
7	330	307	17	4	289	294	-5	4	0	1		-15	286	272	7	
8	1021	1022	0	5	1034	1045	-10	-17	-84	87	-16	-14	582	552	22	
9	98	13	17	6	1034	1045	-9	-16	268	263	2	-13	173	206	-15	
10	127	61	20	7	815	820	-4	-15	-138	16	-25	-12	157	147	4	
11	571	577	-4	8	1445	1458	-8	-14	695	674	15	-11	614	599	13	
12	545	555	-8	9	631	620	9	-13	430	443	-9	-10	351	347	2	
13	513	518	-3	10	249	241	5	-12	-55	17	-5	-9	911	908	2	
14	216	234	-9	11	69	94	-6	-11	642	602	29	-7	699	709	-8	
15	346	355	-5	12	907	896	8	-10	-30	104	-17	-6	673	659	12	
16	-102	16	-12	13	69	167	-32	-9	939	935	3	-5	367	350	15	
				14	-148	32	-31	-8	1155	1144	8	-4	133	104	15	
				15	529	536	-5	-7	608	618	-9	-3	1870	1902	-18	
0	1172	1188	-13	16	-158	46	-33	-6	226	244	-13	-2	131	82	25	
1	857	847	8	17	249	266	-7	-5	207	243	-27	-1	84	37	15	
2	365	367	-1					-4	1391	1418	-19	0	263	246	17	
3	53	24	5	4	-3	1		-3	912	911	0	1	1333	1330	1	
4	-59	18	-9	0	1230	1221	6	-2	920	938	-17	2	273	270	2	
5	1761	1769	-4	1	134	43	42	-1	1379	1410	-23	3	2197	2152	21	
6	57	24	5	2	1211	1219	-6	0	657	652	5	4	230	176	38	
7	69	18	8	3	615	612	3	1	2377	2327	29	5	485	445	35	
8	630	640	-8	4	546	559	-15	2	2166	2181	-7	6	-71	80	-22	
9	296	284	8	5	1640	1624	9	3	247	214	24	7	1762	1769	-3	
10	277	255	15	6	422	419	2	4	578	583	-4	8	174	129	19	
11	677	694	-14	7	245	255	-8	5	513	503	9	9	383	397	-10	
12	633	644	-9	8	833	826	5	6	1918	1895	12	10	714	714	0	
13	463	456	5	9	1279	1281	-1	7	702	683	16	11	69	161	-29	
14	29	139	-24	10	550	547	2	8	437	443	-4	12	463	465	-1	
15	471	482	-8	11	-110	89	-34	9	665	651	10	13	485	501	-11	
16	-63	56	-8	12	736	723	10	10	104	184	-32	14	149	211	-24	
				13	-72	83	-17	11	-33	94	-15	15	180	198	-13	
				14	62	133	-18	12	1004	984	14	15	193	226	-12	
				15	639	636	2	13	-60	144	-31					
				16	-137	70	-28	14	490	467	15	4	3	1		
				17	184	201	-6	15	298	256	20	-17	466	419	28	
0	196	207	-9					16	316	321	-2	-16	161	204	-16	
1	458	448	10	4	-2	1						-15	82	137	-13	
2	1656	1652	2	0	90	19	21	4	1	1		-14	437	435	1	
3	938	938	0	1	731	721	11	-17	288	278	4	-13	-43	115	-20	
4	236	199	30	2	1921	1920	0	-16	380	357	14	-12	560	564	-3	
5	1176	1188	-9	3	67	28	9	-15	45	30	1	-11	805	795	8	
6	705	702	2	4	238	223	13	-14	474	458	11	-10	108	91	4	
7	589	580	8	5	689	710	-21	-13	-118	56	-25	-9	253	253	0	
8	1156	1161	-3	6	1188	1207	-14	-12	318	307	7	-8	70	10	8	
9	132	93	14	7	882	881	1	-11	1035	1021	10	-7	1253	1251	0	
10	131	105	9	8	1191	1192	0	-10	259	285	-16	-6	1174	1195	-16	
11	327	344	-14	9	780	784	-2	-9	522	510	9	-5	613	629	-17	
12	826	838	-9	10	-59	111	-24	-8	349	365	-13	-4	1431	1440	-6	
13	504	496	6	11	395	410	-12	-7	1473	1486	-8	-3	604	598	6	
14	142	172	-11	12	954	953	0	-6	1025	1043	-14	-2	1412	1398	9	
15	557	518	27	13	204	243	-20	-5	862	875	-12	-1	1162	1173	-8	
16	-93	71	-15	14	136	175	-14	-4	597	611	-15	0	323	310	12	
17	-57	120	-18	15	530	526	2	-3	360	366	-7	1	97	105	-3	
				16	190	241	-22	-2	175	101	49	2	542	539	2	
0	643	639	4	17	198	179	6	-1	2554	2540	5	3	1325	1291	23	
1	1949	1906	23					0	390	360	33	4	664	651	12	
2	900	910	-9	4	-1	1		1	577	538	43	5	534	532	2	
3	73	45	9	5	873	870	-2	2	873	870	2	6	983	961	16	
4	619	607	13	6	537	542	-5	3	537	542	-5	7	45	82	-7	
5	1865	1880	-8	7	1269	1272	-1	4	1269	1272	-1	8	283	293	-5	
6	347	354	-7	8	1262	1257	3	5	1262	1257	3	9	1142	1129	9	
7	141	142	0	9	1386	1381	-3	6	1386	1381	-3	10	228	254	-14	
8	814	818	-2	10	855	853	2	7	219	188	16	11	196	224	-12	
9	706	700	5	11	4	234	256	-17	8	84	132	-15	12	144	201	-21
10	405	422	-13	12	1063	1066	-2	8	84	132	-15	13	445	456	-7	
11	303	324	-16					9	872	867	3	14	221	248	-12	
12	678	681	-2					10	314	356	-30					

$$[(Au(dcpe))_2 mu-(dcpe)]_2 + 2[Au(CN)_2]^-$$

Page 19

0	698	709	-10					15	227	281	-26	-15	416	429	-8
1	1112	1093	14	5	-4	1		16	157	157	0	-14	-35	118	-18
2	538	547	-8	0	215	180	28		5	0	1	-13	305	313	-4
3	362	360	1	1	2061	2019	21					-12	565	575	-7
4	343	328	12	2	673	675	-1	-17	219	244	-11	-11	-120	23	-24
5	118	78	14	3	468	468	0	-16	-127	59	-22	-10	603	602	1
6	178	153	14	4	872	873	0	-15	586	558	19	-9	699	695	2
7	1155	1158	-2	5	803	828	-24	-14	391	380	7	-8	563	553	8
8	131	139	-3	6	716	721	-4	-13	1	57	-4	-7	229	256	-19
9	121	81	14	7	1516	1517	0	-12	503	494	7	-6	59	38	3
10	642	651	-7	8	502	489	11	-11	118	176	-24	-5	1646	1662	-9
11	494	489	4	9	382	367	11	-10	604	601	2	-4	777	783	-5
12	509	511	-1	10	197	164	15	-9	1100	1088	8	-3	165	135	19
13	361	355	3	11	926	934	-6	-8	428	431	-2	-2	653	651	2
14	517	505	8	12	55	102	-10	-7	508	538	-26	-1	1236	1221	11
15	49	136	-19	13	69	93	-4	-6	161	195	-20	0	784	786	-1
16	-139	7	-23	14	584	583	0	-5	1207	1201	4	1	1536	1536	0
				15	-100	20	-12	-4	891	873	16	2	202	139	39
				16	193	200	-2	-3	908	915	-6	3	387	398	-10
	5	-7	1					-2	881	883	-2	4	353	358	-4
								-1	216	212	3	5	1602	1577	14
0	1218	1221	-1		5	-3	1	0	1270	1249	16	6	628	641	-10
1	907	907	0	0	588	584	4	1	2154	2152	1	8	867	874	-5
2	119	114	2	1	1450	1417	23	2	454	429	24	9	273	290	-10
3	77	5	13	2	535	526	10	3	-101	8	-22	10	339	347	-5
4	1477	1473	3	3	615	613	1	4	855	858	-2	11	646	644	1
5	193	189	2	4	1571	1564	4	5	1540	1540	0	12	206	263	-27
6	157	187	-19	5	196	160	24	6	792	792	0	13	185	195	-3
7	810	825	-12	6	168	113	28	7	418	431	-9	14	173	202	-11
8	415	418	-2	7	1033	1039	-4	8	740	757	-13				
9	95	60	9	8	1105	1109	-2	9	-159	16	-38	5	3	1	
10	757	766	-8	9	678	681	-1	10	-114	41	-22				
11	325	328	-2	10	251	282	-18	11	954	939	11	-16	-116	35	-16
12	405	384	15	11	726	728	-2	12	-86	106	-24	-15	319	327	-4
13	165	166	0	12	-114	55	-24	13	297	313	-8	-14	-113	63	-21
14	716	714	1	13	130	188	-22	14	414	427	-8	-13	591	598	-5
15	201	218	-7	14	775	755	14	15	391	400	-5	-12	742	737	4
16	33	13	1	15	-118	9	-17					-11	71	101	-7
				16	-123	135	-38	5	1	1		-10	301	297	3
	5	-6	1									-9	120	75	13
0	472	469	3		5	-2	1	-17	396	390	3	-8	988	979	6
1	1080	1077	2	0	572	566	7	-16	-164	9	-32	-7	679	689	-8
2	1123	1120	2	1	2219	2184	17	-15	385	389	-3	-6	681	688	-7
3	742	730	11	2	183	188	-3	-13	308	309	-1	-5	866	876	-8
4	1241	1228	9	3	107	100	3	-12	832	837	-4	-4	201	189	8
5	427	423	3	4	536	529	6	-11	511	514	-2	-3	844	830	13
6	829	825	-2	5	1264	1266	-1	-10	141	165	-9	-2	1558	1582	-15
7	1332	1345	-9	6	840	860	-17	-9	420	405	11	-1	409	418	-9
8	321	313	6	7	1460	1439	13	-8	1179	1154	17	0	182	142	25
9	51	12	4	8	749	751	-1	-7	1108	1096	8	1	386	386	0
10	586	594	-7	9	249	259	-6	-6	767	784	-15	2	951	930	17
11	615	622	-6	10	61	91	-6	-5	600	589	11	3	547	540	5
12	381	379	1	11	790	790	0	-4	50	40	1	4	863	847	13
13	153	187	-14	12	-110	16	-18	-3	216	227	-8	5	771	736	27
14	548	559	-8	13	162	216	-24	-2	1644	1690	-29	6	-124	30	-26
15	119	128	-2	14	687	679	5	-1	555	529	27	7	160	176	-7
16	-157	43	-31	15	192	193	0	0	188	167	16	8	1272	1269	1
				16	178	225	-18	1	742	751	-8	9	247	277	-17
	5	-5	1					2	551	552	0	10	162	207	-19
0	1537	1499	24		5	-1	1	3	834	822	10	11	283	308	-13
1	151	82	37	0	-101	35	-24	4	1163	1176	-9	12	514	521	-5
2	556	539	18	1	1603	1606	-1	5	1302	1301	1	13	175	248	-29
3	289	282	7	2	784	810	-24	6	87	67	4	14	138	162	-6
4	1751	1735	9	3	722	743	-19	7	70	123	-15				
5	118	65	22	4	1086	1090	-3	8	1191	1167	16	5	4	1	
6	227	232	-4	5	547	556	-8	9	149	159	-4				
7	877	871	5	6	202	203	0	10	48	151	-27	-16	163	119	12
8	727	730	-2	7	251	288	-25	11	520	522	-1	-15	411	412	0
9	493	509	-13	8	1459	1459	0	12	132	200	-25	-14	-65	37	-7
10	645	633	9	9	601	621	-15	13	307	335	-15	-13	457	466	-6
11	728	723	4	10	412	430	-13	14	467	448	12	-12	439	436	2
12	70	87	-3	11	589	580	7	15	249	292	-21	-11	421	418	2
13	-127	6	-23	12	-137	118	-46					-10	565	573	-6
14	639	617	16	13	355	373	-11	5	2	1		-9	321	333	-9
15	66	191	-36	14	651	629	15					-8	407	394	10
16	-70	68	-10					-16	151	164	-4	-7	160	112	20
												-6	181	153	15

(Au(depe)) 2 mu-(depe)] 2+ 2[Au(CN)2]-

-5	1537	1529	5	10	231	230	0	-9	-97	53	-15	13	73	67	0
-4	450	463	-12	11	323	319	1	-8	188	124	22				
-3	164	134	16					-7	94	129	-9		6	-10	1
-2	314	297	14		5	7	1	-6	415	422	-4				
-1	852	855	-2					-5	457	447	7	0	422	398	21
0	1090	1091	0	-14	289	286	1	-4	267	230	19	1	777	775	1
1	1172	1161	8	-13	367	377	-6	-3	158	151	2	2	682	712	-28
2	781	776	4	-12	246	208	18	-2	87	47	7	3	179	147	17
3	213	194	11	-11	216	211	2	-1	539	539	0	4	157	148	4
4	290	281	6	-10	339	340	0	0	114	80	8	5	205	183	13
5	725	707	13	-9	143	124	7	1	16	26	0	6	1118	1136	-13
6	-13	56	-5	-8	881	889	-6	2	295	300	-2	7	439	433	4
7	257	261	-2	-7	79	6	10	3	142	152	-3	8	126	94	10
8	898	878	14	-6	308	312	-3					9	484	473	9
9	201	195	2	-5	285	274	8		5	11	1	10	343	346	-1
10	441	459	-12	-4	383	385	-1					11	328	305	14
11	446	457	-6	-3	494	489	3	-4	391	386	2	12	448	446	1
12	238	304	-32	-2	538	550	-11	-3	349	306	25	13	220	216	1
13	-132	61	-22	-1	398	407	-7	-2	128	150	-7	14	183	186	-1
				0	136	146	-4								
	5	5	1	1	103	46	14		6	-14	1		6	-9	1
				2	895	914	-15								
-15	281	273	4	3	307	292	10	0	110	17	14	0	414	399	12
-14	-68	47	-8	4	133	128	1	1	108	93	3	1	181	145	18
-13	656	632	17	5	433	414	13	2	480	472	5	2	258	258	0
-12	491	463	20	6	326	351	-15	3	157	9	30	3	584	571	11
-11	402	396	4	7	456	424	21	4	191	179	5	4	403	385	15
-10	122	124	-1	8	420	425	-2	5	234	223	5	5	465	465	0
-9	59	82	-5	9	332	317	7	6	326	327	0	6	898	920	-19
-8	725	736	-9					7	163	163	0	7	249	202	31
-7	563	561	2		5	8	1	8	297	290	3	8	193	160	18
-6	128	41	24									9	794	801	-6
-5	993	999	-4	-13	102	171	-21		6	-13	1	10	143	172	-13
-4	417	410	6	-12	112	79	7					11	221	216	2
-3	378	359	16	-11	378	372	4	0	321	328	-4	12	357	354	1
-2	1045	1023	16	-10	370	386	-11	1	157	96	20	13	463	458	3
-1	120	46	22	-9	129	45	19	2	373	388	-11	14	263	283	-11
0	485	487	-1	-8	416	423	-5	3	286	245	24	15	89	127	-9
1	169	76	38	-7	274	248	16	4	446	439	5				
2	1523	1504	11	-6	570	566	3	5	306	303	2		6	-8	1
3	671	667	3	-5	748	756	-6	6	324	296	18				
4	123	144	-9	-4	185	154	14	7	145	77	20	0	919	916	2
5	485	481	2	-3	113	110	1	8	242	226	8	1	1011	1005	4
6	340	341	-1	-2	97	83	4	9	417	396	14	2	621	610	10
7	372	366	3	-1	722	740	-14	10	137	122	4	3	699	692	6
8	791	790	0	0	311	314	-2	11	93	87	1	4	353	304	38
9	151	157	-2	1	185	186	0					5	153	89	26
10	171	194	-9	2	317	333	-11		6	-12	1	6	1103	1120	-12
11	272	295	-11	3	-124	29	-24					7	192	201	-4
12	349	353	-2	4	308	278	17	0	101	44	12	8	103	102	0
				5	688	670	13	1	178	174	1	9	712	728	-13
	5	6	1	6	101	136	-9	2	727	741	-11	10	327	320	5
-15	367	347	11	7	188	161	9	3	94	113	-5	11	408	434	-20
-14	93	22	9	8	-53	117	-17	4	246	213	18	12	494	494	0
-13	468	458	6		5	9	1	5	173	149	13	13	577	587	-7
-12	172	153	7					6	518	526	-6	14	193	240	-22
-11	450	444	4					7	291	312	-14	15	-51	35	-4
-10	484	456	22	-11	292	294	0	8	272	254	11				
-9	265	246	12	-10	209	165	18	9	409	395	10		6	-7	1
-8	535	522	10	-9	192	199	-3	10	147	53	23				
-7	231	200	19	-8	429	405	16	11	126	133	-2	0	283	253	23
-6	668	677	-8	-7	96	7	12	12	411	399	8	1	404	412	-7
-5	800	810	-8	-6	205	182	10					2	218	190	20
-4	235	227	5	-5	339	331	5		6	-11	1	3	1399	1400	0
-3	184	150	17	-4	485	478	5					4	512	484	25
-2	713	704	7	-3	463	484	-16	0	275	273	1	5	163	117	23
-1	848	841	5	-2	265	265	0	1	158	141	8	6	876	883	-5
0	615	630	-14	-1	446	432	10	2	458	462	-3	7	497	476	18
1	595	605	-8	0	235	207	15	3	633	635	-2	8	171	147	11
2	402	398	3	1	169	167	0	4	268	247	14	9	820	827	-5
3	140	61	25	2	577	585	-6	5	456	447	8	10	164	118	19
4	187	208	-11	3	261	246	7	6	533	518	13	11	271	278	-4
5	911	919	-5	4	-75	5	-7	7	190	228	-22	12	347	353	-4
6	72	51	3	5	237	230	3	8	49	7	3	13	770	747	17
7	121	118	0	6	394	360	20	9	584	597	-10	14	285	296	-6
8	292	316	-14					10	193	176	7	15	-111	69	-20
9	477	455	14		5	10	1	11	137	116	6				
								12	378	358	13		6	-6	1

(Au(dcpe)) 2 mu-(dcpe)] 2+ 2[Au(CN) 2]-

0	622	618	4	-9	693	704	-9	5	70	109	-10	-3	289	303	-9	
1	222	196	19	-8	545	540	4	6	915	919	-2	-2	378	367	7	
2	1081	1086	-3	-7	513	490	17	7	79	102	-5	-1	577	566	9	
3	632	664	-29	-6	438	456	-14	8	157	156	0	0	498	495	2	
4	503	502	0	-5	109	117	-3	9	768	754	9	1	239	242	-2	
5	1035	1007	20	-4	1394	1403	-5	10	240	266	-12	2	45	39	0	
6	538	561	-18	-3	486	464	19	11	231	274	-19	3	741	752	-8	
7	321	310	7	-2	92	36	14	12	141	193	-16	4	113	129	-4	
8	279	297	-12	-1	626	614	10					5	74	45	4	
9	984	1016	-23	0	727	714	11	7	4	1		6	338	341	-1	
10	291	335	-29	1	864	831	27					7	405	378	16	
11	129	225	-40	2	1240	1237	1	-14	351	355	-2	8	272	301	-14	
12	596	577	14	3	185	165	9	-13	194	202	-3					
13	133	175	-13	4	262	249	7	-12	629	630	0	7	7	1		
14	412	438	-16	5	-98	88	-26	-11	435	435	0					
15	469	458	6	6	1279	1293	-9	-10	217	221	-2	-11	16	86	-8	
				7	282	310	-18	-9	161	181	-9	-10	398	374	15	
					8	-57	147	-33	-8	195	186	5	-9	415	399	11
					9	696	679	12	-7	763	772	-7	-8	130	107	7
					10	-122	118	-36	-6	466	469	-2	-7	431	428	2
0	300	313	-12	11	136	202	-23	-5	83	46	8	-6	380	377	2	
1	949	956	-5	12	508	502	3	-4	706	716	-9	-5	565	556	7	
2	1399	1420	-14	13	237	242	-2	-3	189	124	34	-4	520	527	-5	
3	24	97	-13					-2	493	476	15	-3	-49	28	-4	
4	209	255	-26					-1	738	735	2	-2	57	94	-8	
5	461	461	0					0	379	378	0	-1	76	2	8	
6	1193	1168	16	-15	92	116	-5	1	239	222	11	0	712	707	4	
7	469	454	10	-14	345	350	-3	2	115	15	21	1	354	370	-11	
8	402	425	-18	-13	64	73	-1	3	927	922	3	2	193	212	-9	
9	658	692	-27	-12	568	557	8	4	330	341	-8	3	379	372	4	
10	-47	69	-9	-11	704	683	16	5	332	330	1	4	8	51	-3	
11	-130	37	-23	-10	-87	39	-14	6	396	398	-1	5	329	312	9	
12	670	659	8	-9	203	215	-7	7	-110	75	-23	6	428	451	-15	
13	69	128	-12	-8	-51	6	-4	8	415	407	4					
14	348	354	-3	-7	814	807	6	9	767	771	-2	7	8	1		
				-6	850	854	-3	10	143	171	-8					
				-5	424	437	-11	11	-145	62	-26					
				-4	886	886	0					-9	-47	121	-21	
-16	283	262	9	-3	227	221	4					-8	286	221	33	
-15	-135	84	-28	-2	722	726	-3	7	5	1		-7	490	481	6	
-14	347	359	-7	-1	1131	1113	13	-14	392	385	4	-6	190	82	35	
-13	-56	117	-20	0	169	104	29	-13	153	140	3	-5	244	261	-9	
-12	131	172	-14	1	205	189	9	-12	389	399	-7	-4	268	261	3	
-11	762	758	3	2	572	570	1	-11	135	104	9	-3	426	406	14	
-10	366	405	-29	3	827	811	12	-10	495	485	1	-2	315	332	-11	
-9	405	427	-16	4	548	539	6	-9	452	469	-13	0	141	100	12	
-8	218	259	-22	5	260	244	10	-8	156	114	15	1	85	65	3	
-7	1067	1088	-15	6	684	684	0	-7	397	398	0	2	114	52	12	
-6	845	868	-18	7	-135	81	-37	-6	156	149	3	3	628	603	17	
-5	514	530	-13	8	105	192	-32	-5	524	539	-14	4	214	198	6	
-4	563	539	20	9	928	913	10	-4	911	929	-14					
-3	20	104	-20	10	-145	7	-25	-3	102	30	16	7	9	1		
-2	408	396	10	11	-134	100	-31	-2	98	73	7					
-1	1514	1520	-3	12	-95	128	-26	1	406	387	16	-6	195	222	-12	
0	281	248	26	13	396	393	1	0	764	757	5	-5	435	426	5	
1	134	89	18					1	691	704	-11	-4	466	458	5	
2	738	755	-14					2	255	235	12	-3	235	213	10	
3	804	771	25					3	519	506	10	-2	151	111	12	
4	799	791	5	-15	196	197	0	4	263	281	-11	-1	253	230	11	
5	634	646	-9	-14	502	472	19	5	178	199	-9	0	405	392	8	
6	955	952	2	-13	-88	15	-9	6	611	587	17	1	154	5	26	
7	-137	43	-31	-12	466	445	14	7	-69	37	-7					
8	-100	78	-22	-11	318	313	3	8	151	198	-17	8	-14	1		
9	919	929	-7	-10	427	421	4	9	346	333	6					
10	-61	163	-37	-9	481	499	-15	10	254	282	-12	0	451	429	14	
11	-166	66	-41	-8	126	167	-18					1	259	221	19	
12	525	510	9	-7	326	328	-1	7	6	1		2	-66	8	-5	
13	257	281	-11	-6	309	280	23	-13	301	263	19	3	354	342	8	
14	370	372	0	-4	1320	1326	-4	-12	444	432	7	4	342	310	19	
				-3	166	157	4	-11	201	183	7	5	318	318	0	
				-2	131	81	18	-10	262	274	-7	6	168	195	-11	
-15	284	294	-4	-1	289	267	15	-9	242	214	14	7	190	171	7	
-14	541	510	20	0	967	954	9	-8	285	282	1					
-13	103	123	-5	1	891	892	0	-7	714	717	-2	8	-13	1		
-12	41	151	-25	2	964	949	11	-6	118	102	4	0	244	270	-15	
-11	488	478	6	3	469	470	0	-5	219	222	-2	1	125	97	8	
-10	-94	73	-21	4	-56	69	-13	-4	275	280	-3	2	264	239	14	

[[Au(dcpe)]2 mu-(dcpe)]2+ 2[Au(CN)2]-

Page 24

3	542	524	13	3	135	14	30	9	677	693	-13	1	826	804	18
4	277	256	12	4	837	831	4	10	162	196	-14	2	429	418	8
5	186	183	1	5	364	359	4	11	525	548	-17	3	720	699	16
6	163	102	20	6	159	132	13	12	-100	121	-30	4	999	984	10
7	424	415	6	7	794	801	-5	13	-90	67	-14	5	671	707	-29
8	169	193	-10	8	285	302	-12	14	647	614	21	6	-92	72	-20
9	145	111	10	9	67	118	-14					7	90	151	-18
				10	594	588	4	8	-3	1		8	916	903	9
	8	-12	1	11	236	238	-1					9	245	280	-17
				12	255	256	0	0	554	545	8	10	-114	97	-26
0	601	604	-2	13	224	193	13	1	1708	1706	0	11	489	473	10
1	199	174	11	14	576	581	-3	2	97	22	18	12	161	247	-34
2	209	167	20					3	112	34	21	13	328	335	-3
3	312	327	-10	8	-7	1		4	418	418	0				
4	409	398	8					5	570	571	-1	8	1	1	
5	367	385	-13	0	299	278	15	6	572	565	5				
6	275	288	-8	1	991	995	-3	7	936	937	0	-15	386	381	2
7	460	461	0	2	787	766	17	8	724	740	-13	-14	114	110	0
8	106	83	5	3	520	493	23	9	224	281	-32	-13	148	197	-17
9	76	68	1	4	877	868	7	10	-126	98	-34	-12	272	304	-16
10	485	475	7	5	161	114	21	11	665	677	-9	-11	-58	69	-10
11	117	108	2	6	598	610	-12	12	-143	69	-31	-10	531	538	-5
				7	790	802	-10	13	98	153	-14	-9	640	652	-9
	8	-11	1	8	168	147	10	14	623	593	19	-8	143	184	-18
				9	51	40	1					-7	377	356	16
0	431	449	-14	10	556	558	-1	8	-2	1		-6	70	84	-3
1	314	298	11	11	551	559	-6					-5	1162	1158	3
2	384	375	6	12	400	391	6	0	238	219	12	-4	869	869	0
3	445	438	5	13	134	99	9	1	1099	1108	-7	-3	145	93	20
4	249	217	19	14	501	484	11	2	533	520	11	-2	482	471	8
5	214	220	-3					3	445	457	-10	-1	712	705	6
6	203	200	1	8	-6	1		4	1036	1019	12	0	714	704	8
7	714	716	-1					5	321	336	-9	1	1084	1062	16
8	304	303	0	0	630	609	17	6	277	319	-25	2	66	6	7
9	93	27	11	1	473	466	6	7	-32	146	-32	3	299	269	19
10	366	373	-4	2	372	356	13	8	906	918	-9	4	455	446	7
11	342	341	0	3	142	22	35	9	331	339	-4	5	1034	1027	5
12	226	214	5	4	1421	1419	1	10	305	333	-16	6	326	360	-24
				5	144	91	20	11	554	558	-2	7	-126	48	-24
	8	-10	1	6	302	297	4	12	-140	86	-32	8	603	614	-8
				7	694	694	0	13	299	322	-12	9	-88	21	-9
0	805	807	-2	8	301	300	0	14	679	654	16	10	-70	105	-17
1	288	260	19	9	228	231	-2					11	503	537	-22
2	239	229	6	10	563	546	13	8	-1	1		12	191	236	-17
3	154	109	18	11	582	610	-22								
4	518	521	-2	12	90	117	-6	0	707	710	-3	8	2	1	
5	223	216	4	13	-115	28	-17	1	1364	1352	7				
6	218	176	23	14	574	551	15	2	-93	60	-19	-14	-118	4	-15
7	696	710	-11					3	69	69	0	-13	400	388	7
8	219	199	10	8	-5	1		4	650	652	-1	-12	533	514	13
9	120	104	4					5	989	1001	-7	-11	-164	27	-38
10	541	513	21	0	132	108	10	6	480	514	-27	-10	320	327	-4
11	327	288	23	1	1359	1339	13	7	99	197	-37	-9	-113	23	-20
12	205	186	8	2	946	928	14	8	619	617	1	-8	618	612	5
13	269	272	-1	3	233	200	22	9	-106	123	-33	-7	529	499	24
				4	625	605	17	10	-168	29	-37	-6	395	412	-14
	8	-9	1	5	645	657	-10	11	565	592	-19	-5	717	713	3
				6	669	659	8	12	46	114	-11	-4	293	298	-3
0	423	424	0	7	1099	1094	4	13	238	258	-8	-3	594	575	15
1	789	814	-22	8	283	276	4					-2	902	885	13
2	645	642	2	9	340	350	-7	8	0	1		-1	207	168	21
3	478	473	5	10	212	224	-6					0	224	207	9
4	417	423	-5	11	682	697	-11	-15	223	283	-27	1	438	432	5
5	96	43	13	12	-107	51	-17	-14	-144	47	-26	2	715	709	5
6	195	141	28	13	-97	108	-24	-13	274	304	-16	3	558	533	21
7	967	981	-11	14	569	537	20	-12	570	562	6	4	566	537	23
8	97	52	10					-11	400	422	-14	5	538	532	4
9	56	2	4	8	-4	1		-10	187	236	-23	6	-60	61	-10
10	445	448	-2					-9	493	502	-7	7	201	256	-27
11	304	296	5	0	210	184	16	-8	676	709	-27	8	863	859	3
12	300	300	0	1	1104	1091	9	-7	983	989	-4	9	73	123	-10
13	356	349	4	2	142	84	24	-6	387	369	12	10	127	146	-5
				3	379	374	4	-5	670	647	18	11	285	311	-12
	8	-8	1	4	1028	1015	10	-4	264	241	14				
				5	150	163	-6	-3	368	347	16	8	3	1	
0	818	779	31	6	205	178	14	-2	1102	1103	0				
1	494	485	7	7	754	776	-19	-1	225	202	14	-14	-131	108	-31
2	245	232	9	8	760	790	-25	0	233	208	16	-13	303	345	-23

[(Au(dcpe))₂ mu-(dcpe)]₂₊ 2[Au(CN)₂]₋

-12	365	358	4	-9	170	124	15	10	117	33	15	9	517	503	11	
-11	344	344	0	-8	642	642	0					10	382	360	15	
-10	520	526	-4	-7	132	116	5		9	-11	1	11	294	311	-10	
-9	225	228	-1	-6	266	269	-1					12	251	250	0	
-8	283	291	-5	-5	298	290	5	0	214	156	27	13	545	522	15	
-7	144	165	-9	-4	275	264	6	1	436	435	0					
-6	218	235	-10	-3	310	297	8	2	408	423	-11		9	-6	1	
-5	1160	1170	-7	-2	469	456	10	3	201	180	10					
-4	440	446	-4	-1	238	221	9	4	112	43	15	0	376	373	2	
-3	136	81	20	0	191	165	11	5	135	117	6	1	294	309	-10	
-2	356	344	10	1	176	123	19	6	696	720	-19	2	306	296	7	
-1	580	552	25	2	786	790	-3	7	378	354	16	3	1043	1044	0	
0	802	800	1	3	264	286	-13	8	101	59	9	4	219	208	8	
1	718	736	-18	4	-47	45	-5	9	468	472	-2	5	486	467	16	
2	560	565	-4	5	347	337	5	10	154	134	7	6	694	696	-1	
3	250	225	14	6	253	242	4	11	211	200	4	7	451	460	-7	
4	-74	52	-12									8	400	423	-19	
5	633	648	-12		8	7	1		9	-10	1	9	583	586	-2	
6	23	116	-16									10	357	362	-3	
7	-91	21	-10	-9	101	66	6	0	163	108	21	11	152	136	5	
8	649	635	9	-8	378	360	11	1	317	334	-12	12	-70	53	-9	
9	-137	105	-34	-7	187	112	26	2	222	242	-13	13	577	568	6	
10	317	331	-7	-6	522	524	-1	3	423	425	-1					
				-5	485	484	0	4	215	207	4		9	-5	1	
	8	4	1	-4	47	71	-3	5	186	189	-1					
				-3	140	106	10	6	613	606	5	0	991	961	22	
-13	544	517	17	-2	158	110	16	7	189	167	10	1	928	901	21	
-12	360	334	15	-1	541	537	2	8	158	128	11	2	762	737	20	
-11	180	173	2	0	283	267	9	9	656	650	4	3	767	772	-4	
-10	221	210	5	1	112	133	-6	10	98	103	-1	4	409	396	10	
-9	47	13	2	2	266	298	-18	11	206	161	18	5	403	390	11	
-8	550	553	-2	3	83	100	-3	12	351	330	12	6	871	867	2	
-7	369	392	-18	4	177	174	1					7	267	270	-2	
-6	119	33	19						9	-9	1	8	453	463	-7	
-5	571	572	0		8	8	1					9	442	441	0	
-4	106	115	-3					0	590	605	-13	10	709	706	2	
-3	457	457	0	-6	275	231	21	1	705	727	-19	11	92	141	-13	
-2	821	835	-12	-5	263	269	-2	2	496	498	-1	12	-149	36	-28	
-1	81	48	7	-4	306	265	22	3	280	285	-3	13	475	441	20	
0	274	255	13	-3	431	418	8	4	105	62	12					
1	75	98	-6	-2	164	140	8	5	135	45	26		9	-4	1	
2	972	992	-16	-1	310	302	4	6	846	871	-20					
3	421	413	5	0	182	178	1	7	176	177	0	0	712	694	14	
4	233	261	-16	1	135	141	-2	8	110	108	0	1	368	366	1	
5	277	301	-14					9	452	430	16	2	501	471	25	
6	66	135	-16		9	-14	1	10	125	149	-8	3	895	899	-3	
7	289	284	2					11	285	255	16	4	155	135	9	
8	748	750	-1	0	294	263	16	12	406	384	14	5	128	112	6	
9	82	95	-2	1	126	65	13	13	476	430	28	6	647	641	4	
				2	334	332	1					7	525	540	-12	
				3	172	103	21					8	644	658	-11	
				4	374	372	1		9	-8	1	9	409	416	-5	
				5	221	177	18		0	424	427	-3	10	677	681	-2
-12	162	130	9					1	442	452	-8	11	-126	43	-21	
-11	371	384	-8		9	-13	1	2	187	140	25	12	-129	53	-22	
-10	425	423	1					3	728	734	-4	13	557	561	-2	
-9	-79	108	-24					4	256	235	15					
-8	370	346	16	0	114	48	13	5	112	87	8		9	-3	1	
-7	-96	4	-14	1	173	135	14	6	762	794	-28					
-6	405	400	3	2	600	600	0	7	295	284	8	0	2036	1993	21	
-5	634	638	-3	3	129	56	17	8	264	255	5	1	338	310	21	
-4	62	79	-3	4	287	256	17	9	586	585	1	2	296	272	17	
-3	63	76	-2	5	141	109	9	10	85	98	-3	3	288	249	25	
-2	319	312	5	6	419	409	7	11	243	245	0	4	372	374	-1	
-1	489	487	1	7	240	252	-6	12	279	249	15	5	409	427	-14	
0	662	664	-1	8	158	123	11	13	564	530	23	6	826	843	-14	
1	363	343	14									7	433	460	-20	
2	574	582	-6		9	-12	1					8	361	401	-27	
3	-60	47	-8						9	-7	1	9	139	177	-13	
4	-21	69	-6	0	178	199	-10					10	654	679	-18	
5	485	464	14	1	114	95	5	0	734	707	22	11	-141	89	-33	
6	-54	45	-5	2	332	320	8	1	738	749	-8	12	-174	13	-36	
7	109	130	-5	3	374	360	9	2	466	473	-7	13	590	561	18	
8	364	389	-14	4	321	304	11	3	677	683	-5					
				5	345	349	-2	4	124	63	20					
				6	402	377	18	5	485	484	0		9	-2	1	
				7	246	256	-5	6	939	930	7					
-11	229	213	7	8	122	2	19	7	207	222	-9	0	1246	1230	10	
-10	265	255	5	9	477	482	-3	8	35	39	0	1	310	287	16	

$[(Au(dcpe))_2 mu-(dcpe)]_2+ 2[Au(CN)_2]-$

Page 28

5	112	34	16	9	-142	133	-39	6	-46	95	-11	4	219	197	11
6	247	238	5	10	-184	56	-39					5	315	279	22
7	537	505	24					11	3	1		6	662	637	19
8	295	259	20									7	176	151	9
9	298	265	18					-8	299	301	0	8	174	161	5
10	457	424	21	0	294	320	-22	-7	273	262	5	9	374	345	17
11	328	322	3	1	576	583	-6	-6	96	11	11				
				2	238	261	-12	-5	484	470	10	12	-7	1	
				3	470	492	-15	-4	78	26	7				
				4	537	544	-4	-3	342	332	6	0	292	288	3
0	114	40	17	5	398	416	-11	-2	472	442	21	1	326	322	2
1	797	794	2	6	-112	121	-28	-1	39	36	0	2	118	77	11
2	513	506	6	7	-149	104	-34	0	327	307	12	3	639	644	-4
3	153	84	24	8	510	558	-30	1	157	106	15	4	258	211	25
4	460	451	6	9	94	177	-20	2	653	637	11	5	156	118	13
5	189	227	-21					3	372	345	16	6	485	467	13
6	449	450	0	11	0	1		4	-66	138	-26	7	244	237	3
7	604	576	21									8	360	329	18
8	344	328	10	-11	-141	89	-28	11	4	1		9	403	426	-15
9	225	261	-18	-10	413	421	-4								
10	183	195	-4	-9	407	406	0	-6	357	334	14	12	-6	1	
11	402	431	-17	-8	101	180	-24	-5	510	467	29				
				-7	240	270	-15	-4	135	103	9	0	588	591	-1
				-6	-117	81	-26	-3	150	110	12	1	538	540	-1
				-5	801	796	3	-2	254	222	16	2	66	18	6
				-4	564	556	6	-1	288	255	17	3	631	602	23
0	163	104	23	-3	61	78	-3	0	447	439	5	4	105	37	13
1	696	714	-16	-2	364	344	14	1	248	167	34	5	267	244	13
2	121	51	19	-1	240	238	1	2	452	420	20	6	476	494	-14
3	186	156	15	0	514	491	18					7	246	188	26
4	727	698	23	1	663	674	-9	12	-12	1		8	348	349	-1
5	-117	37	-24	2	48	41	0					9	429	417	7
6	267	293	-16	3	310	336	-16	0	154	55	23				
7	536	523	9	4	345	358	-7	1	323	319	2	12	-5	1	
8	552	565	-9	5	698	706	-5	2	337	336	0				
9	408	431	-15	6	183	258	-31	3	149	122	8	0	426	422	3
10	80	151	-17	7	-150	56	-27	4	169	117	17	1	151	151	0
11	448	448	0	8	440	464	-14					2	363	343	14
								12	-11	1		3	758	756	1
				11	1	1						4	145	84	18
0	280	253	17					0	61	53	1	5	142	74	19
1	909	919	-8	-10	267	270	-1	1	301	301	0	6	349	337	7
2	412	418	-5	-9	165	182	-6	2	183	118	22	7	386	391	-3
3	75	54	4	-8	291	300	-4	3	233	243	-5	8	488	497	-6
4	343	339	2	-7	414	387	17	4	239	225	7	9	351	368	-9
5	325	339	-9	-6	43	72	-4	5	263	223	20				
6	346	333	8	-5	497	481	11	6	445	405	26	12	-4	1	
7	569	573	-2	-4	237	264	-16								
8	409	400	6	-3	460	439	15	12	-10	1		0	798	801	-2
9	368	339	16	-2	632	627	4	0	347	338	5	1	245	236	5
10	-104	74	-17	-1	138	69	20	1	460	460	0	2	291	293	-1
11	508	495	7	0	168	192	-11	2	216	205	5	3	457	460	-2
				1	306	301	3	3	248	244	2	4	220	198	10
				2	301	305	-2	4	167	127	14	5	242	242	0
				3	435	429	3	5	150	2	28	6	496	478	12
0	70	63	1	4	421	414	4	6	516	502	10	7	388	404	-9
1	736	743	-6	5	390	408	-11	7	147	119	9	8	401	398	1
2	98	104	-1	6	-49	72	-7	8	102	85	3	9	-66	135	-23
3	421	417	2	7	94	127	-7								
4	571	570	0					12	-9	1		12	-3	1	
5	165	234	-30												
6	175	207	-12	11	2	1		0	214	173	18	0	584	586	-1
7	153	194	-14	-10	442	427	8	1	384	374	6	1	130	36	22
8	596	600	-3	-9	251	231	9	2	114	121	-2	2	451	461	-7
9	275	296	-10	-8	121	136	-4	3	568	554	10	3	600	588	9
10	-73	147	-27	-7	67	99	-6	4	254	249	3	4	-112	44	-17
				-6	125	63	14	5	151	65	23	5	186	210	-9
				-5	769	753	12	6	495	477	13	6	215	246	-13
				-4	412	395	11	7	176	124	18	7	539	550	-7
0	558	580	-19	-3	242	248	-3	8	220	167	22	8	403	388	8
1	976	980	-3	-2	240	203	19								
2	-180	41	-49	-1	373	366	4	12	-8	1		12	-2	1	
3	-94	131	-34	0	588	552	27								
4	379	412	-20	1	475	455	14	0	377	364	9	0	779	767	9
5	442	491	-32	2	318	323	-3	1	555	537	13	1	59	58	0
6	370	410	-24	3	164	177	-5	2	359	343	11	2	174	235	-24
7	118	208	-29	4	126	57	13	3	428	426	0	3	343	391	-27
8	516	526	-6	5	417	414	1					4	197	274	-31

[(Au(dcpe))₂ mu-(dcpe)]₂+ 2[Au(CN)₂]-

Page 29

5	305	355	-25	-1	366	366	0	13	-6	1										
6	96	173	-19	0	368	355	8						13	0	1					
7	440	466	-15	1	313	279	19	0	385	411	-18									
8	-122	116	-28	2	289	276	6	1	171	120	18	-5	64	35	3					
				3	77	74	0	2	467	454	9	-4	516	511	3					
	12	-1	1					3	134	88	13	-3	80	62	3					
					12	3	1	4	204	166	16	-2	385	385	0					
0	400	398	1					5	411	400	7	-1	336	314	13					
1	259	261	-1	-3	437	418	12	6	175	142	11	0	95	87	1					
2	532	519	9	-2	112	73	8	7	343	319	13	1	245	229	7					
3	664	659	3	-1	188	178	3					2	420	391	18					
4	179	220	-16						13	-5	1									
5	225	250	-10						0	234	219	7		13	1	1				
6	-157	119	-39						1	208	243	-18	-2	225	178	20				
7	578	587	-5	0	333	325	5	2	670	652	13									
				1	218	195	9	3	210	168	18		14	-8	1					
	12	0	1	2	328	311	10	4	35	39	0									
								5	218	208	4	0	253	229	11					
-9	-139	2	-20					6	256	284	-14	1	193	171	8					
-8	279	295	-7					7	383	396	-7	2	387	350	22					
-7	-113	6	-14	0	573	550	16					3	135	46	18					
-6	547	539	5	1	313	292	11		13	-4	1									
-5	490	505	-11	2	189	188	0													
-4	56	19	3	3	91	100	-2													
-3	432	423	6	4	109	38	12		0	359	348	6		14	-7	1				
-2	74	24	6	5	476	444	21		1	262	246	9	0	104	65	7				
-1	328	336	-5						2	557	541	11	1	434	423	7				
0	386	375	7						3	103	83	4	2	435	416	12				
1	103	61	9						4	147	174	-9	3	48	0	2				
2	333	299	20	0	453	422	20		5	290	308	-9	4	357	322	20				
3	447	429	11	1	183	164	7		6	165	180	-4								
4	385	411	-15	2	382	358	15		7	344	344	0		14	-6	1				
5	304	341	-19	3	376	367	6													
6	-173	38	-32	4	114	50	13			13	-3	1	0	89	51	6				
				5	433	403	20						1	427	425	1				
	12	1	1	6	135	78	14			0	-43	101	-13	2	197	187	4			
										1	534	502	23	3	169	161	3			
-8	357	380	-13							2	673	650	16	4	414	392	14			
-7	194	195	0							3	-15	15	0							
-6	286	300	-7	0	400	392	5			4	-172	79	-38		14	-5	1			
-5	351	325	15	1	347	354	-4			5	152	212	-19							
-4	328	288	23	2	377	353	15			6	391	400	-4	0	240	175	27			
-3	696	673	17	3	328	302	15							1	597	574	16			
-2	123	45	16	4	243	163	36			13	-2	1		2	204	171	14			
-1	177	153	9	5	529	524	3							3	185	174	4			
0	230	176	24	6	149	64	21			0	184	149	13							
1	339	356	-11	7	276	240	18			1	351	342	5		14	-4	1			
2	459	444	9							2	381	392	-6							
3	392	386	4							3	-128	80	-22	0	126	122	0			
4	255	250	2							4	368	376	-3	1	517	460	24			
5	-77	91	-14							5	173	291	-44	2	-32	63	-3			
				0	225	200	11							3	330	328	1			
				1	160	129	11													
	12	2	1	2	580	572	6			13	-1	1								
				3	366	320	29													
-6	455	454	0	4	72	82	-1			0	174	161	5		14	-3	1			
-5	488	466	15	5	437	418	13			1	355	341	8	0	300	330	-8			
-4	188	105	27	6	177	154	8			2	585	557	19	1	600	559	18			
-3	381	360	13	7	428	385	27			3	-110	20	-13	2	-184	14	-23			
-2	194	134	22							4	267	304	-17							

Appendix 3 Absorbance traces for recombination rates.

3,4-dicyano-N-methylpyridinium	277
4-cyano-N-methylpyridinium	278
4-carbomethoxy-N-methylpyridinium	279
4-amido-N-ethylpyridinium	280
N-ethylpyridinium	281
2-methoxy-N-methylpyridinium	282
2,6-dimethyl-N-ethylpyridinium	283

DATA FILE: 251-1.002

USER:

TIME RANGE: 5.0 ms INPUT V RANGE: 1.60 V INPUT OFFSET: 0 %

EXPERIMENT: TRANSIENT ABSORPTION

SLOW (100 kHz) VARIABLE GAIN OFFSETTING AMP GAINS: PRE-AMP: x 100 POST-NULL OUTPUT

SHOTS PER CYCLE: 20 CYCLES: 6

EXCITATION WAVELENGTH: 532 nm

OBSERVATION WAVELENGTH: 500 nm

SAMPLE: ircodpz 2

SOLVENT: ch3cn

TEMPERATURE: rt

COMMENT:

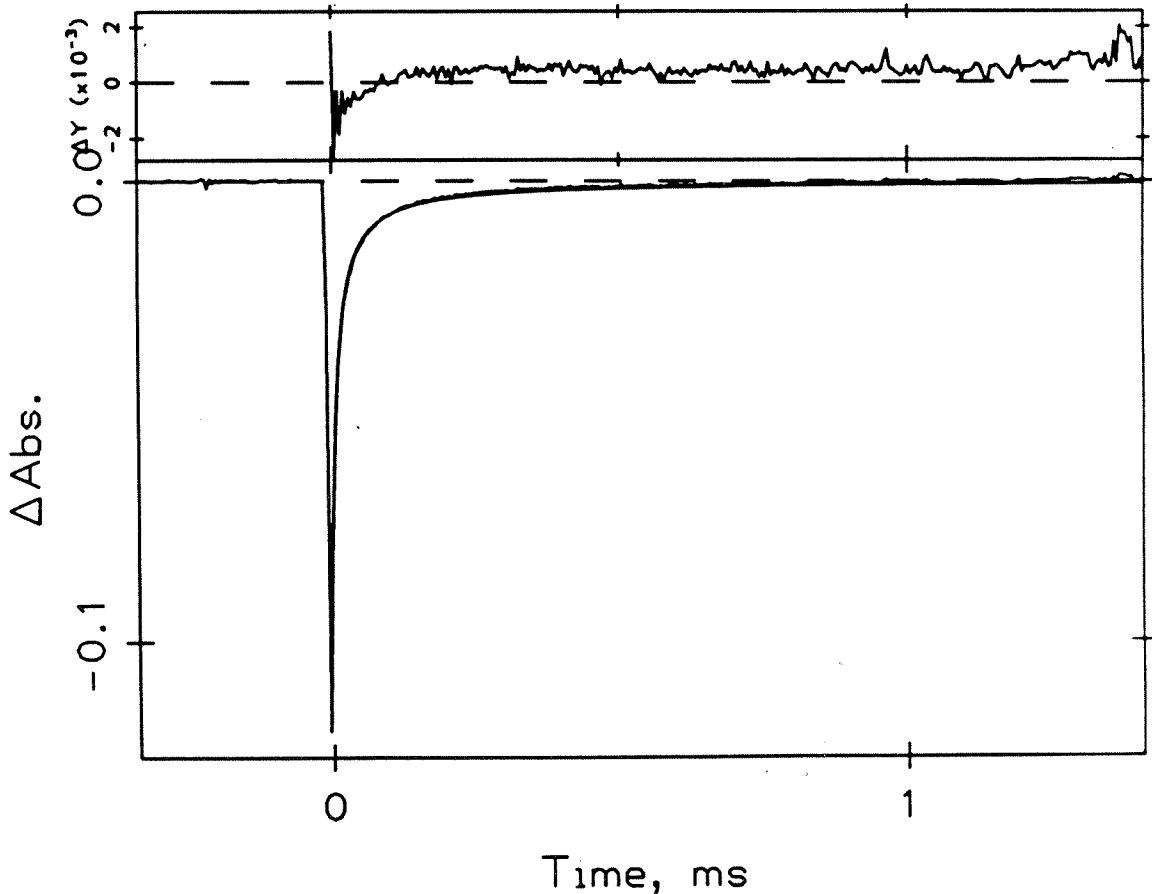
COMMENT:

----> FIXED PARAMETER; ! ----> FIXED SIGN

$$y(t) = 1/(C0+C1*t)$$

C0 = -1.273E+01

C1 = -1.257E+06



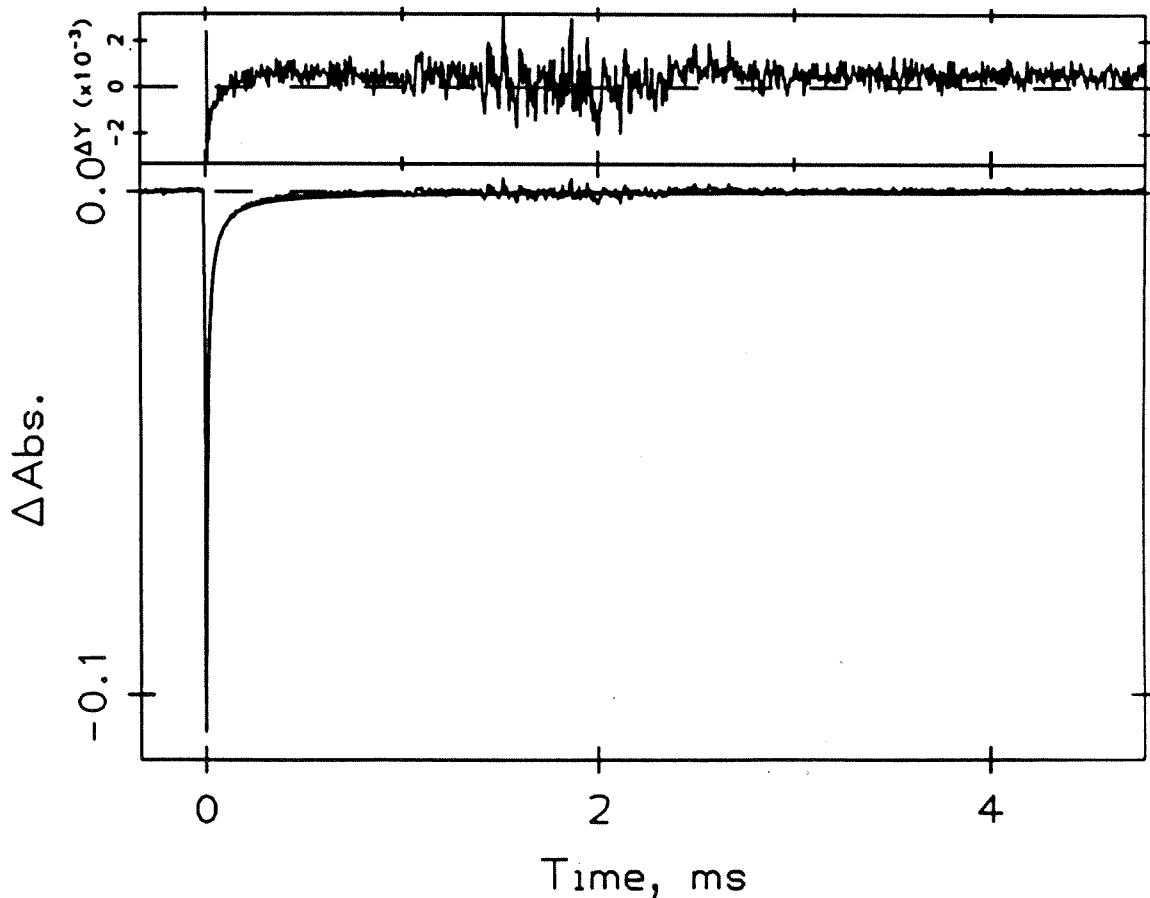
DATA FILE: 251-2.001 USER:
TIME RANGE: 2.5 ms INPUT V RANGE: 1.60 V INPUT OFFSET: 0 %
EXPERIMENT: TRANSIENT ABSORPTION
SLOW (100 kHz) VARIABLE GAIN OFFSETTING AMP GAINS: PRE-AMP: x 100 POST-NULL OUTPUT
SHOTS PER CYCLE: 20 CYCLES: 2
EXCITATION WAVELENGTH: 532 nm OBSERVATION WAVELENGTH: 500 nm
SAMPLE: ircodpz 2
SOLVENT: ch3cn
TEMPERATURE: rt
COMMENT:
COMMENT:

---> FIXED PARAMETER; ! ---> FIXED SIGN

$$y(t) = 1/(C0+C1*t)$$

C0 = -6.842E+00

C1 = -1.408E+06

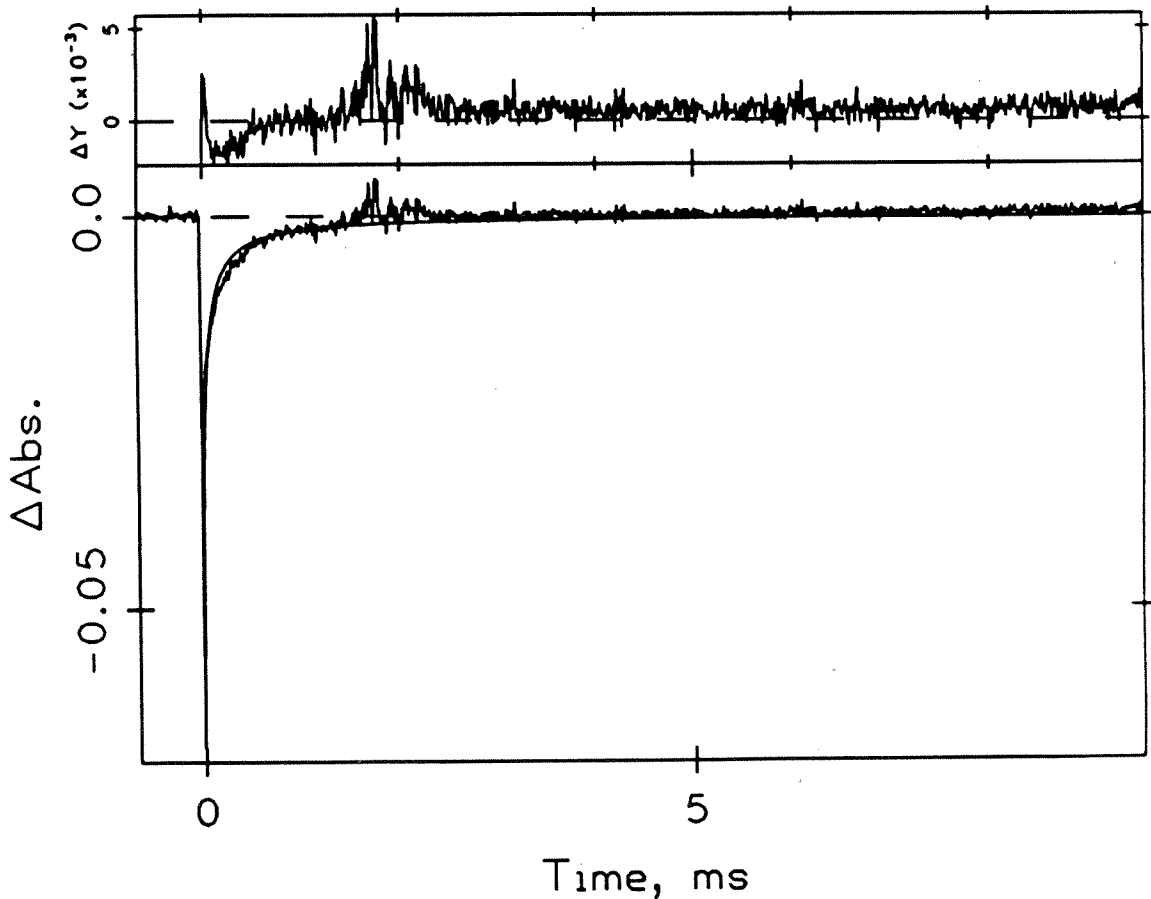


DATA FILE: 251-3.002 USER:
TIME RANGE: 7.5 ms INPUT V RANGE: 1.60 V INPUT OFFSET: 0 %
EXPERIMENT: TRANSIENT ABSORPTION
SLOW (100 kHz) VARIABLE GAIN OFFSETTING AMP GAINS: PRE-AMP: x 100 POST-NULL OUTPUT
SHOTS PER CYCLE: 20 CYCLES: 1
EXCITATION WAVELENGTH: 532 nm OBSERVATION WAVELENGTH: 500 nm
SAMPLE: ircodpz 2
SOLVENT: ch3cn
TEMPERATURE: rt
COMMENT:
COMMENT:

---> FIXED PARAMETER; ! ---> FIXED SIGN

$$y(t) = 1/(C0+C1*t)$$

C0 = -3.045E+01
C1 = -5.434E+05



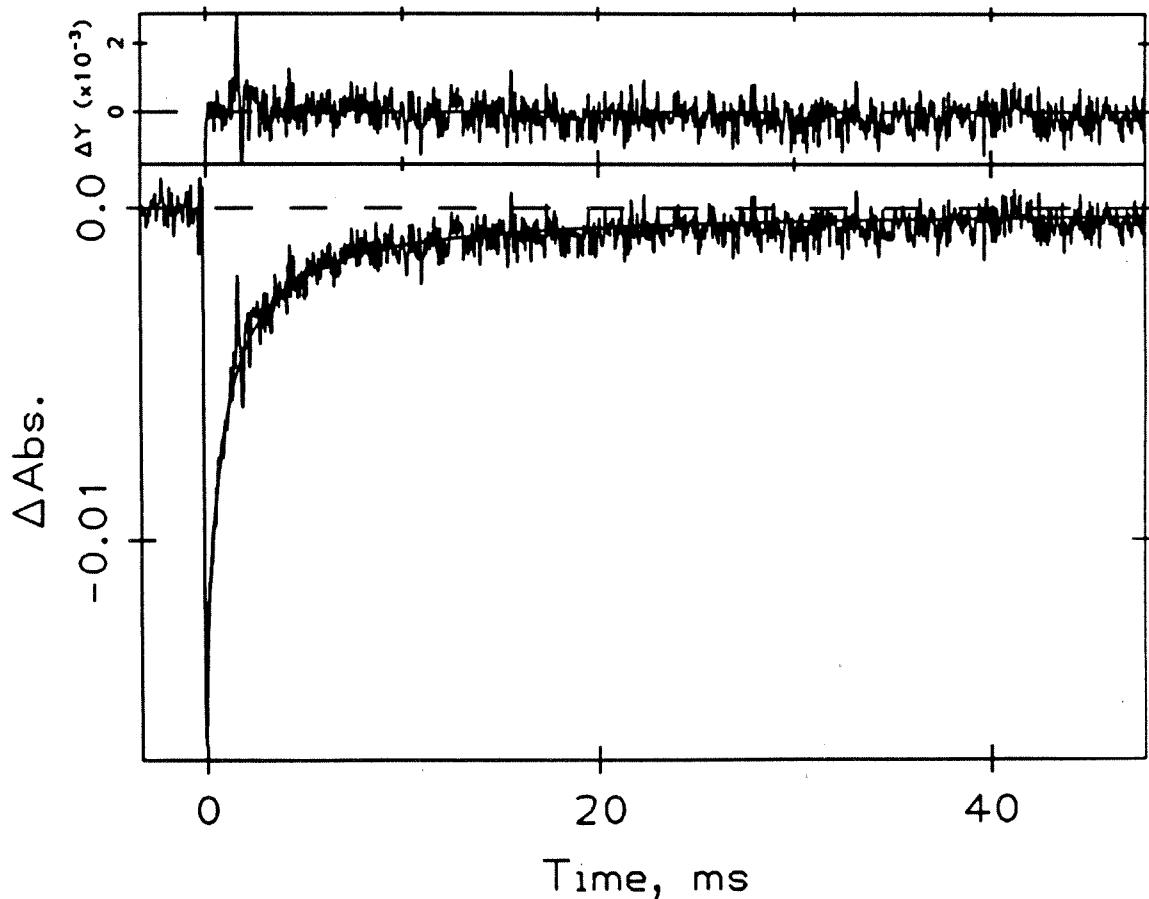
DATA FILE: br211-6.004 USER:
TIME RANGE: 50 ms INPUT V RANGE: 1.60 V INPUT OFFSET: 0 %
EXPERIMENT: TRANSIENT ABSORPTION
SLOW (100 kHz) VARIABLE GAIN OFFSETTING AMP GAINS: PRE-AMP: x 100 POST-NULL OUTPUT
SHOTS PER CYCLE: 1 CYCLES: 30
EXCITATION WAVELENGTH: 532 nm OBSERVATION WAVELENGTH: 500 nm
SAMPLE: ircodpz2
SOLVENT: ch3cn
TEMPERATURE: rt
COMMENT: 10 mg num 06
COMMENT:

----> FIXED PARAMETER; ! ----> FIXED SIGN

$$y(t) = 1/(C0+C1*t)$$

C0 = -7.468E+01

C1 = -8.076E+04



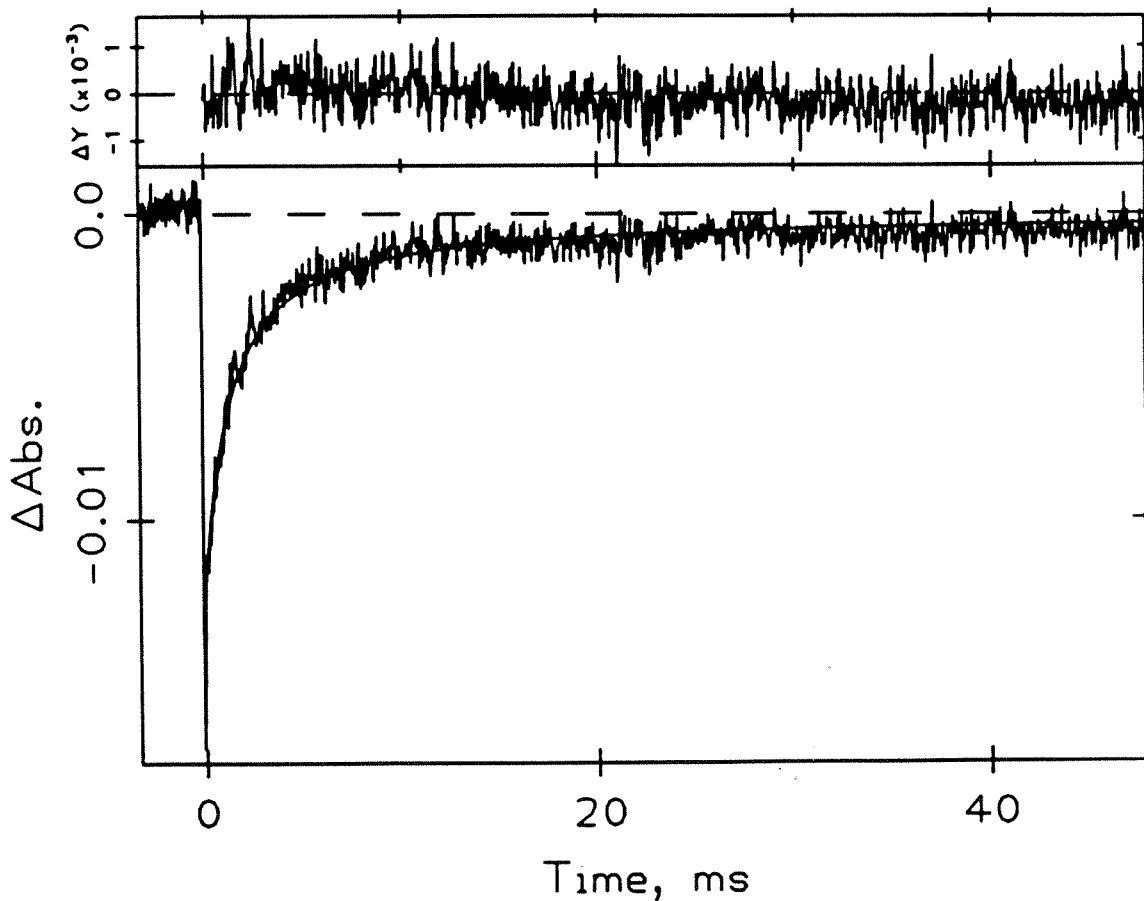
DATA FILE: br211-7.001 USER:
TIME RANGE: 50 ms INPUT V RANGE: 1.60 V INPUT OFFSET: 0 %
EXPERIMENT: TRANSIENT ABSORPTION
SLOW (100 kHz) VARIABLE GAIN OFFSETTING AMP GAINS: PRE-AMP: x 100 POST-
NULL OUTPUT
SHOTS PER CYCLE: 1 CYCLES: 30
EXCITATION WAVELENGTH: 532 nm OBSERVATION WAVELENGTH: 500 nm
SAMPLE: ircodpz2
SOLVENT: ch3cn
TEMPERATURE: rt
COMMENT: 11 mg num 07
COMMENT:

----> FIXED PARAMETER; ! ----> FIXED SIGN

$$y(t) = 1/(C0+C1*t)$$

C0 = -8.217E+01

C1 = -6.412E+04



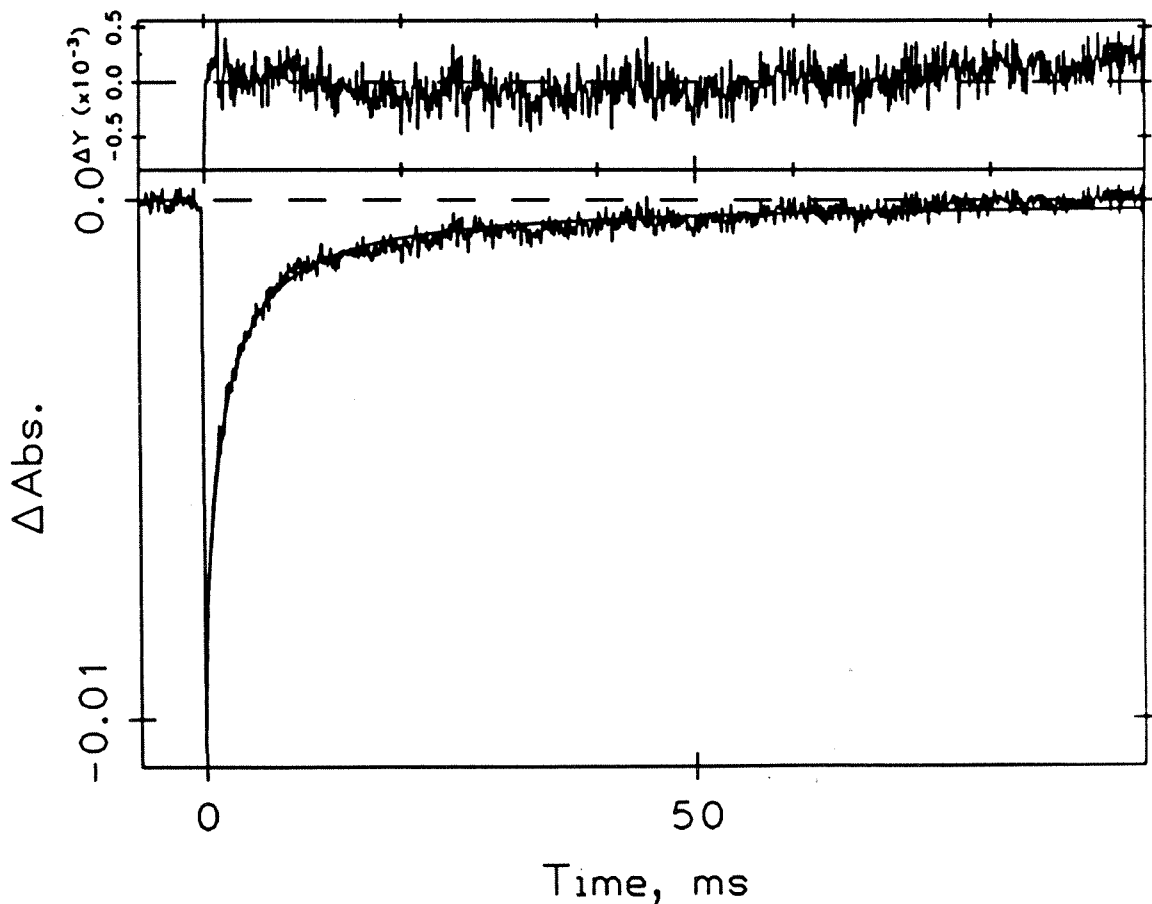
DATA FILE: br211-10.006 USER:
 TIME RANGE: 75 ms INPUT V RANGE: 1.60 V INPUT OFFSET: 0 %
 EXPERIMENT: TRANSIENT ABSORPTION
 SLOW (100 kHz) VARIABLE GAIN OFFSETTING AMP GAINS: PRE-AMP: x 100 POST-
 NULL OUTPUT
 SHOTS PER CYCLE: 1 CYCLES: 30
 EXCITATION WAVELENGTH: 532 nm OBSERVATION WAVELENGTH: 500 nm
 SAMPLE: ircodpz2
 SOLVENT: ch3cn
 TEMPERATURE: rt
 COMMENT: 25 mg num 10
 COMMENT:

----> FIXED PARAMETER; ! ----> FIXED SIGN

$$y(t) = 1/(C0+C1*t)$$

C0 = -1.181E+02

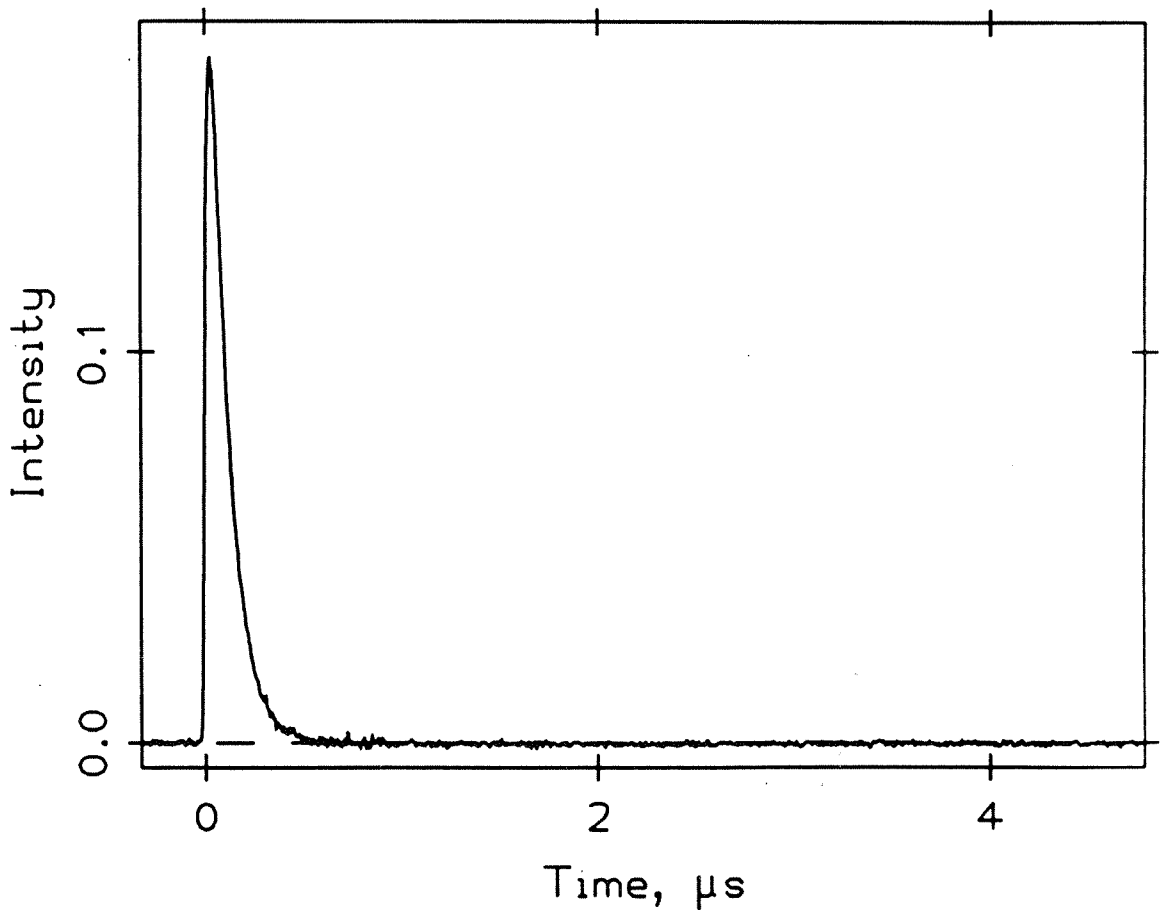
C1 = -6.187E+04



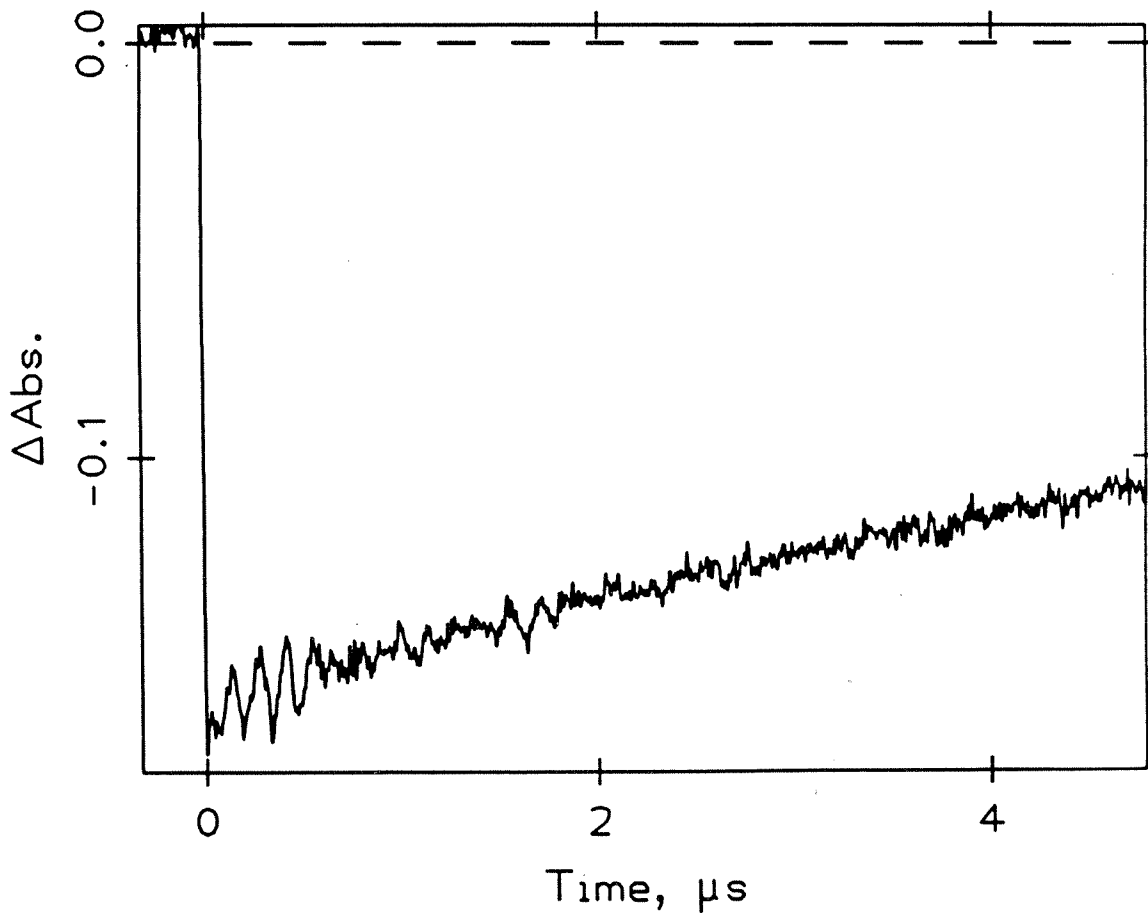
Appendix 4 Absorbance traces used to determine quantum yields.

3,4-dicyano-N-methylpyridinium	
Luminescence Decay	285
Absorbance Trace	286
4-cyano-N-methylpyridinium	
Luminescence Decay	287
Absorbance Trace	288
4-carbomethoxy-N-methylpyridinium	
Luminescence Decay	289
Absorbance Trace	290
4-amido-N-ethylpyridinium	
Luminescence Decay	291
Absorbance Trace	292
N-ethylpyridinium	
Luminescence Decay	293
Absorbance Trace	294
2-methoxy-N-methylpyridinium	
Luminescence Decay	295
Absorbance Trace	296

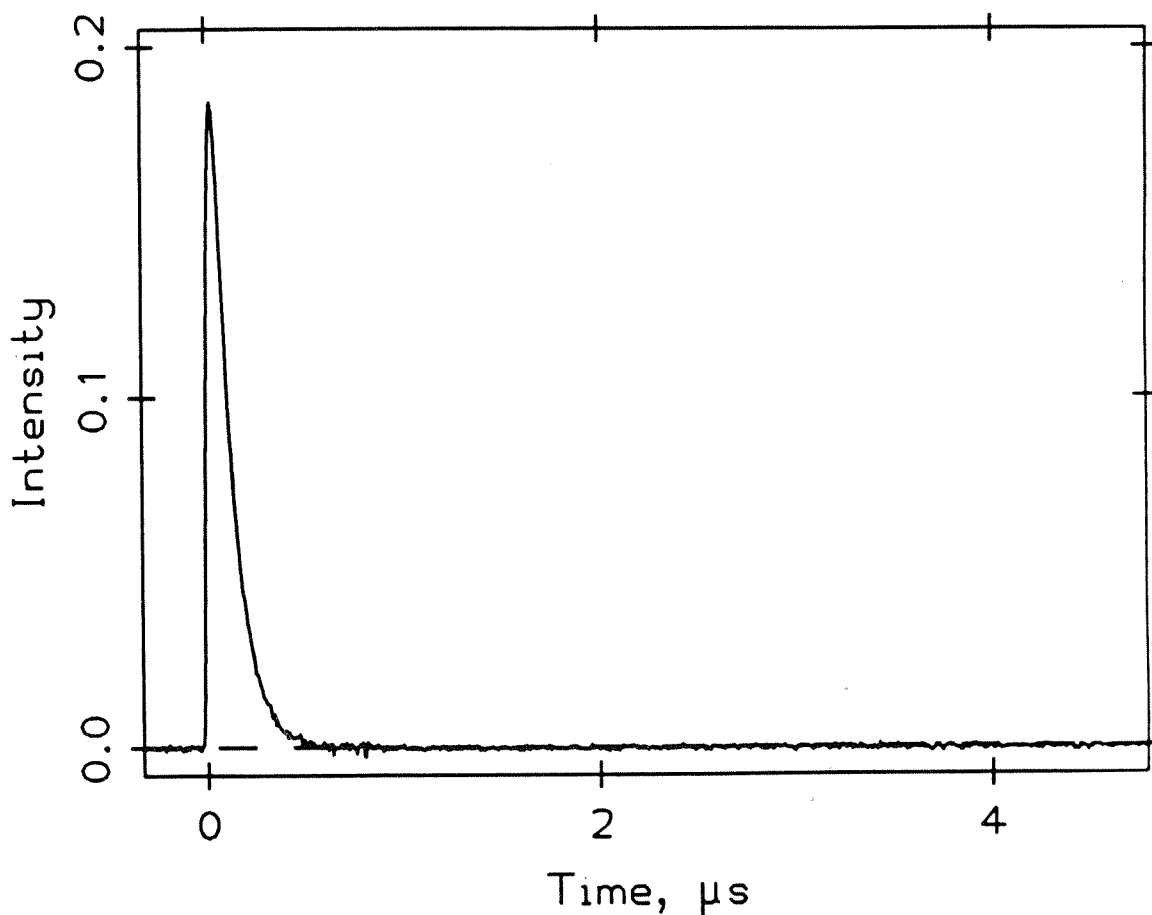
DATA FILE: 247-0.001 USER:
TIME RANGE: 1.25 μ s INPUT V RANGE: 0.250 V INPUT OFFSET: 0 %
EXPERIMENT: LUMINESCENCE DECAY
FAST (200 MHz) QUASI-DIFFERENTIAL AMP MODE: QUASI-DIFFERENTIAL
SHOTS PER CYCLE: 100 CYCLES: 1
EXCITATION WAVELENGTH: 532 nm OBSERVATION WAVELENGTH: 690 nm
SAMPLE: ircodpz 2
SOLVENT: ch3cn
TEMPERATURE: rt
COMMENT:
COMMENT: 250 ul



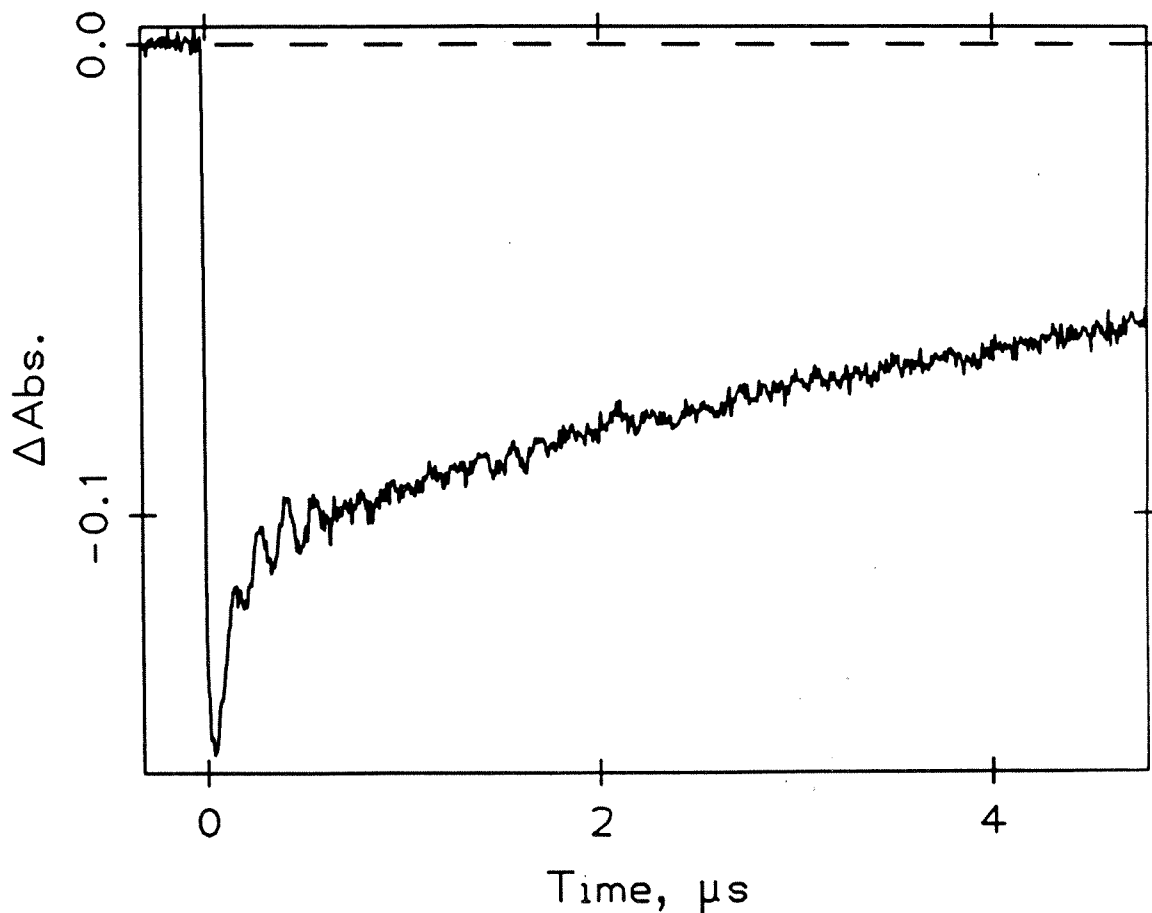
DATA FILE: 247-0.006 USER:
TIME RANGE: 1.25 μ s INPUT V RANGE: 0.250 V INPUT OFFSET: 0 μ
EXPERIMENT: TRANSIENT ABSORPTION
FAST (200 MHz) QUASI-DIFFERENTIAL AMP MODE: QUASI-DIFFERENTIAL
SHOTS PER CYCLE: 100 CYCLES: 1
EXCITATION WAVELENGTH: 532 nm OBSERVATION WAVELENGTH: 500 nm
SAMPLE: ircodpz 2
SOLVENT: ch3cn
TEMPERATURE: rt
COMMENT:
COMMENT: 250 μ l



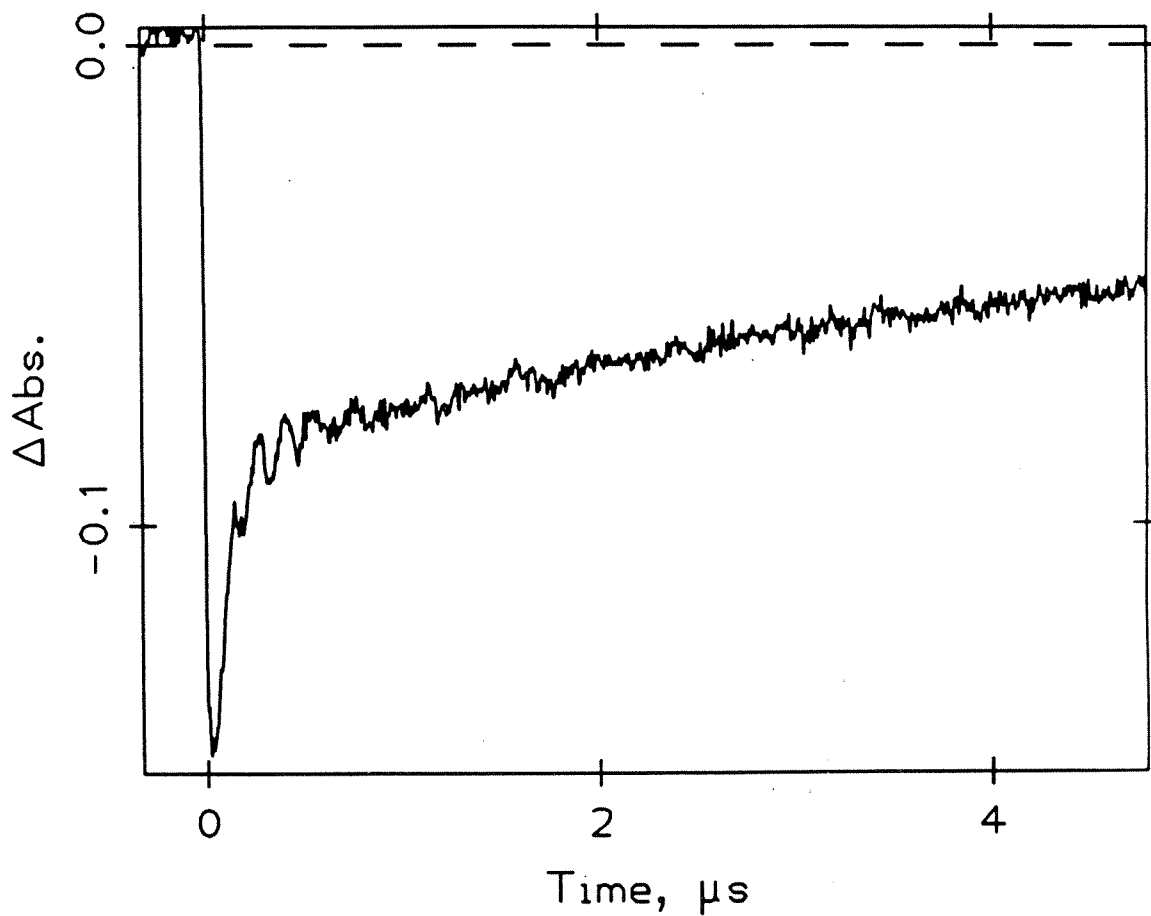
DATA FILE: 247-1.001 USER:
TIME RANGE: 1.25us INPUT V RANGE: 0.250 V INPUT OFFSET: 0 %
EXPERIMENT: LUMINESCENCE DECAY
FAST (200 MHz) QUASI-DIFFERENTIAL AMP MODE: QUASI-DIFFERENTIAL
SHOTS PER CYCLE: 100 CYCLES: 1
EXCITATION WAVELENGTH: 532 nm OBSERVATION WAVELENGTH: 690 nm
SAMPLE: ircodpz 2
SOLVENT: ch3cn
TEMPERATURE: rt
COMMENT:
COMMENT: 250 ul



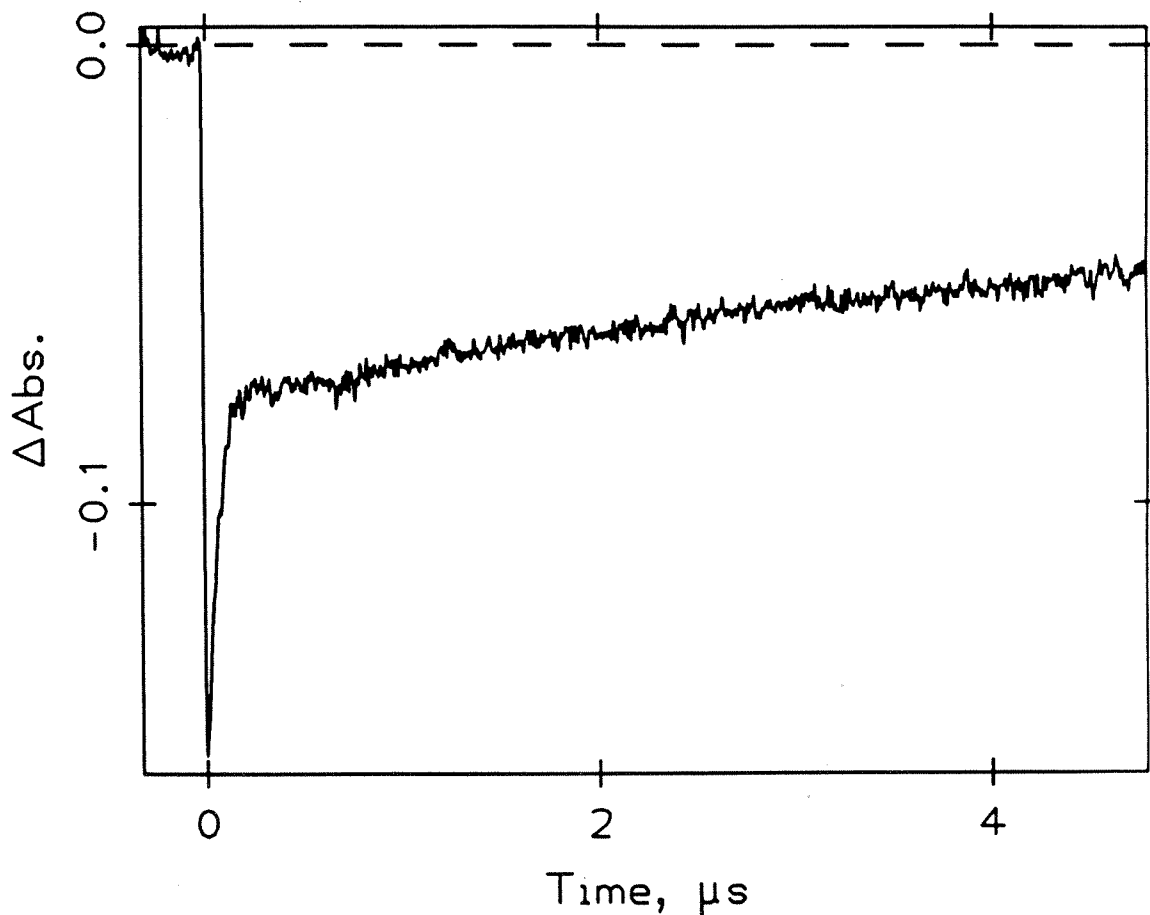
DATA FILE: 247-1.003 USER:
TIME RANGE: 1.25us INPUT V RANGE: 0.250 V INPUT OFFSET: 0 %
EXPERIMENT: TRANSIENT ABSORPTION
FAST (200 MHz) QUASI-DIFFERENTIAL AMP MODE: QUASI-DIFFERENTIAL
SHOTS PER CYCLE: 100 CYCLES: 2
EXCITATION WAVELENGTH: 532 nm OBSERVATION WAVELENGTH: 500 nm
SAMPLE: ircodpz 2
SOLVENT: ch3cn
TEMPERATURE: rt
COMMENT:
COMMENT: 250 ul



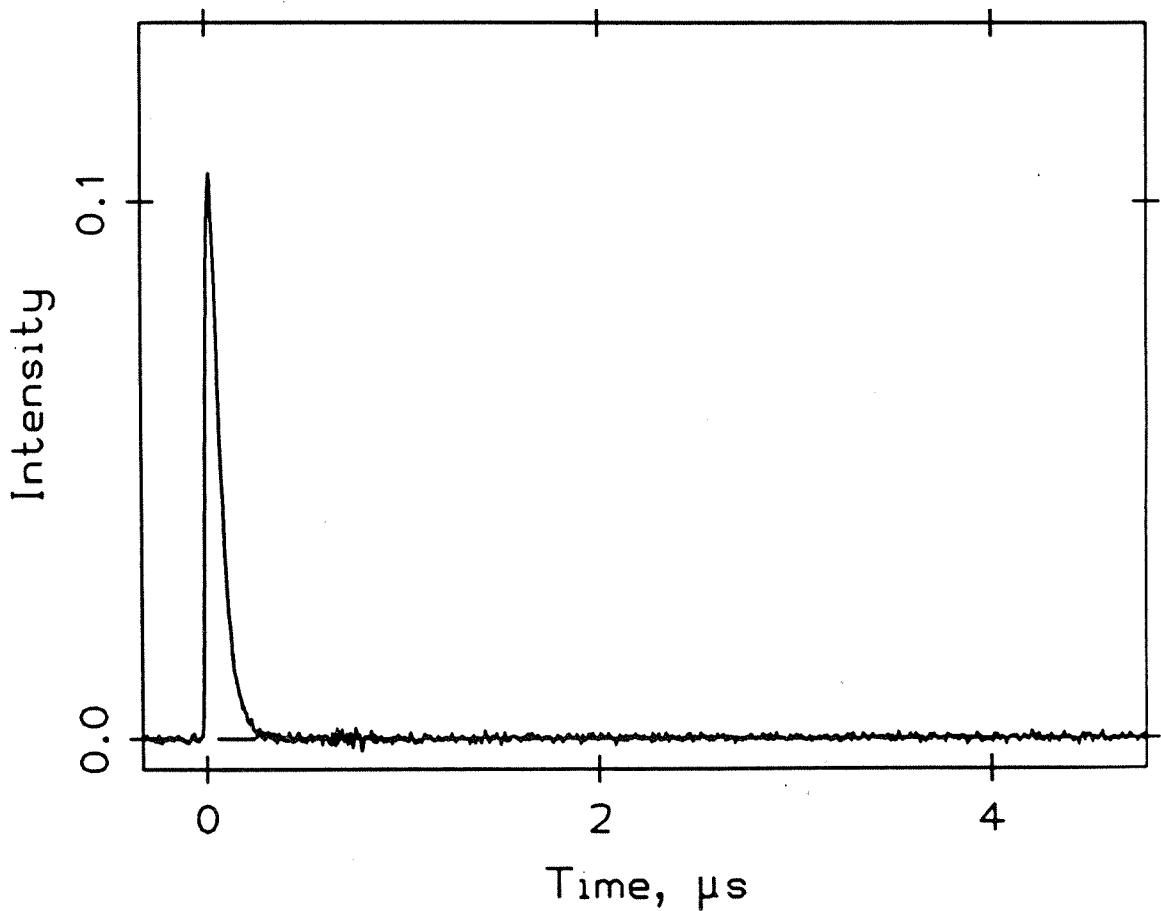
DATA FILE: 247-2.003 USER:
TIME RANGE: 1.25 μ s INPUT V RANGE: 0.250 V INPUT OFFSET: 0 %
EXPERIMENT: TRANSIENT ABSORPTION
FAST (200 MHz) QUASI-DIFFERENTIAL AMP MODE: QUASI-DIFFERENTIAL
SHOTS PER CYCLE: 100 CYCLES: 2
EXCITATION WAVELENGTH: 532 nm OBSERVATION WAVELENGTH: 500 nm
SAMPLE: ircodpz 2
SOLVENT: ch3cn
TEMPERATURE: rt
COMMENT:
COMMENT: 250 μ l



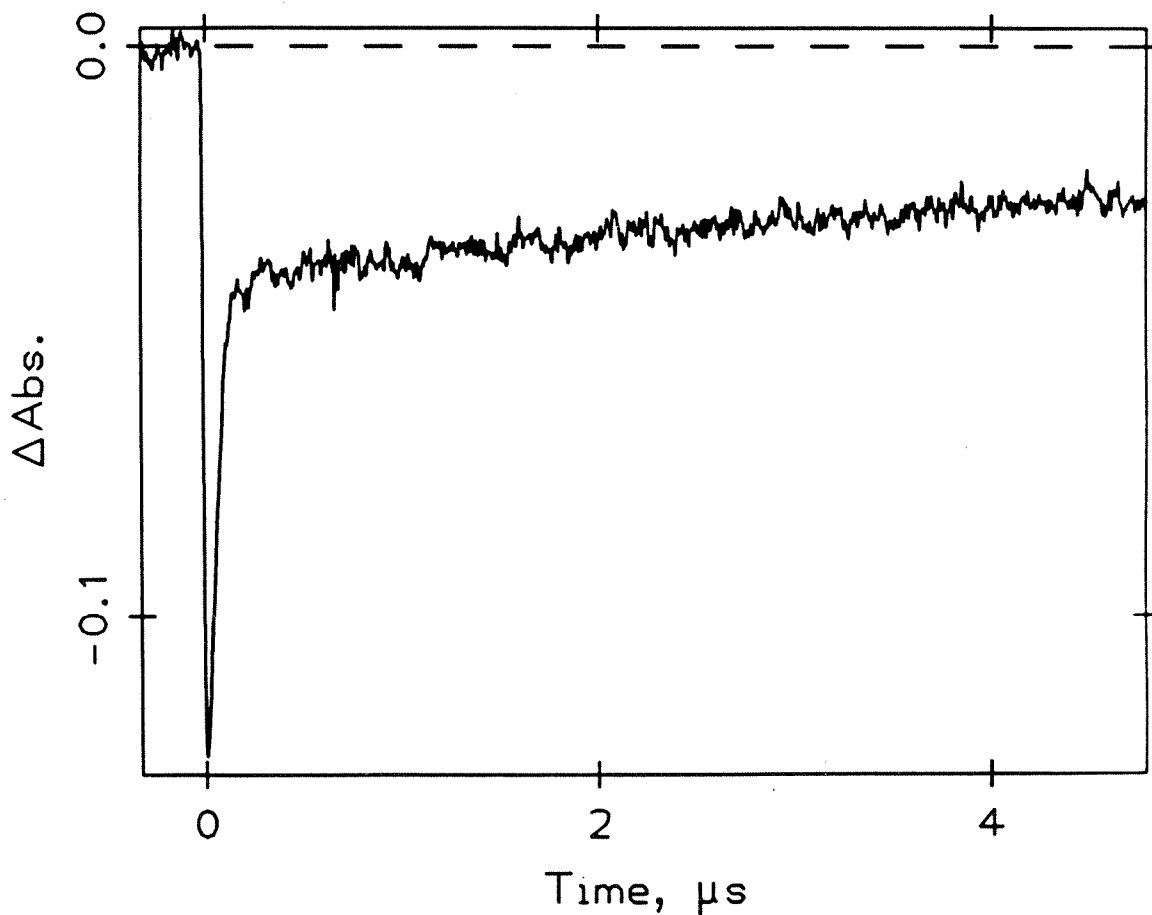
DATA FILE: 247-3.003 USER:
TIME RANGE: 1.25 μ s INPUT V RANGE: 0.250 V INPUT OFFSET: 0 %
EXPERIMENT: TRANSIENT ABSORPTION
FAST (200 MHz) QUASI-DIFFERENTIAL AMP MODE: QUASI-DIFFERENTIAL
SHOTS PER CYCLE: 100 CYCLES: 1
EXCITATION WAVELENGTH: 532 nm OBSERVATION WAVELENGTH: 500 nm
SAMPLE: ircodpz 2
SOLVENT: ch3cn
TEMPERATURE: rt
COMMENT:
COMMENT: 0030mgq



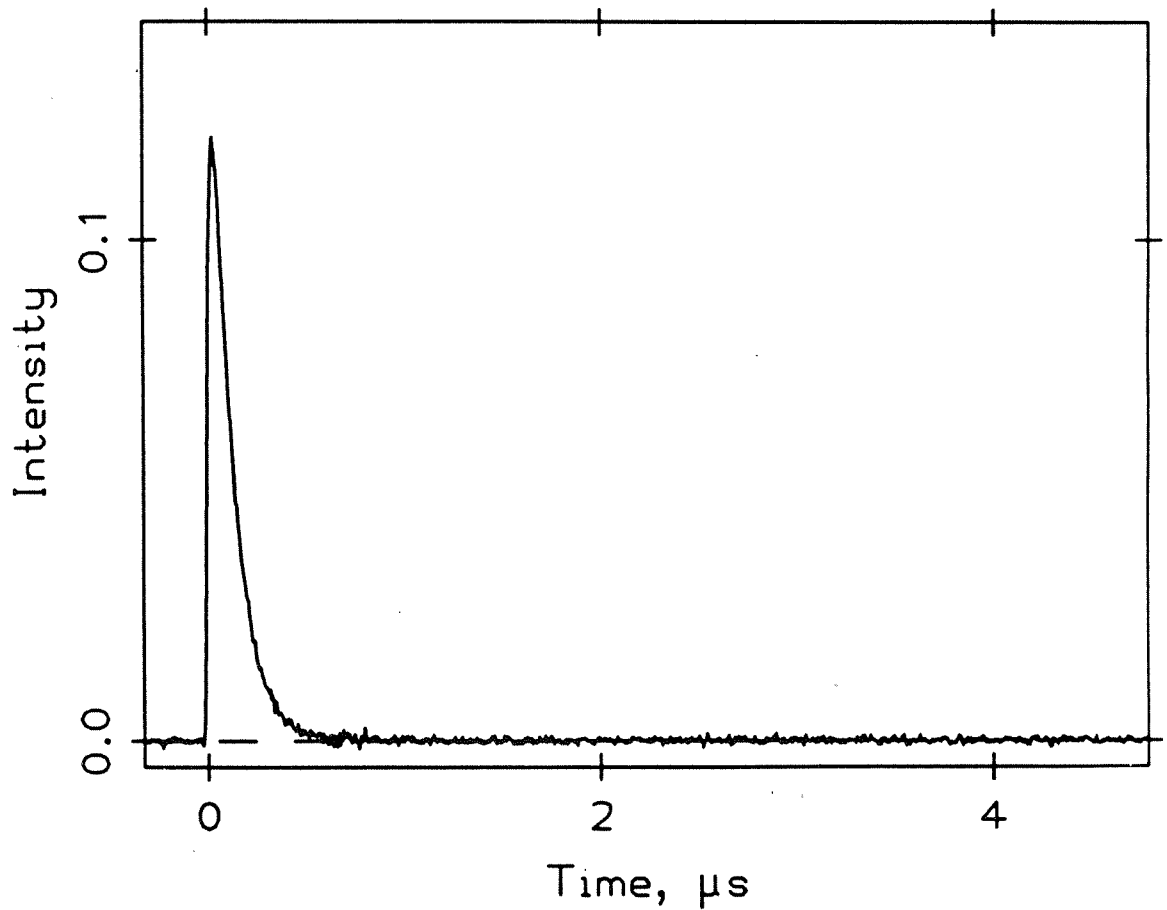
DATA FILE: 247-6.001 USER:
TIME RANGE: 1.25 μ s INPUT V RANGE: 0.250 V INPUT OFFSET: 0 %
EXPERIMENT: LUMINESCENCE DECAY
FAST (200 MHz) QUASI-DIFFERENTIAL AMP MODE: QUASI-DIFFERENTIAL
SHOTS PER CYCLE: 100 CYCLES: 1
EXCITATION WAVELENGTH: 532 nm OBSERVATION WAVELENGTH: 690 nm
SAMPLE: ircdpz 2
SOLVENT: ch3cn
TEMPERATURE: rt
COMMENT:
COMMENT: 6.5mg q



DATA FILE: 247-6.002 USER:
TIME RANGE: 1.25us INPUT V RANGE: 0.250 V INPUT OFFSET: 0 %
EXPERIMENT: TRANSIENT ABSORPTION
FAST (200 MHz) QUASI-DIFFERENTIAL AMP MODE: QUASI-DIFFERENTIAL
SHOTS PER CYCLE: 100 CYCLES: 1
EXCITATION WAVELENGTH: 532 nm OBSERVATION WAVELENGTH: 500 nm
SAMPLE: ircodpz 2
SOLVENT: ch3cn
TEMPERATURE: rt
COMMENT:
COMMENT: 06.5mgq



DATA FILE: 247-7.001 USER:
TIME RANGE: 1.25 μ s INPUT V RANGE: 0.250 V INPUT OFFSET: 0 %
EXPERIMENT: LUMINESCENCE DECAY
FAST (200 MHz) QUASI-DIFFERENTIAL AMP MODE: QUASI-DIFFERENTIAL
SHOTS PER CYCLE: 100 CYCLES: 1
EXCITATION WAVELENGTH: 532 nm OBSERVATION WAVELENGTH: 690 nm
SAMPLE: ircodpz 2
SOLVENT: ch3cn
TEMPERATURE: rt
COMMENT:
COMMENT: 12.5mgq



DATA FILE: 247-7.003 USER:
TIME RANGE: 1.25 μ s INPUT V RANGE: 0.250 V INPUT OFFSET: 0 %
EXPERIMENT: TRANSIENT ABSORPTION
FAST (200 MHz) QUASI-DIFFERENTIAL AMP MODE: QUASI-DIFFERENTIAL
SHOTS PER CYCLE: 100 CYCLES: 1
EXCITATION WAVELENGTH: 532 nm OBSERVATION WAVELENGTH: 690 nm
SAMPLE: ircodpz 2
SOLVENT: ch3cn
TEMPERATURE: rt
COMMENT:
COMMENT: 12.5mgq

